

---

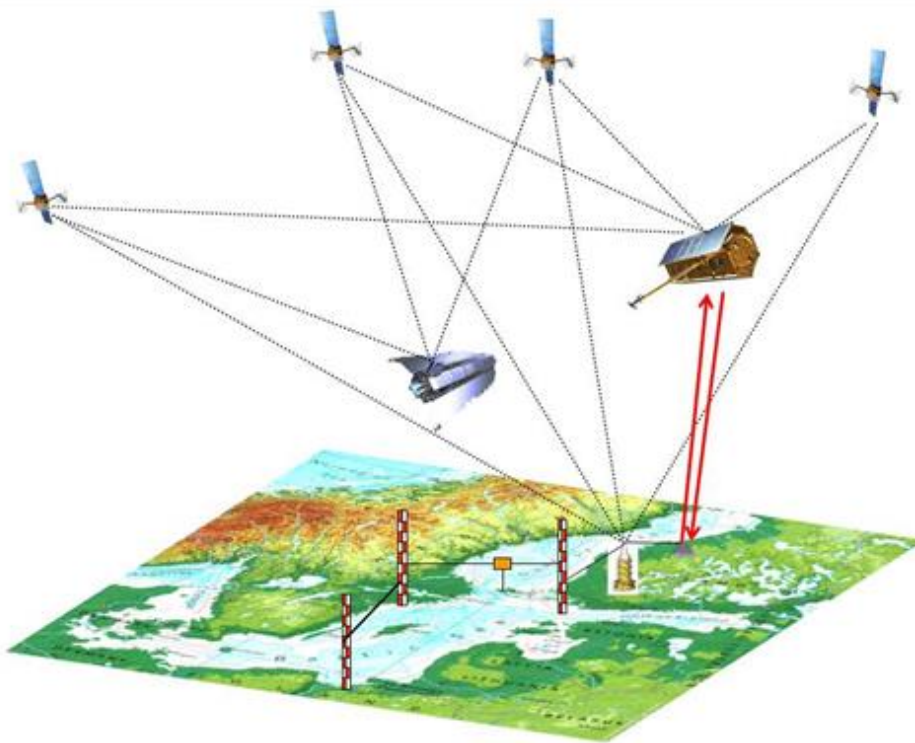
## BALTIC+

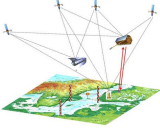
# Geodetic SAR for Baltic Height System Unification and Baltic Sea Level Research

## Final Report

---

Doc. No.: SAR-HSU-FR-0022  
Issue: 1  
Revision: 1  
Date: 07.07.2021



	<b>BALTIC+ Theme 5</b> Geodetic SAR for Baltic Height System Unification and Baltic Sea Level Research	Final Report Doc. Nr: SAR-HSU-SR-0022 Issue: 1.1 Date: 07.07.2021 Page: 1 of 170
---	--	--

### Authors Information

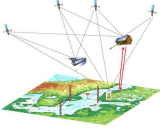
**Authors:** Thomas Gruber, Detlef Angermann, Marius Schlaak,  
 Xanthi Oikonomidou / TUM  
 Christoph Gisinger, Ramon Bric / DLR  
 Markku Poutanen, Simo Marila, Hannu Koivula, Maaria Nordman, Timo  
 Saari / FGI  
 Jolanta Nastula, Ryszard Zdunek / CBK-PAN  
 Art Ellmann, Sander Varbla / TUT  
 Jonas Ågren, Faramarz Nilfouroushan / LM

### Document Change Record

ISSUE /REV.	DATE	REASON FOR CHANGE	CHANGED PAGES / PARAGRAPHS
1.0	11.06.2021	Initial Issue	
1.1	07.07.2021	Revision	Editorials: Some citations updated. Some corrections made throughout the document. Chapter 1.2: Citation added Chapter 1.4: Applicable Documents updated Chapter 1.5: References updated Chapter 1.6 added for not cited literature Chapter 8.7.2: Minor update Chapter 9: Minor update Chapter 10.4.2: Minor update

### Document Approval

CONTRACTOR	DATE	SIGNATURE
Dr. Thomas Gruber Institute of Astronomical and Physical Geodesy, Technical University of Munich		
ESA		
Dr. Jérôme Benveniste Directorate of Earth Observation Programmes EO Science, Applications and Climate Department		

	<b>BALTIC+ Theme 5</b>  Geodetic SAR for Baltic Height System Unification and Baltic Sea Level Research	<b>Final Report</b> Doc. Nr: SAR-HSU-SR-0022 Issue: 1.1 Date: 07.07.2021 Page: 2 of 170
---	--	---

## Abbreviations and Acronyms

ARP	Antenna Reference Point
CBK-PAN	Centrum Badań Kosmicznych Polskiej Akademii Nauk
CODE	Centre for Orbit Determination in Europe
CP	Contact Point
CR	Corner Reflector
DD	Double Differences
DLR	Deutsches Zentrum für Luft- und Raumfahrt
ECMWF	European Centre for Medium-Range Weather Forecasts
ECR	Electronic Corner Reflector
EGM2008	Earth Gravity Model 2008
EPN	European Permanent Network
ESA	European Space Agency
EUREF	Regional Reference Frame Sub-Commission for Europe
EW	Extended Wide-Swath (S-1 SAR mode)
FFT	Fast Fourier Transform
FGI	Finnish Geospatial Research Institute
FM	Frequency Modulation
GNSS	Global Navigation Satellite System
GRS80	Geodetic Reference System 1980
IAG	International Association of Geodesy
IERS	International Earth Rotation and Reference Systems Service
IGS	International GNSS Service
InSAR	Interferometric SAR
IPF	Instrument Processing Facility (S-1 SAR processor)
IPP	Ionospheric Pierce Point
ITRF	International Terrestrial Reference Frame
IW	Interferometric Wide-Swath (S-1 SAR mode)
LM	Lantmäteriet, Swedish Mapping, Cadastral and Land Registration Authority
LOS	Line Of Sight
MSL	Mean Sea Level
NKG	Nordic Geodetic Commission
PDGS	Payload Data Ground Segment
PDOP	Position Dilution of Precision
PPP	Precise Point Positioning
PTA	Point Target Analysis
RMS	Root Mean Square
RP	Reference Point
SAR	Synthetic Aperture Radar
SAR-HSU	Geodetic SAR for Baltic Height System Unification and Baltic Sea Level Research
SCR	Signal to Clutter Ratio
SLC	Single Look Complex
SM	Stripmap (SAR mode)
TEC	Total Electron Content
TG	Tide Gauge
TGCP	Tide Gauge Contact Point
TOPS	Terrain Observation with Progressive Scans
TUM	Technical University of Munich
TUT	Tallinn University of Technology
UTC	Coordinated Universal Time
VLM	Vertical Land Motion
VMF	Vienna Mapping Functions
vTEC	Vertical Total Electron Content
WGS-84	World Geodetic System 1984
ZPD	Zenith Path Delay
ZTD	Zenith Tropospheric Delay

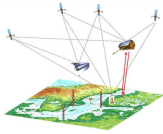
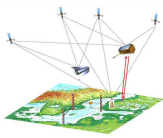


## Table of Content

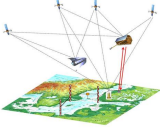
<b>1</b>	<b>Introduction .....</b>	<b>5</b>
1.1	Purpose .....	5
1.2	Project Overview .....	5
1.3	Applicable Documents .....	6
1.4	Project Publications .....	6
1.5	References .....	6
1.6	Additional Literature .....	10
<b>2</b>	<b>Summary .....</b>	<b>12</b>
2.1	Scientific Challenges, Data Base and Network Design .....	12
2.2	Basic Algorithms .....	13
2.3	Data Analyses and Scientific Assessment .....	14
2.4	Conclusions .....	15
<b>3</b>	<b>Scientific Challenges.....</b>	<b>17</b>
3.1	SAR Data Analysis and Value Adding .....	17
3.2	Geometric Positioning .....	18
3.3	Tide Gauge Data Analysis .....	19
3.4	GOCE based Geoid Computation .....	20
3.5	Reference Frames and Joint Standards .....	20
<b>4</b>	<b>Project Data Base.....</b>	<b>22</b>
4.1	SAR Images .....	22
4.2	GNSS Data .....	22
4.3	Tide Gauge Data .....	22
4.4	Local Gravity and GOCE based Global Models.....	23
4.5	Support Data Sets.....	24
<b>5</b>	<b>Baltic Sea Test Network .....</b>	<b>25</b>
5.1	SAR Target Analysis .....	25
5.2	Network Design.....	25
<b>6</b>	<b>Basic Algorithms .....</b>	<b>32</b>
6.1	SAR Data Analysis and Value Adding .....	32
6.2	SAR Positioning .....	42
6.3	GNSS Positioning .....	46
6.4	Tide Gauge Data Analysis .....	49
6.5	GOCE Based Geoid Computation .....	54
6.6	Reference Frames and Joint Standards .....	56
6.7	Height System Unification and Absolute Sea Level.....	59
<b>7</b>	<b>Algorithms Validation and Preliminary Analyses .....</b>	<b>62</b>
7.1	SAR Data Analysis and Value Adding .....	62
7.2	SAR Positioning .....	71
7.3	GNSS Positioning .....	74
7.4	Tide Gauge Data Analysis .....	80
7.5	GOCE based Geoid Computation .....	84
7.6	Reference Frames and Joint Standards .....	90
7.7	Height System Unification and Absolute Sea Level.....	90
<b>8</b>	<b>Data Analyses and Scientific Assessment.....</b>	<b>93</b>
8.1	SAR Data Analysis and Value Adding .....	93
8.2	SAR Positioning .....	98
8.3	GNSS Positioning .....	128
8.4	Tide Gauge Data Analysis .....	134
8.5	GOCE Based Geoid Computation .....	141
8.6	Reference Frames and Joint Standards .....	142
8.7	Height System Unification and Absolute Sea Level.....	144
<b>9</b>	<b>Products and Data Sets .....</b>	<b>149</b>
9.1	SAR Data and Corrections .....	149
9.2	SAR Geometric Positions .....	152
9.3	GNSS Geometric Positions .....	154



**BALTIC+ Theme 5**  
**Geodetic SAR for Baltic Height System  
 Unification and Baltic Sea Level Research**

Final Report  
 Doc. Nr: SAR-HSU-SR-0022  
 Issue: 1.1  
 Date: 07.07.2021  
 Page: 4 of 170

9.4	Tide Gauge Sea Surface Heights.....	154
9.5	GOCE Geoid Heights.....	155
9.6	Unified Heights and Absolute Sea Level .....	155
<b>10</b>	<b>Impact Assessment.....</b>	<b>157</b>
10.1	Electronic Corner Reflectors .....	157
10.2	SAR Data Processing and Positioning.....	160
10.3	GNSS, Tide Gauge and Geoid .....	162
10.4	Data Combination .....	163
10.5	Summary and Outlook.....	164
<b>11</b>	<b>Scientific Roadmap.....</b>	<b>165</b>
11.1	Assessment of Project Results .....	165
11.2	Recommendations for Future Activities .....	167

	<b>BALTIC+ Theme 5</b>	<b>Final Report</b>
	Geodetic SAR for Baltic Height System Unification and Baltic Sea Level Research	Doc. Nr: SAR-HSU-SR-0022
		Issue: 1.1
		Date: 07.07.2021 Page: 5 of 170

# 1 INTRODUCTION

## 1.1 Purpose

The purpose of this final report is to provide a complete description of the project, the obtained results and the conclusions. To a large extent this report is composed by elements from documents generated during the project, but also contains new information, which was the result of the final data processing and the detailed analysis of the obtained results. The list of applicable documents indicates, from which documents information was imported to the final report.

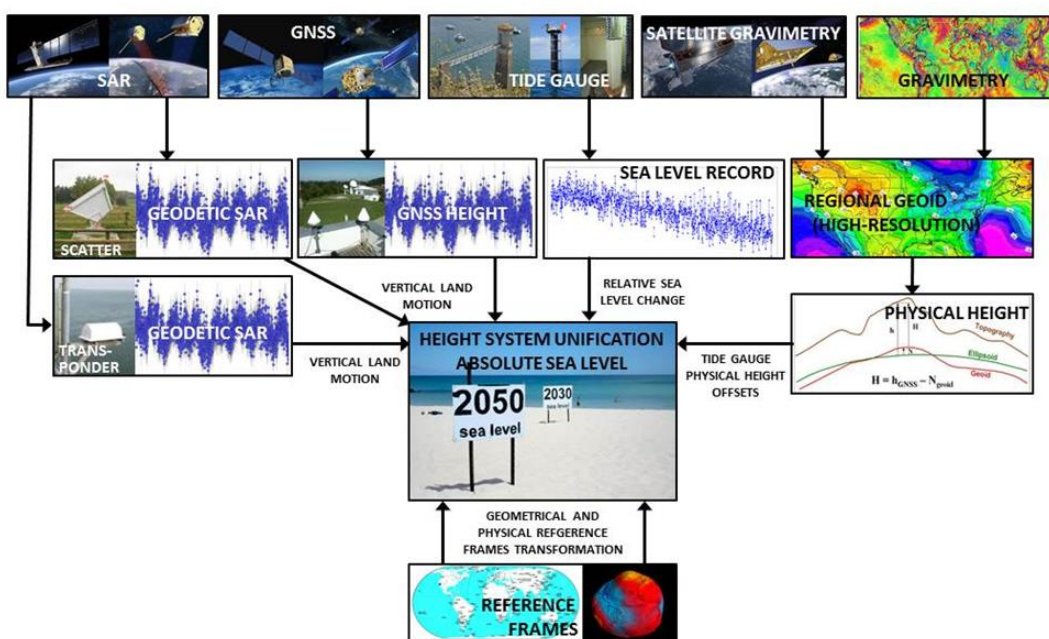
## 1.2 Project Overview

Traditionally, sea level is observed at tide gauge stations, which usually also serve as height reference stations for national levelling networks and therefore define a height system of a country. Thus, sea level research across countries is closely linked to height system unification and needs to be regarded jointly. The project aims to make use of a new observation technique, namely SAR positioning, which can help to connect the GNSS basic network of a country to tide gauge stations and as such to link the sea level records of tide gauge stations to the geometric network. By knowing the geoid heights at the tide gauge stations in a global height reference frame with high precision, one can finally obtain absolute sea level heights of the tide gauge stations in a common reference system and can link them together. By this method, on the one hand national height systems can be connected and on the other hand the absolute sea level at the tide gauge stations can be determined. By analysing time series of absolute sea level heights their changes can be determined in an absolute sense in a global reference frame and the impact of climate change on sea level can be quantified (e.g. by ice sheet and glacier melting, water inflow, global warming).

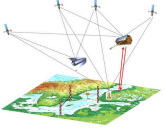
The major scientific challenges to be addressed by this project then can be summarized as follows:

- (1) Connection of the tide gauge markers with the GNSS network geometrically in order to determine the relative vertical motion and to correct the tide gauge readings. For this the new technique of SAR positioning is applied.
- (2) Determination of a GOCE based high resolution geoid at tide gauge stations in order to deliver absolute heights of tide gauges with respect to a global equipotential surface as reference.
- (3) Joint analysis of geometrical and physical reference frames to make them compatible, and to determine corrections to be applied for combined analysis of geometric and physical heights.

In order to provide answers to these challenges the project has been structured accordingly (Figure 1-1). [A detailed overview of the project and its goals is available in Gruber, et-al \(2020\).](#)



**Figure 1-1:** Overview of observations and their combination needed to reach the project goals. The boxes at the top line represent the observations needed to estimate the absolute sea level and its changes at tide gauge locations. All observations need to be processed consistently by applying common standards and reference

	<b>BALTIC+ Theme 5</b>  Geodetic SAR for Baltic Height System Unification and Baltic Sea Level Research	<b>Final Report</b> Doc. Nr: SAR-HSU-SR-0022 Issue: 1.1 Date: 07.07.2021 Page: 6 of 170
---	--	---

frames in order to compute the absolute sea level at tide stations and its changes. Further-on this information then can be used for height system unification between different countries.

### 1.3 Applicable Documents

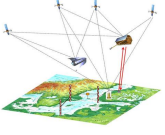
- [AD-1] Requirements Baseline Document, SAR-HSU-RB-0006, Issue 3.0, dated 10.04.2020
- [AD-2] Algorithm Theoretical Basis Document, SAR-HSU-AT-0013, Issue 2.0, dated 12.01.2021
- [AD-3] Product Validation Report, SAR-HSU-PV-0014, Issue 2.0, dated 31.01.2021
- [AD-4] Electronic Corner Reflector Station Description, SAR-HSU-TN-0015, Issue 1.1, dated 07.07.2021
- [AD-5] Dataset User Manual, SAR-HSU-TN-0019, Issue 1.1, dated 07.07.2021
- [AD-6] Impact Assessment Report, SAR-HSU-IA-0020, Issue 1.1, dated 07.07.2021
- [AD-7] Scientific Roadmap, SAR-HSU-SR-0021, Issue 1.1, dated 07.07.2021

### 1.4 Project Publications

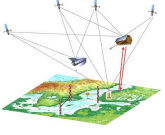
Gruber, T.; Ågren, J.; Angermann, D.; Ellmann, A.; Engfeldt, A.; Gisinger, C.; Jaworski, L.; Marila, S.; Nastula, J.; Nilfouroushan, F.; Oikonomidou, X.; Poutanen, M.; Saari, T.; Schlaak, M.; Świątek, A.; Varbla, S.; Zdunek, R. Geodetic SAR for Height System Unification and Sea Level Research—Observation Concept and Preliminary Results in the Baltic Sea. *Remote Sens.* 2020, 12, 3747. <https://doi.org/10.3390/rs12223747>

### 1.5 References

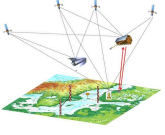
- Abbondanza C., T.M. Chin, R. Gross, M. Heflin, J. Parker, B. Soja, T. van Dam, and X. Wu (2017) JTRF2014, the JPL Kalman filter and smoother realization of the International Terrestrial Reference System. *Journal of Geophysical Research: Solid Earth* 122(8), <https://doi.org/10.1002/2017JB014360>
- Adam N., Rodriguez Gonzalez F., Parizzi A., & Brcic R. (2013): Wide Area Persistent Scatterer Interferometry: Current Developments, Algorithms, and Examples. In proceedings of IEEE IGARSS 2013, July 21-26, Melbourne, Australia, pp. 1857-1860, <https://doi.org/10.1109/IGARSS.2013.6723164>
- Ågren J, Sjöberg LE, Kiamehr R (2009) The new gravimetric quasigeoid model KTH08 over Sweden. *J Appl Geod* 3: 143-153. <https://doi.org/10.1515/JAG.2009.015>
- Ågren, J., G. Strykowski, M. Bilker-Koivula, O. Omang, S. Mårdla, R. Forsberg, A. Ellmann, T. Oja, I. Liepins, E. Parseliunas, J. Kaminskis, L. Sjöberg, and G. Valsson. 2016. The NKG2015 gravimetric geoid model for the Nordic-Baltic region. 1st Joint Commission 2 and IGFS Meeting International Symposium on Gravity, Geoid and Height Systems. Thessaloniki, Greece, 19–23 September. [https://www.isgeoid.polimi.it/Geoid/Europe/NordicCountries/GGHS2016\\_paper\\_143.pdf](https://www.isgeoid.polimi.it/Geoid/Europe/NordicCountries/GGHS2016_paper_143.pdf)
- Altamimi Z., P. Rebischung, L. Metivier, and X. Collilieux (2016) ITRF2014: A new release of the International Terrestrial Reference Frame modeling nonlinear station motions. *Journal of Geophysical Research: Solid Earth* 121(8), pp. 6109–6131, <https://doi.org/10.1002/2016JB013098>
- Altamimi Z. (2018) EUREF Technical Note 1: Relationship and Transformation between the International and the European Terrestrial Reference Systems, Version June 28, 2018, <http://etrs89.ensg.ign.fr/pub/EUREF-TN-1.pdf>
- Angermann D., Gruber T., Gerstl M., Heinkelmann R., Hugentobler U., Sánchez L., Steigenberger P. (2016): GGOS Bureau of Products and Standards: Inventory of standards and conventions used for the generation of IAG products. In: Drewes H., Kuglitsch F., Adám J. (Eds.) *The Geodesist's Handbook 2016*. *Journal of Geodesy*, 90(10), 1095-1156, <http://doi.org/10.1007/s00190-016-0948-z>
- Angermann D., Gruber T., Gerstl M., Heinkelmann R., Hugentobler U., Sánchez L., Steigenberger P. (2020): GGOS Bureau of Products and Standards: Inventory of standards and conventions used for the generation of IAG products. In: Poutanen, M., Rózsa, S. *The Geodesist's Handbook 2020*. *J Geod* 94, 109, <https://doi.org/10.1007/s00190-020-01434-z>
- Balss, U., Cong, X. Y., Brcic, R., Rexer, M., Minet, C., Breit, H., Eineder, M., Fritz, T. (2012): High precision measurement on the absolute localization accuracy of TerraSAR-X. *Proceedings of IGARSS'12 Conference*, July 22–27, Munich, Germany, pp. 1625–1628. <https://doi.org/10.1109/IGARSS.2012.6351217>
- Balss U., Gisinger C., & Eineder M. (2018a): Measurements on the Absolute 2-D and 3-D Localization Accuracy of TerraSAR-X. *MDPI Remote Sensing*, 10(656), 1–21. <http://doi.org/10.3390/rs10040656>
- Balss, U., Gisinger, C., Eineder, M., Breit, H., Schubert, A., Small, D. (2018b): Survey Protocol for Geometric SAR Sensor Analysis. CEOS Cal/Val Technical Note, DLR-FRM4SAR-TN-200, Issue 1.4, 26.04.2018. Online: <http://calvalportal.ceos.org/calibration-methods-guidelines>

	<p style="text-align: center;">BALTIC+ Theme 5</p> <p style="text-align: center;">Geodetic SAR for Baltic Height System Unification and Baltic Sea Level Research</p>	<p style="text-align: right;">Final Report</p> <p>Doc. Nr: SAR-HSU-SR-0022 Issue: 1.1 Date: 07.07.2021 Page: 7 of 170</p>
---	---	---

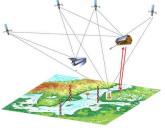
- Barthelmes F (2013) Definition of Functionals of the Geopotential and Their Calculation from Spherical Harmonic Models. Theory and formulas used by the calculation service of the International Centre for Global Earth Models (ICGEM). Scientific Technical Report STR09/02. Revised Edition, January 2013. <http://icgem.gfz-potsdam.de>
- BGR (2021): Bodenbewegungsdienst Deutschland (BBD). (2021): Online Service of the Bundesanstalt für Geowissenschaften und Rohstoffe: <https://bodenbewegungsdienst.bgr.de/>
- Bloßfeld, M., Seitz, M., Angermann, D. (2014) Non-linear station motions in epoch and multi-year reference frames. Journal of Geodesy 88(1), Springer, <https://doi.org/10.1007/s00190-013-0668-6>
- Bloßfeld M., Müller H., Gerstl M., Stefka V., Bouman J., Göttl F., Horwath M. (2015): Second-degree Stokes coefficients from multi-satellite SLR. Journal of Geodesy 89(9): 857-871, <https://doi.org/10.1007/s00190-015-0819-z>
- Boucher C. and Z. Altamimi (2011) Memo: Specifications for reference frame fixing in the analysis of a EUREF GPS campaign, <http://etrs89.ensg.ign.fr/memo-V8.pdf>
- Bourbigot M., Johnsen H., & Piantanida R. (2015): Sentinel-1 Product Definition. Technical note by Sentinel-1 Mission Performance Center (MPC), Doc. S1-RS-MDA-52-7440, Iss. 2, Rev. 6, Date 22.07.2015. Online: [https://sentinels.copernicus.eu/web/sentinel/user-guides/sentinel-1-sar/document-library/-/asset\\_publisher/1dO7RF5fJMbd/content/sentinel-1-product-definition](https://sentinels.copernicus.eu/web/sentinel/user-guides/sentinel-1-sar/document-library/-/asset_publisher/1dO7RF5fJMbd/content/sentinel-1-product-definition)
- Böhm, J., and Schuh, H. (Eds.) (2013): Atmospheric Effects in Space Geodesy. Springer-Verlag Berlin Heidelberg, 2013. <https://doi.org/10.1007/978-3-642-36932-2>
- Cartwright, D. E., and J. Crease. 1963. A comparison of the geodetic reference levels of England and France by mean of the sea surface. Proceedings of the Royal Society of London. Series A, Mathematical and Physical Sciences 273(1355):554–580.
- CSC Mission Management Team (2018): Sentinel-1 High Level Operations Plan (HLOP). Technical note Copernicus Space Component (CSC) Mission Management, Doc. COPE-S1OP-EOPG-PL-15-0020, Iss. 2, Rev. 2, Date 29.03.2018. Online: [https://sentinels.copernicus.eu/web/sentinel/user-guides/sentinel-1-sar/document-library/-/asset\\_publisher/1dO7RF5fJMbd/content/sentinel-high-level-operations-plan](https://sentinels.copernicus.eu/web/sentinel/user-guides/sentinel-1-sar/document-library/-/asset_publisher/1dO7RF5fJMbd/content/sentinel-high-level-operations-plan)
- Cumming, I. G., and Wong, F. H. (2005): Digital Processing of Synthetic Aperture Radar Data. Artech House.
- Dach, R., S. Lutz, P. Walser, P. Fridez (Eds); 2015: Bernese GNSS Software Version 5.2. User manual, Astronomical Institute, University of Bern, Bern Open Publishing. <https://doi.org/10.7892/boris.72297> ; ISBN: 978-3-906813-05-9
- Di Meo, P., Pausini, M., Carnevale, G. (2019): ECR-C User Manual. Technical Note by MetaSensing BV, MS-ECR-C-USER-MANUAL, Issue 1.6, 15.09.2019.
- Doyon, M., J. Smyth, G. Kroupnik, C Carrié, M. Sauvageau, J.F. Lévesque, F. Babiker, V. Abbasi, C. Giguère, J. Bergeron, S. Côté (2018): RADARSAT CONSTELLATION MISSION: Toward launch and operations. Proceedings of SpaceOps Conferences, 28 May - 1 June 2018, Marseille, France. <https://doi.org/10.2514/6.2018-2605>
- Drewes H., F. Kuglitsch, J. Adam, and S. Rozsa (2016) The Geodesist's Handbook 2016. In: vol. 90. 10, pp. 981–982. <https://doi.org/10.1007/s00190-016-0948-z>
- Ekman M (1989) Impacts of geodynamic phenomena on systems for height and gravity. Bull. Géod. 63: pp. 281-296
- Forsberg R., (1984). A study of terrain reductions, density anomalies and geophysical inversion methods in gravity field modelling. Report 355, Depart. Geodetic Science Surveying, Ohio State University, Columbus
- Forsberg, R., Tscherning, C.C. (2008) An Overview Manual for the GRAVSOFTE Geodetic Gravity Field Modelling Programs. 2nd ed. Available at [https://www.academia.edu/9206363/An\\_overview\\_manual\\_for\\_the\\_GRAVSOFTE\\_Geodetic\\_Gravity\\_Field\\_Modelling\\_Programs](https://www.academia.edu/9206363/An_overview_manual_for_the_GRAVSOFTE_Geodetic_Gravity_Field_Modelling_Programs)
- Gisinger, C., Balss, U., Pail, R., Zhu, X. X., Montazeri, S., Gernhardt, S., & Eineder, M. (2015). Precise Three-Dimensional Stereo Localization of Corner Reflectors and Persistent Scatterers With TerraSAR-X. IEEE Transactions on Geoscience and Remote Sensing, 53(4), 1782–1802. <https://doi.org/10.1109/tgrs.2014.2348859>
- Gisinger, Christoph; Willberg, Martin; Balss, Ulrich; Klügel, Thomas; Mähler, Svetlana; Pail, Roland; Eineder, Michael (2017): Differential geodetic stereo SAR with TerraSAR-X by exploiting small multi-directional radar reflectors. In Journal of Geodesy 91 (1), pp. 53–67. <https://doi.org/10.1007/s00190-016-0937-2>
- Gisinger, C., Suchandt, S., Breit, H., Balss, U., Lachaise, M., Fritz, T., Eineder, M., Miranda, N (2019) Towards Operational SAR Imaging Geodesy: An Extended Time Annotation Dataset for Sentinel-1 Image Products. Very High-resolution Radar & Optical Data Assessment workshop, 18.-22. Nov. 2019, Frascati, Italy.

	<b>BALTIC+ Theme 5</b>  Geodetic SAR for Baltic Height System Unification and Baltic Sea Level Research	<b>Final Report</b> Doc. Nr: SAR-HSU-SR-0022 Issue: 1.1 Date: 07.07.2021 Page: 8 of 170
---	--	---

- Gisinger, C., Balss, U., & Eineder, M. (2020a) DLR Geometric Calibration Targets: Status Update and Ongoing Research. CEOS Working Group Cal/Val Workshop 2020, 06.-08. Okt. 2020.
- Gisinger, C., Eineder, M., Brcic, R., Balss, U., Gruber, T., Oikonomidou, X. & Heinze, M. (2020b) First Experiences with Active C-Band Radar Reflectors and SENTINEL-1. IEEE IGARSS 2020, 26. Sept. - 02. Okt. 2020, Virtual Symposium. <https://doi.org/10.1109/IGARSS39084.2020.9324381>
- Gisinger, C., Schubert, A., Breit, H., Garthwaite, M., Balss, U., Willberg, M., Small, D., Eineder, M., Miranda, N. (2021): In-Depth Verification of Sentinel-1 and TerraSAR-X Geolocation Accuracy using the Australian Corner Reflector Array. IEEE Transactions on Geoscience and Remote Sensing, vol. 59, no. 2, pp. 1154-1181. <https://doi.org/10.1109/TGRS.2019.2961248>
- Gruber T, Oikonomidou X., Bruinsma S., Visser P., Mulet S. (2019): Release 6 GOCE Gravity Field Models Validation Report; GOCE High Level Processing Facility Technical Note No. GO-TN-HPF-GS-0337, Issue 1.0, 30.6.2019, <https://earth.esa.int/eogateway/documents/20142/37627/Release-6-gravity-model-validation-report-GO-TN-HPF-GS-0337-1.0.pdf>
- Häkli, P., Lidberg M, Jivall L., Nørbech T., Tangen O., Weber M., Pihlak P., Aleksejenko I., Parseliunas E. (2016). The NKG2008 GPS campaign—final transformation results and a new common Nordic reference frame. Journal of Geodetic Science 6:1–33. <https://doi.org/10.1515/jogs-2016-0001>
- Heiskanen W A., Moritz H (1967) Physical Geodesy. San Francisco. W. H. Freeman and Company.
- Hernández-Pajares M., Juan J. M., Sanz J., Orus R., Garcia-Rigo A., Feltens J., Komjathy A., Schaer S. C., and Krankowski A. (2009): The IGS VTEC maps: a reliable source of ionospheric information since 1998. Journal of Geodesy, vol. 83, no. 3-4, p. 263. <http://doi.org/10.1007/s00190-008-0266-1>
- Hólm E., Forbes R., Lang S., Magnusson L., and Malardel S. (2016): New model cycle brings higher resolution. ECMWF Newsletter, No. 147, ECMWF, Reading, United Kingdom, pp. 14–19. Online: <http://www.ecmwf.int/sites/default/files/elibrary/2016/16299-newsletter-no147-spring-2016.pdf>
- Kouba, J. (2008): Implementation and testing of the gridded Vienna Mapping Function 1 (VMF1). Journal of Geodesy, Vol. 82:193-205. <https://doi.org/10.1007/s00190-007-0170-0>
- Kvas, A., Behzadpour, S., Ellmer, M., Klinger, B., Strasser, S., Zehentner, N., & Mayer-Gürr, T. (2019). ITSG-Grace2018: Overview and evaluation of a new GRACE-only gravity field time series. Journal of Geophysical Research: Solid Earth, 124. <https://doi.org/10.1029/2019JB017415>
- Landskron, D., and Böhm, J. (2018a): VMF3/GPT3: Refined Discrete and Empirical Troposphere Mapping Functions. Journal of Geodesy, vol. 92, pp. 349-360. <https://doi.org/10.1007/s00190-017-1066-2>
- Landskron, D, and Böhm J. (2018b): Refined discrete and empirical horizontal gradients in VLBI analysis, Journal of Geodesy, vol. 92, pp. 1387-1399. <https://doi.org/10.1007/s00190-018-1127-1>
- Leberl, Franz W. (1990): Radargrammetric image processing. Artech House.
- Liibus, A. Ellmann, A., Kõuts, T., Jürgenson, H. (2013). Precise hydrodynamic levelling by using pressure gauges. Marine Geodesy, 36, 138-163.
- Lyszkowicz, A., Nastula, J., Zielinski, J.B., Birylo, M., (2021). A New Model of quasigeoid for the Baltic Sea area, Remote Sens. 2021, 13, 2580. <https://doi.org/10.3390/rs13132580>
- Mäkinen, J. (2008): The treatment of permanent tide in EUREF products. Paper presented at the Symposium of the IAG Sub-commission for Europe (EUREF) in Brussels, June 17-21, 2008. Submitted to the proceedings
- Märdla S, Ågren J, Strykowski G, Oja T, Ellmann A, Forsberg R, Bilker-Koivula M, Omang O, Paršeliūnas E, Liepiņš I, Kaminskis J (2017) From Discrete Gravity Survey Data to a High-resolution Gravity Field Representation in the Nordic-Baltic Region, Marine Geodesy, 40:6, 416-453, <http://doi.org/10.1080/01490419.2017.1326428>
- Mahapatra, P., van der Marel H., van Leijen F.J., Samiei-Esfahany S., Klees R., Hanssen R.F. (2017): Insar datum connection using GNSS-augmented radar transponders. J Geod 92, 21–32 (2018). <https://doi.org/10.1007/s00190-017-1041-y>
- Mayer-Gürr, Torsten; Behzadpur, Saniya; Ellmer, Matthias; Kvas, Andreas; Klinger, Beate; Strasser, Sebastian; Zehentner, Norbert (2018): ITSG-Grace2018 - Monthly, Daily and Static Gravity Field Solutions from GRACE. GFZ Data Services. <http://doi.org/10.5880/ICGEM.2018.003>
- Mikhail, E. M.; Ackermann, F. (1976): Observations and Least: Squares.
- Miranda N. and Meadows, P.J. (2015): Radiometric Calibration of S-1 Level-1 Products Generated by the S-1 IPF. ESA Technical Note, ESA-EOPG-CSCOP-TN-0002, Iss. 1, Rev. 0, Date 21.05.2015. <https://sentinel.esa.int/documents/247904/685163/S1-Radiometric-Calibration-V1.0.pdf>

	<b>BALTIC+ Theme 5</b>  Geodetic SAR for Baltic Height System Unification and Baltic Sea Level Research	<b>Final Report</b> Doc. Nr: SAR-HSU-SR-0022 Issue: 1.1 Date: 07.07.2021 Page: 9 of 170
---	--	---

- Miranda, N. (2015): TOPS Sentinel-1 SLC deramping function for products generated by the S-1 IPF. Sentinel-1 Technical Note COPE-GSEG-EOPG-TN-14-0025, Iss. 1, Rev. 2, 20.04.2015, [https://earth.esa.int/documents/247904/1653442/Sentinel-1-TOPS-SLC\\_Deramping](https://earth.esa.int/documents/247904/1653442/Sentinel-1-TOPS-SLC_Deramping)
- Moritz H (1980) Advanced physical geodesy. Wichmann, Karlsruhe.
- Moritz H. (2000) Geodetic Reference System 1980, Journal of Geodesy 74(1), pp. 128–162, <https://doi.org/10.1007/s001900050278>
- Niell, A.E. (1996): Global mapping functions for the atmosphere delay at 310 radio wavelengths. J. Geophysical Research, vol. 101, pp. 3227–3246.
- Pavlis N., Simon A. Holmes, S. C. Kenyon, and J. K. Factor (2012) The development and evaluation of the Earth Gravitational Model 2008 (EGM2008), Journal of Geophysical Research 117 B04406. <https://doi.org/10.1029/2011JB008916>
- Peter, H., Jäggi, A., Fernández, J., Escobar, D., Ayuga, F., Arnold, D., Wermuth, M., Hackel, S., Otten, M., Simons, W., Visser, P., Hugentobler, U., and Féménias, P. (2017): Sentinel-1A - First precise orbit determination results. Advances in Space Research, vol. 60, no. 5, pp. 879–892. <http://doi.org/10.1016/j.asr.2017.05.034>
- Petit G. and Luzum B. (Eds) (2010): IERS Conventions (2010). Verlag des Bundesamts für Kartographie und Geodäsie, Online: <http://tai.bipm.org/iers/conv2010/conv2010.html>.
- Piantanida, R., Recchia, A., Niccolò, F., Valentino, A., Miranda, N., Schubert, A., Small, D. (2018): Accurate Geometric Calibration of Sentinel-1 Data. Proceedings of EUSAR 2018, pp. 63 – 68.
- Santamaría Álvaro, M. Gravelle, X. Collilieux, M. Guichard, B. Martín Míguez, P. Tiphaneau, G. Wöppelmann (2012), Mitigating the effects of vertical land motion in tide gauge records using a state-of-the-art GPS velocity field, Global and Planetary Change, vol. 98-99, page 6-7, <http://doi.org/10.1016/j.gloplacha.2012.07.007>
- Schaer, S. (1999): Mapping and Predicting the Earth's Ionosphere Using the Global Positioning System. Geodätisch-geophysikalische Arbeiten in der Schweiz, vol. 59
- Schaer, S., Gurtner, W., Feltens, J. (1998): IONEX: The IONosphere Map Exchange Format Version 1, Proc. IGS Analysis Center Workshop, Darmstadt, Germany, Feb. 9-11. Online: <ftp.aiub.unibe.ch/ionex/ionex1.pdf>
- Schubert A., Miranda N., Geudtner D., & Small D. (2017): Sentinel-1A/B Combined Product Geolocation Accuracy. MDPI Remote Sensing, vol. 9, no. 607, pp. 1-16. <http://doi.org/10.3390/rs9060607>
- Schubert A., Small D., Gisinger C., Balss U., & Eineder M. (2018): Corner Reflector Deployment for SAR Geometric Calibration and Performance Assessment. CEOS Cal/Val Calibration Method Guidelines, technical note, Issue 1.03, Online: <http://calvalportal.ceos.org/calibration-methods-guidelines>
- Seitz M., M. Bloßfeld, D. Angermann, R. Schmid, M. Gerstl, and F. Seitz (2016), The new DGFI-TUM realization of the ITRS: DTRF2014 (data), In: Deutsches Geodätisches Forschungsinstitut. <http://doi.pangaea.de/10.1594/PANGAEA.864046>
- Seitz M., M. Bloßfeld, D. Angermann, M. Gerstl, and F. Seitz (2020) DTRF2014 The first secular ITRS realization considering non-tidal station loading. <http://doi.pangaea.de/10.1594/PANGAEA.864046>
- Sjöberg L E (1991) Refined least squares modification of Stokes' formula. Manuscripta Geodetica 16:367–375.
- Sjöberg LE, Bagherbandi M (2017) Gravity Inversion and Integration - Theory and Applications in Geodesy and Geophysics. Springer, Cham. <https://doi.org/10.1007/978-3-319-50298-4>.
- Solari, L., Crosetto, M., Balasis-Levinsen, J., Casagli, N., Frei, M., Moldestad, D. A., and Oyen, A (2020): The European Ground Motion Service: a continental scale map of ground deformation., EGU General Assembly 2020, Online, 4–8 May 2020, EGU2020-3148, <https://doi.org/10.5194/egusphere-egu2020-3148>
- Standish, E.M.: 1990, "The Observational Basis for JPL's DE200, the planetary ephemeris of the Astronomical Almanac", Astronomy & Astrophysics, vol. 233, pp. 252-271.
- Stein, S. (1981): Algorithms for Ambiguity Function Processing. IEEE Transactions on Acoustics, Speech, and Signal Processing, vol. ASPP-29, no. 3, pp. 588–599.
- Torge, W. 2001. Geodesy. 3rd Edition. Berlin-New York: Walter de Gruyter
- Tscherning CC, Rapp RH (1974): Closed covariance expressions for gravity anomalies, geoid undulations, and deflections of the vertical implied by anomaly degree variance models. Rep 355, Dept Geod Sci, Ohio State Univ, Columbus
- Tscherning C.C. (2013) Geoid Determination by 3D Least-Squares Collocation. In: Sansò F., Sideris M. (eds) Geoid Determination. Lecture Notes in Earth System Sciences, vol 110. Springer, Berlin, Heidelberg
- Willberg M, Zingerle P, Pail R (2019) Residual least-squares collocation: use of covariance matrices from high-resolution global geopotential models. J Geod (2019). <https://doi.org/10.1007/s00190-019-01279-1>

	<b>BALTIC+ Theme 5</b>  Geodetic SAR for Baltic Height System Unification and Baltic Sea Level Research	<b>Final Report</b> Doc. Nr: SAR-HSU-SR-0022 Issue: 1.1 Date: 07.07.2021 Page: 10 of 170
---	--	--

Vestøl O, Ågren J, Steffen H, Kierulf H, Tarasov L (2019) NKG2016LU - A new land uplift model for Fennoscandia and the Baltic Region. *J Geod* (2019). <https://doi.org/10.1007/s00190-019-01280-8>.

Villiger A. and Dach R., Eds. (2018): International GNSS Service Technical Report 2017. Astronomical Institute University of Bern. Online: [ftp://igs.org/pub/resource/pubs/2017\\_techreport.pdf](ftp://igs.org/pub/resource/pubs/2017_techreport.pdf)

Villiger, A., Dach, R., Eds. (2019): International GNSS Service Technical Report 2018. Astronomical Institute University of Bern, 2019. Online: <https://kb.igs.org/hc/en-us/articles/360030898551-Technical-Report-2018>

Wang YM, Sánchez L, Ågren J, Huang J, Forsberg R, Abd-Elmotaal HA, Barzaghi R, Bašić T, Carrion D, Claessens S, Erol B, Erol S, Filmer M, Grigoriadis VN, Isik MS, Jiang T, Koç Ö, Li X, Ahlgren K, Krčmaric J, Liu Q, Matsuo K, Natsiopoulou DA, Novák P, Pail R, Pitonák M, Schmidt M, Varga M, Vergos GS, Véronneau M, Willberg M, Zingerle P.; Colorado geoid computation experiment—overview and summary. (2021), submitted to *Journal of Geodesy*, under review, Special Issue on Reference Systems in Physical Geodesy

Willberg M, Zingerle P, Pail R (2019) Residual least-squares collocation: use of covariance matrices from high-resolution global geopotential models. *J Geod* (2019). <https://doi.org/10.1007/s00190-019-01279-1>

Wöppelmann, G., B. M. Miguez, M. N. Bouin, and Z. Altamimi (2007), Geocentric sea-level trend estimates from GPS analyses at relevant tide gauges world-wide, *Global Planet. Change*, 57(3-4), 396–406, <https://doi.org/10.1016/j.gloplacha.2007.02.002>

Wöppelmann, G., M. Marcos, A. Santamaría-Gómez, B. Martín-Míguez, M.-N. Bouin, and M. Gravelle (2014), Evidence for a differential sea level rise between hemispheres over the twentieth century, *Geophys. Res. Lett.*, 41, 1639–1643, <https://doi.org/10.1002/2013GL059039>

Wong L and Gore R (1969) Accuracy of geoid heights from modified Stokes kernels, *Geophysical Journal of the Royal Astronomical Society* 18, 81–91.

Woodworth, P. L., and R. Player (2003), The permanent service for mean sea level: An update to the 21st century, *J. Coastal Res.*, 19(2), 287–295. [https://www.jstor.org/stable/4299170?seq=1#metadata\\_info\\_tab\\_contents](https://www.jstor.org/stable/4299170?seq=1#metadata_info_tab_contents)

## 1.6 Additional Literature

Altamimi Z.: (2017) EUREF Technical Note 1: Relationship and Transformation between the International and the European Terrestrial Reference Systems - Institut National de l'Information Géographique et Forestière (IGN), France, June 2017. <http://etrs89.ensg.ign.fr/pub/EUREF-TN-1.pdf>

Bokun, J. (1961). Zagadnienie wyznaczenia odstępów geoidy w Polsce od elipsoidy Krasowskiego biorąc pod uwagę posiadane materiały astronomiczno-geodezyjne i grawimetryczne. *Prace Instytutu Geodezji i Kartografii*, 1(17), 113–131.

Bruyninx C., A. Araszkiwicz, E. Brockmann, A. Kenyeres, J. Legrand, T. Liwosz, P. Mitterschiffthaler, R. Pacione, W. Söhne, C. Völkens: 'EUREF Permanent Network Technical Report 2017 - International GNSS Service 2017 Technical Report, A. Villiger and R. Dach (eds), IGS Central Bureau and University of Bern; Bern Open Publishing, pp. 105–115; DOI: 10.7892/boris.116377, June 2018. [https://files.igs.org/pub/resource/pubs/2017\\_techreport.pdf](https://files.igs.org/pub/resource/pubs/2017_techreport.pdf)

Capes, R., Marsh, S., Eds. (2009): The TerraFirma Atlas –Terrain-Motion Across Europe. Compendium of results produced by the ESA GMES Service Element project TerraFirma, ESRIN Contract 19366/05/I-EC, 2009. Online: <http://esamultimedia.esa.int/multimedia/publications/TerraFirmaAtlas/>

Chowańska-Otyś, D. (1974). Morskie pomiary grawimetryczne wykonane w obszarze zdjęcia półszczygółowego w 1972 roku.

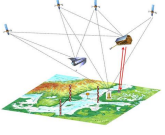
Dahle C, Flechtner F, Murböck M, Michalak G, Neumayer K H, Abrykosov O.; Reinhold A, König R (2019) GRACE-FO Geopotential GSM Coefficients GFZ RLO6. V. 6.o. GFZ Data Services. [https://doi.org/10.5880/GFZ.GRACEFO\\_o6\\_GSM](https://doi.org/10.5880/GFZ.GRACEFO_o6_GSM)

Ellmann, A. (2004). The geoid for the Baltic countries determined by the least-squares modification of Stokes' formula. In *Geoid* (Issue 1061).

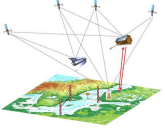
EUREF (2008) 'The EUREF Densification of the ITRF2005', IAG Sub-commission for the European Reference Frame (EUREF), November 27, 2008. <http://www.epncb.oma.be/documentation/publications/technicalreports/EUREFDensificationITRF2005.pdf>

European Environment Agency (2020): European Ground Motion Service: Service Implementation Plan and Product Specification Document, Version 1.01, 28/01/2020, 2020. Online: <https://land.copernicus.eu/user-corner/technical-library/egms-specification-and-implementation-plan>

Forsberg R., S. D. (2000). Geoid of the Nordic/Baltic region from surface/airborne gravimetry and GPS draping.

	<b>BALTIC+ Theme 5</b>  Geodetic SAR for Baltic Height System Unification and Baltic Sea Level Research	<b>Final Report</b> Doc. Nr: SAR-HSU-SR-0022 Issue: 1.1 Date: 07.07.2021 Page: 11 of 170
---	--	--

- Fritz T., and Eineder M. (2013): TerraSAR-X Ground Segment Basic Product Specification Document. DLR Technical Note, Doc. TX-GS-DD-3302, Iss. 1.9, Date 09.10.2013. Online: <https://sss.terrasar-x.dlr.de/docs/TX-GS-DD-3302.pdf>
- Hackel, S., Gisinger, C., Balss, U., Wermuth, M., and Montenbruck, O. (2018): Long-Term Validation of TerraSAR-X and TanDEM-X Orbit Solutions with Laser and Radar Measurements. *Remote Sens.*, vol. 10, pp. 1–20. <https://doi.org/10.3390/rs10050762>
- Hofmann-Wellenhof, B, H. Lichtenegger, E. Wasle - 'GNSS—Global Navigation Satellite Systems GPS, GLONASS, Galileo, and more', Springer Wien New York, 2007, ISBN 978-3-211-73012-6
- Jarmołowski W. (2006). Wyznaczenie przebiegu geoidy na obszarze południowego Morza Bałtyckiego z morskich i lotniczych obserwacji grawimetrycznych oraz altimetrii satelitarnej. Praca Doktorska, UWM Olsztyn, 1–122.
- Kuczynska-Siehien, J., Łyszkowicz, A., & Sideris, M. G. (2019). Evaluation of Altimetry Data in the Baltic Sea Region for Computation of New Quasigeoid Models over Poland. *International Association of Geodesy Symposia*, 149, 51–60. [https://doi.org/10.1007/1345\\_2018\\_35](https://doi.org/10.1007/1345_2018_35)
- Łyszkowicz, A. (2010). Refined astrogravimetric geoid in Poland – Part I. *Geomatics and Environmental Engineering*, 4(1), 57–67.
- Oikonomidou, X., Eineder, M., Gisinger, C., Gruber, T., Heinze, & M., Sdralia, V. (2020) SAR Imaging Geodesy with Electronic Corner Reflectors (ECR) and Sentinel-1 - First Experiences. EGU General Assembly 2020, 4.–8. Mai 2020, Vienna, Austria. Doi: 10.5194/egusphere-egu2020-5608.
- Schwarz, K. P., Sideris, M. G., & Forsberg, R. (1990). The use of FFT techniques in physical geodesy. In *Geophysical Journal International* (Vol. 100, Issue 3, pp. 485–514).
- Tanni L. (1949). The regional rise of the geoid in Central Europe. *Ann. Acad. Sci. Fenn. Series A*, 3(20).
- Vestøl, O., Ågren, J., Steffen, H., Kierulf, H., & ... (2016). NKG2016LU, an improved postglacial land uplift model over the Nordic-Baltic region. ... Working Group of Geoid ....
- Wichiencharoen Ch. (1982). The Indirect Effects on the Computation of Geoid Undulations. Ohio State University, Department of Geodetic Science and Surveying, Report No. 336.

	<b>BALTIC+ Theme 5</b>  Geodetic SAR for Baltic Height System Unification and Baltic Sea Level Research	<b>Final Report</b> Doc. Nr: SAR-HSU-SR-0022 Issue: 1.1 Date: 07.07.2021 Page: 12 of 170
---	--	--

## 2 SUMMARY

### 2.1 Scientific Challenges, Data Base and Network Design

The overall goal of the project is to establish an integrated observing system to monitor sea level change in an absolute sense and to enable height system unification across countries. For this purpose, various types of observations need to be combined consistently. In particular, these are the geometric heights and the geoid height of tide gauge stations and the tide gauge readings. Consistency means that reference frames and processing standards need to be identical for all components, which is crucial as the geometric network intrinsically is defined by a set of reference station coordinates (centre of figure), while gravimetric quantities as the geoid per definition are defined in a physical reference frame defined by the mass distribution of the Earth (centre of figure). As the Earth is a dynamic system the reference frames are not fixed, but undergo temporal variations. This usually is fixed by defining a reference system epoch and by applying transformations between the different frames.

One of the critical issues is vertical land motion, or more general vertical station movements. For this purpose, optimally, a permanent geodetic accuracy GNSS receiver needs to be collocated next to the tide gauge station in order to observe such vertical movements. The number of tide gauge stations collocated with a permanent GNSS station is very limited and by far is not sufficient to monitor vertical station movements at the coast on a systematic basis. Alternatively, regular local surveys to the closest permanent GNSS stations (high effort and costly) or geophysical models (high uncertainty) can be used for this purpose. Therefore, in this study the technique of geodetic SAR positioning is used. Active electronic corner reflectors are installed close to the tide gauge stations and nearby permanent GNSS stations in order to monitor the geometric heights.

Using tide gauge readings and geometric heights determined either by GNSS or SAR positioning still is not sufficient to enable comparisons of sea level from different stations in an absolute sense. This is only possible if one knows the vertical offsets of each tide gauge station from a global high resolution equipotential surface. With the results of the GOCE mission a highly precise global geoid with centimetre accuracy and a spatial resolution of 80–100 km is available. In order to refine the global geoid a local geoid modelling for each tide gauge station is required, which optimally combines the global GOCE gravity field model with local terrestrial gravity observations.

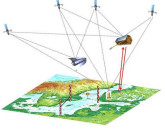
In summary, three major scientific challenges are addressed by the study in order to enable height system unification or absolute sea level computation from tide gauge observations. These are:

- (1) Connecting the tide gauge markers with the GNSS network geometrically in order to determine the relative vertical motion and to correct the tide gauge readings.
- (2) Determine a GOCE based high resolution geoid height at tide gauge stations in order to deliver absolute heights of tide gauges with respect to a global equipotential surface as reference.
- (3) Joint analysis of geometrical and physical reference frames to make them compatible and to determine corrections to be applied for combined analysis of geometric and physical heights.

The main focus is given to the connection of the tide gauge reference marker with the geometric GNSS network applying the geodetic SAR positioning technique. With flexible and compact active transponders, it offers a relatively cheap and simple possibility to connect all tide gauges for an ocean area to the global geometric network. In order to investigate the feasibility of using active SAR transponders for geometric positioning and to use these observations for height system unification and absolute sea level determination, some tide gauge stations in the Baltic Sea area located in different countries are selected as test cases.

For geodetic SAR positioning SAR images captured by the Sentinel-1 mission are used. Both spacecraft, Sentinel-1A and Sentinel-1B, regularly capture the Baltic Sea area and offer unrestricted access to all the data acquired at our study region. Level 1 SLC products, which contain the focused but otherwise unmodified Sentinel-1 SAR data are the main input for the study. Over land areas, Sentinel-1 mainly uses the Interferometric Wide Swath (IW) SAR mode, that covers a swath-width of approximately 250 km on ground. This yields a coverage of each test sites by at least two ascending and two descending pass geometries per site. With a repeat cycle of 6 days, the number of Sentinel-1 SAR observations per test site amounts to some 180 measurements for one year.

For connecting the tide gauge stations to the GNSS network via the SAR targets, a GNSS network covering the study area needs to be defined. After definition of the experiments the reference stations for the double difference method are selected, based on the criteria for optimizing the geometry of the GNSS station network, observation quality, station stability over time, quality of coordinate determination and station velocity vectors, as well as free access for the data. For a few cases, separate agreements with the station/data owners need to be done. Tide gauge readings are acquired from the national authorities operating the tide gauges in each participating country. The project establishes agreements with these authorities and has full access to the pre-processed tide gauge data time series (usually as hourly values). For geoid modelling the fundamental global model is available from the International Centre of Global Earth Gravity Models (ICGEM). For the study the GOCO06S model combining all reprocessed GRACE and GOCE data is used. Local gravity data around the Baltic Sea have for a long time been collected by the Nordic and Baltic countries within the Nordic Geodetic Commission (NKG). A cleaned database including latest gravity datasets observed by different institutions formed is used for the local geoid modelling.

	<b>BALTIC+ Theme 5</b>  Geodetic SAR for Baltic Height System Unification and Baltic Sea Level Research	<b>Final Report</b> Doc. Nr: SAR-HSU-SR-0022 Issue: 1.1 Date: 07.07.2021 Page: 13 of 170
---	--	--

For the Baltic Sea test network, the SAR transponders are installed as close as possible to the tide gauge and, depending on the experiment, to the nearby permanent GNSS station as well. From the perspective of the SAR, the installation sites are selected considering the surroundings of the site. Obstacles above 20° elevation shall be avoided, as well as bright background or spurious signals arising from nearby structures like buildings. Based on the defined test cases, the following installation sites are selected. Collocation sites with local ties of SAR transponder to permanent GNSS station and tide gauge (Władysławowo and Łeba in Poland and Spikarna/Vinberget in Sweden). Tide gauge sites with local ties of SAR transponder to tide gauge (Emäsalo and Rauma in Finland, Loksa in Estonia and Forsmark/Kobben in Sweden). Permanent GNSS network sites with local tie of SAR transponder to permanent GNSS stations (Vergi in Estonia, Mårtsbo, in Sweden and Loviisa in Finland). Transponder calibration site with local ties to permanent GNSS stations and passive corner reflectors (two stations in Oberpfaffenofen, Germany). All together 12 active SAR transponders have been purchased by the project team and are installed at the indicated sites.

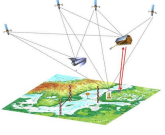
## 2.2 Basic Algorithms

The SAR data analysis algorithms involve accurate extraction of all SAR transponder locations from the acquired Sentinel-1 level 1 single-look complex (SLC) images as well as preparation of dedicated corrections. These corrections comprise the Sentinel-1 systematic effects not accounted for during SAR image generation, the atmospheric path delays, and the solid Earth deformation signals. Moreover, systematic effects of the SAR transponders need to be calibrated (internal signal delay, eccentricity of antennas). The applied computation methods require as data input the SLC Sentinel-1 SAR images, the Sentinel-1 precise orbit solution, the global total electron content (TEC) maps based on GNSS, and the global gridded data for the Vienna mapping function (VMF) model. The analysis system uses approximate coordinates of ECRs to download the applicable SAR image products. Orbit products matching the dates of the SAR images are obtained from the Sentinel-1 PDGS (Payload Data Ground Segment). The same procedure is applied to the atmospheric model data for which the files corresponding to the date of the SAR product are downloaded and ingested into the system. As a result radar observations (range and azimuth) and required corrections for the targets are provided. The geometric relationship between the radar sensor and the radar target is mathematically expressed by the well-known Range-Doppler equations system. For a given epoch, the equations relate the position vector of the radar target with the sensor's state vector (sensor position and sensor velocity) in a Cartesian reference frame. Using range and azimuth and the corresponding corrections finally yields coordinates of the targets and their estimated uncertainties. The process is implemented as an iterative least squares procedure applying pre-selected convergence criteria.

Since heights of the GNSS stations near the SAR transponder stations need to be determined with the highest possible accuracy, GNSS observations with the lowest possible cut off for the elevation angle of the registered satellites are used. Daily observational data ensure the stability of the resulted coordinates. Also for that reason it was decided to apply network computation of GNSS observations in Double Differences (DD) mode, but not Precise Point Positioning (PPP). Before performing calculations, first the network is defined. It contains all necessary permanent GNSS stations useful for the needs of the project – some of them as reference stations and some of them located in close proximity to the SAR transponder stations and/or the selected tide gauge stations. The network should have good and stable in time geometry for determining the coordinates of the stations included in the project and contain GNSS stations as reference points, having long and stable time series of coordinates of these stations, with well-defined parameters of their movements - velocity vectors. The computation process is performed using the Bernese GNSS Software (actually in version 5.2) assuring most precise and stable results. It is clear that for the precise coordinate computation all possible models according to IERS Conventions 2010 must be used and computation are made using dual frequency solutions. For this the standard algorithms for GNSS data processing are applied. Due to the current number of satellites available in orbits and the fact that the GNSS system is in the operational phase, the highest accuracy for the determination of station coordinates is now possible using observational data from GPS or GPS+GLONASS satellites. Galileo is not yet considered as the system still is in its pre-operational phase.

For observing the absolute sea level and enabling unification of height systems, physical heights of the tide gauge stations referring to a common equipotential surface are needed. This is achieved by combining a GOCE based Earth Gravity Model (EGM) with local/regional gravity data (land, airborne and/or marine) and a Digital Elevation Model (DEM). Two regional geoid determination methods are compared, both in a pointwise sense at the tide gauges and over a rectangular area covering the tide gauges (comparison of regular grids). The methods are, three-dimensional Least Squares Collocation (3D LSC method) with Residual Terrain Modeling (RTM) of the topographic corrections, and least squares modification of Stokes' formula with additive corrections (LSMSA method), where the remove-compute-restore philosophy is used for gridding of the surface gravity anomalies. Both methods are tested and it could be shown, that the expected 1 cm geoid accuracy can be achieved. Time variability of the geoid due to vertical land motion is very small, hence negligible for the purpose of the present project as it only covers an analysis period over one year.

Sea level at the coastline is observed with tide gauges that deliver instantaneous sea surface heights relative to a zero marker of the tide gauge station. The standard hourly tide gauge data are the primary data set used for analysis. For reliable mean sea level (MSL), estimation of the sea level measurements should be performed over an adequate time period to filter out data blunders and obtaining statistically meaningful results. An annual water cycle period is assumed to be sufficient for the purpose of the present study. The accuracy of contemporary tide gauge readings remains within 0.2...1.0 cm. However, readings of such sensors need to be compensated due the instrumental phenomena, e.g., drift. Accordingly, the tide gauge data need to be checked for the inclusion of such instrumental corrections. The drift corrected

	<b>BALTIC+ Theme 5</b>  <b>Geodetic SAR for Baltic Height System Unification and Baltic Sea Level Research</b>	<b>Final Report</b> <b>Doc. Nr: SAR-HSU-SR-0022</b> <b>Issue: 1.1</b> <b>Date: 07.07.2021</b> <b>Page: 14 of 170</b>
---	--	--

data are to be further filtered in order to remove data blunders and gross errors. In order to filter out data blunders the tide gauge series are statistically analyzed. The standard deviation (STD) of the readings reflects the inner consistency (for the entire period, or seasonally) of the time series at each tide gauge station. Typically, the larger STD is associated with the rougher sea conditions at individual stations, whereas the smaller STD may also reveal sea sheltered locations. The final mean sea level for the tide gauges will be computed centrally, applying the same methodology and considering also interconnections between the tide gauges and geodetic infrastructure.

In order to compute absolute sea level heights for tide gauge markers with respect to a chosen physical height reference system (an equipotential surface), all individual observation types need to be combined in a consistent way securing that common standards are applied during all processing steps. This includes the geometric heights from GNSS and/or SAR positioning, the geoid heights and the averaged tide gauge readings.

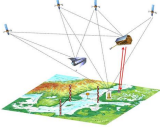
### 2.3 Data Analyses and Scientific Assessment

The SAR data analysis is performed with the surveyed transponder origin coordinates corrected for the geometric transponder phase centre offsets specified for ascending and descending passes. The estimated offsets then mainly show electronic delays of the active transponder, with additional bias contributions from the orbit, the finite correction accuracy and the surveyed coordinates. Several conclusions can be drawn from these results. The SAR range observations of the active transponder generally have a high precision when considering only the individual geometries. Only a few transponders provide relatively homogeneous data across all incidence angles and there is low consistency among the different ECR delay patterns. Despite being built to same specification and stemming from one manufacturing series, the transponder delays can vary between 1.2 m and 3 meters. The experimentally determined electronic delay model can remove the delay effects only within  $\pm 0.5$  m and only for a limited number of transponders. Absolute SAR positioning accuracy is limited to decimetres if these systematic effects are not compensated for. Some stations perform worse because of their less common delay patterns. The azimuth observations are much more consistent and seem less affected by the transponder electronic characteristics. In summary, the attainable precision of Sentinel-1 SAR observations of active transponders is largely equivalent to observations of passive corner reflectors, but absolute accuracy is limited by the delay effects introduced by the active transponder electronics. The effects vary between the individual instruments, which makes an ensemble characterization impossible. In order to achieve better absolute accuracy and improve feasibility for SAR positioning, the active transponders need to be electronically characterized and calibrated by the manufacturer.

For each station the available data since the start of operation of a transponder until the end of 2020 is used. The precision (internal accuracy) of the positioning solutions varies between a few millimetres and one centimetre. The precision is fairly stable, even though the number of data takes vary per stations. This independency is due to the fact that the estimator becomes already stable when more than 20 data takes per station are used. The confidence ellipses of the position solutions only spread over a couple of millimetres or few centimetres. The eccentricity of the ellipses is related to the ratio of observations taken in ascending and descending geometry. The more balanced the number of observations per geometry the more circular the confidence ellipse will become. The confidence ellipses can also be presented with respect to reference coordinates showing the absolute (external) offsets between reference and estimated coordinates. The absolute accuracy in height varies between centimetre offsets and a few decimetres, corresponding to the findings of the initial SAR data analysis. In order to identify if coordinate (height) variations can be observed, position solutions for monthly, bi-monthly, 3-monthly and 4-monthly data sets are computed. In general, one can observe the trend of increasing internal accuracies with increasing number of observations. 3-monthly and 4-monthly solutions perform for most stations as good as the solutions using all available observations. Results show that the time series of transponder position solutions exhibit much larger variability than the IGS trend model for these stations. This indicates, that coordinate variations of a few cm per year so far hardly can be estimated with the current active transponders due to their limited performance.

The processing of GNSS daily observations is performed as daily network solutions using the Bernese GNSS Software ver. 5.2 in the double-difference mode (DD method). As the reference frame the ITRF2014 is used, in which all IGS global products are available for the calculations: precise orbits, the Earth's rotation parameters and the corrections of GNSS satellite clocks. The daily network solutions are related to the middle of the development period of each daily session. Based on these solutions, time series of X, Y, Z Cartesian coordinates covering the entire year 2020 are generated. From these series, for the purposes of the project, time series of B, L, h geodetic coordinates are then created, related to the GRS80 geocentric ellipsoid. The averaged coordinate solutions for all stations and the complete year 2020 is computed from the daily solutions and provided for epoch 2020.50 in terms of geodetic coordinates referred to the GRS80 ellipsoid. Error estimates show that the 1 centimetre goal easily can be achieved for all stations.

Tide gauge data series for the year 2020, also relevant station documentation and metadata are delivered by the national authorities operating the tide gauges. All tide gauge data are un-normalized, i.e. presenting the actual hourly sea level heights at the tide gauge stations. Vertical land motion estimates (reaching up to 9 mm/year) were either embedded in the tide gauge records (Sweden) or accounted for separately (Estonia, Finland, Poland). In order to filter out data blunders the tide gauge series are statistically analysed. The initial TG time series are quality checked in several tests for identifying gross errors and systematic biases. Typically, the standard deviation of the annual sea level series remains within 2 decimetre, whereas the larger standard deviation is associated with the rougher sea conditions at individual tide

	<b>BALTIC+ Theme 5</b>  Geodetic SAR for Baltic Height System Unification and Baltic Sea Level Research	<b>Final Report</b> Doc. Nr: SAR-HSU-SR-0022 Issue: 1.1 Date: 07.07.2021 Page: 15 of 170
---	--	--

gauge station. The smaller standard deviation revealed sea sheltered locations of certain tide gauges. The data series is used for computing the mean sea level estimates for each TG station averaged over the year 2020.

For the regional geoid computation, the least squares modification of Stokes' formula approach is applied. The computed model is then converted to the project mean epoch 2020.5 by applying a land uplift correction. The final geoid heights in the Swedish, Finnish and Estonian tide gauges are given by this model. As can be judged from the comparison to GNSS/levelling, the standard uncertainty of the geoid heights in Sweden, Finland and Estonia is estimated to be approximately 0.010 m in a relative sense. The GNSS/levelling fit standard deviation after correction of country biases is 0.013–0.015 m. Considering that there are also errors in the GNSS ellipsoidal heights and in the levelled heights, 0.010 m should be a reasonable estimate. In order to get consistent geoid heights for the whole test area, the geoid model is selected also for the Polish stations. For these stations, however, the uncertainty should be somewhat higher due to a slightly reduced terrestrial data quality.

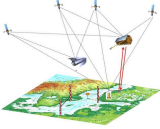
In order to ensure consistent results for the different products, it is essential that any differences regarding the underlying reference frames and inconsistencies with respect to the implemented standards and models are taken properly into account. The standards and models used for the processing of the different observations used within this project are applied accordingly with the IERS Conventions 2010. In addition, technique-specific processing standards are applied for the individual observation techniques (e.g., IGS- and EPN-Standards, SAR Standards, GOCE Standards, standards for gravity and tide gauge data). For the transformation between 3-D Cartesian coordinates and ellipsoidal coordinates it was specified that the conventional GRS80 parameters are used.

For the transponder stations co-located to a permanent GNSS station the resulting heights are compared by applying the relative height difference between the GNSS antenna reference point and the ECR reference point. Results show that the absolute height differences between the 2 techniques are varying. While three stations exhibit good to reasonable agreement at decimetre level or below, for three other stations height differences are at a level of several decimetres to half a meter. As one can assume that the GNSS derived heights are accurate at a level of a few centimetres, the transponder derived heights are the main driver for the absolute performance results. From the ECR stations co-located to a tide gauge station the resulting physical heights of the tide gauge zero markers above the reference equipotential surface are computed with equation. The results show that some stations seem to provide very good results with only a few centimetres offset, while other stations exhibit an offset of several decimetres up to a meter. These results need to be further analysed together with the performance of the individual active transponder stations and also with respect to the length of the data time series. There seems to be some correlation of the physical height results with the SAR observation quality, the SAR residuals and the length of the SAR observation time series. Relative height differences are compared between GNSS or tide gauge stations and those observed with the active transponders. The results again show a diverse behaviour. Basically, the differences between GNSS and ECR observed height differences vary between a few centimetres and some decimetres. For stations, which exhibit a large absolute offset the differential height error between these stations becomes small, while the differential error between one of these stations with the other stations becomes significantly larger. This indicates, that there is a systematic height offset in the ECR positioning results with the same sign, as it is also shown in the absolute comparisons.

## 2.4 Conclusions

The active transponders are designed such that they shall be able to operate without the need of on-site user interaction and with energy supply either by connecting it to the electrical power supply at a station or, if not available, by charging the batteries with solar panels. The project team operated 12 transponders from late 2019 until now and made a lot of experiences, which led to some conclusions related to operability and calibration of the devices. Generally, it can be stated that a consistent long-term operation of the transponders in the demanding environment of the Baltic sea region is not possible with the present transponder design. The current design requires improvements related of the hardware and software. In particular, major points of concern are the sealing of the instrument against water intrusion, the power supply, the remote access to transponder by electronic means (WiFi or others), the transponder software for user interaction and time synchronization. Because the transponder is an active electronic instrument, an initial calibration after fabrication by the manufacturer is advised in order to correct for possible system delays. Ideally, this calibration shall be identical for all transponders of the same design. From the results obtained during the project there are indicators that each transponder somehow has its own characteristics and individual calibration sessions need to be performed. A major limitation for obtaining very good geodetic positioning results from this technique comes from the delays introduced by the active transponder electronics which was found to vary significantly between 1.2 m and 3 m for different pass geometries and different devices. This is a very critical items and needs to be solved. The transponders should be investigated by the manufacturer and if possible calibrated in laboratories to determine their individual electronic characteristics.

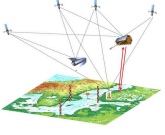
The project gives a good overview on possibilities of geodetic SAR and possible applications. With the results, the potential of the method, a way to develop the technique in future, and a lot of information how to improve it in future has been achieved. As such, it fulfilled the goals one may expect with such a new technique. Active transponders can give additional information for areas of no previous observations, but cannot replace current positioning techniques. In a wider perspective, the number of observations is very small comparing to GNSS observations. Therefore, the geodetic SAR technique in general is not suitable to observe temporal coordinate variations with shorter temporal resolution than a month, except more C-band SAR satellites become available. But, it can be used for observations of large movement

	<b>BALTIC+ Theme 5</b> <b>Geodetic SAR for Baltic Height System  Unification and Baltic Sea Level Research</b>	<b>Final Report</b> Doc. Nr: SAR-HSU-SR-0022 Issue: 1.1 Date: 07.07.2021 Page: 16 of 170
---	---	--

(>decimeter/month) in areas with critical slopes undergoing landslides, for volcanos and fast subsidence. Additionally, it might be applicable for determining absolute reference coordinates to fix the orientation of SAR interferometry.

The project team learned about these new geodetic devices, and the geodetic SAR project was the first step to add such electronic corner reflectors to geodetic infrastructure and co-locate them with other geodetic instruments/benchmarks. Having such transponders co-located with GNSS (for example) can provide additional data for local deformation monitoring at the site, 3D absolute positioning and atmospheric studies and can be compared with GNSS data and time series in long run. In addition, such reflectors as artificial persistent scatterers (PS) co-located with GNSS permanent stations can be useful for future calibration of the European ground motion service (EGMS) products and to transform the deformation maps and rates into a global reference frame.

Within the project a very valuable data set has been compiled, which offers the possibility to enhance methods and procedures in order to develop the SAR positioning technique towards operability. The data set will be publicly available and can attract new users to develop processing strategies and to investigate new possible applications for the SAR positioning technique.

	<b>BALTIC+ Theme 5</b>  Geodetic SAR for Baltic Height System Unification and Baltic Sea Level Research	<b>Final Report</b> Doc. Nr: SAR-HSU-SR-0022 Issue: 1.1 Date: 07.07.2021 Page: 17 of 170
---	--	--

### 3 SCIENTIFIC CHALLENGES

For each contributing observing system (refer to Figure 1-1, top line) the challenges are regarded separately in order to achieve the highest possible precision for the sub-system (refer to chapters 3.1 to 3.4). In parallel it is analysed, what is needed to be done when processing the observation data in order to make the compatible and absolute, such that they can be combined (chapter 3.5 on reference frames and joint standards, Figure 1-1, bottom line). Both items are equally important and needed to be considered jointly.

#### 3.1 SAR Data Analysis and Value Adding

The task of SAR data analysis and value adding involves both the extraction of the 2D radar coordinates (range and azimuth) of the installed radar point targets from the level 1 single look complex (SLC) images as well as the computation of the entire set of necessary data corrections. The main challenges to be addressed are the assessment of new technology of active transponders, i.e. the electronic corner reflectors (ECRs), and the monitoring of the project's SAR ground infrastructure consisting of ECRs and passive CRs. Regarding the SAR data, the project mainly relies on the publicly accessible Sentinel-1 data along with the precise orbit distributed separately, (cf. chapter 4.1).

While the extraction of radar coordinates at sub-pixel level by means of image analysis techniques is well defined (see e.g. Schubert et al., 2018), the computations of corrections for the perturbing effects of the atmosphere and the solid Earth dynamic demand care in order to obtain SAR range and observations that are compliant with the other techniques employed in the project. The consistent modelling and removal of atmospheric delays and surface deformation signals related to geodynamic effects according to the common geodetic standards is crucial to facilitate accurate SAR positioning (see chapter 3.2) and the fusion of the different results as shown in Figure 1-1. The methods for SAR are firmly established through earlier studies (e.g. Gisinger et al, 2015, Balss et al., 2018, Gisinger et al., 2021), but they need to be inspected to ensure that the overall standards as defined in chapter 3.5 are properly met.

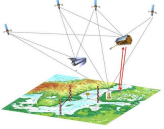
The geodynamic effects can be directly computed following the IERS 2010 conventions and standards (Petit and Luzum, 2010). The atmospheric path delays, on the other hand, require a few technique-specific considerations. In principle, the signal propagation delays affecting the range measurements can be treated similar to GNSS because SAR also makes use of radio signals. The neutral troposphere part can be either treated globally, by integration of weather models (e.g. ECMWF, VMF), or locally, by GNSS tropospheric delay products (e.g. through IGS, EUREF). For the dispersive ionosphere part, global ionospheric maps provided by CODE are employed to derive the corrections. All these methods have been tried and tested and are available through the DLR processing environment (Balss et al., 2018, Gisinger et al., 2021). They ensure that the primary requirement for the SAR data analysis is properly addressed, i.e. the consistent spatiotemporal modelling and correction of the SAR observation. In addition, the availability of regional geodetic GNSS networks and of co-locations with the SAR targets offers a mean to test alternative approaches and products for correcting the SAR data in this study.

Furthermore, SAR system corrections have to be provided, i.e. the additional corrections specifically required for the Sentinel-1 data to achieve accurate zero Doppler geometry (see Gisinger et al., 2021), and the system calibration of the SAR sensors against reference targets defined in global geodetic reference frame (ITRF2014) has to be performed. The Sentinel-1 system corrections are part of the DLR processing environment and are thus derived and applied as part of the automated image analysis. The determination of the total internal signal delay within the satellite's central electronics is part of its geometric calibration. It is estimated along with all external unconsidered biases by comparing the measured range and azimuth of reference reflectors with expected values derived from terrestrial surveying and the satellite's trajectory.

The main scientific challenge for the consistency of the SAR data is the new technology of C-band ECRs for Sentinel-1. Whereas passive SAR targets (e.g. corner reflectors) are known for their long-term stable behaviour if properly maintained, the active ECRs are expected to introduce an additional electronic delay (equivalent to decimetres). Moreover, the long-term stability of this delay is not yet known and needs to be monitored. The definition of a physical reference point on the transponder housing, the survey of the local tie to the co-located GNSS (if available at a test site), and the usage of the same orientation for all transponder installations allow us to derive and apply a delay compensation for all the used ECRs.

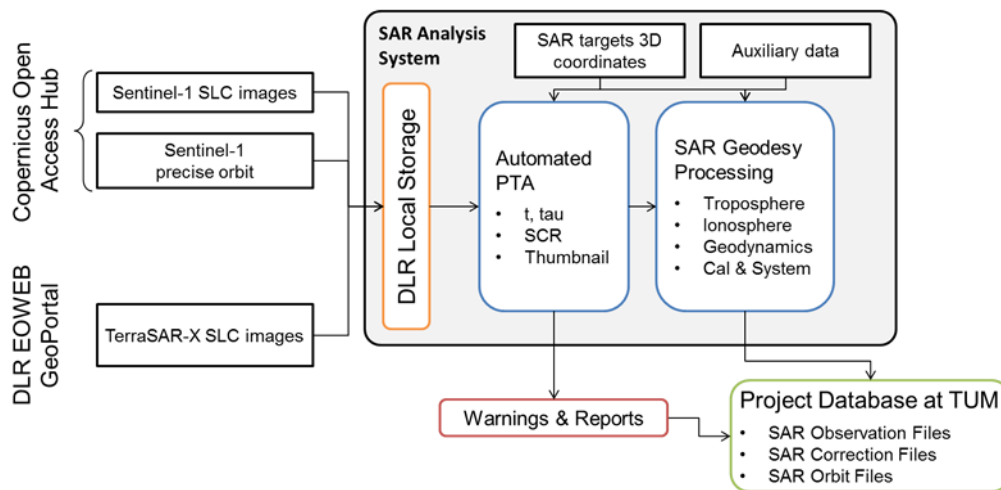
Monitoring the status of the overall SAR network is performed during the image processing by checking the signal-to-clutter ratio (SCR) of the point response. Problems with an ECR or signal degradation, which may occur for either ECR or CR, can be detected as a drop in the SCR under a predefined threshold, e.g. 10 dB below the average SCR (Schubert et al., 2018). The SCR along with the image thumbnails of the each analysed image is archived to allow later inspection of the point response history if needed. In the case of an anomaly, a warning is issued to initiate an on-site investigation.

Figure 3-1 summarizes the workflow as described above. After becoming available, the SAR images of the test sites are retrieved and injected into the analysis system. Knowledge of test sites enables automated point target analysis (PTA) that yields the SAR range and azimuth as well as the monitoring data, i.e. SCR and image thumbnails allowing for warnings and quality reports. Subsequently, the corrections are derived by the usage of the applicable background data for tropospheric and ionospheric modelling. The SAR observation files are placed in the project database along with the

	<b>BALTIC+ Theme 5</b> Geodetic SAR for Baltic Height System Unification and Baltic Sea Level Research	<b>Final Report</b> Doc. Nr: SAR-HSU-SR-0022 Issue: 1.1 Date: 07.07.2021 Page: 18 of 170
---	--	--

corresponding correction files and the precise orbit data to be accessed in the subsequent SAR positioning. The files themselves are already an important outcome of this project as the database are publicly available, allowing other users to experiment with these SAR datasets.

The SAR images themselves are not part of the project database, as they are available through the mission's image databases. The experimental differential InSAR processing is performed with DLR's wide area persistent scatterer interferometry system IWAP (Adam et al., 2013). Differential InSAR estimates relative height changes between the selected SAR targets using the same underlying dataset (stacks of SAR images) as the SAR positioning. The results support the comprehensive final impact assessment of the geodetic SAR positioning method with respect to the established differential InSAR method.



**Figure 3-1:** SAR data work flow for analysis and value adding.

## 3.2 Geometric Positioning

Geometric positioning is performed for the SAR ECRs and the GNSS stations of the Baltic Sea network (see chapter 5.2).

### SAR Positioning

The SAR positioning deals with the determination of the 3D coordinates of the SAR targets at the different test sites using the methods of absolute SAR positioning (Gisinger et al., 2015) and differential SAR positioning (Gisinger et al., 2017). The computations solve the linearized Range-Doppler equations in an iterative way by combining the SAR observations files from the project database (see chapter 3.1).

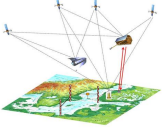
The main challenges to be addressed include the outlier detection, the data combination for the differential setups, and the identification of the optimum temporal sampling for the data processing (monthly, bi-monthly, seasonal solution). With respect to the outlier detection, major outliers are already captured by Signal-to-Clutter ratio monitoring and data takes affected by low point target response are removed. However, for the removal of further errors, least squares residuals analysis and statistical tests are required. For relative coordinate transfer experiments two or more targets need to be observed within the same data take. For this, pass information is used in order to plan the experiments accordingly. For the optimum temporal sampling, a trade-off between the estimated precision (confidence) of the estimated positions (driven by the amount underlying data) versus the temporal sampling of the position time series is needed. Different setups are investigated for optimum solutions, i.e. monthly computations, bi-monthly, seasonal data batches.

Additionally, SAR positioning results have to be compliant with standards that will allow data combination with other observations (e.g. GNSS, tide gauges). The same reference ellipsoid shall be used for all height conversions. For all locations where GNSS observations are available, an error analysis and a cross-validation of the SAR positioning coordinates against the GNSS-based coordinates is performed. The coordinate solutions of the targets, along with the quality information (error budget) are placed in the project data base.

### GNSS Positioning

An overview about the GNSS stations in the Baltic Sea area is performed, specifically regarding how they are linked to tide gauges in the area.

*Collocation measurements:*

	<b>BALTIC+ Theme 5</b>  Geodetic SAR for Baltic Height System Unification and Baltic Sea Level Research	<b>Final Report</b> Doc. Nr: SAR-HSU-SR-0022 Issue: 1.1 Date: 07.07.2021 Page: 19 of 170
---	--	--

Local ties of reference points of SAR transponders to GNSS (ARP – Antenna Reference Point) and to tide gauge stations (TGCP – Tide Gauge Contact Point) are identified and measured. Height component for short eccentricities can be done by levelling relatively easy. Full 3D collocation is more complicated and needs more effort. To determine the precise three-dimensional eccentricities between reference points of different types of instruments, additional GNSS measurements at few selected tide gauge stations are performed. In such cases, coherent measurement principles are developed for short campaigns (minimal length and number of sessions, measuring equipment, principles of measurements).

In the project, for all proposed tests and scenarios using the Geodetic-SAR technique very stable and precise reference frame is strongly required. The use of Double Differencing and Precise Point Positioning methods are applied for comparison and evaluation of systematic errors existing in the used methods and software packages, dedicated for GNSS data processing. In Double differences method (DD) stable and strong network design (set of reference stations) is required in long time scale, while in Precise Point Positioning (PPP) computations are performed only for GNSS stations close to selected tide gauge stations. Reference stations are not required. However, the DD method gives higher precision in determining the station coordinates. For the DD method, careful selection of GNSS reference stations has been carried out, taking into account a number of important elements, including: location in place with no abnormal movements (the GNSS site and tide gauge need move in the same way), stabilisation (concrete pillar or comparable, ensuring high precision of results), preferences regarding the quality of station observation, coordinate accuracy and time series. Analysis and comparison of different existing solutions and time series of coordinates from global and regional permanent networks (IGS, EPN) is required for ensuring stable results of coordinates computation.

*Processing conditions:*

Calculations are performed using GPS and GLONASS systems. The project takes into account studies made using one or several software packages: The Bernese GNSS Software ver. 5.2, (DD & PPP), GAMIT/GLOBK, ver. 10.70, (DD), GIPSY/OASIS, (PPP), CSRS-PPP, NRCan, Canada, (PPP-AR), PRIDE PPP-AR, a new open-source software from Wuhan University, China, (PPP-AR).

Same standards are applied for all geometric techniques. For SAR and GNSS processing ITRF2014 is used. All models, products and parameters must be compatible with IERS Conventions (2010). For GNSS measurements IGS/EPN standards are implemented. RINEX ver.2.1x is used as data format for GPS and GLONASS. Error budgets for all geometric positioning techniques are determined for the selected stations.

In GPS/GNSS it is necessary to develop a method for obtaining the final, total determination of station movements either by choosing one "best" solution (with predefined selection of the criteria) or as a combined solution of all Analysis Centre solutions, with the adoption of the weighing method.

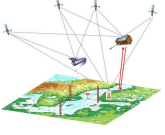
*Geometric Positions Time Series with Error Budget:*

For time series analysis of geometric positions obtained from GNSS data one or more from the following commercial/scientific software, CATREF (IGN), Bernese GNSS Software ver. 5.2, GITSA (in Matlab environment), GGMatlab (in Matlab environment), iGPS (in IDL), Hector (Linux), Statistica, TSAlyser 2.0 (Linux) is selected, or alternatively an own developed Software is used. In the time series analysis process, for each station, before determining linear trend (station velocity vector), based on the information collected in headers of RINEX files, log files and any collected metadata, all effects generating discontinuities in analysed time series are examined and removed. For each GNSS station, time series constrained from different solutions are compared for identification of changes characteristic caused by different solution and between neighbourhood stations – as reference frame impact for the time series.

### 3.3 Tide Gauge Data Analysis

At the coasts, sea level is usually observed with tide gauges delivering instantaneous sea surface heights relative to a zero marker of the tide gauge station (Woodworth and Player, 2003; Wöppelmann et al, 2014). After eliminating ocean and Earth tides from the observations, one gets a time series of sea heights and consequently its changes. These height changes, as they are observed at the tide gauges, at this point can be only regarded as relative changes of the sea surface with respect to the zero marker. For a long term analysis and for the determination of absolute height changes with respect to a reference height one needs to know if the zero marker of the station is stable or undergoes changes in height as well. Therefore, on-site observation of the relative motion of the zero marker with respect to a global geometric reference frame is required. By subtracting the identified land uplift rate from sea level change rate observed with the tide gauge, one obtains the actual sea level change rate at this location (Wöppelmann et al, 2007; Santamaria et al, 2012).

The tide gauge observations are required in order to use these data for height system unification and sea level research and make them compatible in an absolute sense. Therefore, all relevant issues need to be taken into account for the definition of case studies. This includes studying and defining the common standards for tide gauge processing data, followed by the collection of suitable tide gauge records from Estonia, Finland, Poland and Sweden. The records of existing tide gauges are analysed in terms of consistency and systematic distortions due to external artificial disturbances. From this analysis unreliable stations or low-quality observation data are excluded to generate a good data basis for investigating the applicability of the geodetic SAR concept for tide gauges.

	<p style="text-align: center;"><b>BALTIC+ Theme 5</b></p> <p style="text-align: center;">Geodetic SAR for Baltic Height System Unification and Baltic Sea Level Research</p>	<p style="text-align: right;">Final Report</p> <p>Doc. Nr: SAR-HSU-SR-0022 Issue: 1.1 Date: 07.07.2021 Page: 20 of 170</p>
---	--	--

### 3.4 GOCE based Geoid Computation

Tide gauge data and collocated GNSS/SAR are not sufficient to enable comparisons of sea level at different stations in an absolute sense, meaning in relation to a global high-resolution equipotential surface (Gruber et al, 2020). In other words, physical heights are needed for the tide gauge stations with respect to the global high-resolution geoid. Today, the long to medium wavelengths of the global gravity field can be very accurately determined by GOCE (limited to 80-100 km resolution), possibly in combination with other satellite missions. A high-resolution geoid, however, must be derived by combining the GOCE based model with local/regional gravity data (land, airborne and/or marine), a Digital Elevation Model (DEM) and possibly other types of data using a so-called regional geoid determination method.

During the years, several regional geoid modelling methods have been developed. Examples of relevant methods are,

- Least Squares Collocation (Moritz 1980; Tscherning and Rapp 1974) using the remove-compute-restore method with Residual Terrain Modelling (RTM) of topographic corrections. A recent and improved version of this method is presented by Willberg et al. (2019).
- Least squares modification of Stokes' formula with additive corrections (LSMSA method), where the remove-compute-restore philosophy is used for gridding of the surface gravity anomalies; e.g. Sjöberg and Bagherbandi (2017) and Ågren et al. (2009).
- Modified Stokes' formula using Wong and Gore (1969) kernel modification. Remove-compute-restore with RTM (cf. the first bullet point above).

All these methods imply that a GOCE based geopotential model is combined with regional gravity data. It is a major challenge to find the method that is most suitable for this task. This is, to some extent, investigated in the project by comparing a few regional geoid determination methods, both in a pointwise sense and over a larger area surrounding the tide gauges. Geoid heights computed as the differences between GNSS heights and levelled heights are also utilized to check and evaluate the methods in a relative sense (referring to the existing national height systems in the area). The goal of the tests is not only to find the most suitable method but also to estimate how large part of the uncertainty that is due to the choice of method. Other important problems are to study the combination of GOCE and local/regional gravity data for the chosen method(s) and to estimate realistic standard uncertainties for the geoid heights.

The (static) regional geoid determination above is made at a selected reference epoch. As the geoid is not static a method to determine the geoid change is identified. The main reason behind the time variations in the current area is postglacial rebound. It is well known that the land is rebounding after the last deglaciation, and with the land, the geoid is also rising. The maximum land uplift (about 1 cm/year land uplift, 0.7 mm/year geoid rise) occurs close to the southern part of the Bay of Bothnia, which is in the northern part of the target area for the project; tide gauges are included at both the Swedish and Finnish coasts close the maximum. The way the Nordic and Baltic countries usually deal with the land uplift is to make use of a model to correct all the affected observations as needed. The latest postglacial land uplift model is NKG2016LU, which has been computed in Nordic/Baltic cooperation under the umbrella of the Nordic Geodetic Commission (NKG) by combining an optimized Glacial Isostatic Adjustment (GIA) model with geodetic observations (long GNSS time series and repeated levelling); see Vestøl et al. (2019). Another alternative to determine the geoid change is to measure it directly using from the GRACE mission. The major scientific question in this context is which method (geoid rise rate from NKG2016LU vs monthly mean values from GRACE) that is most suitable to estimate the geoid time series (refer to section 8.5.1).

### 3.5 Reference Frames and Joint Standards

Within this project, a survey of the main scientific challenges and an assessment of gaps and scientific problems concerning the underlying geometric and gravimetric reference frames for the contributing space techniques, such as geodetic SAR, GNSS, GOCE and terrestrial/airborne gravity data is conducted. The outcome is an inventory summarizing the state-of-the-art concerning geometric and gravimetric reference frames and standards needed for the work envisaged in this project, and providing recommendations how to resolve possible deficiencies and inconsistencies.

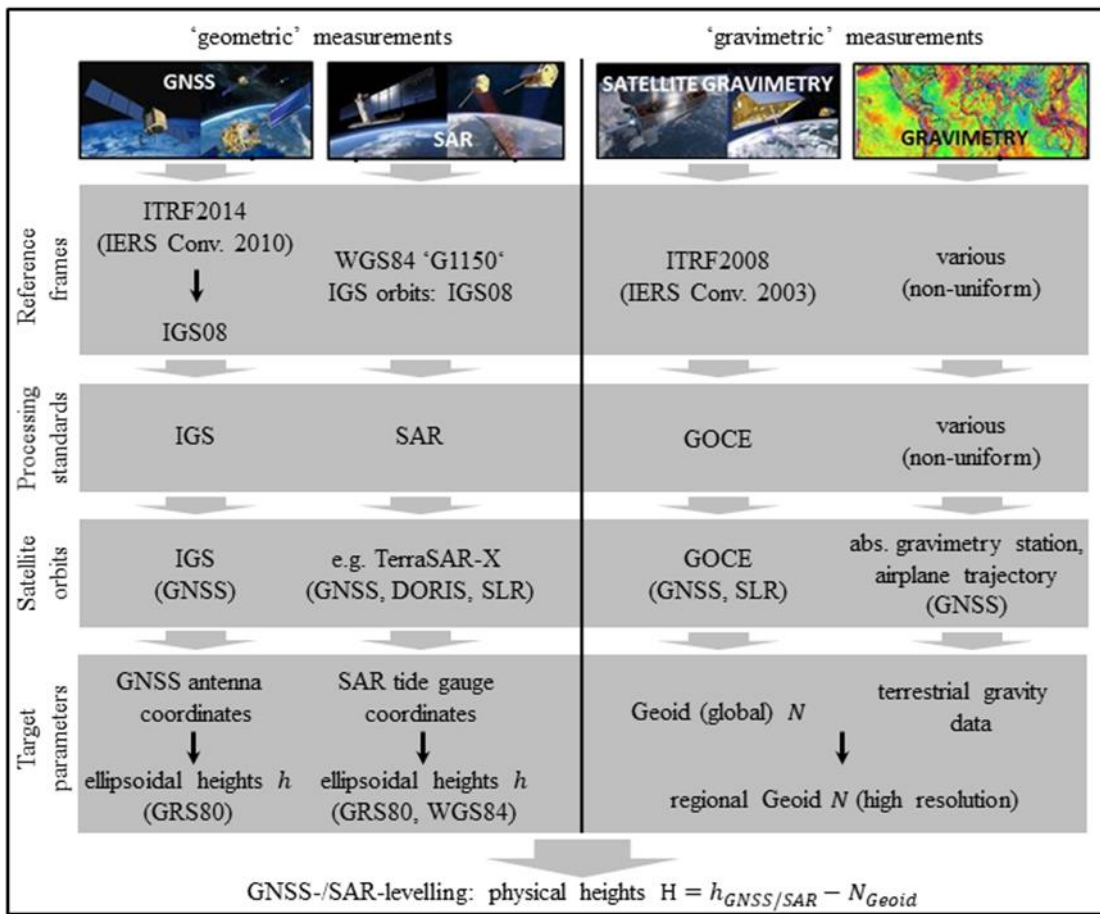
It is obvious from Figure 3-2 that the processing of the different geometric and gravimetric observations is based on different reference frames, e.g., ITRF2014, IGS14, WGS84. Taking into account the proposed case study in the Baltic sea area, also regional and national reference frames (e.g., EUREF, GREF, SWEPOS) and transformations between them have to be considered. Furthermore, different numerical standards (e.g., IERS Conventions, GRS80) and different technique-specific processing standards (e.g., IGS, GOCE, SAR) are in use for determining the required geometric and gravimetric quantities.

A further challenge results from the fact that the present realization (i.e., the ITRF2014) of the International Terrestrial Reference System (ITRS) is primarily based on a linear model (station positions and constant velocities). As a consequence, non-linear motions (e.g., caused by non-tidal loading displacements or other phenomena) are visible in the station position residuals. Moreover, by applying such a linear model, the ITRF origin is realized as a mean center of mass (CM) averaged over the time span of SLR observations. This leads to the fact that the ITRF station coordinates differ from an instantaneous geocentric position (as specified in the ITRS definition), which may cause systematic shifts between the geometric and gravimetric reference frames. In this context, the results of an SLR multi-satellite solution with station positions, Earth orientation parameters and low-degree spherical harmonic coefficients of the Earth's gravity

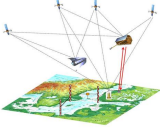
field (computed for example at DGFI-TUM, Bloßfeld et al., 2015) provides valuable input for the integration of geometric and gravimetric reference frames.

This work on reference frames makes use of the literature and documentations of standards for geometric and gravimetric quantities such as geometric positioning, tide gauge data analysis, geoid computation, the IERS Conventions and processing standards for the different geometric and gravimetric observations (e.g., IGS, EPN, SAR, GOCE). The inventory of standards and conventions used for the generation of IAG products, which has been compiled by the GGOS Bureau of Products and Standards (Angermann et al., 2016), provides a good basis for the envisaged work.

In summary, the tasks comprise the evaluation of the present status concerning the standards for the computation of ellipsoidal heights from the geodetic SAR technique and GNSS observations, as well as for the gravimetric quantities from GOCE and other gravity data. As a result, an inventory will be compiled which provides the present status, gaps and recommendations on how to resolve possible inconsistencies. As a major outcome, recommendations of common standards for geometric and gravimetric quantities and for a unification of the underlying reference frames is provided.



**Figure 3-2:** Simplified scheme for the determination of ellipsoidal heights from the geodetic SAR technique (left) and the determination of physical heights referring to a common physical reference surface based on GOCE and terrestrial/airborne data (right).

	<b>BALTIC+ Theme 5</b>  Geodetic SAR for Baltic Height System Unification and Baltic Sea Level Research	<b>Final Report</b> Doc. Nr: SAR-HSU-SR-0022 Issue: 1.1 Date: 07.07.2021 Page: 22 of 170
---	--	--

## 4 PROJECT DATA BASE

The individual observing systems are separately analysed related to available data sets used for the project (chapters 4.1 to 4.5).

### 4.1 SAR Images

The project primarily relies on the SAR images captured by the Sentinel-1 mission, which is operated in the framework of Europe's Copernicus programme targeting the European region. Therefore, both spacecraft, Sentinel-1A and Sentinel-1B, regularly capture the Baltic Sea area, as outlined in the mission's high-level operations plan (CSC, 2018). Moreover, the open access policy of the Copernicus programme allows unrestricted access to all the data acquired at our study region.

We use the level 1 SLC products (Bourbigot et al, 2015), which contain the focussed but otherwise unmodified Sentinel-1 SAR data that are required by our methods. Over land areas, Sentinel-1 mainly uses the Interferometric Wide Swath (IW) SAR mode, that covers a swath-width of approximately 250 km on ground. In combination with the latitude of our test area (above 50 degrees), this yields a coverage of each test sites by at least two ascending and two descending pass geometries, i.e. at least four independent SAR viewing geometries per site. With both spacecraft active, the repeat cycle of the Sentinel-1 data is six days, but one should be aware that during the winter months Sentinel-1B becomes unavailable for the Baltic region due to its assignment to ice monitoring that is carried out for the Arctic region. Nevertheless, the number of Sentinel-1 SAR observations per test site amounts to some 180 measurements if we assume the one year of Sentinel-1 data that is analysed by the project. In addition, we use the precise orbit solution, which is provided through the Sentinel-1 PDGS quality control website with a latency of 20 days. This latency is not an issue for our project, as the analysis is carried out in post-processing to achieve the best possible accuracy. Passive CR installations are used for 2 sites at DLR premises in Oberpfaffenhofen, Germany and in Metsähovi, Finland.

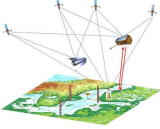
### 4.2 GNSS Data

After definition of the experiments the reference stations for the DD method are selected, based on the criteria for optimizing the geometry of the GNSS station network, observation quality, station stability over time, quality of coordinate determination and station velocity vectors, as well as free access for the data. Some GNSS stations in the vicinity of tide gauges are included in regional (EPN) and/or global (IGS) non-commercial GNSS networks. For a few cases, however, these may be stations for which access to data is not open. In such cases, separate agreements with the station/data owners are prepared.

The created structure on the GNSS data server also stores data of 'global products' (precise satellites orbits, satellite clock corrections, Earth Orientation Parameters (EOP)) and any complementary data sets, necessary in the GNSS data processing (global / regional / local / in situ models). The selection of parameters and products ensures internal consistency and comply with applicable conventions (IERS Conventions 2010). The data server resources also include well verified metadata for all GNSS stations (log files, site description documents) and data provided by individual partners regarding 3D eccentricities for selected stations (TG, GNSS, Geodetic-SAR, levelling benchmarks), enabling the linking of various observational techniques on each station (including measurement method/technique, accuracy, frequency of measurements, date of last measurements). In separate parts of the server structure, the final results of GNSS data processing (station coordinates, variance-covariance matrices, intermediate models calculated during the main development process (eg. ZTD, TEC, ...), obtained from project partners using different software and different methods) are stored. There are also successively constrained time series of GNSS station coordinates and the results of their analysis.

### 4.3 Tide Gauge Data

Based on preliminary analysis a set of tide gauge stations around the Baltic Sea is chosen, see Table 4-1 below. These tide gauges (TG) are connected to national height network in order to monitor and predict adequately the sea level fluctuations and oceanographic processes, as well as vertical land motions (VLM) along the entire shore of respective countries. All the participating countries are using the European Vertical Reference System (EVRS), that is referred to the Normaal Amsterdam Peil (NAP). Regardless, possible height system offsets between the participating countries are investigated and the detected systematic biases eliminated. Note that in the post glacial land uplift at the selected TG sites reaches up to 10 mm/year, hence the VLM effect is considered. The revision leads to coherent time series for all the participating tide gauges.

	<b>BALTIC+ Theme 5</b>  Geodetic SAR for Baltic Height System Unification and Baltic Sea Level Research	<b>Final Report</b> Doc. Nr: SAR-HSU-SR-0022 Issue: 1.1 Date: 07.07.2021 Page: 23 of 170
---	--	--

**Table 4-1:** Overview of tide gauges at the Baltic sea considered in this project

Country	Station
Estonia	<p>There is a tide gauge station in Loksa and a national GNSS station some 20 kilometres away from it. This is a good test case to link them by geodetic SAR. The area is affected by postglacial rebound up to 1.5 mm/year, which could offer the possibility to observe temporal height changes as well. The station is located on the Southern coast of the Gulf of Finland and the distance to the SAR transponder in Finland is close enough to be observed by single SAR scenes, meaning that coordinate transfer by relative SAR positioning across the Gulf of Finland might be feasible.</p> <p>In Loksa a modern pressure sensor based tide gauge is used. Note also that usually the station is also equipped with level staff, the visual readings of which are to be used for verification of the pressure gauge records and determining/elimination the sensor drift. In 2013 the level staff of the Loksa TG station was changed and relevelled, and thus reliable TG records can be obtained for this 6-year period. The Loksa TG readings are hourly averaged and drift corrected.</p>
Finland	<p>The Emäsalo (some 30 km eastwards from Helsinki, near Porvoo) tide gauge station is selected on the northern shore of Gulf of Finland. With the transponders/reflectors one could link the tide gauge station to a nearby national GNSS CORS station (Loviisa).</p> <p>The Rauma tide gauge at the West coast of Finland is selected as additional site. This tide gauge station is linked to the Swedish stations across the Baltic sea.</p>
Poland	<p>Tide gauge station in Wladyslawowo is selected as primary point. This station is connected with the GNSS ground network and very well linked to the Polish height network. This station plays the role of a very well equipped station in order to identify the potential of SAR based geometric heights.</p> <p>As second tide gauge station to Łeba is selected which is roughly 50 km away from Wladyslawowo. There is a nearby permanent GNSS station which can be used as well for connecting the SAR transponder to the Polish GNSS network. This could be a typical situation to apply relative positioning by geodetic SAR and to check the performance relative to the GNSS network.</p>
Sweden	<p>Spikarna tide gauge in middle Sweden not far away from the postglacial land uplift maxima, in the vicinity of a SWEPOS permanent GNSS station Vinberget, well connected to the Swedish height frame RH 2000 (connection checked once every third year). This station probably is a good representative station with significant geometric height change to be used as a test case.</p> <p>As a second tide gauge station Forsmark in Southern Sweden is selected. This station also is collocated with a SWEPOS permanent GNSS station.</p>

#### 4.4 Local Gravity and GOCE based Global Models

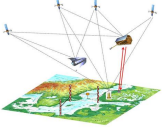
The high-resolution regional geoid computation is made by combining a geopotential model based on GOCE with local/regional gravity data. Below an overview is given of the available data sets that will be used in the project.

##### Local/regional gravity data

Gravity data in and around the Baltic Sea have for a long time been collected by the Nordic and Baltic countries within the Nordic Geodetic Commission (NKG). The last major update of the NKG gravity database was made in the NKG2015 geoid model project (Ågren et al. 2016; Märdla et al. 2017). In this project, all the involved countries cleaned their datasets and updated the database with their latest gravity datasets.

The following standards were agreed upon in the NKG2015 project: The computation of the gravimetric model and evaluation using GNSS/levelling is (as far as possible) to be made in common reference systems/frames for the whole area, in the postglacial land uplift reference epoch 2000.0 and in the zero permanent tide system. It should be mentioned that the used gravity systems are consistent with modern Absolute Gravimetry (AG) using the zero permanent tide system (thus agreeing with the up-coming International Gravity Reference System, IGRS). It should be added here that the released NKG2015 quasigeoid model also included a tide correction making it compatible to use together with tide free GNSS heights above the ellipsoid. However, the NKG2015 gravimetric model was originally computed in the zero tide system. It is also this zero degree gravimetric model that is evaluated below, in Section 7.5.

The NKG2015 version of the NKG gravity database contains up-to-date versions of the national gravity datasets from Sweden, Finland, Estonia, Latvia, Lithuania, Denmark and Norway. The dataset over the Baltic Sea is currently being improved in the FAMOS project by making new marine gravimetry measurements. A project database has also been created in FAMOS, which includes the NKG2015 gravity database, German gravity data above 52 degree of latitude and the newly measured FAMOS marine gravity data. Polish gravity data has yet not been released to the FAMOS project.

	<b>BALTIC+ Theme 5</b>  Geodetic SAR for Baltic Height System Unification and Baltic Sea Level Research	<b>Final Report</b> Doc. Nr: SAR-HSU-SR-0022 Issue: 1.1 Date: 07.07.2021 Page: 24 of 170
---	--	--

For regional geoid computation, gravity data is required over an area that overlaps the geoid target area (i.e. selected tide gauge locations) with at least around 100 km in all directions. This is required to obtain sufficient spectral overlap between the GOCE based model and the regional gravity data. Ultimately, as many gravity data as possible are collected in order to achieve ideally a complete coverage of the test area.

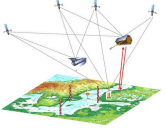
Regarding standards for the project, those applied for NKG2015 are followed as far as possible, meaning that the zero permanent tide system and land uplift epoch 2000 are to be used for gravity data and gravimetric geoid computation. For this project the  $W_0$  value derived in the NKG2015 project is used as the height reference.

#### GOCE based Geopotential Models

As global model, state-of-the-art satellite-only solutions combining reprocessed satellite data from GOCE and GRACE and combined models adding information from ground, sea and airborne gravimeter data are considered. The best performing background model is used for the regional geoid modelling.

## 4.5 Support Data Sets

Different support data are required for the computation of the atmospheric corrections of the SAR data, i.e. the ionospheric and tropospheric delays. The computation of the tropospheric delays relies on the operational integrated forecast model of ECMWF (Hólm et al., 2016). DLR can retrieve these data sets because access has already been established as part of other DLR research activities. Additional data sets for tropospheric calculations include the GNSS-based tropospheric delays for cross-validation, which are freely available for some of the selected test sites. These GNSS-based products are derived by several analysis centers from the IGS and EUREF GNSS networks (Villiger and Dach, 2018). The ionospheric delay computation makes use of the global ionospheric maps provided by the Center for Orbit Determination in Europe (CODE) (Hernández-Pajares et al., 2009), which are distributed free of charge through the FTP services of the IGS. For all these cases, the atmospheric background data sets are converted to slant path delay product files matching the SAR observations. These correction files are stored in the project database.

	<b>BALTIC+ Theme 5</b>  Geodetic SAR for Baltic Height System Unification and Baltic Sea Level Research	<b>Final Report</b> Doc. Nr: SAR-HSU-SR-0022 Issue: 1.1 Date: 07.07.2021 Page: 25 of 170
---	--	--

## 5 BALTIC SEA TEST NETWORK

Different types of test cases are defined in order to investigate the feasibility of the new SAR positioning technique for this kind of scientific analyses (refer to chapter 5.2). In this context the selected stations are analysed prior to installation regarding their reflectivity pattern by available Sentinel-1 SAR images in these areas (refer to chapter 5.1).

### 5.1 SAR Target Analysis

For the Baltic Sea test network, the transponders (ECRs) are installed as close as possible to the tide gauge and, depending on the experiment, to the nearby permanent GNSS station as well. From the perspective of the SAR, the installation sites are selected considering the surroundings of the site. Obstacles above 20 degree elevation need to be avoided, as well as bright background or spurious signals arising from nearby structures like buildings. The SAR requirement is a stable dark image area of at least 7 by 7 pixels, assuming that the central peak point response is typically located within 3 x 3 pixels. Because many of the tide gauges are located in harbour areas with moored ships or ships passing by, the installations are selected with care.

Based on the defined test cases, possible installation sites are proposed by each local partner by taking into account the given boundary conditions. Preliminary 3D coordinates derived by GIS or other mapping data is used to accurately project the proposed location into the Sentinel-1 or TerraSAR-X images of the site by applying the techniques of imaging geodesy (Balss et al., 2018). Calibration of the incidence angle by computing the radar cross section (sigma nought; Miranda and Meadows, 2015) enables the analysis of the proposed sites across the different SAR viewing geometries. Repeating this analysis for two seasons (summer and winter) enables a reliable judgement of the site and if needed iteration with the local partner to decide the final location. Thereby, we can consider not only the requirements of the SAR, but also the additional requirements demanded by the individual test sites. This procedure together with local boundary conditions led us to the test network described in the following chapter.

### 5.2 Network Design

Test cases and experiments were discussed intensively by the project team. All project partners investigated the initial station selection about feasibility of installing active transponders and about SAR reflection properties of the nearby environment (accessibility; local tie possibility w.r.t. tide gauge and/or GNSS; obstacles surrounding the site; radio frequency interference). For the selected stations, approval from national authorities to operate active instruments at specific locations was acquired before installation. This led to some delays in installation meaning that not all selected ECR stations could be occupied for the complete year 2020, which is the designated data analysis period. The final network design is shown in Figure 5-1.

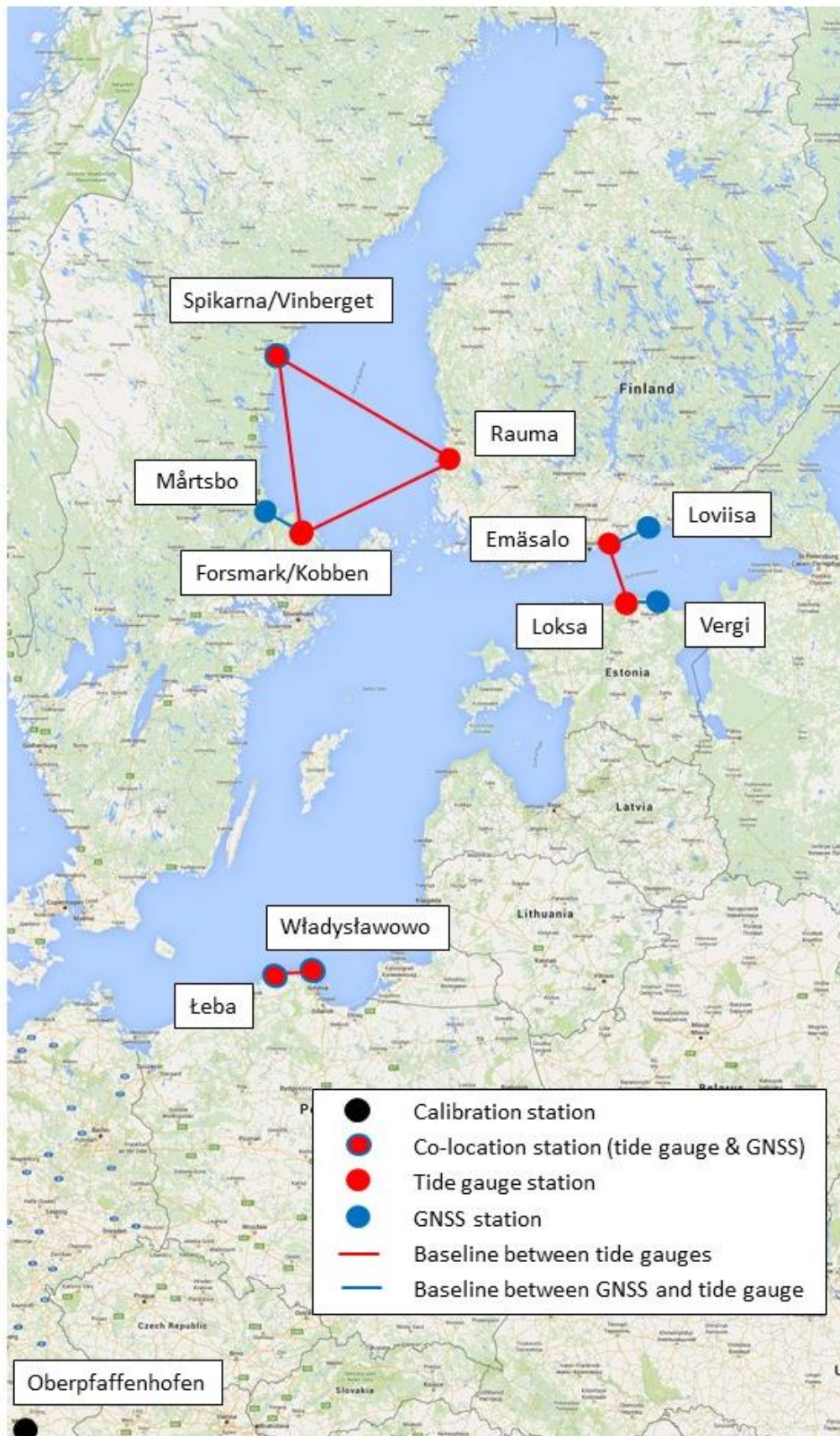
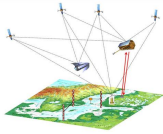
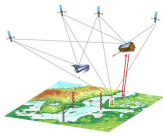


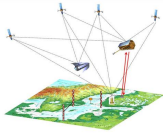
Figure 5-1: Baltic Sea Test Network



The individual ECR stations are characterized as follows (all details are described in [AD-4]. In addition, two fixed mounted corner reflectors at the calibration site in Oberpfaffenhofen are included in the test network.

**Table 5-1:** Summary of ECR Stations occupied for the Baltic Sea Test Network and ECR/CR stations at the calibration site in Oberpfaffenhofen Germany

<b>Station</b> Owner/Operator ECR ID Local Tie Data Takes 2020	<b>Images</b>	
<b>Vergi, Estonia</b> TUT/TUT 18_0086 GNSS 01.03.-31.12. 81 Data Takes		
<b>Loviisa, Finland</b> FGI/FGI 18_0091 GNSS 11.02.-31.12. 106 Data Takes		
<b>Loksa, Estonia</b> TUM/TUT 18_0098 Tide Gauge 16.02.-31.12. 164 Data Takes		
<b>Leba, Poland</b> TUM/CBK-PAN 18_0104 Tide Gauge, GNSS 18.05.-27.12. 116 Data Takes		



BALTIC+ Theme 5

Geodetic SAR for Baltic Height System  
Unification and Baltic Sea Level Research

Final Report

Doc. Nr: SAR-HSU-SR-0022

Issue: 1.1

Date: 07.07.2021

Page: 28 of 170

**Spikarna/  
Vinberget, Sweden**  
LM/LM  
19\_0106  
Tide Gauge, GNSS  
27.09.-27.12.  
57 Data Takes



**Mårtsbo, Sweden**  
LM/LM  
19\_0107  
GNSS  
07.01.-27.12.  
218 Data Takes

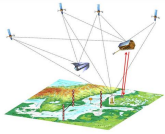


**Forsmark/Kobben,  
Sweden**  
LM/LM  
19\_0108  
Tide Gauge  
01.06.-27.12.  
97 Data Takes



**Emäsalo, Finland**  
DLR/FGI  
19\_0110  
Tide Gauge  
25.01.-31.12.  
185 Data Takes





**BALTIC+ Theme 5**  
**Geodetic SAR for Baltic Height System  
 Unification and Baltic Sea Level Research**

**Final Report**  
 Doc. Nr: SAR-HSU-SR-0022  
 Issue: 1.1  
 Date: 07.07.2021  
 Page: 29 of 170

**Rauma, Finland**  
 DLR/FGI  
 19\_0111  
 Tide Gauge  
 26.04.-22.12.  
 76 Data Takes



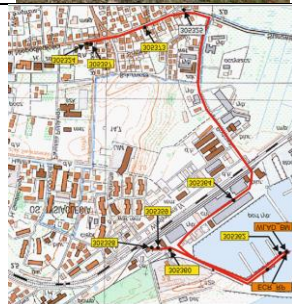
**Oberpfaffenhofen,  
 Germany (DLR2)**  
 DLR/DLR  
 19\_0112  
 GNSS  
 10.01.-29.12.  
 85 Data Takes

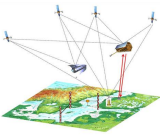


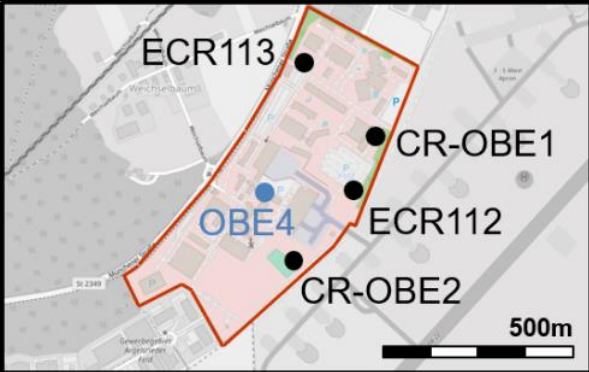
**Oberpfaffenhofen,  
 Germany (DLR3)**  
 DLR/DLR  
 19\_0113  
 GNSS  
 10.01.-29.12.  
 177 Data Takes



**Władysławowo,  
 Poland**  
 CBK-PAN/CBK-PAN  
 19\_0114  
 Tide Gauge, GNSS  
 21.03.-29.12.  
 142 Data Takes

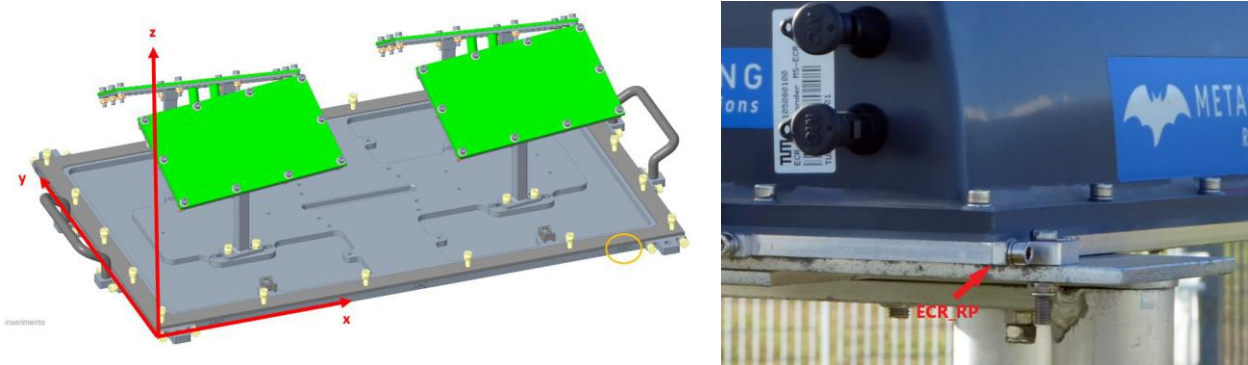


	<p style="text-align: center;"><b>BALTIC+ Theme 5</b></p> <p style="text-align: center;">Geodetic SAR for Baltic Height System Unification and Baltic Sea Level Research</p>	<p style="text-align: right;">Final Report</p> <p>Doc. Nr: SAR-HSU-SR-0022 Issue: 1.1 Date: 07.07.2021 Page: 30 of 170</p>
---	--	--

<p><b>Oberpfaffenhofen, Germany</b> DLR/DLR CR-OBE1 GNSS 03.01.-29.12. 117 Data Takes (Ascending only)</p>		
<p><b>Oberpfaffenhofen, Germany</b> DLR/DLR CR-OBE2 GNSS 01.01.-26.12. 60 Data Takes (Descending only)</p>		

All together, the project team ordered 12 transponders from Metasensing BV. 10 out of these 12 are devoted to the project, while 2 transponders owned by DLR will be used for other purpose. Nevertheless DLR offered to implement their 2 transponders calibration purposes at the DLR site in Oberpfaffenhofen.

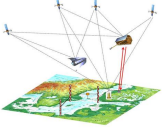
It is required that all transponders are installed in the same orientation (roughly within 1 degree). A common reference point has been defined for the transponders. According to the ECR user manual, the ECR reference point is defined as the point at the bottom of the NW corner of the base plate as shown in Figure 5-2.



**Figure 5-2:** Definiton of the ECR Reference Point (RP); Left picture Copyright MetaSensing BV.

Apart from the site location criteria the network design also considered the possibility to perform a number of specific experiments. Such experiments mostly are defined by connecting different ECR stations and to check if and how good a height transfer between these stations can be performed. A second criteria was to identify possible calibration stations, where additional satellite positioning capabilities are available (e.g. permanent GNSS station). This led to the following station selection.

**ECR Calibration:** Two DLR owned transponders are installed at the DLR premises in Oberpfaffenhofen as calibration stations. Both transponders are close to a permanent GNSS station. Additionally, the transponder locations were surveyed by a local campaign with high precision GNSS receivers. At the calibration site there are also available conventional corner reflectors, which can be used as well (refer to station description for Oberpfaffenhofen shown in Table 5-1).

	<b>BALTIC+ Theme 5</b>  Geodetic SAR for Baltic Height System Unification and Baltic Sea Level Research	<b>Final Report</b> Doc. Nr: SAR-HSU-SR-0022 Issue: 1.1 Date: 07.07.2021 Page: 31 of 170
---	--	--

**Collocation Sites:** Some ECRs are installed at collocation sites with local ties to a tide gauge and a permanent GNSS station. In particular these are the stations in Władysławowo and Łeba in Poland and Spikarna/Vinberget in Sweden.

**Tide Gauge Sites:** A number of tide gauges is equipped with ECRs. These stations are linked to permanent GNSS stations by using the ECRs. These are the stations in Emäsalo and Rauma in Finland, Loksa in Estonia and Forsmark/Kobben in Sweden.

**Permanent GNSS Network Sites:** Several ECRs are installed next to permanent GNSS stations and used for coordinate transfer from the GNSS station via the ECRs to the tide gauge stations. These are the stations Vergi in Estonia, Mårtsbo, in Sweden and Loviisa in Finland.

With these ECR stations and co-located GNSS and/or tide gauge stations a number of experiments can be conducted, which are described in the following:

**Long Baseline Experiment:** Long baseline experiments crossing the Baltic Sea.

- Emäsalo to Loksa (North-South baseline) – tide gauge to tide gauge baseline with GNSS station connection of both tide gauge stations (Loviisa to Emäsalo, Vergi to Loksa)
- Spikarna/Vinberget to Rauma and Forsmark/Kobben to Rauma (East-West baselines) – tide gauge to tide gauge baselines with GNSS connection of Swedish station.

**Short Baseline Experiment:** Several experiments with short baselines are possible by which the coordinate transfer from a GNSS station to a tide gauge station is tested.

- Finland: GNSS Loviisa to Emäsalo tide gauge
- Estonia: GNSS station Vergi to Loksa tide gauge
- Sweden: GNSS station Mårtsbo to Forsmark tide gauge
- Poland: GNSS station Władysławowo to Łeba

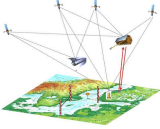
**Tide Gauge Linking Experiment:** Two nearby tide gauges are directly linked by means of ECRs.

- Poland: Władysławowo tide gauge to Łeba tide gauge

**Absolute versus Relative Coordinate Transfer:** Coordinate transfer between two nearby ECRs is done either by absolute or by relative positioning technique. This only considers ECR to ECR coordinate transfer disregarding local ties.

- Poland: Władysławowo to Łeba
- Sweden: Mårtsbo to Forsmark
- Estonia: Vergi to Loksa
- Finland: Loviisa station to Emäsalo

In section 8.7 results for selected experiments are shown. It shall be noted that not all planned experiments could have been executed as the performance of the ECR transponders did not meet expectations. For details about the ECR performance and the impact it is referred to section 10.1.

	<b>BALTIC+ Theme 5</b> Geodetic SAR for Baltic Height System Unification and Baltic Sea Level Research	<b>Final Report</b> Doc. Nr: SAR-HSU-SR-0022 Issue: 1.1 Date: 07.07.2021 Page: 32 of 170
---	--	--

## 6 BASIC ALGORITHMS

### 6.1 SAR Data Analysis and Value Adding

#### 6.1.1 Introduction

The SAR data analysis algorithms are responsible for preparing the geometric SAR observations to support global positioning of the ECRs installed at tide gauges or at reference markers. This involves accurate extraction of all ECR locations from the acquired Sentinel-1 level 1 single-look complex (SLC) images as well as preparation of dedicated corrections. These corrections comprise the Sentinel-1 systematic effects not accounted for during SAR image generation, the atmospheric path delays, and the solid Earth deformation signals associated with global geodetic reference frames. Moreover, systematic effects of the ECRs need to be calibrated (internal signal delay, eccentricity of antennas). The applied computation methods require as data input the SLC Sentinel-1 SAR images, the Sentinel-1 precise orbit solution, the global total electron content (TEC) maps based on GNSS, and the global gridded data for the Vienna mapping function (VMF) model. Table 2 1 summarizes the datasets and their sources.

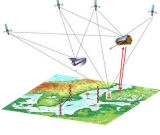
**Table 6-1:** External data sets required for SAR data analysis and value adding algorithms.

Dataset	Provider	Format	Description
Sentinel-1 L1 Images	ESA, Copernicus Open Access Hub <a href="https://scihub.copernicus.eu">https://scihub.copernicus.eu</a>	SAFE	Sentinel-1 images acquired for the Baltic sea area in the Interferometric Wide-Swath mode; single-look complex level 1 products
Sentinel-1 precise orbit product	ESA PDGS, Sentinel-1 Quality Control <a href="https://scihub.copernicus.eu/gnss">https://scihub.copernicus.eu/gnss</a>	XML	Sentinel-1 precise state vectors (position & velocity) with 10s sampling; provided as daily files spanning 26 hours (1 hour daily boundary overlaps)
Global TEC maps	IGS, Center for Orbit Determination in Europe <a href="https://www.igs.org/products">https://www.igs.org/products</a>	IONEX	Global total electron content (TEC) maps with 5° by 5° spatial resolution and 1 hour temporal resolution; files provided as daily data cubes
VMF3 gridded products	TU Vienna <a href="https://vmf.geo.tuwien.ac.at/">https://vmf.geo.tuwien.ac.at/</a>	ASCII	Global gridded parameter data for Vienna mapping function model; 1° by 1° spatial resolution and 6 hours temporal resolution; one file per timestamp (00h, 06h, 12h, 18h)

The overall processing scheme is outlined in Figure 6-1. The analysis system uses the database file containing the approximate coordinates of all the installed ECRs to download the applicable SAR image products by querying the Copernicus Open Access Hub. The approximate ECR positions (1 meter or better) are determined during installation, e.g., through differential GNSS, or derived from mapping data. Orbit products matching the dates of the SAR images are obtained from the Sentinel-1 PDGS quality control website. Same procedure is applied to the atmospheric model data for which the files corresponding to the date of the SAR product are downloaded and ingested into the system. This process is carried out on a routine basis during the project period in order to supply the SAR data files for ECR position computation.

The subsequent sections describe the methods and algorithms applied for each installed ECR to generate the information stored in the SAR data files:

- *Point target analysis:* extraction of the ECR raw SAR timings and azimuth ( $\tilde{\tau}$ ,  $\tilde{\ell}$ ) from the Sentinel-1 level 1 SLC image products.
- *Sentinel-1 system effects:* computation of corrections for the bistatic shifts in azimuth, for the Doppler shifts in range, and for the azimuth shifts due to azimuth FM-rate mismatch ( $\Delta t_{BAC}$ ,  $\Delta t_{DRC}$ ,  $\Delta t_{FMMC}$ ). The raw SAR timings are corrected for these effects and stored in the SAR observation file as  $(\tau, t)$ . In addition, the raw SAR timings and the correction values are preserved in a separate file to maintain traceability of all applied corrections. The corrections are approximately 2-4 m (bistatic azimuth shifts),  $\pm 0.4$  m (Doppler shifts in range), and up to 1 m (FM-rate mismatch shifts).
- *Tropospheric delay correction:* evaluation of the VMF3 model for ECR location at date and time of the SAR acquisitions to obtain the tropospheric delays in slant range ( $\Delta \tau_{tro}$ ). The delays are stored in a dedicated correction file matching the observation file. The slant range tropospheric delays are on the order of 3 meters.
- *Ionospheric delay correction:* interpolation of the TEC maps for ECR location at date and time of the SAR acquisitions to derive the ionospheric delays in slant range ( $\Delta \tau_{ion}$ ). The delays are stored in a dedicated correction file matching the observation file. The slant range ionospheric delays in Sentinel-1 C-band may reach up 0.5 m.

	<b>BALTIC+ Theme 5</b> Geodetic SAR for Baltic Height System Unification and Baltic Sea Level Research	<b>Final Report</b> Doc. Nr: SAR-HSU-SR-0022 Issue: 1.1 Date: 07.07.2021 Page: 33 of 170
---	--	--

- *Solid Earth effects correction*: evaluation of geophysical models describing the tidal-related surface deformations as defined in the conventions of the geodetic ITRF. The cumulative 3D deformation is computed for ECR location at date and time of the SAR acquisitions which is converted into SAR slant range and azimuth corrections ( $\Delta\tau_{sec}, \Delta t_{sec}$ ). The corrections are stored in a dedicated correction file matching the observation file. The combined effect is up to 0.3 m.
- *ECR system corrections*: modelling of the ECR systematic effects that affect the SAR range and azimuth observations. Signal delay caused by the ECR electronics, eccentricities of ECR transmission and reception antennas, and possibly other unknown effects have to be converted into range and azimuth correction values ( $\Delta\tau_{ecr}, \Delta t_{ecr}$ ). The corrections are stored in a dedicated ECR correction file.

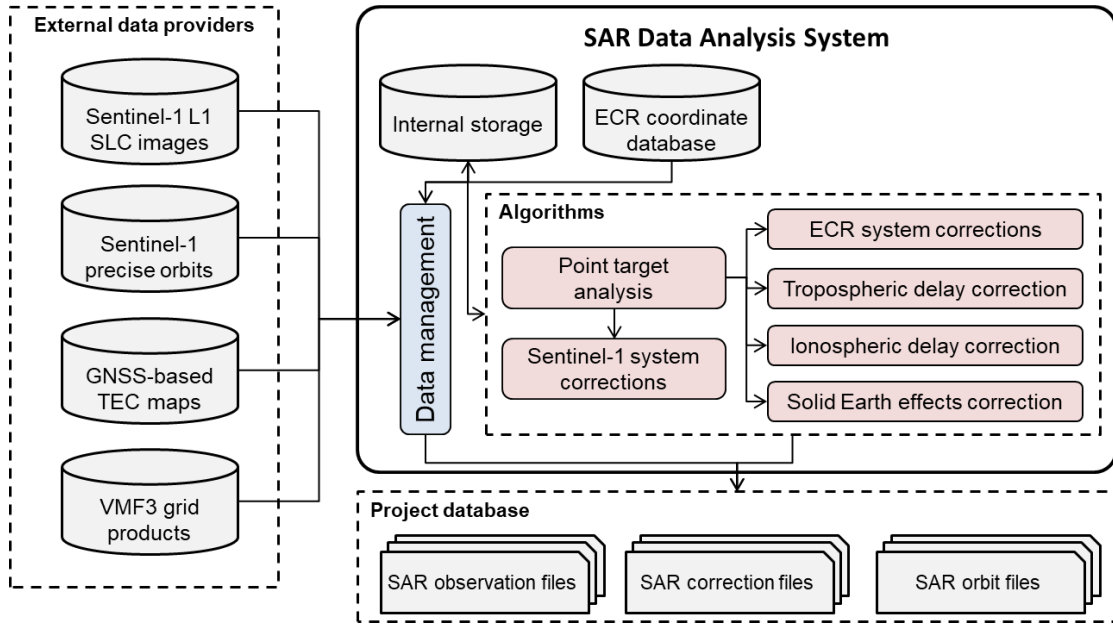


**Figure 6-1:** SAR data analysis system. Data sets and output files are marked in grey. Red boxes refer to methods and algorithms

The corrections are computed by the algorithms and stored in the files such that they can be applied as follows:

- *Sentinel-1 system effects*: to compute accurate radar timings obeying zero-Doppler convention the raw SAR timings are corrected as follows:

$$\begin{aligned}\tau &= \tilde{\tau} + \Delta\tau_{DRC} \\ t &= \tilde{t} + \Delta t_{BAC} + \Delta t_{FMMC}\end{aligned}\quad (6.1)$$

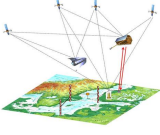
- *Correction of atmospheric, solid Earth, and ECR effects*: to remove the atmospheric path delays, the conventionally defined solid Earth displacements, and the ECR-related systematic effects from the ECR observations the corrections are applied as follows:

$$\begin{aligned}\tau_{corrected} &= \tau - \Delta\tau_{tro} - \Delta\tau_{ion} - \Delta\tau_{sec} - \Delta\tau_{ecr} \\ t_{corrected} &= t - \Delta t_{sec} - \Delta t_{ecr}\end{aligned}\quad (6.2)$$

### 6.1.2 SAR Image Point Target Analysis

Single isolated point scatterers like the ECRs represent the impulse response of the SAR system. They appear as sinc-like functions that spread over several pixels in cross-shaped signatures and can be accurately localized in the image grid. The determination of signature locations in the SLC image is part of the point target analysis (PTA). It yields not only the sub-pixel position, but can be also used to derive further quality parameters like the impulse response width (a measure for the image resolution) or the peak sidelobe ratio (a measure for the contrast) (Cumming and Wong, 2005).

Assuming a given image resolution of 1 m and aiming at a SAR measurement accuracy on the order of 1 cm, then the PTA must provide the peak location with about 1/100 of a pixel. An efficient way to achieve such a precision is to apply spectral zero padding for the image subset containing the point target signature. This corresponds to an oversampling of the complex data using a sinc-like interpolator. The oversampling factor is equivalent to the number of inserted zeros, but

	<b>BALTIC+ Theme 5</b> Geodetic SAR for Baltic Height System Unification and Baltic Sea Level Research	<b>Final Report</b> Doc. Nr: SAR-HSU-SR-0022 Issue: 1.1 Date: 07.07.2021 Page: 34 of 170
---	--	--

large numbers of 1024 or 2048 lead to a computationally expensive inverse Fourier transformation of the padded spectrum. This can be overcome by performing a two-step procedure as suggested in Stein 1981. Firstly, one performs moderate oversampling of a factor of 32 to determine a coarse peak location. Secondly, this peak location is refined by fitting an analytical paraboloid surface to the moderately oversampled central peak area.

Consequently, the procedure is applied as follows (see Figure 6-2). The approximate location of the ECR is projected into the SAR image and a search space of  $32 \times 32$  pixels is defined around this location. Within this area, the maximum amplitude pixel is determined and the patch is centered w.r.t. this position. Following the FFT of this patch defined as complex number  $(I + iQ)$ , with  $I$  and  $Q$  denoting the complex SAR image bands, the zeros are inserted (32 in both dimensions) at spectral minimum in order to generate an oversampled patch after computation of the inverse FFT. Finally, an elliptic paraboloid of the shape

$$f(i, j) = a_0 + a_1(i - m_i)^2 + a_2(j - m_j)^2 + a_3(i - m_i)(j - m_j) \quad (6.3)$$

is fitted (least squares adjustment) to the central  $3 \times 3$  pixel of oversampled maximum amplitude to refine peak location. The  $i$  and  $j$  denote the pixel indices,  $a_{0,1,2,3}$  are the coefficients of the paraboloid, and  $m_i$  and  $m_j$  are the refined pixel indices of the peak location. The subpixel peak position is converted into radar timings by using the SAR image annotation, i.e. first sample azimuth time and range time as well as the range sampling frequency and the azimuth time interval.

From our tests comparing zero-padding with high oversampling factors (2048, 4096) against the two step approach we can confirm that the latter method is capable of maintaining the required accuracy of better than 1/100th of a pixel (Bals et al., 2012).

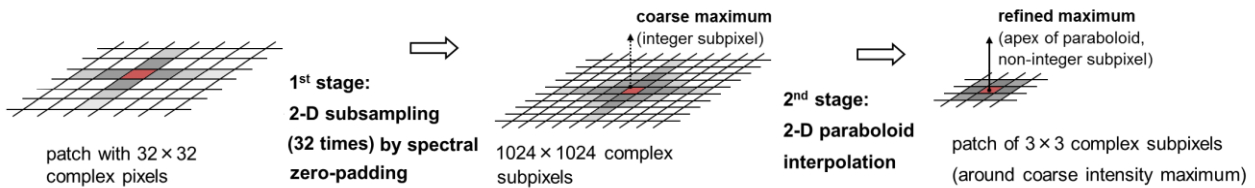


**Figure 6-2:** Subpixel-level target location extraction by applying spectral zero padding and fitting of a paraboloid

### 6.1.3 Sentinel-1 Systematic Effects Correction

The Sentinel-1 system specific corrections deal with the sub-pixel level deviation of the IPF SLC product annotation from the conventional zero-Doppler SAR geometry. The corrections allow the refinement of the  $t$  and  $\tau$  annotation by post-processing without modifying the actual SLC image. Because of the TOPS mode (Terrain Observation with Progressive Scans) used by Sentinel-1 to generate the IW and EW products, these corrections have to be computed following the internal SAR data structure (swathes and burst; Bourbigot et al, 2015). Three corrections are required (Piantanida et al., 2018, Gisinger et al., 2020):

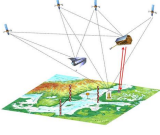
- Bistatic effects in azimuth: correction for the movement of the platform between pulse transmission and echo reception (quasi-bistatic situation); up to 4 meters in azimuth
- Doppler shifts in range: removal of the Doppler frequency shifts in the range pulses;  $\pm 0.4$  meter in range
- FM-rate mismatch in azimuth: removal of the shifts caused by the mismatch of the azimuth FM-rate used by the processor (assuming a constant scene height) and the true azimuth FM-rate for target position; up to 1 meter in azimuth

The computation of these corrections only requires the Sentinel-1 product annotation.

#### Bistatic effects in azimuth

The movement of the Sentinel-1 satellites between pulse transmission and echo reception approximately amounts to 30-40 m. This quasi-bistatic situation is commonly neglected in digital SAR processing when focussing the raw image data with spectral methods applying the stop-and-go approximation: it is assumed that the satellite stops between transmission and reception of a single pulse and only moves after each cycle. The stop-and-go approximation is beneficial for efficient SAR processing, but the implications have to be carefully considered in order to generate SAR images of rigorous zero-Doppler geometry, i.e. with orthogonal  $t$  and  $\tau$  (azimuth and range) annotation. The Sentinel-1 IPF applies a simple shift (referred to as "bulk correction") to modify the azimuth timing annotation because of the assumed stop-and-go situation. This leads to sub-pixel distortions and range dependent shifts of 2-4 m in the azimuth measurements of Sentinel-1 IW products (Piantanida et al., 2018, Gisinger et al., 2020b).

The post-processing correction of the stop-and-go approximation removes the original IPF bulk shift and applies the rigorous correction (Gisinger et al., 2020b). For the extracted ECR location in an image  $(\tilde{r}, \tilde{t})$  the computation reads:

	<b>BALTIC+ Theme 5</b> Geodetic SAR for Baltic Height System Unification and Baltic Sea Level Research	<b>Final Report</b> Doc. Nr: SAR-HSU-SR-0022 Issue: 1.1 Date: 07.07.2021 Page: 35 of 170

$$\Delta t_{BAC} = \frac{\tau_{mid}}{2} + \frac{\tilde{\tau}}{2} - rank \cdot PRI \quad (6.4)$$

with:

$\tau_{mid} / 2$  the IPF bulk correction using the mid-range time of the swath, i.e.:  $\tau_{mid}$  of the SM product;  $\tau_{mid,IW2}$  for the IW product; and  $\tau_{mid,EW3}$  for the EW product;

$rank, PRI$  = rank (number of travelling pulses) and pulse repetition interval as given in the annotation of the applicable beam (SM, IW1-3, EW1-5).

An example for the correction across three bursts of a Sentinel-1 IW product is shown in Figure 6-3:

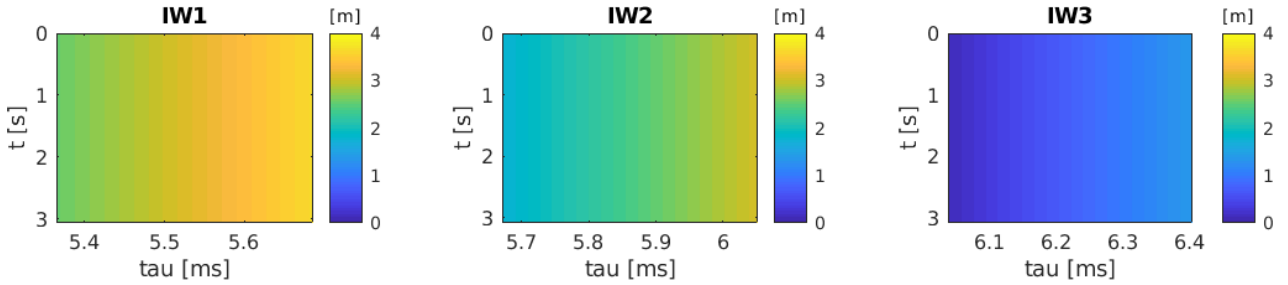


**Figure 6-3:** Bistatic azimuth correction for TOPS bursts of the three sub-swaths IW1, IW2 and IW3 of a Sentinel-1 IW product. Results scaled to meter. The correction changes significantly when computed across the entire IW TOPS swath, as the Sentinel-1 sensor adapts the pulse repetition frequency (inverse of the PRI) and the rank according to the slant range distance of the swaths IW1, IW2 and IW3.

### Doppler shifts in range

The transmitted radar pulses experience frequency shifts from the Doppler effect caused by the movement of the satellite. These shifts are usually ignored by SAR image processing, because the effect cancels almost completely for SAR modes with azimuth spectra close to zero-Doppler, e.g., stripmap SAR with zero-Doppler steering. However, for the TOPS mode used by Sentinel-1, which generates data with large Doppler centroid variations across the bursts, the impact of the Doppler shift becomes significant, especially towards the edge of the bursts where the Doppler effect is maximum. During spectral range compression performed by the Sentinel-1 IPF, the Doppler frequency leads to a proportional spatial shift of the compressed pulses. This cannot be handled by the matched filter, because at this stage the pulse echo data contain all the superimposed Doppler shifts of the entire swath. Consequently, the shifts have to be removed at later stage in the SAR processor, but the Sentinel-1 IPF processor does not consider the effect for the IW and EW data.

The post-processing correction  $\Delta \tau_{DRC}$  requires the reconstruction of the Doppler centroid  $f_{DC}$  depending on the ECR location  $(\tilde{x}, \tilde{\tau})$  in the image, which has to consider the additional beam steering carried out for the TOPS mode.

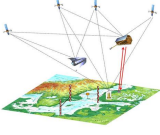
$$\Delta \tau_{DRC} = \frac{f_{DC}}{K_r} \quad (6.5)$$

$K_r$  is the FM-rate of the range chirp and is explicitly annotated in the products. The Doppler centroid is obtained as follows (Miranda 2015):

$$\begin{aligned} f_{DC} &= f_{DC,g}(\tilde{\tau}) + k_t(\tilde{\tau}) \cdot (\tilde{t} - t_{mid}) \\ f_{DC,g}(\tilde{\tau}) &= a_0 + a_1(\tilde{\tau} - \tau_0) + a_2(\tilde{\tau} - \tau_0)^2 \\ k_t(\tilde{\tau}) &= \frac{k_a(\tilde{\tau}) \cdot k_s}{k_a(\tilde{\tau}) - k_s} \\ k_a(\tilde{\tau}) &= b_0 + b_1(\tilde{\tau} - \tau_0) + b_2(\tilde{\tau} - \tau_0)^2 \\ k_s &= \frac{2v_s}{c} \cdot f \cdot k_\psi \end{aligned} \quad (6.6)$$

where:

- $f_{DC,g}$  = annotated Doppler centroid frequency at ECR location
- $k_t$  = Doppler rate of focused SLC data [Hz/s]
- $k_a$  = annotated azimuth FM-rate [Hz/s]
- $k_s$  = Doppler rate introduced by antenna steering [Hz/s]
- $a_{0,1,2}$  = annotated coefficients of the Doppler centroid polynomials

	<b>BALTIC+ Theme 5</b> Geodetic SAR for Baltic Height System Unification and Baltic Sea Level Research	<b>Final Report</b> Doc. Nr: SAR-HSU-SR-0022 Issue: 1.1 Date: 07.07.2021 Page: 36 of 170
---	--	--

$b_{0,1,2}$  = annotated coefficients of the azimuth FM-rate polynomial s  
 $\tau_0$  = reference range time of the annotated polynomials [s]  
 $t_{mid}$  = mid azimuth time of burst for which the parameters are evaluated  
 $f$  = the Sentinel-1 radar frequency [Hz]  
 $c$  = speed of light in vacuum [m/s]  
 $v_s$  = satellite velocity (from precise orbit file) [m/s]  
 $k_\psi$  = antenna beam steering rate [rad/s]

Note that the polynomial coefficients are also dependent on the azimuth time  $t$  and therefore the respective quantities have to be computed for the given ECR image position.

Figure 6-4 shows an example spanning across three bursts of an IW product. Because of the adaptation of antenna steering rate and chirp FM-rate, the slope of the correction changes across the different sub-swaths, and also from near range to far range because of the varying sensor-to-ground geometry.

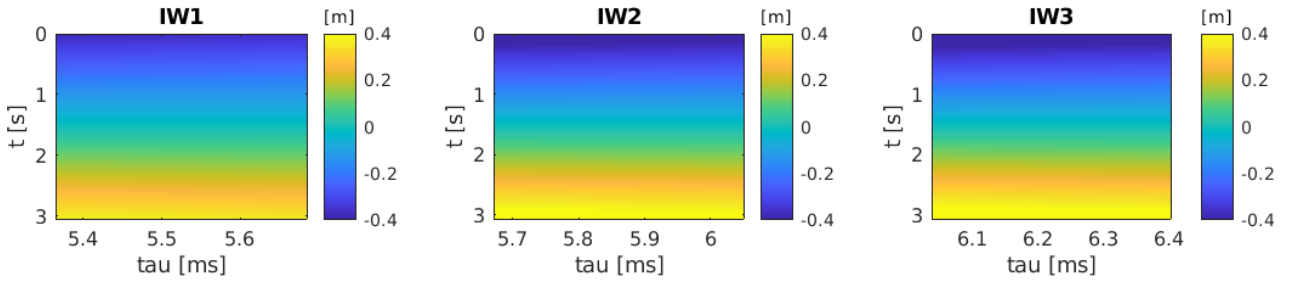


**Figure 6-4:** Correction of the Doppler shift in the ranges for TOPS bursts of the three sub-swaths IW1, IW2 and IW3 of a Sentinel-1 IW product. Results scaled to meter one-way slant range

#### Azimuth shifts due to FM-rate mismatch

Spectral focussing of the azimuth signal requires the reconstruction of the azimuth FM-rate, which is driven by the sensor-to-ground geometry. The change with distance (range) is modelled with sufficient detail when defining the matched filter. However, the effective velocity parameter underlying the azimuth FM-rate computation is kept constant during the processing of large azimuth blocks. These blocks comprise up to several seconds in azimuth dimension, e.g., the 3s burst size of Sentinel-1 IW data. For the stripmap SAR mode with zero-Doppler steering, the effect of the mismatch (quadratic phase error) is mainly a blurring of the image (defocussing), whereas for the Sentinel-1 IW and EW modes the outcome is a shift in azimuth. Shifts of up to 1m were found at the edge of the burst if the assumed height in the computation of the azimuth FM-rate deviates about 1000 m.

The correction of the FM-rate mismatch requires the computation of the Doppler centroid  $f_{DC}$ , the azimuth FM-rate  $k_a$  used by the Sentinel-1 IPF, and the true azimuth FM-rate  $k_{a,true}$  derived from the orbit and the ECR coordinates.

$$\Delta t_{FMMC} = -f_{DC} \cdot \left( \frac{1}{-k_a(\tilde{\tau})} - \frac{1}{-k_{a,true}} \right) \quad (6.7)$$

The computation for the Doppler centroid and the IPF azimuth FM-rate at ECR location  $(\tilde{t}, \tilde{\tau})$  is given in equation (6.6). The true azimuth FM-rate is calculated as:

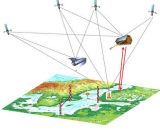
$$k_{a,true} = -\frac{2}{\lambda \cdot |X_S - X_{ECR}|} \left[ (X_S - X_{ECR}) \cdot \ddot{X}_S + \dot{X}_S \cdot \dot{X}_S \right] \quad (6.8)$$

with

$\lambda$  = wavelength of Sentinel-1 SAR carrier signal [m]  
 $X_{ECR}$  = position vector of the ECR [m]  
 $X_S, \dot{X}_S, \ddot{X}_S$  = Sentinel-1 orbit state vector corresponding to ECR zero-Doppler [m, m/s, m/s<sup>2</sup>]

#### 6.1.4 Tropospheric Delay Correction

The tropospheric delay correction makes use of the Vienna Mapping Function (VMF3) model. The VMF3 is the latest development in a series of widely used mapping functions to convert tropospheric zenith path delays into slant path delays, which also provides tropospheric delays from numerical weather data integration allowing for observation correction (Landskron and Böhm, 2018a).

	<b>BALTIC+ Theme 5</b>  Geodetic SAR for Baltic Height System Unification and Baltic Sea Level Research	<b>Final Report</b> Doc. Nr: SAR-HSU-SR-0022 Issue: 1.1 Date: 07.07.2021 Page: 37 of 170

The time-dependent VMF3 coefficients are computed from zenith path and slant range path integrations of the operational numerical weather model of ECMWF. For each grid location, the slant path integration is performed for 8 equally spaced horizontal directions ( $0^\circ, 45^\circ, \dots, 360^\circ$ ), covering the anisotropy of the atmosphere (Landskron and Böhm, 2018a). This anisotropy is converted into a horizontal gradient model also provided with the grids. The spatial resolution of the gridded VMF3 solution is  $1^\circ$  by  $1^\circ$  (approximately 110 by 110 km) and the temporal sampling is in line with operational ECMWF model (00, 06, 12, 18 UT). The grids are offered as a service by Vienna Technical University with a timeliness of less than 1 day.

The primary goal of the VMF3 is the *a priori* modelling of the path delays for the space geodetic techniques, which estimate the turbulent wet delay when computing the position. However, the integrated path delays, the mapping function, and the horizontal gradient also provide a mean to efficiently model the tropospheric path delay at a global scale. Figure 6-5 shows an example for the zenith delays provided with the VMF3 product.

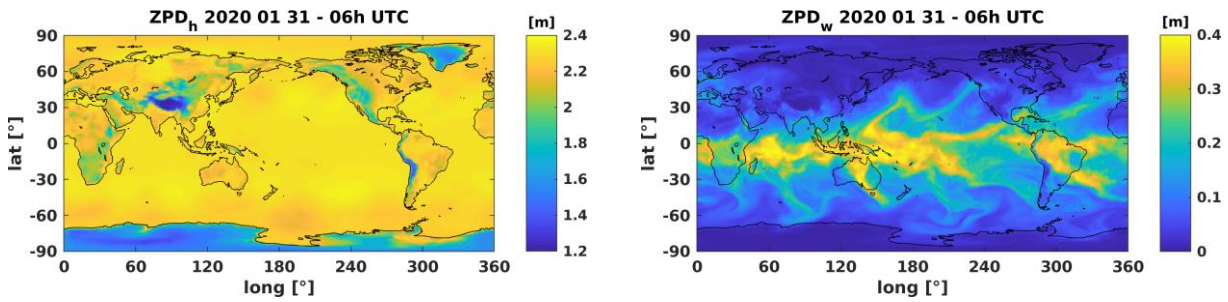


**Figure 6-5:** Examples for the global grids ( $1^\circ \times 1^\circ$ ) of hydrostatic path delay (left) and wet path delay (right) distributed with the VMF3 model

The tropospheric slant delay computation from the VMF3 product is defined as (Landskron and Böhm, 2018a, Landskron and Böhm, 2018b):

$$\Delta\tau_{tro} = (zpd_h \cdot MF_h + zpd_w \cdot MF_w + \Delta L_h + \Delta L_w) \cdot 2 / c \quad (6.9)$$

where  $zpd$ ,  $MF$ , and  $\Delta L$  denote the zenith path delay, the mapping function, and the horizontal gradient contribution, respectively. All computations are performed separately for the hydrostatic and wet path delay (subscripts  $h, w$ ). Conversion to delay in units of seconds uses the speed of light  $c$ . The mapping functions solely depend on the elevation  $E$  as inferred from the sensor-to-ground LOS:

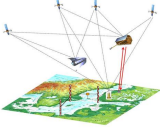
$$MF_{h,w}(E) = \frac{1 + \frac{a}{b}}{1 + c} \cdot \frac{\sin(E) + \frac{a}{\sin(E) + \frac{b}{\sin(E) + c}}}{\sin(E) + \frac{b}{\sin(E) + c}} \quad (6.10)$$

where the coefficients  $a, b, c$  are independently provided for the wet ( $w$ ) and the hydrostatic ( $h$ ) version of the function. The two sets of  $b$  and  $c$  coefficients are pre-defined through empirical models that were computed with least squares adjustments fitting 9 years of monthly ray-traced ECMWF data on global  $5^\circ$  by  $5^\circ$  grid (Landskron and Böhm, 2018a). The more demanding parameters are the  $a$  coefficients, which need to be updated on a daily basis by using the operational ECMWF model. The Vienna University of Technology computes these  $a$  coefficients as global grids with 6 hour temporal sampling together with integrated ZPDs (hydrostatic and wet delays in units of meters, 1-way) and the horizontal gradient components  $G_n$  and  $G_e$  (north, east). Using the azimuth  $A$  defined by the sensor-to-ground LOS, the gradient contributions are computed as (Landskron and Böhm, 2018b):

$$\Delta L_{h,w} = MF_{h,w} \cdot [G_n \cdot \cos(A) + G_e \cdot \sin(A)] \quad (6.11)$$

To apply equation (6.9), the model information (delays, gradient components,  $a$ -coefficients) is interpolated in space and time (trilinear interpolation) for the location and acquisition of the ECRs. This requires the two VMF3 products to enclose the time of the ECR observation.

While this interpolation step resolves the temporal and horizontal dimensions, special care must be taken for the vertical dimension. The vertical integration of the ECMWF model is performed with respect to a global elevation model

	<b>BALTIC+ Theme 5</b> Geodetic SAR for Baltic Height System Unification and Baltic Sea Level Research	<b>Final Report</b> Doc. Nr: SAR-HSU-SR-0022 Issue: 1.1 Date: 07.07.2021 Page: 38 of 170
---	--	--

(*orography\_ell*) having a resolution of  $1^\circ$  by  $1^\circ$ . The height difference of the ECR with respect to this underlying elevation model has to be taken into account to derive proper slant path delays for the observed SAR ranges.

In order to transform the hydrostatic ZPD, the delay is first converted to its corresponding pressure value, which is updated for the height difference between the station and the elevation grid. Converting the modified pressure back to path delay yields the hydrostatic ZPD. The wet ZPD is directly obtained through an empirical decay law that accounts for the height difference. The details of the height correction are given in (Kouba, 2008):

$$p(h_g) = \frac{zpd_h(h_g)}{0.0022768} \left( 1 - 0.00266 \cos(2\varphi_{ECR}) - 0.28 \cdot 10^{-6} h_g \right) \quad (6.12)$$

$$p(h_{ECR}) = p(h_g) \cdot \left( 1 - 0.0000226(h_{ECR} - h_g) \right)^{5.225} \quad (6.13)$$

$$zpd_h(h_{ECR}) = 0.0022768 \frac{p(h_{ECR})}{1 - 0.00266 \cos(2\varphi_{ECR}) - 0.28 \cdot 10^{-6} h_{ECR}} \quad (6.14)$$

$$zpd_w(h_{ECR}) = zpd_w(h_g) \cdot e^{-\frac{(h_{ECR} - h_g)}{2000}} \quad (6.15)$$

where:

$zpd_h$  = hydrostatic ZPD at ECR location

$zpd_w$  = wet ZPD at ECR location

$p$  = pressure in millibar

$\varphi_{ECR}$  = ECR geodetic latitude (WGS-84 ellipsoid)

$h_{ECR}$  = ellipsoidal height of ECR (WGS-84 ellipsoid)

$h_g$  = height of the VMF3 elevation model (*orography\_ell*) at ECR location

In a similar way, also the hydrostatic mapping function is corrected for the height difference  $\Delta h$  by applying the differential correction (Niell, 1996):

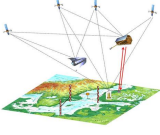
$$\overline{MF}(E) = MF_h(E) + \Delta h \cdot \left( \frac{1}{\sin E} - MF(E, \bar{a}, \bar{b}, \bar{c}) \right) \quad (6.16)$$

where the equation (6.10) is evaluated using empirical correction coefficients,  $\bar{a} = 2.53 \cdot 10^{-5}$ ,  $\bar{b} = 5.49 \cdot 10^{-3}$ ,  $\bar{c} = 1.14 \cdot 10^{-3}$ . For the hydrostatic gradient components, such a correction is not available in existing literature and therefore the gradient model equation (6.11) is applied as interpolated for the location of the ECRs.

### 6.1.5 Ionospheric Delay Correction

The ionization of the upper part of Earth's atmosphere (about 50 to 1500 km altitude) is driven by solar radiation. This region is referred to as ionosphere and contains free electrons and charged particles, which cause frequency dependent (dispersive) path delays for microwave signals. Peak concentration of electrons and charged particles occurs around an altitude of 400 km (Böhm and Schuh, 2013).

As in the case of SAR, the L-band carrier signals of GNSS are sensitive to the ionospheric delay, but simultaneous observations with two or more frequencies enables the GNSS to determine the ionospheric delay. This ability is exploited to generate global ionospheric maps from the GNSS observations of the global IGS network (Schaer, 1999, Hernández-Pajares, 2009). Several analysis centers generate such maps for the International GNSS Service (IGS), which are averaged for the official IGS product (Hernández-Pajares, 2009). However, the product by the Center of Orbit Determination in Europe (CODE) is used because of the underlying methodology. Its computation is based on a consistent least squares inversion of daily GNSS observations that yields not only the  $vTEC$  maps but also the corresponding RMS information (Schaer, 1999). The latter is used to quantify the error in the ionospheric path delay correction. Figure 6-6 shows an example of the  $vTEC$  distribution at 12 UTC extracted from the CODE product of January 31<sup>st</sup> 2020. The main bulge trails the location of the sun by about two hours, i.e. it is always located around 2PM local time. Sentinel-1 uses a sun-synchronous orbit in dusk-dawn configuration, which leads to equator crossings around 6AM and 6PM local time, causing the satellites to cross either ahead of the main bulge or behind the bulge in its tail region. This leads to typical TEC values of approximately 20-30 TECU (1 TECU =  $10^{16}$  electrons per  $m^2$ ), or 0.3 to 0.4 meters when converted to delays in Sentinel-1 C-band.

	<b>BALTIC+ Theme 5</b> Geodetic SAR for Baltic Height System Unification and Baltic Sea Level Research	<b>Final Report</b> Doc. Nr: SAR-HSU-SR-0022 Issue: 1.1 Date: 07.07.2021 Page: 39 of 170

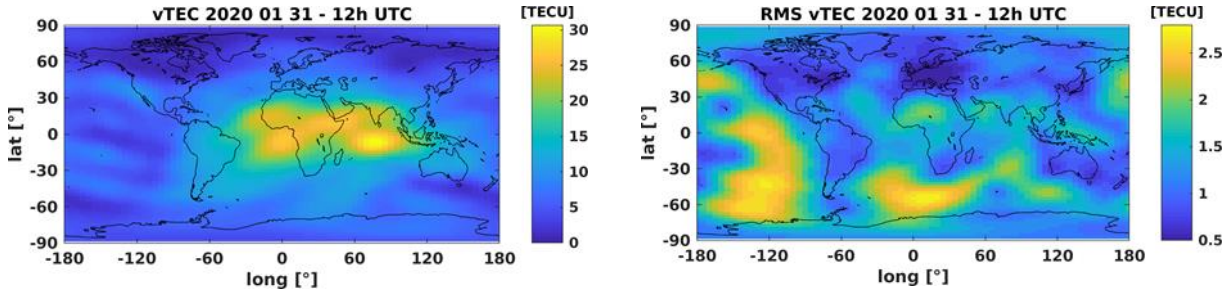


**Figure 6-6:** Examples for the global TEC maps computed by CODE. TEC map (left) and TEC RMS map (right).

The GNSS-based ionospheric modelling uses the total electron content, because it is independent of the frequency. Therefore, the TEC can be readily scaled to frequency-dependent delays for Sentinel-1 by applying the first order ionospheric model underlying the TEC map generation (Schaer, 1999):

$$\Delta\tau_{ion} = \frac{40.3 \cdot 10^{16}}{f^2} \cdot vTEC \cdot MF(z') \cdot \alpha \cdot \frac{2}{c} \quad (6.17)$$

where:

- f = the Sentinel-1 radar frequency [Hz]
- vTEC = total number of electrons (vertical) in TEC units (1 TECU =  $10^{16}$  electrons per  $m^2$ )
- MF( $z'$ ) = mapping function for conversion into slant delay using the zenith angle  $z'$
- $\alpha$  = scaling of vTEC due to Sentinel-1 orbit altitude (set to 0.9)
- c = speed of light in vacuum [m/s]

The method of the TEC modelling is illustrated in Figure 6-7. It consists of a single spherical layer assumed at the altitude of the maximum electron concentration (specified with 450 km in the CODE product), which contains the total number of vertically integrated electrons, i.e. the vTEC. For the known ECR position, the vTEC is interpolated at the ionospheric pierce point (IPP) defined by the analytical LOS intersection with the spherical layer as given in the product (Figure 6-7). Because the original determination of the global vTEC is carried out in a solar fixed frame, each map was rotated for the earth fixed frame according to the 1 hour temporal sampling interval (Schaer et al., 1998). Therefore, the temporal interpolation for the azimuth times of the ECR should take into account this time variant transformation by accordingly modifying the longitude argument for the time difference  $T_i - t$  with respect to the two involved TEC maps (before and after the observation of the ECR at time  $t$ ) (Schaer et al., 1998):

$$vTEC(\varphi, \lambda, t) = \frac{T_{i+1} - t}{T_{i+1} - T_i} vTEC_i(\varphi, \lambda'_i) + \frac{t - T_i}{T_{i+1} - T_i} vTEC_{i+1}(\varphi, \lambda'_{i+1}) \quad (6.18)$$

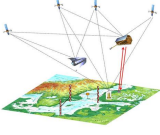
where:

- $T_i \leq t < T_{i+1}$
- $\varphi, \lambda$  = geocentric latitude and longitude of the ionospheric pierce point
- $\lambda'_i = \lambda + (t - T_i) \cdot \omega_e$ , with  $\omega_e = \frac{360^\circ}{24h}$

The spatial interpolation to obtain the  $vTEC_i$  from the gridded maps is performed with a bilinear approach. Finally, the mapping to slant path delay accounts for the spherical model geometry:

$$MF(z') = \frac{1}{\cos(z')} \quad (6.19)$$

with  $z'$  denoting the zenith angle stemming from the LOS intersection with the shell (see Figure 6-7). The actual mapping function remains isotropic – it only depends on  $z'$  – but the vTEC depends on the direction of the LOS through the derivation of the IPP. In order to gauge the model error at the location of the IPP, the RMS of the vTEC is processed like the vTEC itself. Inserting the derived RMS into equation (6.17) yields an estimate for the slant delay error of the computed ionospheric delay.

	<b>BALTIC+ Theme 5</b> Geodetic SAR for Baltic Height System Unification and Baltic Sea Level Research	<b>Final Report</b> Doc. Nr: SAR-HSU-SR-0022 Issue: 1.1 Date: 07.07.2021 Page: 40 of 170

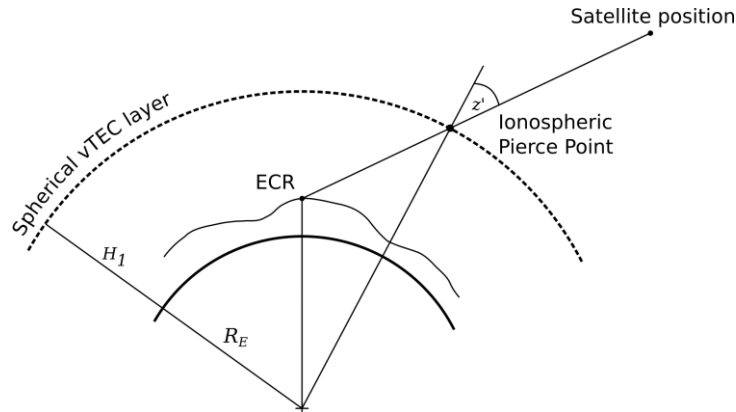


**Figure 6-7:** Concept of the ionospheric mapping function assuming a single layer ionospheric model

An additional point considered in equation (6.17) is the fact that the Sentinel-1 orbit lies still within the upper region of the ionosphere. Strictly speaking, resolving this would require the 3-D distribution of the free electrons and the integration of the electrons along the observed slant-range path. To our knowledge, there is not yet any global model, which can provide such information with sufficient quality. Therefore, we decided for this empirical approach using the scaling parameter  $\alpha$  to resolve this problem to some degree. An extrapolation based on the 75% value found for TerraSAR-X (Balss et al., 2012) yields a scaling of 90% for Sentinel-1.

#### 6.1.6 Solid Earth Effects Correction

During determination of the International Terrestrial Reference Frame (ITRF), the effects of the solid Earth causing displacements of the reference stations are removed by applying conventionally defined geodynamic models. The ITRF is therefore realized through so-called regularized station coordinates representing the average state of the Earth's crust (Petit and Luzum, 2010). Consequently, the observations of targets made by the SAR satellites, which refer to the dynamic state of the Earth's surface at the time of observation, have to be corrected using the same procedures to obtain proper ITRF coordinates from the SAR.

The instantaneous positions of the ECRs during a SAR acquisition are modelled by the displacements computed from the conventional dynamic models at the date and time of SAR observation. These models encompass all the tidal related effects deforming the Earth's crust (solid Earth, ocean, atmosphere) as well as secondary effects related to the dynamics of the Earth's rotational axis, see the overview given in Table 6-2. In total, these effects add up to displacements of approximately 0.3m in the vertical direction and to approximately 0.06m in the horizontal direction. The conventions of IERS (International Earth Rotation and Reference Systems Service) describe in detail all these models and sample programs are provided, which may be used to verify the calculations. Therefore, the models are not repeated here.

All geodynamic models as listed in Table 6-2 have been implemented such that the displacement results can be generated in the global ITRF as differential offsets  $\Delta X_i$  at date, time and position of the ECRs. Thus, the total solid Earth deformation correction  $\Delta X_{sec}$  can be computed as:

$$\Delta X_{sec} = \sum_{i=1}^5 \Delta X_i \quad (6.20)$$

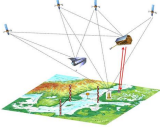
Conversion into corrections for the range and azimuth radar timings is performed by an iterative solution of the SAR range-Doppler equations by usage of the precise orbit data  $(X_s, \dot{X}_s)$ . The Doppler equation (6.21) is solved for zero-Doppler time  $t$  for the given ECR position  $X = X_{ECR}$ , as well as for the given ECR position including the displacement correction  $X = X_{ECR} + \Delta X_{sec}$ . The range equation yields the range time  $\tau$  by inserting the corresponding zero-Doppler satellite position  $X_s(t)$ .

$$\frac{\dot{X}_s(t) \cdot (X - X_s(t))}{|\dot{X}_s(t)| \cdot |X - X_s(t)|} = 0 \quad (6.21)$$

$$\tau = c / 2 \cdot |X - X_s(t)| \quad (6.22)$$

The difference between both timing solutions yields the solid Earth deformation corrections for the SAR observations of the ECRs.

$$\begin{aligned} \Delta \tau_{sec} &= \tau_{ECR} - \tau_{ECR,sec} \\ \Delta t_{sec} &= t_{ECR} - t_{ECR,sec} \end{aligned} \quad (6.23)$$

	<b>BALTIC+ Theme 5</b> Geodetic SAR for Baltic Height System Unification and Baltic Sea Level Research	<b>Final Report</b> Doc. Nr: SAR-HSU-SR-0022 Issue: 1.1 Date: 07.07.2021 Page: 41 of 170
---	--	--

**Table 6-2:** Magnitude of the solid Earth displacement effects based on the geodynamic models listed in the IERS conventions (Petit and Luzum, 2010).

Effect	Horizontal [mm]	Vertical [mm]
Solid Earth tides	± 60.0	± 250.0
Ocean loading	± 10.0	± 50.0
Pole tides	± 1.5	± 6.0
Atmospheric tidal loading	± 0.2	± 1.5
Ocean pole tide loading	± 0.3	± 0.5

### 6.1.7 ECR system corrections

The ECR are active devices that receive and re-transmit the SAR signal coming from the Sentinel-1 satellites. In between, the signal is amplified such that the radar cross section of an ECR is approximately equivalent to a passive triangular trihedral corner reflector with an edge-size of 1.8 meters. The ECR activations are performed for programmed time windows matching either ascending or descending satellite passes (Di Meo et al., 2019).

Internally, the devices consist of four rectangular antennas. Two antennas are oriented towards East direction (one for reception and one for transmission) to support the descending satellite passes, whereas the other two antennas are facing West to support the ascending satellite passes (of right-looking SAR sensors). Consequently, the ECRs need to be mounted horizontally and aligned to geographic North to ensure proper signal response. In this configuration, the antenna boresights are pointing towards the SAR satellites (approximately the mid-swath of the Sentinel-1 and RADARSAT SAR payloads; Di Meo et al., 2019)

The different locations of these antennas as well as the signal delay introduced by ECR electronics have to be taken into account when combining the measurements for SAR positioning. Approximate geometric antenna positions are listed in the ECR-C manual (Di Meo et al., 2019). The electronic delay is presently not characterized and needs to be determined in an experimental calibration setup. As this is the first time these ECRs are used in the field, the methods have to be developed from experience and are not yet fully defined. The selected approach builds on the methods for characterizing the absolute geolocation errors of SAR instrument (Balss et al., 2018, Gisinger et al., 2020a). By validating SAR observations against passive corner reflector targets with known ITRF reference coordinates, the SAR instruments are calibrated for their respective residual payload biases. If this analysis is performed for a reference corner reflector and a close-by ECR with known coordinates, the contributions stemming from the ECR can be characterized.

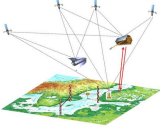
Our current assumption is a comparable behaviour across the different ECRs and therefore we will do such an assessment for a small subset of the installed ECRs, for which the reference coordinates have been determined. Further details will be provided in the version 2.0 of this document.

### 6.1.8 Parameter Summary

Table 6-3 summarizes the input parameters needed for SAR data analysis and the output parameters generated by the processor. In particular, it is described from where the input parameters are taken and for which follow-on processing task the output parameters are needed. Refer also to Figure 6-1 where the internal data flow of this processing task is shown.

**Table 6-3:** Overview of Input/Output Parameters for SAR Data Analysis and Value Adding

Parameter Name	Description	Type	Source (Input)/ Target (Output)	Comment
S1-L1-SLC	Sentinel-1 Level 1 Single Look complex images	Input	ESA Copernicus open access hub	Sentinel-1 images acquired for the Baltic sea area in the Interferometric Wide-Swath mode; single-look complex level 1 products
S1-PSO	Sentinel-1 Precise Orbits	Input	ESA PDGS, Sentinel-1 Quality Control	Sentinel-1 precise state vectors (position & velocity) with 10s sampling; provided as daily files spanning 26 hours (1 hour daily boundary overlaps)
IGS-TEC	Global total Electronic Content Maps	Input	IGS Center for Orbit Determination in Europe	Global total electron content (TEC) maps with 5° by 5° spatial resolution and 1 hour temporal resolution; files provide daily data cubes
VMF3	Vienna Mapping Function Model	Input	Technical University of Vienna	Global gridded parameter data for Vienna mapping function model; 1° by 1° spatial resolution and 6 hours temporal resolution; one file per timestamp (00h, 06h, 12h, 18h)
IERS-2010	IERS Conventions 2010	Input	International Earth Rotation and	Solid Earth tidal deformations; Ocean loading; Atmospheric pressure loading;

	<b>BALTIC+ Theme 5</b> Geodetic SAR for Baltic Height System Unification and Baltic Sea Level Research	<b>Final Report</b> Doc. Nr: SAR-HSU-SR-0022 Issue: 1.1 Date: 07.07.2021 Page: 42 of 170
---	--	--

			Reference System Service (IERS)	Rotational deformation due to polar motion; Ocean pole tide loading
ECR-LOC-A	Approximate Locations of ECR Stations	Input	Project Team	Approximate coordinates of all the installed ECRs to download the applicable SAR image. Approximate ECR positions (1 meter or better) determined during installation.
PTA-RES	Extracted Target Locations from Point Target Analysis	Output	PTA-OBS	File contains results from point target analysis: date/time, range, peak/background power, SCR, range/azimuth resolution, standard dev. range azimuth, range/azimuth in image coordinates, corrections for azimuth/range effects (bistatic, FM-rate, Doppler shift)
PTA-OBS	SAR Raw Measurements	Output	SAR-Positioning	Generated from the point PTA-RES. Processor specific corrections are applied to range and azimuth representing raw SAR measurements.
COR-TD	Tropospheric Delays	Output	SAR-Positioning	Generated from PTA-OBS and VMF3. Tropospheric delays as 1-way path delay in units of meters.
COR-ID	Ionospheric Delay	Output	SAR-Positioning	Generated from PTA-OBS and IGS-TEC. Ionospheric delays are stored as 1-way path delay in units of meters.
COR-GC	Geodynamic Corrections	Output	SAR-Positioning	Generated from PTA-OBS and IERS-2010. Cumulative impact on range and azimuth are stored in the correction file. The range corrections are available in units of meters 1-way.
COR-SC	Sentinel-1 Systematic Effects Corrections	Output	SAR-Positioning	Sensor specific calibration constants (S1A, S1B) stored in dedicated calibration files. The numbers need to be applied to the raw range and azimuth observations to ensure unbiased observations. The numbers primarily account for SAR payload internal signal delays.
COR-EC	ECR System Corrections	Output	SAR-Positioning	The different locations of ECR antennas as well as the signal delay introduced by ECR electronics have to be taken into account.

## 6.2 SAR Positioning

### 6.2.1 Absolute Positioning

The geometric relationship between the radar sensor and the radar target is mathematically expressed by the well-known range-Doppler equations system (Leberl 1990). For a given time instant, the equations relate the position vector  $X$  of the radar target with the sensor's state vector (sensor position  $X_s$  and sensor velocity  $\dot{X}_s$ ) in a Cartesian reference frame. At this time instant, the geometry between the sensor and the target is expressed by the signal travel time one-way distance to the target times the velocity of light  $c$  (the one-way travel time is considered), and the squint angle  $\alpha$  (Gisinger et al. 2015; Gisinger et al. 2017):

$$\begin{aligned}
 |X_s(t) - X| - \frac{c}{2} \cdot \tau &= 0 \\
 \frac{\dot{X}_s(t)(X - X_s(t))}{|\dot{X}_s(t)||X - X_s(t)|} &= \sin \alpha
 \end{aligned}
 \tag{6.24}$$

For radar images focused to zero-Doppler geometry, the right hand-side of the Doppler equation equals 0. The times  $t$  and  $\tau$  correspond to the two known radar observations azimuth and range.

As one might observe, the azimuth  $t$  is not directly included in the range-Doppler equations. It is introduced via an analytical trajectory model i.e. a polynomial orbit model of degree  $n$ , with coefficients  $a_0 - a_n$ ,  $b_0 - b_n$  and  $c_0 - c_n$  that can be estimated by least squares methods from the sensor trajectory state vectors, which are usually provided by the

orbit determination of the SAR satellite (Gisinger et al, 2015; Gisinger et al, 2017). Polynomials of degree six are typically used.

$$X_S = \sum_{i=0}^n \begin{bmatrix} a_i \\ b_i \\ c_i \end{bmatrix} t^i \quad ; \quad \dot{X}_S = \sum_{i=0}^n \begin{bmatrix} a_i \\ b_i \\ c_i \end{bmatrix} i t^{(i-1)} \quad (6.25)$$

If equation (6.25) is introduced into the zero-Doppler equations, the 3D location of a target with  $t$  and  $\tau$  is reduced to a circle perpendicularly oriented to the satellite's flight direction (Gisinger et al, 2015). Figure 6-8 depicts three image acquisitions, one from an ascending and two from a descending satellite pass, all containing the same target with position vector  $X$ . It is evident that in order to solve for  $X$ , at least two acquisitions are required, most preferable acquired from different geometries.

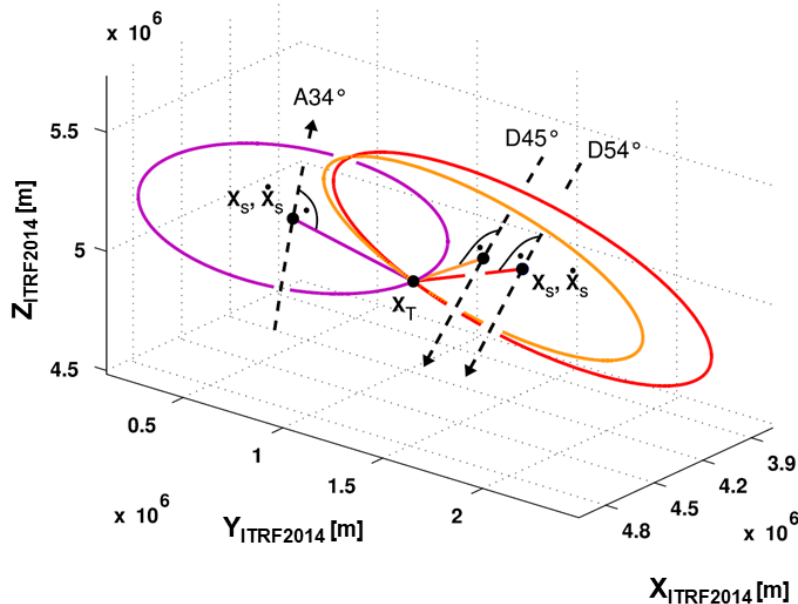


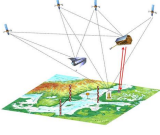
**Figure 6-8:** Graphical representation of the range-Doppler equation system in zero-Doppler mode (Gisinger et al. 2017)

Mathematically, the equation system can be fully linearized and solved according to the concept of adjustment of conditions with additional parameters (Mikhail and Ackermann, 1976).

$$\begin{aligned} B(l + v) + Ax &= b \\ Bv + Ax + w &= 0 \end{aligned} \quad (6.26)$$

Matrix B holds the conditions for the observations  $t$  and  $\tau$ ,  $l$  is the observation vector, A is the design matrix for the three unknown target coordinates, and  $x$  is the unknown parameters vector. Vector  $v$  contains the observations residuals and  $w = Bl - b$  accounts for inconsistencies of the system demanding the outcome  $b$ , which is resolved by  $x$  and  $v$  (Gisinger et al, 2015; Gisinger et al, 2017). B and A are generated by differentiating the range-Doppler equations including the polynomial orbit model as described in (Gisinger et al, 2015). The observation residuals are minimized by the adjustment, stating the L2 norm:  $v^T P v$  is minimized. The weight matrix P is defined as the inverse of the observations variance-covariance matrix.

The adjustment is performed iteratively, starting from an initial guess  $X_0$  for the target location. As the solution converges, the inconsistencies eventually decay, while the residuals  $v$  are minimized. Since the image acquisitions are independent from each other, the matrix B has a quadratic block diagonal structure that allows the inversion  $B^{-1}$ . Therefore, if we denote  $\bar{l} = B^{-1}w$  and  $\bar{A} = -B^{-1}A$  equation (6.26) can be converted to a Gauss-Markov model, which can be solved as (Mikhail and Ackermann, 1976):

	<b>BALTIC+ Theme 5</b> Geodetic SAR for Baltic Height System Unification and Baltic Sea Level Research	<b>Final Report</b> Doc. Nr: SAR-HSU-SR-0022 Issue: 1.1 Date: 07.07.2021 Page: 44 of 170

$$\hat{x} = (\bar{A}^T P \bar{A})^{-1} \bar{A}^T P \bar{l}$$

$$\sum(\hat{x}) = (\bar{A}^T P \bar{A})^{-1} \frac{(\bar{A} \hat{x} - \bar{l})^T P (\bar{A} \hat{x} - \bar{l})}{2n - 3} \quad (6.27)$$

Vector  $\hat{x}$  denotes the estimates of the unknown parameters, while  $\sum(\hat{x})$  is the 3x3 variance-covariance matrix which provides the standard deviations of the target coordinates and the error ellipsoid.

The weighting of the different observation types within the parameters estimation is done via variance component estimation (VCE), which yields additionally estimated range and azimuth standard deviations. Details about the quality indicators and the variance component estimation can be found in Gisinger et al, 2015.

### 6.2.2 Differential Extension

Similar to the principle of differential GNSS, a target with known a priori coordinates can be used to solve for the coordinates of additional targets. In the differential geodetic SAR setup, the velocity of the reference target within the ITRF needs to be additionally considered, since the reference coordinates must be established for the individual epochs of the SAR observations (Gisinger et al. 2017).

For a reference target  $X^R$  at an epoch of an acquisition (derived from the range-Doppler equation (6.24), the range and azimuth observations of k targets can be considered differentially with respect to the observations of the reference target (Gisinger et al, 2017):

$$\Delta \tau^{R,k} = \tau^R - \tau^k \quad ; \quad \Delta t^{R,k} = t^R - t^k \quad (6.28)$$

The coordinates to be solved can be expressed as coordinate differences:

$$X^k = X^R + \Delta X^{R,k} \quad (6.29)$$

The range-Doppler equation system for the zero Doppler case, then takes the form:

$$\left| X_S - X^R \right| - \left| X_S - X^R - \Delta X^{R,k} \right| - \frac{c}{2} \cdot \Delta \tau^{R,k} = 0$$

$$\frac{\dot{X}_S (X^R - X_S)}{\left| \dot{X}_S \right| \left| X^R - X_S \right|} - \frac{\dot{X}_S (X^R + \Delta X^{R,k} - X_S)}{\left| \dot{X}_S \right| \left| X^R + \Delta X^{R,k} - X_S \right|} = 0 \quad (6.30)$$

with the polynomial orbit model being extended as:

$$\mathbf{X}_S = \sum_{i=0}^n \begin{bmatrix} a_i \\ b_i \\ c_i \end{bmatrix} \left( t^R + \Delta t^{R,k} \right)^i \quad ; \quad \dot{\mathbf{X}}_S = \sum_{i=0}^n \begin{bmatrix} a_i \\ b_i \\ c_i \end{bmatrix} i \left( t^R + \Delta t^{R,k} \right)^{(i-1)} \quad (6.31)$$

The solution of the differential case follows the procedure described in 6.2.1, with B and A computed from (6.30) and (6.31),  $\Delta \tau^{R,k}$  and  $\Delta t^{R,k}$  as input observations and  $\Delta X^{R,k}$  as the unknown to be resolved.

For the differential setup at a local site spatial correlation of the external disturbances can be assumed, therefore eliminating the need of applying corrections to the range and azimuth observations of the targets. There is however an increase of the random SAR observation error due to the data combination, with an estimated growth by approximately a factor of 2 (Gisinger et al, 2017).

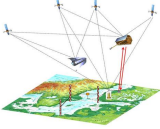
More details on the differential extension of the SAR positioning can be found in Gisinger et al, 2017.

### 6.2.3 Data Processing Chain

The procedures described for the standard (section 6.2.1) and the differential (section 6.2.2) geodetic SAR, are applied by the '3D Stereo SAR' module of a SAR processor software developed in MatLab by C. Gisinger. The processing scheme steps for both the standard and the differential approach are shown in Figure 6-9, and further described in detail below.

#### Standard Geodetic SAR - Processing steps

- 1) Azimuth  $t_{a,raw}$  and range  $t_{r,raw}$  are extracted at subpixel level from the zero-Doppler SLC Sentinel-1 images using Point Target Analysis (PTA) (see section 6.1).

	<b>BALTIC+ Theme 5</b> Geodetic SAR for Baltic Height System Unification and Baltic Sea Level Research	<b>Final Report</b> Doc. Nr: SAR-HSU-SR-0022 Issue: 1.1 Date: 07.07.2021 Page: 45 of 170
---	--	--

- 2) The raw timings are corrected for the geodynamic and atmospheric effects and calibration parameters.
- 3) The polynomial orbit model's coefficients are estimated by means of least squares fit.
- 4) The Geodetic SAR algorithm as described in section 6.2.1 is applied.

#### Differential Geodetic SAR - Processing steps

- 1) Azimuth  $t_{a,raw}$  and range  $t_{r,raw}$  are extracted at subpixel level from the zero-Doppler SLC Sentinel-1 images using Point Target Analysis (PTA) (see section 6.1).
- 2) The polynomial orbit model's coefficients are estimated by means of least squares fit.
- 3) The azimuth  $\tau_a^R$  and range  $\tau_r^R$  of the reference target are derived from the range-Doppler equations.
- 4) The Geodetic SAR algorithm as described in section 6.2.2 is applied.

#### L1b images

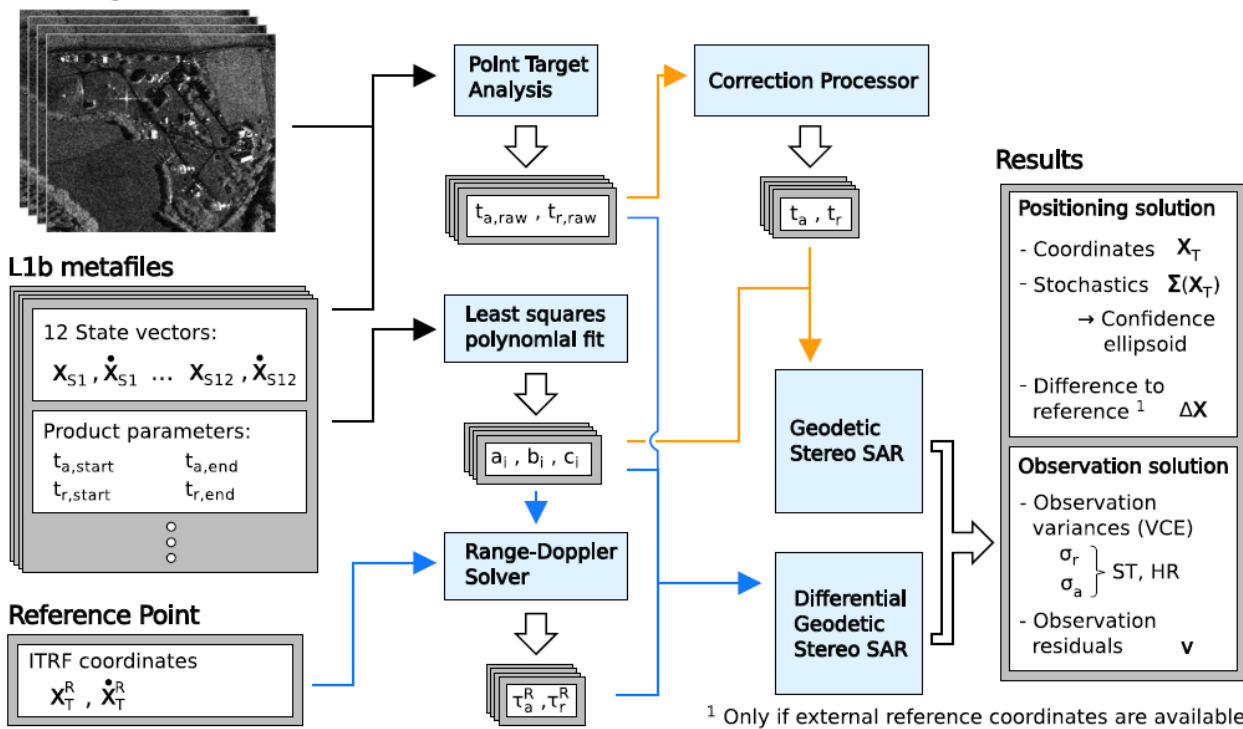


**Figure 6-9:** Processing scheme of geodetic stereo SAR for the standard (orange arrows) and the differential approach (blue arrows) (Gisinger et al. 2017)

#### Data input

The Geodetic SAR processor solves for the unknown X, Y, Z target coordinates, which has been observed from at least two different acquisitions. For a reliable solution, acquisitions from both ascending and descending passes, as well as acquisitions from different adjacent tracks, should be considered. For the solution of the system, the data inputs required are:

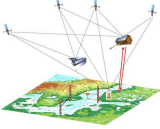
- the range and azimuth timings of the target extracted at subpixel level from the different SAR images,
- the trajectory model of the SAR antenna phase centre during the acquisitions.

In order to ensure an unbiased estimation, the range and azimuth timings need to be corrected for the disturbing effects (atmospheric path delays, geodynamic effects, geometrical calibration) prior to the parameter estimation. It should additionally be mentioned that the uncertainty of the orbit accuracy is not individually handled, since it cannot be distinguished from the remaining errors of the observations. Therefore, the variance component estimation includes contributions from the orbit, the SAR observations and the external corrections (Gisinger et al, 2015).

#### Data output

The results of the parameter estimation include:

- the X, Y, Z target coordinates in the ITRF2014.
- the uncertainties  $\sigma_x, \sigma_y, \sigma_z, \sigma_{xy}, \sigma_{xz}, \sigma_{yz}$ , derived from the variance-covariance matrix  $\Sigma(\hat{\mathbf{x}})$ .
- the confidence ellipsoid, which can be obtained by performing eigenvalue and eigenvector decomposition of  $\Sigma(\hat{\mathbf{x}})$  scaled to a 95% confidence level as described in Gisinger et al, 2017.

	<b>BALTIC+ Theme 5</b> Geodetic SAR for Baltic Height System Unification and Baltic Sea Level Research	<b>Final Report</b> Doc. Nr: SAR-HSU-SR-0022 Issue: 1.1 Date: 07.07.2021 Page: 46 of 170
---	--	--

- In case external reference coordinates for the same target are also available (e.g. from a terrestrial survey), the  $\Delta X_{x,y,z}$  coordinate differences are computed.
- The range and azimuth standard deviations  $\sigma_r$  and  $\sigma_a$ , provided by the variance component estimation.
- The observation residuals.

#### 6.2.4 Parameter Summary

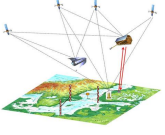
Table 6-4 summarizes the input parameters needed for SAR positioning and the output parameters generated by the processor. In particular, it is described from where the input parameters are taken and for which follow-on processing task the output parameters are needed. Refer also to Figure 6-9 where the internal data flow of this processing task is shown.

**Table 6-4:** Overview of Input/Output Parameters for SAR Positioning

Parameter Name	Description	Type	Source (Input)/ Target (Output)	Comment
S1-PSO	Sentinel-1 precise orbits	Input	ESA PDGS, Sentinel-1 Quality Control	Sentinel-1 precise state vectors (position & velocity) with 10s sampling; provided as daily files spanning 26 hours (1 hour daily boundary overlaps)
PTA-OBS	SAR raw measurements	Input	SAR Data Analysis and Value Adding	Range and azimuth representing raw SAR measurements.
COR-TD	Tropospheric delays	Input	SAR Data Analysis and Value Adding	Tropospheric delays as 1-way path delay in units of meters.
COR-ID	Ionospheric delay	Input	SAR Data Analysis and Value Adding	Ionospheric delays are stored as 1-way path delay in units of meters.
COR-GC	Geodynamic corrections	Input	SAR Data Analysis and Value Adding	Cumulative impact of geodynamic corrections. The range corrections are available in units of meters 1-way.
COR-SC	Sentinel-1 systematic effects corrections	Input	SAR Data Analysis and Value Adding	Sensor specific calibration constants (S1A, S1B).
COR-EC	ECR system corrections	Input	SAR Data Analysis and Value Adding	ECR specific corrections due to antenna locations and internal signal delay.
SAR-POS	SAR positioning solution	Output	Height System Unification and Absolute Sea Level	Time series of coordinates of the SAR target as X, Y, Z coordinates in the ITRF2014 and uncertainties $\sigma_X, \sigma_Y, \sigma_Z, \sigma_{XY}, \sigma_{XZ}, \sigma_{YZ}$ , derived from the variance-covariance matrix $\Sigma(\hat{x})$ . Confidence ellipsoid from eigenvalue and eigenvector decomposition of $\Sigma(\hat{x})$ scaled to a 95% confidence level. In case external reference coordinates for the same target are also available (e.g. from a terrestrial survey), the $\Delta X_{x,y,z}$ coordinate differences are computed.
SAR-OBS	SAR observation solution	Output	Height System Unification and Absolute Sea Level	Time series of range and azimuth standard deviations $\sigma_r$ and $\sigma_a$ , provided by the variance component estimation and observation residuals.

### 6.3 GNSS Positioning

Since we need to determine the height of the GNSS stations near the ECR stations with the highest possible accuracy, we should use GNSS observations with the lowest possible cut off for the elevation angle of the registered satellites. Daily observational data will ensure the stability of the resulted coordinates. Also for that reason we have decided to choose the

	<b>BALTIC+ Theme 5</b>  Geodetic SAR for Baltic Height System Unification and Baltic Sea Level Research	<b>Final Report</b> Doc. Nr: SAR-HSU-SR-0022 Issue: 1.1 Date: 07.07.2021 Page: 47 of 170
---	--	--

network computation of GNSS observations in Double Differences (DD) mode, but not PPP. This computation procedure is used for networks and ensures most precise results.

Before performing calculations, first the network has to be defined. It should contain all necessary permanent GNSS stations useful for the needs of the project – some of them as reference stations and some of them located in close proximity to the ECR stations and/or the selected tide gauge stations. The network defined in this way should have good and stable in time geometry for determining the coordinates of the stations included in the project and contain GNSS stations as reference points, having long and stable time series of coordinates of these stations, with well-defined parameters of their movements - velocity vectors.

The computation process is resulted by the Bernese GNSS Software (actually in version 5.2) (Dach et al, 2015) in way assured the most precise and stable results. It is clear that for the precise coordinate computation all possible models according to IERS Conventions 2010 (Petit et al, 2010) must be used and computation should be made using dual frequency solutions. Here the standard algorithms for GNSS data processing are not repeated, instead we refer to the standard literature on this topic. It is more important to define models, data formats and other standards to be used in the GNSS data analysis and for the determination of the GNSS station positions.

The GNSS observation files in RINEX v2.11 or 3.02 format is planned to be used as input data in the GNSS data processing. The precise orbit files (\*.sp3) as well as the global products, satellite's clock correction (\*.clk), Earth rotation parameters (\*.erp) are available on several FTP servers, e.g. <ftp://garner.ucsd.edu/archive/garner/products/>.

#### Satellite Systems

Due to the current number of satellites available in orbits and the fact that the GNSS system is in the operational phase, it is clear that obtaining the highest accuracy for the determination of station coordinates is now possible using observational data from GPS or GPS+GLONASS satellites.

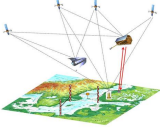
Because Galileo system is still in pre-operational phase the gaps in observations could occur (number of satellites visible above horizon can be not sufficient or the PDOP value can exceed 6). Additional there are no dedicated antenna phase centre variation model for Galileo. Such circumstances cause the occurrence of periods of significantly lower accuracy and for such reason the computations using Galileo observations could be considered only as a test.

#### Applied models in GNSS Processing

During GNSS data processing and for computing the GNSS positions for a number of parameters models need to be used. Table 6-5 provides an overview of these models.

**Table 6-5:** Models to be used in data processing for GNSS positioning

<b>Parameter</b>	<b>Models</b>	<b>Comments</b>
Station velocities	Most proper is to use the station velocities deliver by IERS, at least for reference stations	Station coordinates (especially of reference sites) should, therefore, always be propagated from the reference epoch to the observation epoch based on the corresponding station velocities. This ensures consistency with the IGS satellite orbits and prevents network deformations induced by moving plates.
Solid and Ocean Pole Tides, and Permanent Tides	TIDE2000 according to IERS Conventions 2010	Effects of solid Earth tides have to be taken into account because they are two orders of magnitude larger than the accuracies currently achieved for GNSS– derived coordinates.
Ocean Tidal Loading	OT_FES2004 according to IERS Conventions 2010	The crustal deformation caused by the changing mass distribution due to ocean tides (ocean tidal loading).
Centre of mass corrections for ocean and atmospheric tidal loading	These CMC have to be given in the header of the tidal loading file	For tidal loading models, centre of mass corrections (CMC) are provided for the transformation.
Geopotential model	EGM2008	The official Earth Gravitational Model EGM2008 has been publicly released by the U.S. National Geospatial-Intelligence Agency (NGA) EGM Development Team.
Earth orientation Parameters/ Pole coordinates	IERS Co4 EOP, files: Co4_yyyy.ERP, BULLET_A.ERP	The pole files contain time series of pole coordinates, length of day, etc., necessary to perform the transformation between the terrestrial and the celestial (inertial) reference frame. We recommend to use the homogeneous 'global products'(SP3 precise orbit, CLK clocks and ERP) from IGS final solutions.

	<b>BALTIC+ Theme 5</b> Geodetic SAR for Baltic Height System Unification and Baltic Sea Level Research	<b>Final Report</b> Doc. Nr: SAR-HSU-SR-0022 Issue: 1.1 Date: 07.07.2021 Page: 48 of 170
---	--	--

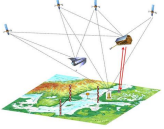
Planetary ephemeris file	DE405	Development ephemeris file from the Jet Propulsion Laboratory (JPL) (Standish 1990), the gravitational attraction of Sun, Moon and the major planets (Jupiter, Venus, and Mars) are taken into account.
Receiver antenna phase centre offsets and phase centre variations	ANTEX files containing absolute antenna phase centre variations	We recommend using individual antenna calibrations if they exist for individual stations, e.g. from EPN.
Sun radiation pressure model	The corresponding coefficients are contained in the satellite information file SATELLIT.IYY	The acceleration due to the solar radiation pressure is switched off when the satellite is in the Earth's shadow and scaled according to the fraction of the solar disk covered by the Moon during partial lunar eclipses that regularly occur during New Moon.
Nutation model	IAU2000R06 as the nutation model approved by the International Astronomical Union (IAU) and IERS2010XY according to the IERS Conventions 2010 for the model describing the subdaily tidal variations of the pole and the rotation of the Earth.	
Troposphere: GMF/GPT and VMF1 for GNSS		VMF1 requires 6-hour ECMWF data.

### Parameter Summary

Table 6-6 summarizes the input parameters needed for GNSS positioning and the output parameters generated by the processor. In particular, it is described from where the input parameters are taken and for which follow-on processing task the output parameters are needed.

**Table 6-6:** Overview of Input/Output Parameters for GNSS Positioning

Parameter Name	Description	Type	Source (Input)/ Target (Output)	Comment
GNSS-OBS	GNSS Observations	Input	GNSS Receiver Data at Stations	GNSS observation files in RINEX v2.11 or 3.02 format. Data with lowest possible elevation angle to be used.
GNSS-ORB	GNSS Precise Orbits	Input	IGS	Orbit files of GNSS satellites (positions and velocities)
GNSS-CLK	GNSS Clock Corrections	Input	IGS	Satellites clock corrections
GNSS-BM	Background Models	Input	Various (refer to Table 6-5)	Background models required for GNSS processing. Station velocities, Solid and ocean pole tides, Permanent tides, Center of mass corrections for tidal loading, Geopotential model, Earth orientation parameters, Pole coordinates, Planetary ephemeris, Receiver antenna phase center offsets and variations, Sun radiation pressure model, Nutation model, Troposphere for GNSS
GNSS-POS	GNSS positioning solution	Output	Height System Unification and Absolute Sea Level	Time series of coordinates of the GNSS stations as X, Y, Z coordinates in the ITRF2014 and uncertainties.

	<b>BALTIC+ Theme 5</b>  Geodetic SAR for Baltic Height System Unification and Baltic Sea Level Research	<p style="text-align: right;">Final Report</p> Doc. Nr: SAR-HSU-SR-0022 Issue: 1.1 Date: 07.07.2021 Page: 49 of 170
---	--	--

## 6.4 Tide Gauge Data Analysis

Sea level at the coastline is usually observed with tide gauges (TG) that deliver instantaneous sea surface heights relative to a zero marker of the tide gauge station. Incorporation of TG data into present study is needed for comparing sea level records in an absolute sense and to connecting height systems of different countries across the ocean. In this study it is conducted by comparing mean sea level (MSL) estimates at the participating TG stations. This classical method is meant to support the modern SAR and GNSS based estimates.

Contemporary automatic sea level gauge stations track water level changes continuously and are capable via data communication devices to transfer data in real-time. Since the sea level observations are mainly used for marine navigation then most commonly the TG-s are installed at harbours, where the necessary infrastructure exists. At the present stage ECR transponders are mounted at or nearby seven suitable TG stations (Loksa, Emäsalo, Rauma, Leba, Wladyslawowo, Forsmark and Spikarna) in Estonia, Finland, Poland and Sweden. All the participating tide gauge stations utilise automatic sea level detection (e.g. pressure gauges etc).

### Retrieving data from the national tide gauge authorities

The TG data are delivered by the national tide gauge authorities of Estonia, Finland, Poland and Sweden. It is expected thus that also relevant TG station documentation and meta-data is available. These include: definition of the TG station location, used sensor types, datums, benchmarks, levelling information, maintenance, malfunctioning, etc. It is also of interest to identify whether the submitted TG data is „raw“ or is it corrected to account for certain phenomena, e.g. ocean and Earth tides.

If there is any reliable weather station installed (e.g. by national meteorological authority) nearby the participating tide gauge station, then also such data that affect the sea level fluctuations (e.g. wind speed and direction, wave heights) can also be optionally retrieved for further analysis.

### Data sampling interval and the time period

The same time sampling intervals need to be used for each TG station. For the project the standard hourly tide gauge data are the primary data-set to be used for analysis. The advantage of the hourly TG data is that these contain no high frequency noise (i.e. sudden spikes in the time series), that usually is eliminated by the averaging procedure. For reliable mean sea level (MSL) estimation the sea level measurements should be performed over an adequate time period to filter out data blunders and obtaining statistically meaningful results. As a working hypothesis an annual water cycle period is assumed to be sufficient for the purpose of the present study. Alternatively, also seasonal MSL estimates can be tested. The period of the TG data starts from 01.01.2020, i.e. no earlier than the collocated ECR transponders became operational. The latest TG data records to be included into analysis is 31.12.2020.

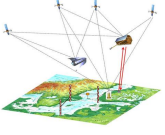
### Accounting for the drift correction of tide gauge sensors

The accuracy of contemporary TG readings remains within 0.2...1.0 cm. However, readings of such sensors need to be compensated due the instrumental drift phenomenon. Note that usually a TG station is also equipped with level staff, the visual readings of which are to be used for verification of the automatic gauge records and determining/elimination the sensor drift. The instrumental drift can be an important issue which has to be taken under control through regular control readings from a nearby staff gauge. Regular field checks of the tide gauge readings are advisable (this could be a standard routine for the tide gauge authorities anyways.). The visual control measurements are taken to compare the level staff readings with that of the pressure sensor at the same time instant. If the readings differ more than a certain threshold (e.g. three centimetres, the threefold accuracy of the visual reading), then the automatic records of the preceding period need to be corrected retrospectively. Accordingly, the TG data received from the tide gauge authorities to be checked for the inclusion of the drift correction. The drift corrected data are to be further filtered in order to remove data blunders and gross errors.

### Analysis of TG records for computing MSL

The records of existing tide gauges maybe analysed in terms of consistency and systematic distortions due to external artificial disturbances. From this analysis one should exclude unreliable records or low-quality observation data. The data content and problematic quality issues can be consulted with the respective national tide gauge authority. In order to filter out data blunders the tide gauge series can be statistically analysed. The primary goal is preliminary check of TG records for identifying gross errors and systematic biases. For the removal of gross errors the sea values need to be studied (e.g. visually or using numerical constraints). The occasional data jumps (defined as a single reading differing from its adjacent readings by some threshold, due to sea vessels manoeuvring close to TG station) need to be identified, studied and eliminated. Abrupt sea level changes (e.g. >10 cm over an hour) could be an indication of gross errors, such occasions need to be examined individually and verified with contemporary weather conditions. The detected gross errors need to be eliminated from the further analysis.

The data gaps (e.g. due to malfunctioning of instruments) in TG data series also may occur. These need to be identified, also the occurrence of data gap in one station may yield removal of the same time-epoch from related (e.g. opposite side of the sea) TG stations as well. The standard deviation (STD) of the readings reflects the inner consistency (for the entire period, or seasonally) of the time series at each tide gauge station. Typically, the STD of the annual sea level series should

	<b>BALTIC+ Theme 5</b>  <b>Geodetic SAR for Baltic Height System Unification and Baltic Sea Level Research</b>	<b>Final Report</b> <b>Doc. Nr: SAR-HSU-SR-0022</b> <b>Issue: 1.1</b> <b>Date: 07.07.2021</b> <b>Page: 50 of 170</b>
---	--	--

remain within selected limit, whereas the larger STD is associated with the rougher sea conditions at individual TG station. The smaller STD may also reveal sea sheltered locations of certain tide gauges.

The data series are to be used for computing the tentative mean sea level estimates for each TG station. The final mean sea level for the participating tide gauges to be computed centrally applying the same methodology and considering also interconnections (e.g. local ties by precise levellings, GNSS) between the tide gauges and geodetic infrastructure. Also possible inconsistencies between the national vertical datums are to be eliminated in the final TG processing stage. For the consistency of the TG analysis it is requested that TG data is presented in same sea level datum. The TG series is uniformly formatted into an ASCII (or Excel) data file for further processing. These resulting data series will serve as an input for the next stage, which is the processing of corrected Tide Gauge Sea Level Heights. The MSL at individual TG-s can then be uniquely determined from these corrected TG records.

#### Common vertical datum

After eliminating ocean and Earth tides from the observations, one gets a time series of sea heights and consequently its changes. These height changes, as they are observed at the tide gauges, at this point can be only regarded as relative changes of the sea surface with respect to the zero marker. For proper interconnection of oversea tide gauge series the TG measurements need to be converted into the same vertical/chart datum. It is necessary to establish a reliable connection through the national levellings to the pan-European precise levelling Network (such as United European Levelling Network – UELN). Alternatively, the GNSS height determination in conjunction with the precise regional precise geoid model could also be used. The European Vertical Reference System (EVRS) referred to the Normaal Amsterdam Peil (NAP) will be used as reference for the tide gauge data analysis. At this also possible differences in between national EVRS realisations can be considered.

#### Determining the TGZ height and accounting for the vertical land motion

Usually a special tide gauge benchmark (TGBM) is installed within a few hundred meters from the tide gauge station. The height of such a TGBM is determined (by using high precise levelling) with respect to the national height network at the time of the TG installation. Note that tide gauge readings are expressed with respect to the tide gauge zero (TGZ), i.e., the reference height value on the level staff. The TGZ height ( $H_i^{TGZ}$ ) is assigned with respect to contact point (CP) at the installation by measuring the vertical distance (T). The tide gauge contact point (CP, on the top of level staff) is connected to the tide gauge benchmark (TGBM) also by precise spirit levelling (at the time of its installation). Figure 6-10 depicts inter-relations in between the tide gauge zero (TGZ), contact point (CP) and tide gauge benchmark TGBM.

TGZ is a pre-determined point (e.g. a metrical reading on the staff gauge), with respect of which the sea level fluctuations are measured. Often the planned height of the TGZ is aimed at to correspond to the value  $H=0.000$  m in the national vertical datum. In this way the TG readings are directly referred to the national height datum. For a long term analysis and for the determination of absolute height changes with respect to a reference height one needs to know if the zero marker of the station is stable or undergoes changes in height as well. The entire Fennoscandia is affected by apparent land uplift at the velocity rate up to +9 mm/year, primarily due to the viscoelastic response of the solid Earth resulting from the de-glaciation of the Pleistocene ice-sheets. Over a time span this causes notable distortions of height system realisations even within a country. Therefore, the land uplift corrections should be also taken into account in sea level series, which are used for modelling and forecasting of sea level changes. Over the time the vertical land motion (either the postglacial rebound or the local subsidence) will affect the correctness of TG data series. Therefore, on-site observation of the relative motion of the TGZ with respect to a global geometric reference frame is required. In order to obtain coherent time series the tide gauges then it is necessary to consider this VLM effect on the TGBM height as well. The Nordic Geodetic Commission developed land uplift model NKG2016LU (Vestöl et al, 2019) is to be used for estimating the postglacial rebound values for the epoch 2000.0 at the locations of the TG stations. The effect of the postglacial land uplift to the tide gauge series in this rather short-period study is expected to be insignificant. However, in long lasting (multi-year) studies the VLM effect on the TG series need to be strictly accounted for.

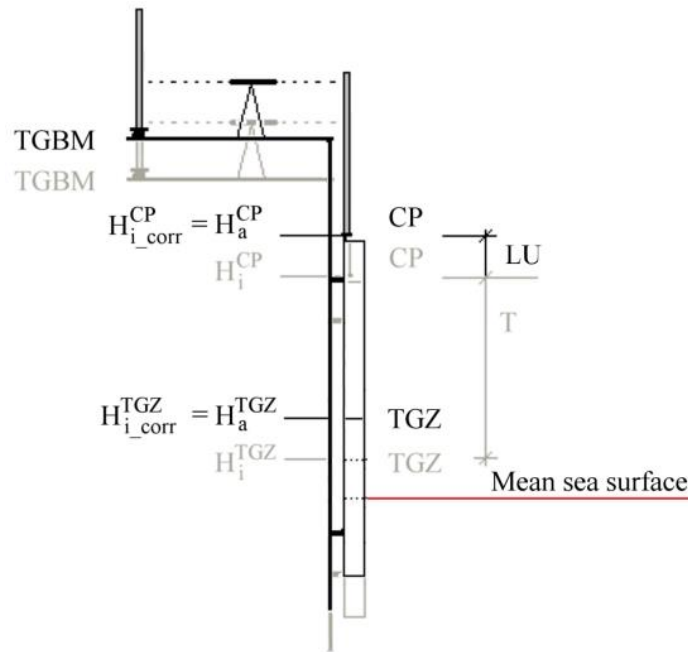


**Figure 6-10:** The tide gauge reference points and influence of vertical land motion (in this case - land uplift) to the tide gauge data series. The tide gauge contact point (CP, on the top of staff) is connected to the tide gauge benchmark (TGBM) by precise spirit levelling. The height of the tide gauge zero (TGZ) ( $H_i^{TGZ}$ ) is assigned with respect to CP at the installation by measuring the vertical distance (T). The shaded grey figure indicates the position of the TG and its reference heights ( $H_i^{CP}$  and  $H_i^{TGZ}$ ) at moment of installation. The black figure denotes the contemporary TG position with heights  $H_i^{CP}$  and  $H_i^{TGZ}$  due to the land uplift (LU).  $H_{i\_corr}^{CP}$  and  $H_{i\_corr}^{TGZ}$  are land uplift-corrected heights of CP and TGZ, respectively. Mean sea surface indicates the zero level of the height system. Note that due to various reasons (e.g. land uplift, levelling errors and eustatic sea level rise) the mean sea level is not necessary coinciding with the zero-reading of the TGZ and the zero of the height system either.

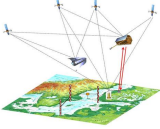
Levelling guidelines

The ECR reference points (RP) need to be connected to the TGBM and levelling network as well. Since TG are collocated with an ECR transponders, then it is advisable, that also the tide gauges are to relevelled, in order to perform checks of the stability of the tide gauges. Hence the following height differences:

TGBM-> ECR (RP) -> TG (CP) -> TGBM

need to be determined by high- precise levelling, see also Figure 6-11. Precise (foot) levelling in forward and backward directions need to be conducted. Recommended levelling sights in each levelling stations are in the following order: back-forward-forward-back. Also equality (<0.2 m) of levelling shoulders should strictly be followed.

Usage of modern digital levelling equipment in conjunction with calibrated invar barcode staffs is recommended. The expected precision 0.3...0.5 mm/km of the system (instrument & staffs) is recommended. At the processing of levelling data standard least squares adjustment should be used; in case of longer levelling distances also rod calibration or temperature corrections should be included. The precise levelling results (specified height differences between TGBM and TGZ, also possibly accounting for VLM) are to be used for correcting the TG data series either at the national level or centrally.

	<b>BALTIC+ Theme 5</b> Geodetic SAR for Baltic Height System Unification and Baltic Sea Level Research	Final Report Doc. Nr: SAR-HSU-SR-0022 Issue: 1.1 Date: 07.07.2021 Page: 52 of 170
---	--	---



**Figure 6-11:** An example of levelling connections in the collocated TG/ECR site

Tide gauge data processing

Incorporation of the tide gauge results into present study is needed for comparing sea level records in an absolute sense and to connecting height systems of different countries across the ocean. In this study it is conducted by comparing mean sea level (MSL) estimates at the participating TG stations by the method of hydrodynamic levelling. Hydrodynamic levelling is connoted with sea level observations for determining height (potential) differences between coastal points or over oceanic regions (e.g., Torge 2001). The observations have to be averaged and reduced due to the sea surface topography (SST), which is a deviation of the mean sea level (MSL) from an equipotential surface (e.g., marine geoid). The hydrodynamic levelling is to be conducted in between six paired TG stations as follows: (1) across-sea connections Emäsalo-Loksa, Rauma-Spikarna, Rauma-Forsmark; (2) land-connected connections Wladyslawowo-Leba, Forsmark-Spikarna, Emäsalo-Rauma. It is also of interest to combine a closed loop of across-sea tide-gauge measurements Rauma-Forsmark-Spikarna-Rauma. The misclosure values of the loop would indicate the possible errors either in the TG data-series, assigned TG heights or adopted SST models. In hydrodynamic levelling it is important to identify the same level surface that was adopted at the initial TG. At Station A (see Figure 6-12) the CPA height (HA) can be determined precisely by connecting it to TGBMA by spirit levelling.

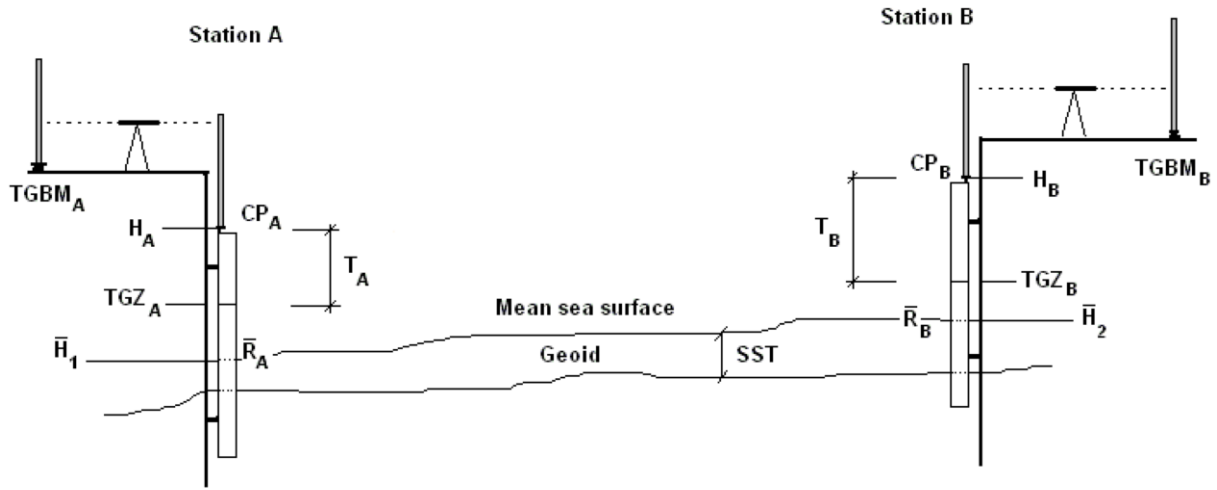
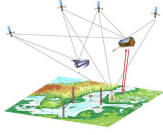


**Figure 6-12:** Hydrodynamic levelling between paired tide gauges. The height difference between respective contact point (CP) and tide gauge benchmark (TGBM) can be measured by spirit levelling. Readings of the MSL values ( $\bar{R}_A$ ,  $\bar{R}_B$ ) are obtained by averaging. Other values are either calculated (heights:  $\bar{H}_1$ ,  $\bar{H}_2$ ,  $H_A$ ,  $H_B$ ) or assigned (tide gauge zeros:  $TGZ_A$  and  $TGZ_B$ ). (Liibusk et al 2013)

At across-sea Station B the  $CP_B$  height ( $H_B$ ) needs to be determined with respect to  $H_A$  by using periodic or continuous sea level observations. Observation equations for determining the heights of the MSL ( $\bar{H}_1$  and  $\bar{H}_2$ ) at paired Stations A and B can be represented as:

$$\bar{H}_1 = (H_A - T_A) - (R_{TGZ}^A - \bar{R}_A) + \epsilon_A \quad (6.32)$$

and

$$\bar{H}_2 = (H_B - T_B) - (R_{TGZ}^B - \bar{R}_B) + \epsilon_B \quad (6.33)$$

where  $T_A$  and  $T_B$  are vertical distances between the corresponding CP and TGZ at Stations A and B, respectively (cf. Figure 6-12). Thus, the first bracketed term on the right hand side of Eqs. (6.32) and (6.33) denotes the height of the corresponding TGZ. The readings  $R_{TGZ}^A$  and  $R_{TGZ}^B$  correspond to the TGZ location (determined at the instalment of the TG) of Station A and B, respectively. The overbared symbols denote values obtained by simple arithmetical averaging over the given time period. The averaged readings  $\bar{R}_A$  and  $\bar{R}_B$  correspond to the MSL at Station A and B, respectively, i.e.

$$\bar{R} = \frac{1}{n} \sum_{i=1}^{n=i \max} R(t_i) + d(t_i) \quad (6.34)$$

where  $R(t_i)$  is the reading at the  $i$ -th time-epoch of measurements ( $t_i$ ) and  $d(t_i)$  denotes relevant corrections (e.g. due to drift of pressure sensors, for a more extended discussion see the TG data analysis section above) at the same instant. Symbols  $\epsilon_A$  and  $\epsilon_B$  denote a random variable (error of measurements at Stations A and B) with the mathematical expectation of zero, i.e.  $E(\epsilon_A) = E(\epsilon_B) = 0$ . Note that the quantities  $T_A$ ,  $T_B$ ,  $R_{TGZ}^A$ ,  $\bar{R}_A$ ,  $R_{TGZ}^B$ ,  $\bar{R}_B$ ,  $H_A$ ,  $\bar{H}_1$  can be measured directly or obtained from simple averaging. The only unknowns are  $\bar{H}_2$  and  $H_B$  which need to be determined from solving the system of equations. Subtracting Eq. (6.33) from Eq. (6.32) yields:

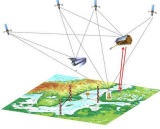
$$H_B - \bar{H}_2 = (H_A - T_A) - \bar{H}_1 + T_B - (R_{TGZ}^A - \bar{R}_A) + (R_{TGZ}^B - \bar{R}_B) \quad (6.35)$$

where the two unknowns are grouped on the left hand side and the values of random measurement errors are henceforth neglected for the sake of brevity of discussion. Recall, that in general the MSL does not coincide with an equipotential surface, say, the geoid (see Figure 6-12). The height  $\bar{H}_2$  can also be expressed via SST, which is dependent on currents, wind drag, water depth and bottom friction, water density, atmospheric pressure, Coriolis force and gravity (Torge, 2001). The height of the MSL at Station B can then be written as (see also Figure 6-12):

$$\bar{H}_2 = \bar{H}_1 - \overline{SST}_A + \overline{SST}_B \quad (6.36)$$

where  $\overline{SST}_A$  and  $\overline{SST}_B$  are the mean sea surface topography values at Stations A and B, respectively. Now Eq. (6.35) can be expressed as:

$$H_B = (H_A - T_A) + T_B - (R_{TGZ}^A - \bar{R}_A) + (R_{TGZ}^B - \bar{R}_B) - (\overline{SST}_A - \overline{SST}_B) \quad (6.37)$$

	<b>BALTIC+ Theme 5</b>  Geodetic SAR for Baltic Height System Unification and Baltic Sea Level Research	<b>Final Report</b> Doc. Nr: SAR-HSU-SR-0022 Issue: 1.1 Date: 07.07.2021 Page: 54 of 170
---	--	--

Certain assumptions need to be introduced in order to determine  $H_B$ . For instance, the mean  $\overline{SST}$  values can be taken from a suitable SST model. The estimated SST values are to be verified using land-connected tide-gauge connections. Note that the above expressions are somewhat simplified. More elaborated expressions for hydrodynamic levelling can be found in Cartwright and Crease (1963).

The results of hydrodynamic levelling could be various estimates (monthly, annual, seasonal) of height differences between the paired tide gauge stations.

#### Parameter Summary

Table 6-7 summarizes the input parameters needed for tide gauge data analysis and the output parameters generated by the processor. In particular, it is described from where the input parameters are taken and for which follow-on processing task the output parameters are needed.

**Table 6-7:** Overview of Input/Output Parameters for Tide Gauge Data Analysis

Parameter Name	Description	Type	Source (Input)/ Target (Output)	Comment
TG-RAW	Raw Sea Surface Height at Tide Gauge Station	Input	National Tide Gauge Authorities	Sea surface height with respect to zero marker of tide gauge station with hourly resolution including information about applied corrections (e.g. ocean and Earth tides).
TG-COR	Tide Gauge Sensor Corrections	Input	National Tide Gauge Authorities	Information about instrument corrections like drifts or sensor outages/problems as well as information about gross errors.
TG-SSH	Corrected Sea Surface Height at Tide Gauge Stations	Output	Height System Unification and Absolute Sea Level	Time series of corrected sea surface heights observed at tide gauges with respect to the tide gauge benchmark with hourly temporal resolution.

## 6.5 GOCE Based Geoid Computation

The project aims to determine physical heights at the tide gauge stations with respect to a global high-resolution geoid. This will be achieved by combining a GOCE based Earth Gravity Model (EGM) with local/regional gravity data (land, airborne and/or marine) and a Digital Elevation Model (DEM). There are several such methods that has been proposed and validated by the scientific community and they have so far *not* converged to a single state-of-the-art method. In Wang et al. (2021), most of the available regional geoid determination methods are compared and evaluated using a test dataset supplied by National Geodetic Survey (NGS) in Colorado, US. This upcoming publication also contains references to all the tested methods.

In this project, basically two regional geoid determination methods are compared, both in a pointwise sense at the tide gauges and over a rectangular area covering the tide gauges (comparison of regular grids). The methods to be tested are,

- Three-dimensional Least Squares Collocation (3D LSC method) (Moritz 1980; Tscherning and Rapp 1974; Tscherning 2013) using the remove-compute-restore method with Residual Terrain Modelling (RTM) of the topographic corrections (Forsberg 1984).
- Least squares modification of Stokes' formula with additive corrections (LSMSA method), where the remove-compute-restore philosophy is used for gridding of the surface gravity anomalies; see e.g. Sjöberg (1991), Sjöberg and Bagherbandi (2017) and Ågren et al. (2009).

Both these methods will be tested with the following GOCE based EGMs,

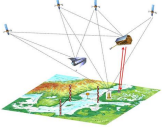
- GO\_CONS\_GCF\_2\_DIR\_R6 ( $M = 300$ )
- GOCOo6S ( $M = 300$ )

where  $M$  is the spherical harmonic maximum degree of the model; see <http://icgem.gfz-potsdam.de> for more information and detailed references.

The algorithms implied by these two regional geoid determination methods are described in detail in the literature, for instance in the references given above. To summarize, the main steps and algorithms are the following,

- Selection of local/regional gravity data from the NKG and Polish gravity databases including only the datasets available to the countries participating in the project (excluding for instance Latvian and Lithuanian data) and computation of surface gravity anomalies using the Geodetic Reference System 80 (GRS 80). The algorithms for the latter step are given in Moritz (2000).

To obtain a sufficient spectral overlap between the local/regional gravity and the GOCE based EGM, gravity point data will be selected from a rectangular *gravity area* overlapping the rectangular *geoid area* with at least 110 km in all directions (corresponding to 1-degree spherical distance in each direction). In the geoid

	<p>BALTIC+ Theme 5</p> <p>Geodetic SAR for Baltic Height System Unification and Baltic Sea Level Research</p>	<p style="text-align: right;">Final Report</p> <p>Doc. Nr: SAR-HSU-SR-0022 Issue: 1.1 Date: 07.07.2021 Page: 55 of 170</p>
---	---	--

computation tests, two computation areas, one in area to the North over the Bay of Bothnia/Gulf of Finland (Sweden, Finland and Estonia) and one large area surrounding also the Polish tide gauges are defined. Most methodological tests described below will be made over the North main area. In addition, CPK-PAN has made complementary geoid computations aiming to compute and check the quasigeoid particularly for the Polish tide gauges; see further in Łyszkowicz et al (2021).

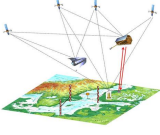
- Computation of topographic RTM effects based on a Digital Elevation Model (DEM) using the algorithms in Forsberg (1984). In this step, the NKG2015 DEM (called NKG\_DEM2014) is used for Sweden, Finland and Estonia (Latvian and Lithuanian DEMs might have to be excluded).

The RTM effect on the surface gravity anomaly is computed both for each gravity observation and for the gravity grid. The RTM effect on the *height anomaly* is computed for the geoid grid and for the tide gauges stations. As we in this project are at or close to sea with limited topographic heights, the height anomaly is very close to the geoid height (Heiskanen and Moritz 1967).

- Computation of the EGM effects for the gravity anomaly and height anomaly grids using the GOCE based EGMs above. This is standard synthesis of solid spherical harmonics; see for instance (Barthelmes et al. 2013). An important parameter here is the maximum degree used for the synthesis. This parameter is chosen based on numerical tests with respect to the NKG2015 GNSS/levelling height anomalies in the North geoid area.
- Computation of reduced surface gravity anomalies by subtracting the EGM and RTM effects. Gross error detection is made using cross validation exactly as described in Märdla et al. (2017).
- For the LSMSA method: The surface gravity anomalies are gridded using Least Squares Collocation (LSC) with a 2<sup>nd</sup> order Gauss Markov covariance function. After that, the RTM gravity anomaly grid is restored to get gridded surface gravity anomalies. All details can be found in Märdla et al. (2017).
- For the LSMSA method: The final geoid height (height anomaly) are computed using the LSMSA method as implemented in Ågren et al. (2009), which is also summarized in Märdla et al. (2017). The least squares modification of Stokes' formula is chosen according to the formulation in Sjöberg (1991). The most crucial parameter choices here are to choose as realistic signal and noise degree variances as possible (for the EGM and for the local/regional gravity data). The chosen parameters will be validated using GNSS/levelling data (refer to section 7.5).
- For the 3D LSC method: The reduced height anomaly is computed using to the well-known standard formulas of three-dimensional LSC (e.g. Moritz 1980). An empirical covariance function is estimated from the reduced gravity anomalies, to which a Tscherning and Rapp (1974) covariance function is then fitted (Tscherning 2013). The standard uncertainties of the observations are taken from the NKG2015 version of the NKG gravity database (Ågren et al. 2016). To speed up the grid computations, the height anomaly grid is divided into small 1 x 1-degree grids with some small overlap, which are finally merged to obtain the final height anomaly grid. The point height anomalies in the tide gauges will be computed without this approximation and compared to the grid values.
- For the 3D LSC method: The final geoid height (height anomaly) is computed by restoring the EGM and RTM effects, both pointwise in the tide gauges and grid wise.
- The standards agreed upon in the current SAR project will be followed for both methods. The standards are the same as in the NKG2015 geoid model project (Ågren et al. 2016) implying zero permanent tide system and postglacial land uplift epoch 2000.0. Besides, the  $W_0$  value is chosen to the values obtained in the NKG2015 project ( $W_0 = 62\,636\,858.18\text{ m}^2/\text{s}^2$ ).
- The tested methods, EGMs and parameter choices will be evaluated in a *relative sense* using Finnish, Swedish, and Estonian GNSS/levelling height anomalies (inside the North geoid area over the northern/middle Baltic Sea including parts of Gulf of Finland). The GNSS/levelling should refer either to the national realizations of the European Vertical Reference System (EVRS) with postglacial land uplift epoch 2000.0 or to EVRF2007 (as for Poland). The GNSS observations in question must also be transformed from non-tidal to zero permanent tide system.

The methods above aim for absolute geoid heights (height anomalies) at standard epoch 2000.0. The next part is to compute the same quantity for the epochs with geodetic SAR observations. As outlined in chapter 3.4, two methods are evaluated to compute the geoid variation. The first is to take the geoid change from the official NKG2016LU postglacial land uplift model (Vestøl et al. 2019), while the second is to compute it based on the GRACE mission. The computations and tests are made in the following way,

- The NKG2016LU model is used to convert the absolute geoid heights from epoch 2000.0 to the *mean epoch* for the Geodetic SAR project.
- In the next step, NKG2016LU is compared with Grace for the project time. The study is limited to evaluating monthly the model ITSG-Grace2018 (Mayer-Gürr et al. 2018) incorporated into GOCO06s (Kvas et al. 2019). It is based on the full time series from the whole GRACE mission. Spherical harmonic analysis will be made at all tide gauge locations and the corresponding geoid time series will be computed and analysed. The long term

	<b>BALTIC+ Theme 5</b>  Geodetic SAR for Baltic Height System Unification and Baltic Sea Level Research	<b>Final Report</b> Doc. Nr: SAR-HSU-SR-0022 Issue: 1.1 Date: 07.07.2021 Page: 56 of 170
---	--	--

geoid change in the large area is around 0.2–0.6 mm/year (Vestøl 2019), so we are talking about pretty small effects here.

### Parameter Summary

Table 6-8 summarizes the input parameters needed for GOCE based geoid computation and the output parameters generated by the processor. In particular, it is described from where the input parameters are taken and for which follow-on processing task the output parameters are needed.

**Table 6-8:** Overview of Input/Output Parameters for GOCE based Geoid Computation

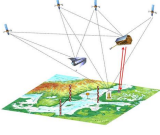
Parameter Name	Description	Type	Source (Input)/ Target (Output)	Comment
GEO-GRA	Local Gravity Data	Input	NKG / National authorities	Local terrestrial and/or airborne gravity data around tide gauge stations (at least 110 km around station)
GEO-DEM	Digital Elevation Model	Input	NKG / IfE	Digital elevation model NKG2015 DEM (called NKG_DEM2014) will be used for Sweden, Finland and Estonia. For Poland the DEM compiled by Heiner Denker at IfE in the European geoid project may be used.
GEO_EGM	Global Gravity Field Model	Input	ICGEM	GOCE based Earth gravity field models
GEO-TVG	Time-Variable Gravity Field	Input	NKG2016LU / GRACE-FO	Time-variable gravity due to land uplift in the Baltics from land-uplift model and/or GRACE results
GEO-HGT	Geoid Heights	Output	Height System Unification and Absolute Sea Level	Time series of geoid heights or height anomalies for tide gauge stations.

## 6.6 Reference Frames and Joint Standards

The tasks comprise the evaluation of the present status concerning the standards for the computation of ellipsoidal heights from the geodetic SAR technique, GNSS observations, gravimetric quantities from GOCE and other gravity data, as well as Tide Gauges. Figure 3-2 gives an overview about the different geometric and gravimetric observations that are relevant for this project, along with their major characteristics regarding reference frames, processing standards, satellite orbits and other target parameters. As shown in this figure, the processing of the various observation types is based on different reference frames, e.g., ITRF2014, IGS14, ITRF2008, WGS84. The various data sets and methods developed in this project will be tested in the Baltic Sea area, and thus, also regional and national reference frames (e.g., EUREF, GREF, SWEPOS) and transformations between them have to be considered. Furthermore, different numerical standards (e.g., GRS80, IERS Conventions, WGS84, GOCE) and different technique-specific processing standards (e.g., IGS, GOCE, SAR, Tide Gauges) are in use for determining the required geometric and gravimetric quantities.

Within this project the evaluation of the present status concerning standards for the processing of the different data sets and an assessment of gaps and scientific problems concerning the underlying geometric and gravimetric reference frames for the contributing space techniques, such as geodetic SAR, GNSS, GOCE, terrestrial/airborne gravity data and tide gauges have been performed. The outcome is an inventory summarizing the state-of-the-art concerning geometric and gravimetric reference frames and standards needed for this project. As a major output, recommendations and guidelines for common standards for geometric and gravimetric quantities and for the unification of the underlying reference frames are provided.

Table 6-9 summarizes the numerical standards that are relevant for the processing of the different geometric and gravimetric observations within this project. These standards are given in different sources, namely the conventional GRS80 constants (Moritz 2000), the EGM 2008 (Pavlis et al. 2012), the IERS Conventions 2010 (Petit and Luzum 2010), and the updated version (2017) of the IERS Conventions 2010, which contain the new conventional geopotential value  $W_0$  issued in the IAG (2015) Resolution No. 1 (Drewes et al. 2016). WGS84 ellipsoid parameters are (except for small negligible rounding errors) identical with GRS80.

	<b>BALTIC+ Theme 5</b>  Geodetic SAR for Baltic Height System Unification and Baltic Sea Level Research	<b>Final Report</b> Doc. Nr: SAR-HSU-SR-0022 Issue: 1.1 Date: 07.07.2021 Page: 57 of 170
---	--	--

**Table 6-9:** Overview on numerical standards that are relevant for this project

	semi-major axis $a$ [m]	Geocentric Grav. Constant $GM$ [ $10^{12} \text{m}^3 \text{s}^{-2}$ ]	Dyn. form factor $J_2$ [ $10^{-6}$ ]	Earth's rotation $\omega$ [ $\text{rad s}^{-1}$ ]	Normal potential $U_0$ or $W_0$ [ $\text{m}^2 \text{s}^{-2}$ ]
GRS80	6 378 137	398.600 5	1 082.63	7.292 115	62 636 860.850
EGM2008	6 378 136.3	398.600 4415 <sup>(1)</sup>	1 082.635 9	7.292 115	62 636 856.0
IERS Conv. 2010	6 378 136.6 <sup>(2)</sup>	398.600 4418 <sup>(3)</sup>	1 082.635 9	7.292 115	62 636 856.0
IERS Conv. 2010 (update 2017)	6 378 136.6 <sup>(2)</sup>	398.600 4418 <sup>(3)</sup>	1 082.635 9	7.292 115	62 636 853.4
IAG 2015					62 636 853.4

(1) TT-compatible value; (2) value given in zero-tide system; (3) TCG-compatible value

As shown in Table 6-9, different sets of numerical standards are in use in geodesy. This has to be considered within this project when combining the different geometric and gravimetric quantities. The same holds for tide and time systems, which are not uniquely defined for the different geodetic quantities. While gravimetric products, such as the GOCE gravity field models, are given in the zero-tide system (in agreement with IAG resolution No. 16 of the 18th General Assembly 1983), the geometric quantities, such as the ITRF, are given in the conventional tide free system. The difference between these two tide systems is latitude dependent, and this effect is more than 10 cm for station heights in the Baltic Sea area. The formulae for the transformation between different tide systems are provided in Section 7 of the IERS Conventions 2010 (Petit and Luzum 2010). Please also note that the gravitational constant  $GM$  of the IERS Conventions refers to TCG (Coordinated Geocentric Time), whereas the EGM2008 value is expressed in the Terrestrial Time (TT). Both values displayed in Table 6-9 are fully consistent (the small difference can be explained by the different time systems). For the transformation of 3-D Cartesian coordinates into ellipsoidal coordinates, the conventional GRS80 parameters shall be used for all the different observation types and products to ensure consistency of the combination results. For example, the difference for the equatorial radius  $a$  between GRS80 and the IERS Conventions 2010 is about 40 cm. It is also strongly recommended to use the conventional  $W_0$  value (IAG 2015) as the reference value for the geopotential at the geoid. More details on standards-related issues are provided in the inventory of standards and conventions compiled by the GGOS Bureau of Products and Standards (Angermann et al. 2016 and 2020).

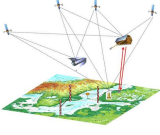
Furthermore, also the background models and standards used for the processing of the different geometric and gravimetric quantities should be consistently applied with the project. The IERS Conventions 2010 and its updates as provided at the Website of the IERS Conventions Center ([http://iers-conventions.obspm.fr/conventions\\_versions.php](http://iers-conventions.obspm.fr/conventions_versions.php)) should be applied for the processing of the different observations. Moreover, individual technique-specific standards need to be considered for the processing of the GNSS data (IGS- and EPN-Standards), the SAR data (SAR standards), the tide gauge data (EUROGOOS, BOOS, PSMSL) and the gravimetric quantities (IAG Resolutions No. 1/2, 2015; GOCE Standards).

In summary, the standards used for the different data types and products need to be clearly documented, and in the case of any deviations regarding numerical standards, time or tide systems, transformations between different sets have to be performed to get consistent results. Furthermore, also the background models and processing standards need to be consistently applied for the different observation types used within this project.

The geometric and gravimetric quantities refer to different global terrestrial reference frame realizations (e.g., ITRF2008, ITRF2014) and technique-specific frames (e.g., IGS08, IGS14). Thus, similarity transformations might have to be performed between the different realizations, or the transformation parameters published at the ITRF Website ([http://itrf.ensg.ign.fr/ITRF\\_solutions/2014/ITRF2014.php](http://itrf.ensg.ign.fr/ITRF_solutions/2014/ITRF2014.php)) could be used instead. For a combination and comparison of results expressed in different reference frames, it has to be considered that the results of these transformations depend on the network geometries and on the selected stations, including the weighting.

In the context of global reference frames, there are the three following issues (see below), which are important for the combination of different geometric and gravimetric quantities as well as for the comparison and validation of different products:

- (1) **Non-linear station motions:** The ITRF realizations are primarily based on a linear model (station positions and constant velocities), and thus, non-linear motions are visible in the station position residuals. The time series analysis of station positions reveal non-linear motions of several millimeters or even more (up to a few centimeters) for some stations, which are caused by various effects such as neglected surface loading (e.g. Bloßfeld et al., 2014). These non-linear station motions may cause errors in the order of a few millimeters when transforming the (regional) GNSS solutions into the global reference frame. This is a dominating error source within this project, which can affect the combinations and comparisons of different geometric and gravimetric quantities. Thus, it is strongly recommended to study this issue in detail, e.g., by using the periodic signals of the ITRF2014 results (available on request from IGN, Altamimi et al. 2016), by using the DTRF2014 results

	<b>BALTIC+ Theme 5</b>  Geodetic SAR for Baltic Height System Unification and Baltic Sea Level Research	<b>Final Report</b> Doc. Nr: SAR-HSU-SR-0022 Issue: 1.1 Date: 07.07.2021 Page: 58 of 170
---	--	--

(which consider for the first time non-tidal loading corrections, Seitz et al. 2020), and by using geophysical models for the atmospheric, hydrological and oceanic loading from the Global Geophysical Fluids Center (GGFC) or from other available sources.

- (2) **Extrapolation of ITRF results:** The ITRF2014 and DTRF2014 contain data until the end of 2014. If GNSS (or SAR) solutions (processed for example in 2020) need to be transformed to the global reference frame, the station positions must be extrapolated over a time period of about ten years, since the reference epoch of ITRF2014 station positions is 2010.0. Assuming that station velocities may have an error of 2 mm/yr, the required extrapolation will cause a position error of about 2 cm. Since the non-linear effects in station position time series (as discussed above) are visible mainly in the height components, this issue is very critical for this project.
- (3) **Realization of the ITRF origin, Center of Mass (CM) versus Center of Figure (CF):** The ITRF origin is realized by SLR observations. Through the orbit dynamics, SLR determines the Center of Mass (CM). According to the IERS Conventions 2010 (Petit and Luzum 2010), the ITRF2014 (and DTRF2014) origin follows the mean Earth center of mass, averaged over the time span of SLR observations used and modeled as a secular (linear) function in time. For the first time, the ITRF2014 provides an annual geocenter motion model derived from the same SLR data that defines the ITRF2014 long-term origin (Altamimi et al. 2016). The DTRF2014 delivers the time series of the SLR translation parameters as an additional product (Seitz et al. 2016), and the JTRF2014 realizes the origin at the quasi-instantaneous CM as sensed by SLR (Abbondanza et al. 2017).

#### Transformations between ITRF and EUREF

Taking into account the case study in the Baltic sea area, also regional and national reference frames (e.g., EUREF, GREF, SWEPOS) and transformations between them are involved. The orientation rate of the ITRF is aligned to that of the geophysical no-net-rotation model (NNR-NUVEL-1A), whereas for EUREF the European Terrestrial Reference System 89 (ETRS89) has been adopted in 1990. This definition follows the EUREF Resolution 1 that states: "The IAG Subcommission for the European Reference Frame recommends that the system to be adopted by EUREF will be coincident with the ITRS at the epoch 1989.0 and fixed to the stable part of the Eurasian Plate and will be known as European Terrestrial Reference System 89 (ETRS89)" (Altamimi 2018). The ETRS89 definition follows two conditions:

- The ETRS89 coincides with the ITRS at epoch 1989.0. This condition leads to consider that the 7 transformation parameters between ITRS and ETRS89 are all zeros at epoch 1989.0.
- The ETRS89 is fixed to the stable part of the Eurasian tectonic plate. This condition implies that the ETRS89 is co-moving with the Eurasian tectonic plate, hence defining its time evolution. Therefore, the time derivatives of the 7 parameters between ITRS and ETRS89 are zeros, except the three rotation rates. The three rotation rates are in fact the three components of the Eurasia angular velocity in the ITRF<sub>yy</sub> frames.

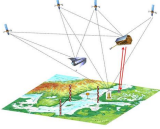
As a consequence of the above two conditions, it becomes straightforward to derive the transformation formulae allowing to link the ETRS89 to the ITRS, for both station positions and station velocities, using the equations published for example in Boucher and Altamimi (2011) and Altamimi (2018). When transforming station coordinates from ITRS to ETRS89 at a specific epoch  $t$ , the users are strongly advised to validate their obtained station coordinates in their preferred ETRS89 frame, by using the web-based tool available at the EUREF Permanent Network (EPN) website: [http://epncb.oma.be/productservices/coord\\_trans/](http://epncb.oma.be/productservices/coord_trans/).

#### Parameter Summary

Table 6-10 summarizes the input and output for references frames and joint standards. In particular, it is described which standards need to be addressed when combining the results of the different processors.

**Table 6-10:** Overview of Input/Output Parameters for Reference Frames and Joint Standards

Parameter Name	Description	Type	Source (Input)/ Target (Output)	Comment
STD-NUM	Numerical Standards	Input Output	Services/ Literature Height System Unification and Absolute Sea Level	Numerical standards relevant for the project and collected from literature (GRS80, EGM2008, IERS Conventions 2010, IAG)
STD-NLSM	Non-linear Station Motions	Output	Height System Unification and Absolute Sea Level	Non-linear motions of ECR and GNSS stations due to periodic signals given by ITRF2014 or DTRF2014 results and by geophysical models for the atmospheric, hydrological and oceanic loading.
STD-ITRF	Extrapolation of ITRF Results	Output	Height System Unification and	Extrapolation parameters for geometric coordinates (SAR, GNSS) from reference epoch 2010.0. to observation time (2020).

	<b>BALTIC+ Theme 5</b> Geodetic SAR for Baltic Height System Unification and Baltic Sea Level Research	<b>Final Report</b> Doc. Nr: SAR-HSU-SR-0022 Issue: 1.1 Date: 07.07.2021 Page: 59 of 170
---	--	--

			Absolute Sea Level	
STD-ORI	Center of Mass versus Center of Figure	Output	Height System Unification and Absolute Sea Level	Geocenter motion needed for the combination of geometric heights (SAR, GNSS) with gravimetric geoid heights.
STD-EUREF	Transformations between ITRF and EUREF	Output	Height System Unification and Absolute Sea Level	Transformation formulae allowing to link the ETRS89 to the ITRS, for both station positions and station velocities.

## 6.7 Height System Unification and Absolute Sea Level

In order to compute absolute sea level heights for tide gauge markers with respect to a chosen physical height reference system (an equipotential surface) all individual observation types need to be combined in a consistent way securing that common standards are applied during all processing steps. For a defined epoch  $t$  the formula to compute an absolute sea level heights reads as follows:

$$S^{TG}(t) = h^{TG}(t) - N^{TG}(t) + z^{TG}(t) \quad (6.38)$$

- where:  $t$  Observation epoch
- $z^{TG}(t)$  Tide gauge sea level height above tide gauge zero marker at epoch  $t$  (relative sea level)
- $h^{TG}(t)$  Height of tide gauge zero marker above reference ellipsoid at epoch  $t$  (ellipsoidal height)
- $N^{TG}(t)$  Height of reference equipotential surface above reference ellipsoid at tide gauge location at epoch  $t$  (geoid height)
- $S^{TG}(t)$  Sea level height above reference equipotential surface at epoch  $t$  (absolute sea level height)

If we target for physical heights at a tide gauge station referring to a unique reference equipotential surface at an epoch  $t$  and not considering the absolute or relative sea level, we can apply the following formula:

$$H^{TG}(t) = h^{TG}(t) - N^{TG}(t) \quad (6.39)$$

- where:  $H^{TG}(t)$  Physical height of tide gauge zero marker above reference equipotential surface.

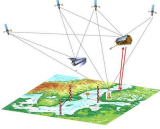
If offsets of the tide gauge zero markers physical heights (as computed with equation (6.39)) shall be computed with respect to physical heights given in the national or regional height system, levelled heights of the tide gauge zero marker are needed. These offsets then can be further used to unify national or regional height systems.

### Parameter Summary

Table 6-11 summarizes the input and output for computing absolute sea level observations and offsets for height system unification.

**Table 6-11:** Overview of Input/Output Parameters for Height System Unification and Absolute Sea Level

Parameter Name	Description	Type	Source (Input)/ Target (Output)	Comment
SAR-POS	SAR Positioning Solution	Input	SAR Positioning	Time series of coordinates of the SAR target as X, Y, Z coordinates in the ITRF2014 and uncertainties $\sigma_X, \sigma_Y, \sigma_Z, \sigma_{XY}, \sigma_{XZ}, \sigma_{YZ}$ , derived from the variance-covariance matrix $\Sigma(\hat{\mathbf{x}})$ . Confidence ellipsoid from eigenvalue and eigenvector decomposition of $\Sigma(\hat{\mathbf{x}})$ scaled to a 95% confidence level. In case external reference coordinates for the same target are also available (e.g. from a

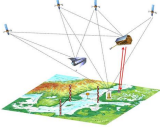
	<b>BALTIC+ Theme 5</b> Geodetic SAR for Baltic Height System Unification and Baltic Sea Level Research		<b>Final Report</b> Doc. Nr: SAR-HSU-SR-0022 Issue: 1.1 Date: 07.07.2021 Page: 60 of 170

				terrestrial survey), the $\Delta X_{x,y,z}$ coordinate differences are computed.
SAR-OBS	SAR Observation Solution	Input	SAR Positioning	Time series of range and azimuth standard deviations $\sigma_r$ and $\sigma_a$ , provided by the variance component estimation and observation residuals.
GNSS-POS	GNSS Positioning Solution	Input	GNSS Positioning	Time series of coordinates of the GNSS stations as X, Y, Z coordinates in the ITRF2014 and uncertainties.
TG-SSH	Corrected Sea Surface Height at Tide Gauge Stations	Input	Tide Gauge Data Analysis	Time series of corrected sea surface heights observed at tide gauges with respect to the tide gauge benchmark with hourly temporal resolution.
GEO-HGT	Geoid Heights	Input	GOCE based Geoid Computation	Time series of geoid heights or height anomalies for tide gauge stations.
STD-NUM	Numerical Standards	Input	Reference Frames and Joint Standards	Numerical standards relevant for the project and collected from literature (GRS80, EGM2008, IERS Conventions 2010, IAG)
STD-NLSM	Non-linear Station Motions	Input	Reference Frames and Joint Standards	Non-linear motions of ECR and GNSS stations due to periodic signals given by ITRF2014 or DTRF2014 results and by geophysical models for the atmospheric, hydrological and oceanic loading.
STD-ITRF	Extrapolation of ITRF Results	Input	Reference Frames and Joint Standards	Extrapolation parameters for geometric coordinates (SAR, GNSS) from reference epoch 2010.0. to observation time (2020).
STD-ORI	Center of Mass versus Center of Figure	Input	Reference Frames and Joint Standards	Geocenter motion needed for the combination of geometric heights (SAR, GNSS) with gravimetric geoid heights.
STD-EUREF	Transformations between ITRF and EUREF	Input	Reference Frames and Joint Standards	Transformation formulae allowing to link the ETRS89 to the ITRS, for both station positions and station velocities.
SL-ABS	Absolute Sea Level Heights	Output	ESA & Public	Time series of absolute sea level heights of tide gauge stations involved in the project.

### Parameter and Processing Flow

Chapters 6.1 to 6.7 in detail define all parameters needed to perform the individual processing tasks. For height system unification and absolute sea level determination all intermediate results are combined into one final output. This is shown in Figure 6-13, which in details specifies the complete data and processing flow from the original observations to the final products.



	<b>BALTIC+ Theme 5</b>  Geodetic SAR for Baltic Height System Unification and Baltic Sea Level Research	<b>Final Report</b> Doc. Nr: SAR-HSU-SR-0022 Issue: 1.1 Date: 07.07.2021 Page: 62 of 170
---	--	--

## 7 ALGORITHMS VALIDATION AND PRELIMINARY ANALYSES

The algorithms specified and described in chapter 6 are validated based on preliminary data or subsets of final data sets not covering the full analysis period for the year 2020. The validation results show that the algorithms are properly implemented and that the results obtained from the different processors are meaningful.

### 7.1 SAR Data Analysis and Value Adding

#### 7.1.1 SAR Data End-to-End Validation

The validation of the SAR products of the range and azimuth measurements as listed in Table 7-1 was performed for the passive corner reflectors at DLR Oberpfaffenhofen, at Metsähovi geodetic observatory, and at Wettzell geodetic observatory (see Table 7-2), as well as for selected ECRs. Using the known reference coordinates of these targets, the correctness of the generated products is validated by combining measurement files and correction files and comparing them with reference values derived from the known positions and the precise Sentinel-1 orbits. The conversion of the azimuth results to units of meters uses an average Sentinel-1 swath velocity of 6842 m/s. The procedure for assessing the SAR geolocation quality of targets with known reference coordinates is well established in literature (Balss et al., 2018a, Balss et al., 2018b, Gisinger et al., 2021). The reference values for range and azimuth ( $\tau_{ref}, t_{ref}$ ) are inferred from the given precise orbit state vectors ( $X_S, \dot{X}_S$ ) and the target's ITRF position at the epoch of observation  $X_{ref}$ . First, the Doppler equation, which defines the zero-Doppler plane with respect to satellite trajectory, is iteratively solved for the reference azimuth as time of closest approach. The obtained zero-Doppler satellite position is then inserted into the range equation to compute the corresponding reference range value.

$$\frac{\dot{X}_S(t) \cdot (X_{ref} - X_S(t))}{|\dot{X}_S(t)| \cdot |X_{ref} - X_S(t)|} = 0 \rightarrow t_{ref} \quad (7.1)$$

$$\tau_{ref} = c / 2 \cdot |X_{ref} - X_S(t_{ref})|$$

Finally, range and azimuth geolocation residuals are computed by comparing the measurements with the reference values as follows:

$$\Delta\tau_{res} = (\tilde{\tau} + \Delta\tau_{DRC} - \Delta\tau_{tro} - \Delta\tau_{ion} - \Delta\tau_{sec} - \Delta\tau_{cal} - \tau_{ref}) \cdot c / 2 \quad (7.2)$$

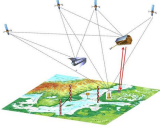
$$\Delta t_{res} = (\tilde{t} + \Delta t_{BAC} + \Delta t_{FMCC} - \Delta t_{sec} - \Delta t_{cal} - t_{ref}) \cdot v_{swath}$$

where the different input quantities are provided by the SAR data products listed in Table 7-1:

- $\tilde{\tau}, \tilde{t}$  = raw range and azimuth observations as extracted from Sentinel-1 SAR images
- $\Delta\tau_{DRC}$  = correction for Doppler shifts in range
- $\Delta t_{BAC}$  = correction for bistatic shifts in azimuth
- $\Delta t_{FMCC}$  = correction for azimuth shifts due to FM-rate mismatch
- $\Delta\tau_{tro}$  = correction for tropospheric slant range delay
- $\Delta\tau_{ion}$  = correction for ionospheric slant range delay
- $\Delta\tau_{sec}, \Delta t_{sec}$  = corrections in range and azimuth for tidal-related displacements of solid Earth
- $\Delta\tau_{cal}, \Delta t_{cal}$  = Sentinel-1 geometric range and azimuth calibration constants
- $c$  = speed of light in vacuum
- $v_{swath}$  = average Sentinel-1 swath velocity

**Table 7-1:** Set of intermediate products generated by SAR data analysis and value adding. Corresponding algorithms and methods are outlined in chapter 6.1.

Product Type	Description
Point target analysis	Raw slant range and azimuth radar observations of ECRs and selected CRs as extracted from Sentinel-1 IW image products. Additional Sentinel-1 system corrections for the bistatic shifts in azimuth shifts, for the Doppler-induced shifts in range, and for the shifts in azimuth due to mismatch of the azimuth FM-rate.
Sentinel-1 precise orbit ephemerides	Daily precise orbit ephemerides product as provided by Sentinel-1 PDGS.
SAR observations	Slant range and azimuth observations of ECRs and CRs corrected for the Sentinel-1 system effects. These observations are the basic SAR measurements obeying the orthogonal zero-Doppler convention.
Tropospheric path delays	Slant range corrections for the tropospheric slant path delay derived from the VMF3 model (Vienna Mapping Function, release 3).
Ionospheric path delays	Slant range corrections for the ionospheric slant path delay derived from the GNSS-based global ionospheric maps distributed by the IGS.

	<b>BALTIC+ Theme 5</b> Geodetic SAR for Baltic Height System Unification and Baltic Sea Level Research	<b>Final Report</b> Doc. Nr: SAR-HSU-SR-0022 Issue: 1.1 Date: 07.07.2021 Page: 63 of 170
---	--	--

Solid Earth tidal deformations	Slant range and azimuth corrections for the sum of tidal-related solid Earth deformations as defined in the conventions of the geodetic ITRF.
Sentinel-1 system calibration	Sentinel-1 geometric calibration constants to compensate for the internal electronic delays of the SAR payloads and the residual biases of the SAR systems. Two constants (range and azimuth) for each Sentinel-1 sensor (S1A and S1B), i.e. four constants in total.
ECR system effects	Systematic observation errors introduced by the ECRs (electronic delays, antenna phase center offsets).
Time series of ECR phase	Time series of ECR phase w.r.t. passive reference CR at the DLR calibration site to assess ECR phase stability
PS-InSAR vertical deformation rates	Linear vertical deformation rates between two ECRs derived from PS-InSAR line-of-sight deformation velocity estimates

**Table 7-2:** Calibration sites used for SAR data end-to-end validation

Calibration Site	Site Location (latitude / longitude)	SAR Ground Infrastructure	Description
DLR Campus Oberpfaffenhofen	Germany (48.0856° / 11.2802°)	1.5m CR (1), ECR (2)	CR facing West (Sentinel-1 ascending tracks); Reference coordinates from differential GNSS survey (< 1.5 cm); Permanent IGS GNSS station (OBE4)
Wetzell Geodetic Observatory	Germany (49.1447° / 12.8783°)	1.5m CR (2)	CRs facing East and West (Sentinel-1 ascending and descending tracks); Reference coordinates from terrestrial local tie survey (< 5 mm); Permanent IGS GNSS stations (WTZA, WTZR, WTZS, WTZZ)
Metsähovi Geodetic Observatory	Finland (60.2176° / 24.3945°)	1.5m CR (1)	CR facing East (Sentinel-1 descending tracks); Reference coordinates from terrestrial local tie survey (< 5mm); Permanent IGS GNSS station (METS)

Figure 7-1 shows the residuals using the measurement files after applying all the corrections from the products and considering the Sentinel-1 range and azimuth timing calibration constants. The data covers all Sentinel-1A and Sentinel-1B passes of 2020 at the different CR test sites. The results show the measurement files as is, which means that measurements with low signal-to-clutter are already removed (they remain accessible in the raw data file of the point target analysis), but otherwise the data is unchanged, i.e., no further outlier detection has been applied.

The residuals across all test sites are in line with the results reported for Sentinel-1 absolute geolocation (Gisinger et al., 2021). The standard deviations in range and azimuth vary between 4-5 cm and 25-42 cm, respectively, see Table 7-3. The accuracy is on the order of 5 cm in range and 15 cm in azimuth. Overall, these numbers are within expectation. They are in accordance with the limits given by the Sentinel-1 system (orbit, SAR payload), the applied corrections, and the dimension of the used corner reflectors. In conclusion, the end-to-end validation results confirm the correctness of our SAR data analysis system and the generated SAR data products for Sentinel-1 range and azimuth time measurements.

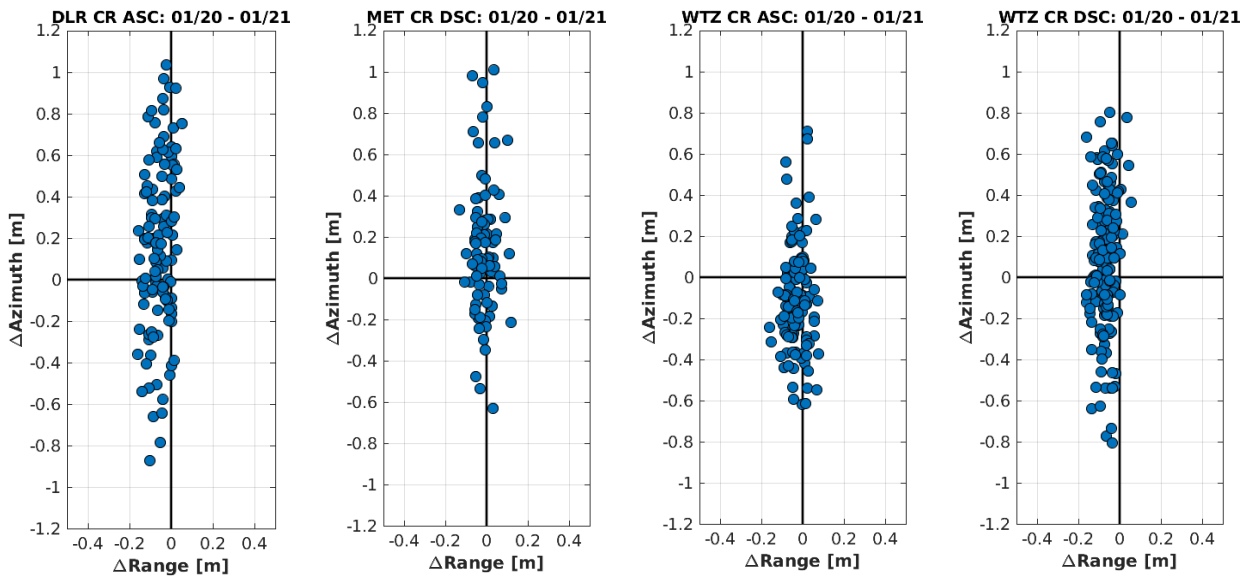
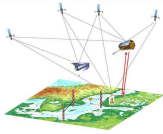


**Figure 7-1:** Residuals in range and azimuth obtained with the SAR data products when applying the end-to-end SAR geolocation analysis at the corner reflector test sites described in Table 7-2 From left to right: DLR Oberpfaffenhofen, Metsähovi geodetic observatory, Wettzell geodetic observatory (2 CRs).

Compared to passive CR, the active ECR demand for two additional corrections that have to be considered in the analysis: Firstly, the locations of the geometric phase centers which differ for ascending and descending measurements and which are specified in the ECR user manual (Di Meo et al. 2019). These geometrical phase centers are applied when modelling the target position (see equation (7.1)) and are therefore not provided with the SAR measurement products. Secondly, there is the delay introduced by the ECR electronics, which has not been characterised by the manufacturer. Therefore, the characterization was performed as part of this project, yielding an experimental model that distinguishes the delay for ascending and descending measurements with respect to incidence angle, see section 7.1.2 for details.

Verification of the ECR delay model is performed with the ECR 113 at DLR Oberpfaffenhofen and the ECR 107 at Mårtsbo, Sweden. The latter was selected due to malfunctions of the second ECR installed at DLR site. The reference positions of both ECRs are known with 1-2 cm from differential GNSS survey. The residuals of the ECR end-to-end processing, applying the phase center offsets and the delay model, are shown in Figure 7-2. Even with an angular-dependent delay model considering ascending and descending passes, there remain systematic differences between the individual measurement geometries, see Table 7-3. Without applying additional outlier detection, the noise level of the ECR range observations is approximately 2-3 times larger when compared to the passive CR, whereas the azimuth data are on par or better. The results of the different geometries also listed in Table 7-3 confirm that most stacks are centred to zero and that overall data consistency depends on individual device characteristics. In conclusion, ECR data precision lies within expectation, but the measurement accuracy is currently limited by ECR electronic delay patterns. Their resolution would require an individual device characterization by the manufacturer.

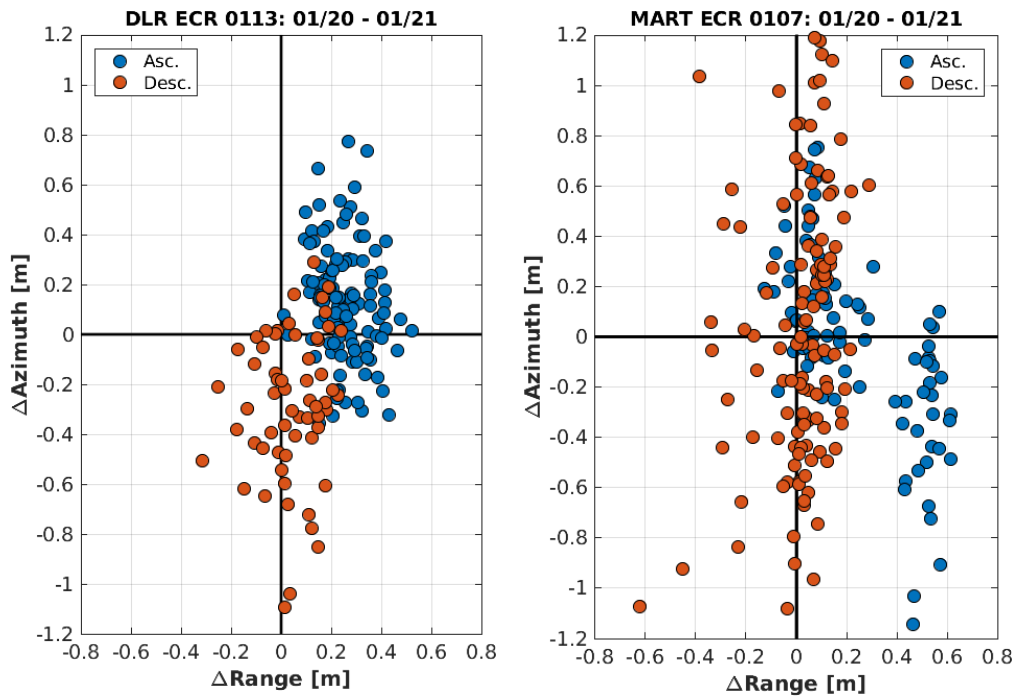
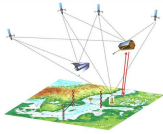


**Figure 7-2:** Residuals in range and azimuth obtained with the SAR data products when applying the end-to-end SAR geolocation analysis for transponders (ECR) installed at DLR Oberpfaffenhofen and Mårtsbo (Sweden). The colours mark the results as ascending and descending data.

**Table 7-3:** Results of the SAR data product end-to-end validation performed with the data acquired in 2020. Statistics of the range and azimuth residuals as shown in Figure 7-1 and Figure 7-2

Test Site	Samples [#]	Range			Azimuth		
		Mean [m]	STD [m]	RMS [m]	Mean [m]	STD [m]	RMS [m]
DLR OP CR Asc.	119	-0.056	0.050	0.075	0.145	0.423	0.445
Metsähovi CR Desc.	85	-0.011	0.047	0.048	0.146	0.318	0.348
Wettzell CR Asc.	123	-0.028	0.046	0.054	-0.098	0.251	0.269
Wettzell CR Desc.	162	-0.069	0.040	0.080	0.093	0.338	0.350
DLR OP ECR 113 Asc.	119	0.254	0.097	0.272	0.130	0.228	0.262
DLR OP ECR 113 Desc.	61	0.041	0.122	0.128	-0.300	0.319	0.436
Mårtsbo ECR 107 Asc.	95	0.236	0.230	0.328	0.019	0.456	0.454
Mårtsbo ECR 107 Dsc.	127	0.017	0.145	0.145	0.035	0.804	0.802
DLR OP ECR 113 All	180	0.182	0.146	0.233	-0.0156	0.332	0.331
Mårtsbo ECR 107 All	222	0.111	0.215	0.241	0.028	0.676	0.675

### 7.1.2 SAR Data Component Validation

This section reports on the results of the additional validation that was performed for selected SAR data products as described in Table 7-1.

#### Point Target Analysis

The product file of the point target analysis contains the raw range and azimuth times and corrections for the three Sentinel-1 system effects: Bistatic effects in azimuth, Doppler shifts in range, and the azimuth shifts due to FM-rate mismatch. The SAR data analysis system applies these corrections when generating the SAR measurement files. To test the proper behaviour of these corrections, the end-to-end analysis was performed with the raw measurements instead of the final measurement files. The results of the CRs located at DLR Oberpfaffenhofen and Wettzell geodetic observatory are displayed in Figure 7-3. Compared to the fully corrected results shown in Figure 7-1, the Sentinel-1 system corrections perform as expected: the bistatic azimuth correction centers the azimuth measurements to zero and removes the systematic difference among the different TOPS beams (see IW1 and IW2 for the DLR CR). The Doppler shifts in range correct for the systematic effects in the range measurements, which are clearly visible in the Wettzell measurements, because the CR is located in a burst overlap, i.e., it is measured twice during one pass. Finally, the FM-rate mismatch correction removes systematic azimuth effects between different bursts, which are again visible in the Wettzell CR results, i.e., the difference in azimuth between the two residual groups.

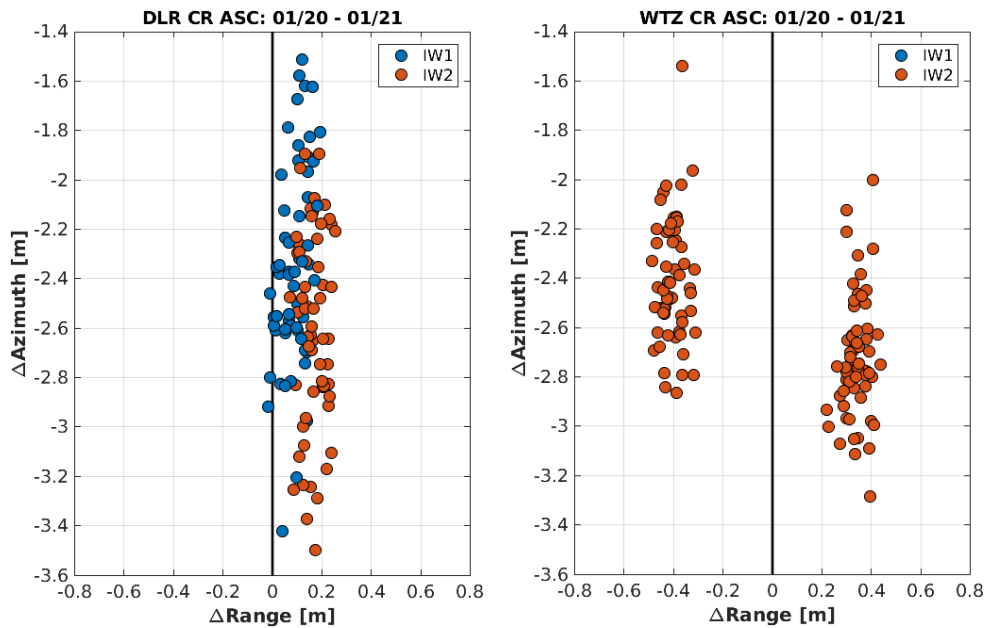


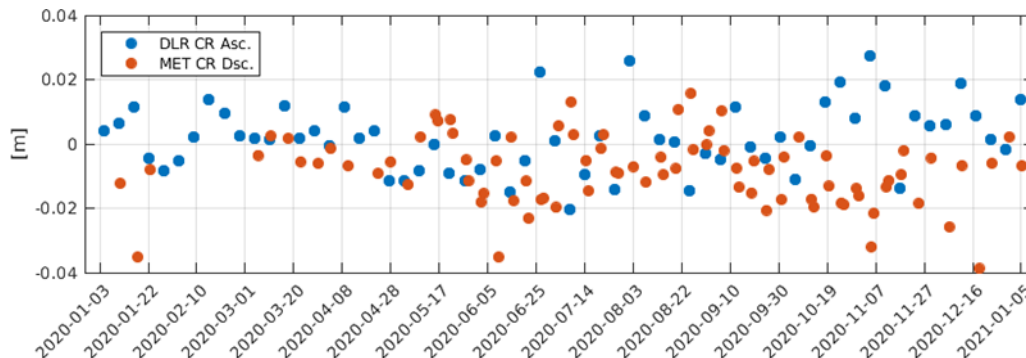
**Figure 7-3:** Residuals in range and azimuth obtained with the raw SAR measurements not corrected for the Sentinel-1 system errors when applying the end-to-end SAR geolocation analysis. Results for the CR at DLR Oberpfaffenhofen (left) and for the CR at Wettzell geodetic observatory (right). The colours mark the different beams of the Sentinel-1 TOPS acquisition mode (IW1 not observed in Wettzell).

#### Sentinel-1 Precise Orbit Ephemerides

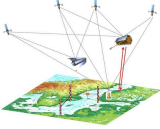
The precise orbit ephemerides distributed by Sentinel-1 Quality Control can be used as is for the analysis of the project at hand. The quality of the product is tested by the end-to-end SAR data validation shown in section 7.1.1. It confirms the accuracy of 5 cm or better that was reported for the Sentinel-1 orbits (Peter et al., 2017). Because the orbit ephemerides are currently not considered a limiting factor of the Sentinel-1 SAR system, the cross-validation of the alternative precise orbit ephemerides solution available at Sentinel-1 PDGS was not performed.

#### Tropospheric Delay

At geodetic observatories, accurate corrections for the tropospheric delay of SAR measurements can be derived from the zenith path delay data of permanently operated GNSS receivers (Gisinger et al. 2015). To validate the tropospheric delay corrections generated for this project, the tropospheric corrections files are compared with corrections computed from the path delay products distributed by the IGS (Villiger and Dach 2019). The comparison is performed for 2020 for the tropospheric delay products of Wettzell and Metsähovi. The results are shown in Figure 7-4 and Table 7-4. The RMS of the correction difference amounts to 1.5 cm and 1.1 cm, which confirms correctness of the VMF3-based tropospheric delay corrections generated by the SAR data analysis system.



**Figure 7-4:** Difference between the tropospheric delay correction files generated by the SAR data analysis system and the tropospheric delay corrections derived from GNSS-based IGS delay products. Analysis performed for the tropospheric delay correction files of the Wettzell CR (Ascending) and the Metsähovi CR (Descending).

	<b>BALTIC+ Theme 5</b>  Geodetic SAR for Baltic Height System Unification and Baltic Sea Level Research	<b>Final Report</b> Doc. Nr: SAR-HSU-SR-0022 Issue: 1.1 Date: 07.07.2021 Page: 67 of 170
---	--	--

**Table 7-4:** Comparison of tropospheric path delays generated by the SAR data analysis system and the delays computed from the IGS tropospheric zenith delay product. Statistics of the correction differences as shown in Figure 7-4

Site	Mean [m]	STD [m]	RMS [m]
Metsähovi CR	-0.009	0.012	0.015
Wetzell CR Ascending	0.002	0.0104	0.011

### Ionospheric Delay

The total electronic content (TEC) maps used to model the ionospheric delay contain RMS maps, which quantify the accuracy of the TEC solutions estimated with the global GNSS network. The SAR data analysis system converts this RMS information into an accuracy estimate of the computed ionospheric delay correction and reports this in the corresponding SAR correction files. Figure 7-5 shows an analysis of the maximum RMS values found in the ionospheric correction files of each ECR installation site. The reported numbers confirm that for most of the stations the ionospheric delay corrections are estimated with 1 cm or better. The RMS level of the ionospheric correction are not limiting the Sentinel-1 SAR system performance and confirm the applicability of the generated products.

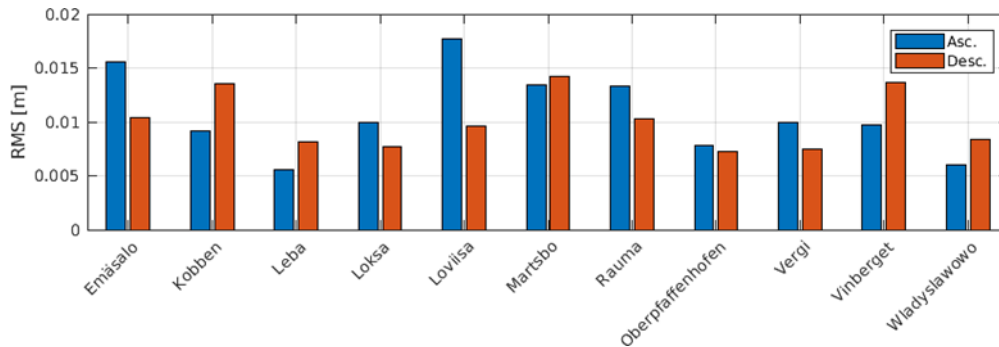


**Figure 7-5:** Maximum RMS as reported in the ionospheric delay correction products of the different ECR installation sites. Results for all data of 2020. The colours mark the RMS of the ascending and descending correction data of each site.

### Solid Earth Tidal Deformations

The additional validation of the geodynamic correction products following IERS 2010 conventions against tidal deformations computed by GNSS software was not performed. The results obtained for the end-to-end SAR data analysis are considered an appropriate validation of the correction files generated by the SAR analysis system.

### Sentinel-1 System Calibration

The Sentinel-1 system calibration constants primarily account for the electronic delay of the SAR payloads. They were determined with the CR at Metsähovi geodetic observatory and three years of Sentinel-1A and Sentinel-1B data. The same procedure was already used for the re-calibration of the TerraSAR-X mission, which confirmed the stability of Metsähovi geodetic observatory as SAR calibration site (Balss et al. 2018a).

Table 7-5 lists the constants contained in the two calibration file products used in this project. To ease interpretation, the numbers are also shown in units of meters. Applying these calibration constants mitigates the systematic difference of the Sentinel-1 sensors and centers the measurements close to zero, see the results obtained for the different CRs (section 7.1.1). Therefore, no further changes are required to calibrate the Sentinel-1 SAR data of this project.

**Table 7-5:** Range and azimuth time calibration constants for Sentinel-1A and Sentinel-1B as provided in the calibration product file. The numbers in units of meters are listed only for interpretation

	Range [s]	Azimuth [s]	Range [m]	Azimuth [m]
<b>Sentinel-1A</b>	1.1281e-9	1.2873e-5	0.1691	0.0881
<b>Sentinel-1B</b>	6.4566e-11	-4.9701e-5	0.0881	-0.3400

### ECR System Effects

The ECR electronic delay calibration has to be performed empirically, because an accurate delay calibration is not yet provided by the ECR manufacturer. The ECRs installed at DLR Oberpfaffenhofen, Märtsbo and Vinberget (both Sweden), and Vergi and Loksa (both Estonia) were used to determine the delay model, because their positions are known within 5 centimetres or better from differential GNSS surveys carried out during the installations.

The SAR data products containing the data of 2020 were processed for range and azimuth residuals as described in section 6.1. The residuals of the individual stacks were cleaned from outliers using the median and the 95% confidence interval, assuming normal distribution. Subsequently, mean estimates were performed per stack, which have an estimated precision (95% confidence) of 4 cm in range and 10 cm in azimuth and which are displayed in Figure 7-6. The results show significant offsets among the different ECRs and the observed pass geometries, which are attributed to ECR delay characteristics. The differences between ascending and descending results could be explained with the two amplification chains employed by the ECRs (Di Meo et al. 2019), whereas the causes for the variations among the ECRs built to same specification and deviations between incidence angles are not known. Because of these results, linear angular-dependent delay models, discriminating ascending and descending data, were fitted to the averaged residuals by using least-squares adjustment. The model coefficients are listed in Table 7-6. They allow for a delay compensation in most ECR measurements with an accuracy of approximately 10 cm, but systematic differences of up to 40 cm may remain in certain geometries, which was already confirmed by the ECR results of the end-to-end validation discussed in section 7.1.1.

In order to validate the methods applied for ECR delay model computation, the same processing was also performed for the data of the passive CR. The results are shown in Figure 7-7. The range results underline the high quality of the Sentinel-1 ranging system and they confirm that the observed effects are not part of the Sentinel-1 system but are caused by the active ECRs. The hypothetical constant delay model estimated for the CRs is effectively zero. The azimuth data have small residual offsets that indicate the accuracy limit of Sentinel-1 azimuth measurements, but they are approximately two times smaller than the azimuth offsets observed for the ECRs. In conclusion, the results confirm correctness of the empirical delay calibration approach.

**Table 7-6:** ECR range and azimuth time delay model coefficients for ascending and descending measurements as derived from ECR residuals of the different installation sites, see Figure 7-6. The  $a_0$  denotes the mean offsets and the  $a_1$  denotes linear component that depends on the incidence angle.

	$a_0$ [s]	$a_1$ [s/°]
ECR Range Delay Ascending	7.2416e-09	1.1405e-10
ECR Range Delay Descending	1.1243e-08	-4.7810e-11
ECR Azimuth Delay Ascending	9.5494e-05	-2.102e-06
ECR Azimuth Delay Descending	1.0584e-05	-2.3110e-06

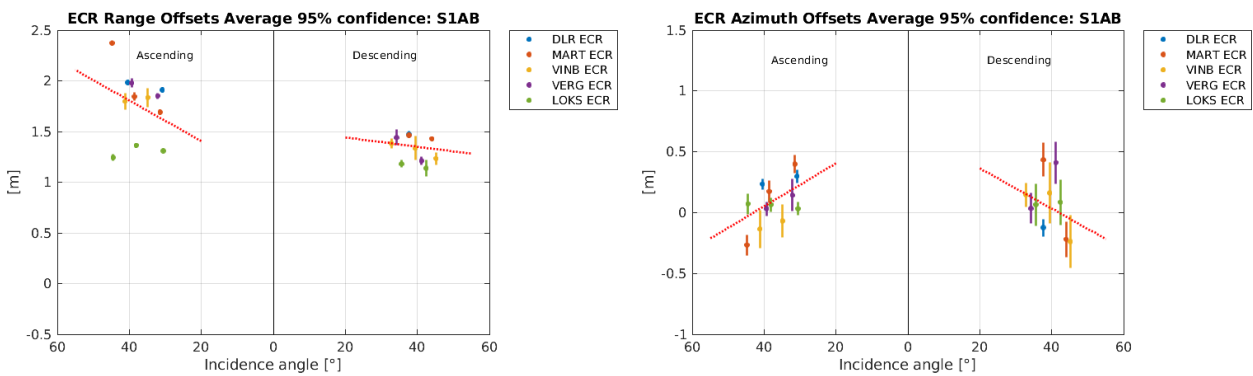


**Figure 7-6:** Average ECR residuals for the different pass geometries of selected ECR sites after applying an outlier detection per geometry, assuming normal distribution and five percent outliers. Visualization according to SAR data incidence angles and ascending and descending geometries, amounting to 22 stacks in total. Range results (left) and azimuth results (right). The red lines visualize the linear delay models as listed in Table 7-6.

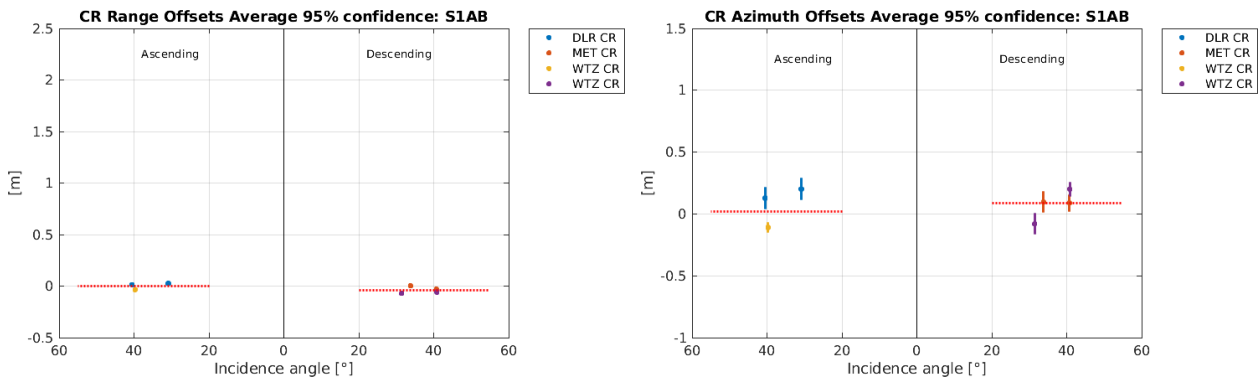


**Figure 7-7:** Average CR residuals for the different pass geometries of selected CR sites after applying an outlier detection per geometry, assuming normal distribution and five percent outliers. Visualization according to SAR data incidence angles and ascending and descending geometries, amounting to 7 stacks in total. Range results (left) and azimuth results (right). The red lines visualize a hypothetical CR delay model

### 7.1.3 InSAR Results Validation

Various passive reflectors and active transponders are installed at the DLR Oberpfaffenhofen premises for test and calibration purposes (see Table 7-2). Several trihedral CRs, of suitable size (1.5 m edge length) for C-band measurements and oriented for both ascending and descending geometries, are available. The single functioning ECR installed at this site (ECR 113) is compared to a subset of the trihedral CRs. Since the distances between the reflectors are all less than 1km, the spatial variation in propagation delay from the troposphere, geodynamics and ionosphere is quite small so as to be negligible when considering the relative phase between (E)CRs.

The simulated phase, comprised of components due to the WGS84 ellipsoid and height of the point above the ellipsoid, is compensated for in the interferometric phase. Here, there is an error due to the actual height of the point with respect to the DEM. However, due to the small spatial baseline of Sentinel-1 and the small height error of the points (the heights of the phase centres are about 1m above the DEM), this can also be neglected.

#### *InSAR and PSI Processing*

InSAR coregistration and PSI processing was performed with IWAP (Integrated Wide Area Processor) which was used to generate the German national motion map (BGR, 2021). The interferometric (temporally between a secondary and reference acquisition) phase is calculated for all detected PSs, among which the (E)CR and CRs should be found, for every secondary acquisition in the coregistered stack yielding a time series of double differenced phases. IWAP provides the interferometric phase already corrected for the simulated phase. The processing steps are as follows:

1. All secondary acquisitions in the stack are coregistered to high accuracy to a single reference acquisition.
2. PSs are detected in the coregistered stack. These are strong point-like scatterers with temporally stable amplitude and phase behaviour. PS detection is the first step in PSI. The positions of the PS are determined from the average calibrated amplitude image of the coregistered stack which is in the radar geometry of the reference acquisition. This reduces the effect of clutter shifting the location of the PS's peak amplitude in individual acquisitions which would otherwise dominate the phase.
3. The amplitude and phase are determined at the location of each PS in every coregistered acquisition using bandpass oversampling. Geometric parameters such as the simulated phase are calculated from coregistration parameters, orbit state vectors and a DEM.

#### *Phase Stability Analysis*

After InSAR and PSI processing, all necessary information for the phase stability analysis is available which consists of 3 major steps:

1. For each (E)CR, determine the position of the nearest detected PS. This PS should correspond to the (E)CR. Extract the calibrated amplitude (Sigma Zero), interferometric phase and other necessary information for these PSs = (E)CRs.
2. For each (E)CR, from the calibrated amplitude time series, discard any acquisition with an amplitude whose value is less than the stack median minus 3 times the median absolute deviation (corrected to be unbiased for normally distributed values). This may occur when precipitation (snow in winter) collects in a trihedral CR. Also, discard any E(CR)s whose amplitude behaviour is visually unstable, e.g. with long periods of reduced amplitude indicating a change in orientation.

For each (E)CR pair, compute the relative interferometric phase. Remove linear and seasonal trends. A linear trend, i.e. a relative velocity, may be caused by the loose grounding of CRs on grassland, leading to settling. Seasonal trends may be caused by soil expansion and contraction due to moisture or effects related to temperature. Note that in this case, any temperature dependent effects of the ECR's electronics are mitigated and will have to be determined by other means. Any

(E)CRs displaying visually aberrant behaviour, such as phase jumps due to an altered phase centre, are removed. The standard deviation of the residual phase on a pair is then used as a proxy for phase stability.

*Results*

This analysis was carried out for two stacks, relative orbit 44 in ascending geometry (44A) and relative orbit 168 in descending geometry (168D) with relevant details in Table 7-7. The temporal coverage of each stack is almost exactly 1 year, allowing the estimation and mitigation of any seasonal or temperature dependent trends.

**Table 7-7:** Stack details for the 2 geometries analysed for phase stability

Stack	Number of Acquisitions	Temporal Coverage	Reference Acquisition Date
44A	60	10-01-2020 – 16-01-2021	16-03-2020
168D	62	13-01-2020 – 19-01-2021	06-04-2020

The (E)CRs used in the phase stability analysis along with their orientations and positions are listed in Table 7-8. Note that CR OBE5 refers to two CRs, each with a different geometry and physical location. The ECR contains two practically co-located transponders for ascending and descending orientations.

**Table 7-8:** (E)CR used in the phase stability analysis

Type	ID	Orientation	Position (WGS-84)		
			Latitude (deg)	Longitude (deg)	Height (m)
ECR	19-0113	Ascending	48.087834	11.279231	623.000
ECR	19-0113	Descending	48.087834	11.279231	623.000
CR	OBE1	Ascending	48.085832	11.281787	624.853
CR	OBE5	Ascending	48.082541	11.277944	628.186
CR	OBE2	Descending	48.083685	11.278317	624.811
CR	OBE3	Descending	48.082869	11.278443	627.664

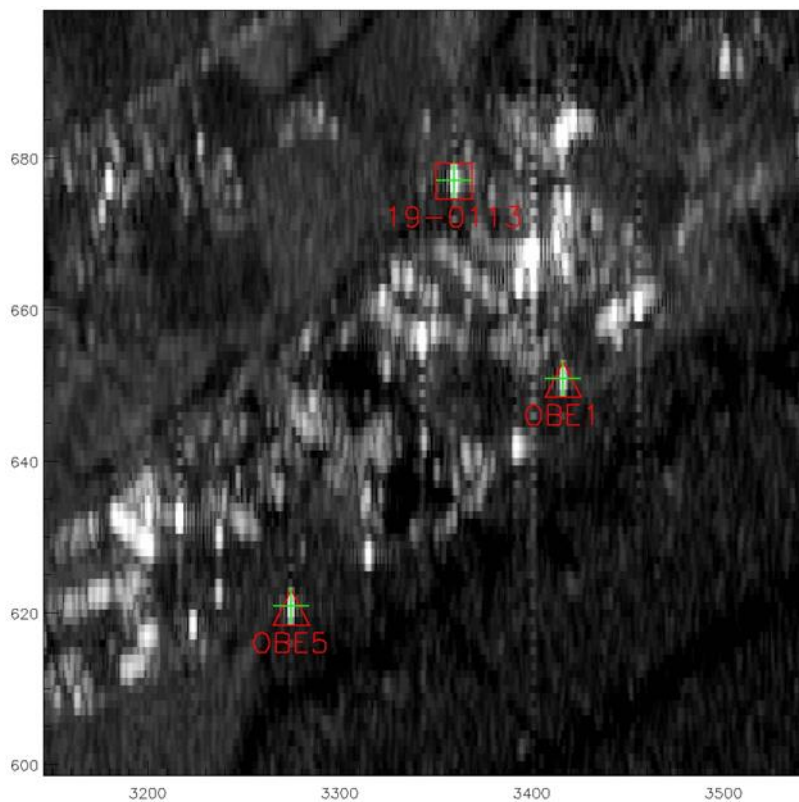


**Figure 7-8:** Detected (E)CRs overlaid on the stack average calibrated amplitude image in radar geometry for stack 44A. The ground dimensions of the image are approximately 1km in range (x-axis) and azimuth (y-axis). The known positions projected onto radar geometry are shown for the ECR (red box) and CRs (red triangles), along with the positions determined during PS detection from the stack average calibrated amplitude image (green crosses).

An example of the detected (E)CRs overlaid on the stack average calibrated amplitude image in radar geometry for stack 44A is shown in Figure 7-8. Note the presence of other strong scatterers due to infrastructure such as buildings and

satellite dishes which are distributed over the site. These may cause strong contaminating signals. The special airfield at Oberpfaffenhofen is visible as an area of low backscatter in the lower right of the image. Likewise, the upper left portion of the image consists predominantly of agricultural fields, also with a low backscatter. The sidelobes of several very strong scatterers appear as a series of points along azimuth centred on the scatterer. Strong sidelobes such as these can contaminate the measurements of other scatterers lying directly on them and so should be avoided.

An example of the residual time series for stack 44A, pair (ECR)19-0113 ← (CR)OBE1, converted to one-way slant range difference values in millimetres, is shown in Figure 7-9. The time values are referenced to the master acquisition, although this is irrelevant for the analysis. It should, however, be ensured that the calibrated amplitude of the (E)CR in the master acquisition is above the threshold.

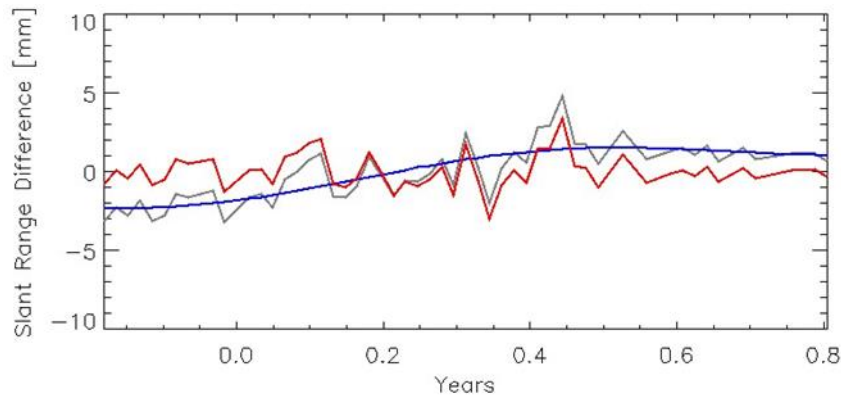


**Figure 7-9:** Residual time series (red) for stack 44A, pair (ECR)19-0113 ← (CR)OBE1, converted to one-way slant range difference values in millimetres. Also shown is the time series before trend removal (grey) and the estimated linear and seasonal trend (blue).

The results of the phase analysis for each (E)CR pair are shown in Table 7-9. As already mentioned, the absolute phase stability of a single (E)CR was not determined from this inherently relative analysis. What can be seen, however, is that the residual standard deviation of pairs with an ECR (1.34mm or 17.3° on average) is higher than those with only CRs (1.01mm or 13.1° on average), suggesting that the phase stability of the ECR is less than that of the CRs. These results seem to be comparable to the values 0.6 mm to 1.4 mm published in (Mahapatra et al. 2017). In conclusion, the results confirm principle usability of the ECRs for InSAR processing and correctness of the IWAP software.

**Table 7-9:** Phase stability analysis results derived with IWAP

Stack	Pair to ← from	Acquisitions in Time Series	Residual Standard Deviation	
			mm	degrees
44A	19-0113 ← OBE1	54	1.05	13.66
44A	19-0113 ← OBE5	56	1.42	18.38
44A	OBE1 ← OBE5	54	1.03	13.39
168D	19-0113 ← OBE2	58	1.60	20.72
168D	19-0113 ← OBE3	57	1.27	16.49
168D	OBE2 ← OBE3	58	0.98	12.78

## 7.2 SAR Positioning

The positioning results show internal accuracies in the centimetre-level that can reach millimetre-level for some ECR stations, e.g. Vergi when using a post positioning bias correction. This is illustrated in the confidence ellipsoids in Figure 7-10. Comparing the confidence ellipsoids of ECRs and CRs one can see a clear difference. The CRs show a strong directionality in their uncertainties especially in the height component, which is caused due to the limited observation geometry. CRs can only be observed in either ascending or descending orbit geometries. The ECR uncertainties are much smaller and show much less dependence in a specific direction as both ascending and descending orbit geometries are included in the observations. Directionalities in the uncertainties might still occur eventually, due to different number of observations in ascending/descending geometries.

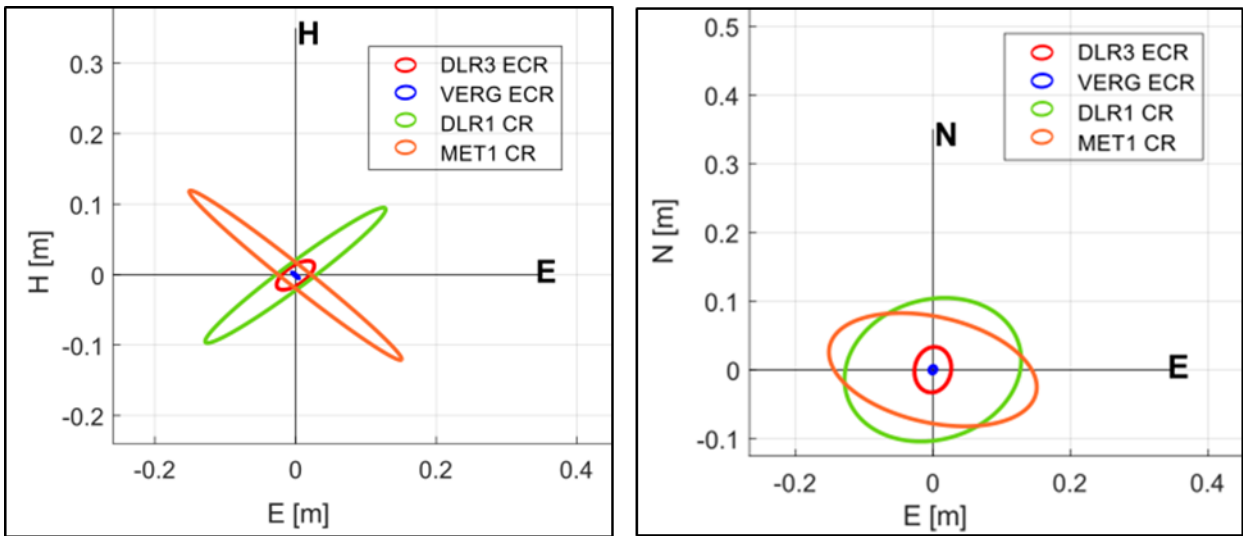


**Figure 7-10:** Internal positioning accuracy is illustrated through confidence ellipsoids of CR Stations at DLR and Metsähovi as well as ECRs at DLR and Vergi. The figure displays the magnitude of the uncertainties of the positioning results in the local Height-East (left) and North-East (right) coordinates.

The absolute positioning accuracy with respect to positions from terrestrial survey at mm level is shown by the offset of the estimated position from the origin in Figure 7-11. The CRs and ECRs can be both positioned with an accuracy of few decimetres after an outlier removal. In addition to the outlier removal, an ECR delay model has been applied to ECR observations to compensate for electronic delay of the transponders (see section 7.1.2).

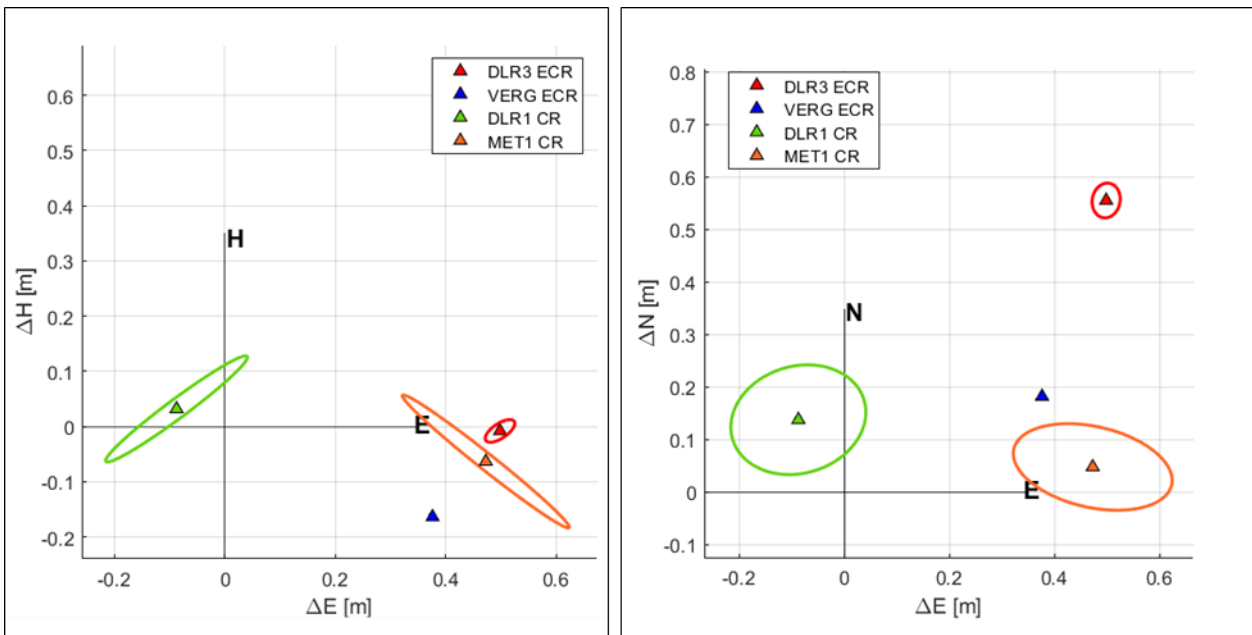
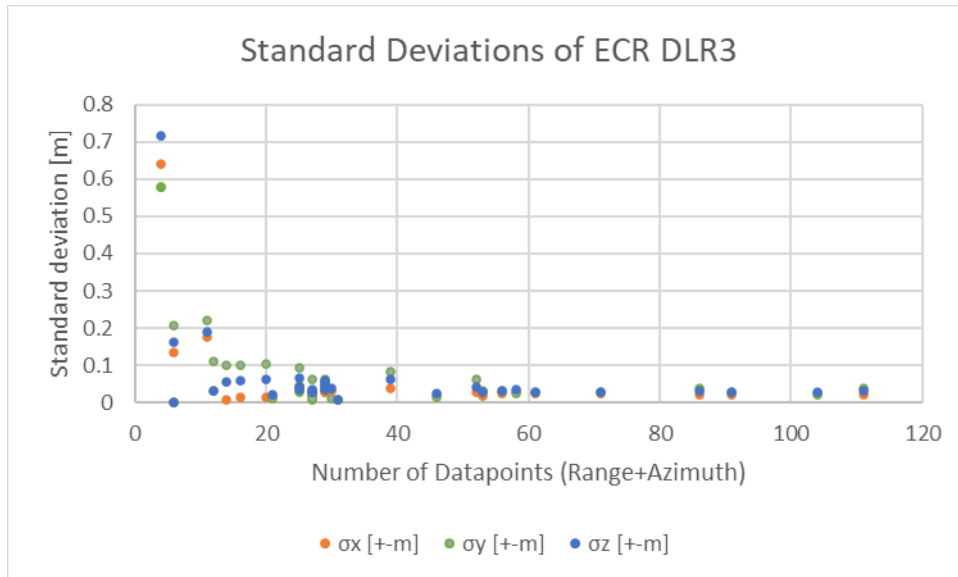


**Figure 7-11:** Absolute positioning accuracy with confidence Ellipsoid of Corner Reflector Stations at DLR and Metsähovi as well as ECRs at DLR and Vergi (error ellipsoid not visible). The positioning results are given with respect to the reference coordinates of each station in local Height-East-coordinates (left) and local North-East-coordinates (right).

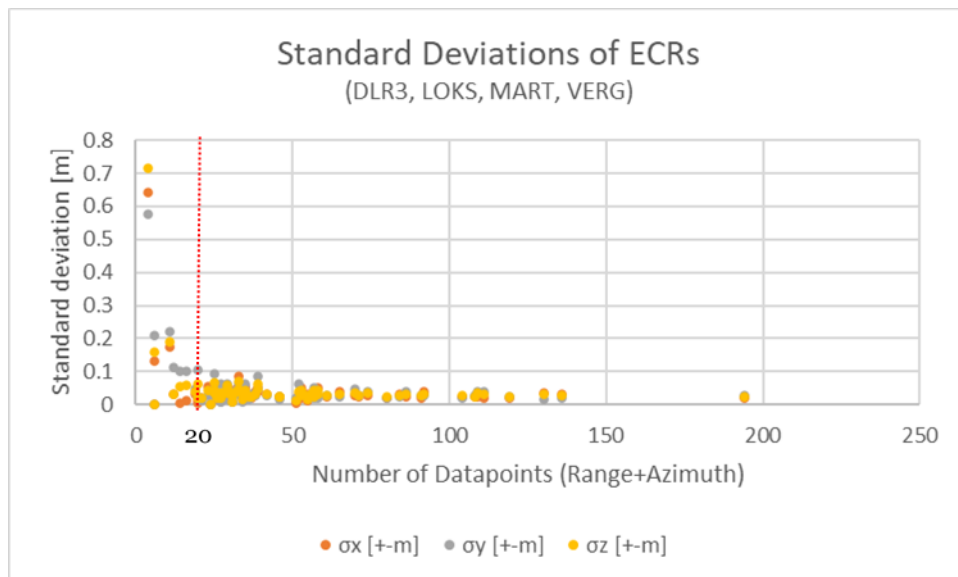
The minimum number of observation data points required to achieve a reasonable positioning solution is derived by looking at the resulting standard deviations of the least squares adjustment. Each observation epoch consists of one range data point and one azimuth data point. A valid data point is defined as a data point, which is no outlier nor were orbit information flagged for this epoch.

From multiple processing of the reference stations, taking different number of observation data points into account, the least squares statistics show that at least 20 valid range and azimuth data points shall be used to allow a stable positioning estimation. This results in a minimum number of observation epochs of 10, if these observation epochs contain no outliers. For smaller number of data points the standard deviations increases exponentially and starts to deviate significantly (Figure 7-12 and Figure 7-13). Furthermore, the results in Figure 7-13 show that the results become more

stable with increasing number of data points. Ideally more than 50 data points lead to the most stable solution. Current observation of the reference stations show that monthly solutions provide more than 20 valid data points for a station. For the reference ECR DLR3, bimonthly solutions contain between 50 and 60 data points. Trimonthly solutions of the current observations contain between 60 and 85. Four-monthly solutions contain 90 to 120 data points. Depending on the latitude of the station position, the data points can increase as the observable incidence angles increases with latitude.

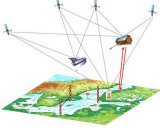


**Figure 7-12:** Least Squares standard deviations (x,y,z) for a different number of data points of the DLR3 ECR. Each observation epoch consists of one data point in azimuth and one data point in range.



**Figure 7-13:** Least squares standard deviations (x,y,z) of reference Stations (DLR3,LOKS, MART, VERG) with respect to the number of data points. Each observation epoch consists of one data point in azimuth and one data point in range.

The results obtained for the ECR test stations show that the SAR positioning processor is delivering absolute position errors comparable with those obtained with CRs, when applying all required corrections (including the ECR system correction per station). Because with ECRs ascending and descending arcs can be observed, the internal accuracy is more consistent than for CRs, which is shown by the achieving near circular error ellipsoids for ECR position solutions. Finally, it was identified that for obtaining stable positioning solutions at least 10 epochs of valid azimuth and range observations are needed. This implies that average position solutions per month can be computed with reasonable internal accuracy.

	<b>BALTIC+ Theme 5</b>  Geodetic SAR for Baltic Height System Unification and Baltic Sea Level Research	<b>Final Report</b> Doc. Nr: SAR-HSU-SR-0022 Issue: 1.1 Date: 07.07.2021 Page: 74 of 170
---	--	--

## 7.3 GNSS Positioning

### 7.3.1 GNSS Network Adjustment

Because the coordinates of the reference points of ECR-C transponders obtained from GNSS technique will be treated as reference values for the determination of the Geodetic-SAR technique, in the project we need to determine the height of the GNSS stations near the ECR-C stations with the highest possible accuracy.

Before making the decision to include certain stations of the IGS and EPN networks into the project's GNSS network, the site-log files and the observation data from these stations were reviewed in terms of their quality, gaps and missing sessions, using the data quality check program like e.g. TEQC. The geometry of the created network, the mutual distances between the stations as well as the availability and quality of station velocity vectors were also very important. Finally, 45 stations were qualified for preliminary analyses of the test networks, of which various variants are tested.

Observation data in RINEX format from stations of IGS and EPN networks are available. Access to data from national stations of the EUPOS system, which usually provide services for a fee, is slightly different. After approving the final locations of the ECRs, we obtained the access conditions (logins and passwords) for observation data files from selected stations of the FinnRef, ESTREF, ASG-EUPOS and SWEPOS networks, located near the transponders using the contact persons in each country participating in the project. Table 7-10 summarizes all available permanent GNSS stations in the vicinity of the included tide-gauge stations and the installed transponders.

**Table 7-10:** List of GNSS stations close to the ECR-C transponders installed in the project

Nearest GNSS station	City, Country	Network	Data available since	ECR-C installed
OBE4	DLR Oberpfaffenhofen, Germany	IGS/EPN	2019:DOY001	ECR_19_0113
LEBI	Leba, Poland	Leica network	2020:DOY001	ECR_18_0104
WLAD	Wladyslawowo, Poland	ASG-EUPOS	2019:DOY001	ECR_19_0114
VERG	Loksa, Estonia	ESTPOS	2019:DOY129	ECR_18_0098
VERG	Vergi, Estonia	ESTPOS	2019:DOY129	ECR_18_0086
LOV3	Loviisa, Finland	FinnRef	2019:DOY091	ECR_18_0091
METS,LOV3	Emasalo, Finland	IGS/EPN,FinnRef	2019:DOY091	ECR_19_0110
OLK2	Rauma, Finland	EPN	2019:DOY001	ECR_19_0111
SUN6, VINB	Vinberget, Sweden	EPN, SWEPOS	2019:DOY121	ECR_19_0106
MAR6, MAR7	Martsbo, Sweden	IGS/EPN	2019:DOY001	ECR_19_0107
KOBB	Kobben (Forsmark), Sweden	SWEPOS	2019:DOY121	ECR_19_0108

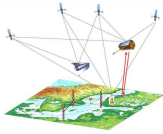
**Table 7-11:** GNSS equipment installed on selected stations close to ECR transponders or tide-gauge stations, involved in the Baltic+ project (period: 2020-01-01 – 2020-12-31, 2020: DOY001 – 2020:DOY366). (Stations with firmware update are marked in blue).

STAT	Receiver type	Firmware	Antenna type	Radome type	Rec./Ant. No.	H_ARP
KOBB	TRIMBLE NETR9	5.43	TPSCR.G5	OSPS	0852/11913	0.0000 m
LEBI	LEICA GR30	4.31-7.403	LEIAR10	NONE	5364/	0.0000 m
LOV3	JAVAD TRE_3 DELTA	3.7.7/4.0.0	JAVRINGANT_DM	SCIS	02750/02064	0.0000 m
MAR6	SEPT POLARX5	5.3.0	AOAD/M_T	OSOD	3025729/221	0.0710 m
MAR7	TRIMBLE ALLOY	5.43 / 5.45	LEIAR25.R3	LEIT	40025/40009	0.0030 m
METS	JAVAD TRE_3 DELTA	3.7.7	ASH700936C_M	NONE	02876/11761	0.0000 m
OBE4	JAVAD TRE_G3TH DELTA	3.7.6//3.7.9/3.7.10	JAV_RINGANT_G3T	NONE	214 / 340	0.0700 m
OLK2	JAVAD TRE_3 DELTA	3.7.7	JAVRINGANT_DM	SCIS	02874/0746	0.0000 m
SUN6	TRIMBLE NETR9	5.43 / 5.45	LEIAR25.R3	LEIT	0836/90012	0.0030 m
VERG	LEICA GR25	4.31-6.712 4.31-6.713	LEIAR25.R4	LEIT	1281 / 6291	0.0000 m
VINB	SEPT POLARX5	5.3.0	JNSCR_C146-22-1	OSOD	8053 / 0279	0.0710 m
WLAD	LEICA GR30	4.31/7.403	LEIAR20	LEIM	1932 / 4005	0.0000 m

RINEX data is available without delay for most of these stations. Only for KOBB and VINB stations from the SWEPOS network, the data is available in the data resources made available for the project with a delay of about 70 days.

For this reason, as well as because of the delay of about 14 days of the IGS global product availability (IGS combined), to the end of 2020 preliminary variants of network calculations were made in the network configuration shown in Figure 7-14, for several methods of defining vectors. All variants are implemented in the 'minimally constrained' network





All computations are performed using the Bernese GNSS Software in Double Differences (DD) mode. As reference frame the ITRF2014 (IGS14) with suitable coordinates and velocity vectors of all reference stations of the project's GNSS network is used. During GNSS data processing and for computing the GNSS stations positions, all parameters and models (accordingly with IERS Conventions 2010, Petit et al., 2010) described in Table 2-5 of the mentioned document are implemented:

- Station velocities - at least for the selected reference stations of the network are delivered by IERS to ensure consistency with the IGS satellite orbits and prevents network deformations induced by plates moving,
- TIDE2000 model for Solid and Ocean Pole Tides and Permanent Tides
- OT\_FES2004 model for Ocean Tidal Loading
- CMC for Centre of Mass corrections for ocean and atmospheric tidal loading
- EGM2008 as Geopotential model
- IAU2000Ro6 and IERS2010XY – as Nutation model and model of sub daily tidal variations of the pole and the Earth rotation
- DE405 - for modelling planetary ephemeris
- Antenna calibration model from I14.ATX (Antex)
- GMF/GPT and VMF1 models for ZTD computations

As Output of daily network solutions by the Bernese GNSS Software v.5.2 we obtain \*.crd files with X, Y, Z coordinates of all stations of the network in the ITRF2014 reference frame on the epoch of observation. On their basis, time series of coordinates of the GNSS stations as X, Y, Z and B, L, h coordinates in ITRF2014 and uncertainties are created. Analyses of test calculations of various variants of the designed GNSS station network are performed before the final network is fixed. On their basis, the optimal solution variant will be selected, in which all available observational data for the period until the end of 2020 will be computed.

From the different tests of GNSS network computations, obtained results look realistic. Below are presented the results from two COMPAR.Lxx files, which contain comparison of coordinates of each stations from each daily solution of the network. Both contain comparisons of the 100 daily network solutions from 2020. The first is a comparison from 2020: DOY001 to 2020: DOY099, the second is from 2020: DOY100 to 2020: DOY199.

45 stations, 2020:DOY001 - 202:DOY099

-----  
MEAN VALUES OF GEOCENTRIC X,Y,Z - COORDINATES  
RMS1: RMS OF UNWEIGHTED AVERAGE OF EACH COORDINATE COMPONENT  
RMS2: FORMAL ACCURACY OF EACH COORDINATE COMPONENT FROM COMBINED SOLUTION USING EQUAL WEIGHTS  
-----

STAT	#FIL	X (M)		Y (M)		Z (M)	
		RMS1	RMS2	RMS1	RMS2	RMS1	RMS2
KOBB	98	2999027.73439	0.00022	987782.37956	0.00013	5523181.10913	0.00029
LEBI	91	3517620.33599	0.00019	1111450.72273	0.00010	5185644.53221	0.00019
LOV3	98	2828365.38755	0.00021	1396873.05798	0.00013	5524911.18720	0.00019
MAR6	98	2998189.20674	0.00016	931451.99429	0.00007	5533398.88232	0.00019
MAR7	98	2998198.24738	0.00019	931450.11598	0.00014	5533393.04220	0.00024
OLK2	98	2866981.07407	0.00013	1129669.00350	0.00010	5565665.87001	0.00026
SUN6	98	2838910.79994	0.00016	903817.40938	0.00010	5620661.34778	0.00027
VERG	98	2905540.95985	0.00014	1423460.04167	0.00010	5478170.73945	0.00024
VINB	98	2829293.31782	0.00023	888151.51431	0.00021	5628086.96712	0.00032
WLAD	97	3496344.48597	0.00020	1164350.43431	0.00010	5188401.99433	0.00024

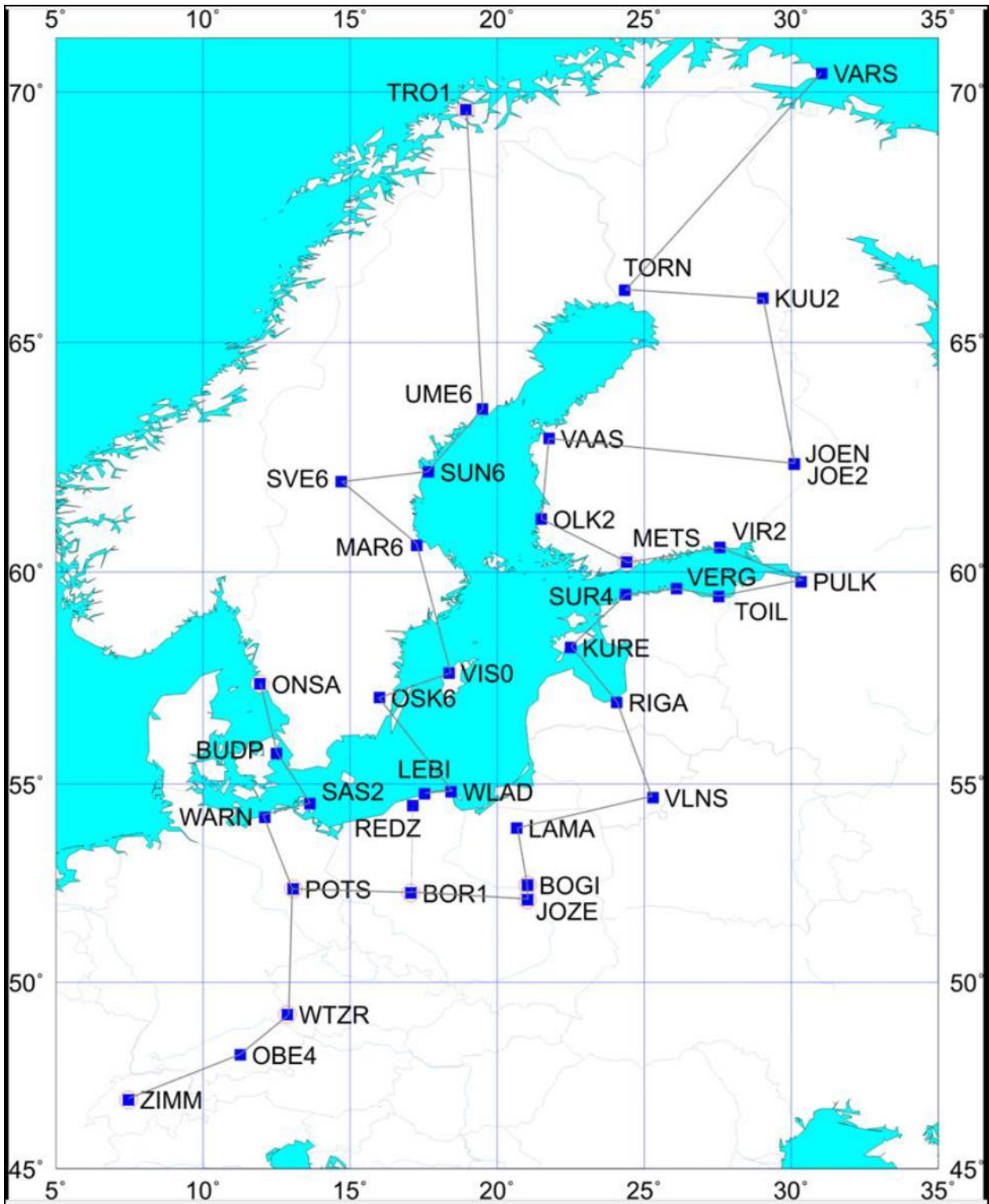
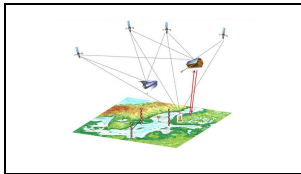
-----

45 stations, 2020:DOY100 - 202:DOY199

-----  
MEAN VALUES OF GEOCENTRIC X,Y,Z - COORDINATES  
RMS1: RMS OF UNWEIGHTED AVERAGE OF EACH COORDINATE COMPONENT  
RMS2: FORMAL ACCURACY OF EACH COORDINATE COMPONENT FROM COMBINED SOLUTION USING EQUAL WEIGHTS  
-----

STAT	#FIL	X (M)		Y (M)		Z (M)	
		RMS1	RMS2	RMS1	RMS2	RMS1	RMS2
KOBB	100	2999027.73082	0.00018	987782.38304	0.00012	5523181.11367	0.00036
LEBI	97	3517620.33128	0.00018	1111450.72641	0.00008	5185644.53452	0.00017
LOV3	100	2828365.38268	0.00015	1396873.06147	0.00014	5524911.18981	0.00033
MAR6	100	2998189.20393	0.00014	931451.99758	0.00008	5533398.88698	0.00029
MAR7	98	2998198.24427	0.00019	931450.12013	0.00021	5533393.04664	0.00047
OLK2	100	2866981.06905	0.00016	1129669.00791	0.00009	5565665.87318	0.00030
SUN6	99	2838910.79625	0.00015	903817.41153	0.00009	5620661.35047	0.00026
VERG	99	2905540.95573	0.00019	1423460.04603	0.00014	5478170.74246	0.00029
VINB	100	2829293.31413	0.00018	888151.51645	0.00013	5628086.97054	0.00024
WLAD	97	3496344.48457	0.00023	1164350.44347	0.00030	5188401.99653	0.00022

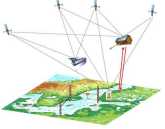
-----



**Figure 7-15:** Vectors configuration between selected GNSS stations involved in the Baltic+ project network using ‘minimally constrain’ strategy. An example of the construction of a network consisting of 37 GNSS stations.

7.3.2 GNSS to ECR Eccentricity Vectors and Vertical Connections

In order to compare ECR positioning results with those from co-located permanent GNSS stations eccentricity vectors need to be determined. By this geometric coordinates of the ECR reference point is determined in the ITRF2014 reference frame. The technique applied is exemplarily described for the ECR stations in Władysławowo and Łeba in Poland. Results of the eccentricity vectors are provided in the station description technical note (refer to [AD-4]).

	<b>BALTIC+ Theme 5</b>  Geodetic SAR for Baltic Height System Unification and Baltic Sea Level Research	Final Report Doc. Nr: SAR-HSU-SR-0022 Issue: 1.1 Date: 07.07.2021 Page: 78 of 170
---	--	---

Observation sessions were carried out immediately before the transponder installation and/or, during the levelling measurements in September 2020. At both stations, during the observation sessions, the GNSS antennas were positioned directly above the transponder reference points. For this purpose, previously made special adapters attached to a steel frame for mounting the ECR-C were used (see Figure 7-16).

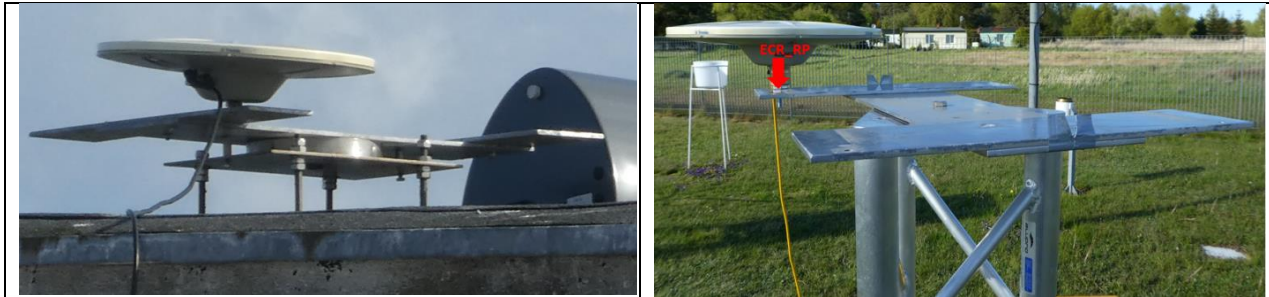


**Figure 7-16:** GNSS antenna installed on the adapter vertically above the ECR\_RP points: left in Władysławowo, right in Łeba station

### ***Eccentricity Vectors***

#### Władysławowo:

GNSS observation sessions performed on ECR\_RP point:

Year:DayOfYear	SessionDate	StartTime	StopTime	Duration
2020:DOY080	2020-03-20	12:50:55	15:36:05	02:45:10
2020:DOY254	2020-09-10	10:50:00	14:34:30	03:44:30
2020:DOY254	2020-09-10	14:53:30	23:59:55	09:06:25
2020:DOY255	2020-09-11	00:00:00	08:39:10	08:39:10

Result:

WLAD (GNSS) to WLAS (ECR) vector:

dLat = +2.456 m    sdLat = 0.0003 m  
 dLon = -0.080 m    sdLon = 0.0002 m  
 dh = -0.1348 m    sdh = 0.0005 m

Preliminary coordinates of the reference point of ECR\_19\_0114 in ITRF2014, epoch 2020.42:

Lat = 54° 47' 48.42044357"  
 Lon = 18° 25' 07.52248105"  
 h = 34.6233 m

#### Łeba:

GNSS observation sessions performed on ECR\_RP point:

Year:DayOfYear	SessionDate	StartTime	StopTime	Duration
2020:DOY255	2020-09-11	13:46:00	23:59:55	10:13:55
2020:DOY256	2020-09-12	00:00:00	05:54:45	05:54:45

Result:

LEBI (GNSS) to LEBS (ECR) vector:

dLat = -12.892 m    sdLat = 0.0003 m  
 dLon = +4.698 m    sdLon = 0.0003 m  
 dh = -3.9317 m    sdh = 0.0005 m

Preliminary coordinates of the reference point of ECR\_18\_0104 in ITRF2014, epoch 2020.42:

Lat = 54° 45' 13.17744414"  
 Lon = 17° 32' 05.54830034"  
 h = 33.9531 m

### ***Vertical Connections***

#### Władysławowo

Vertical connections of primary benchmark of Władysławowo tide-gauge (BM305362), tide-gauge reference point (TG\_BM), reference benchmark of WLAD GNSS station (WLAD\_BM), reference point of GNSS antenna (WLAD\_ARP) and reference point of ECR (ECR\_RP) were made using geometric levelling method. Height difference between WLAD\_BM and WLAD\_ARP is measured and controlled by calibrated steel and measuring rod, designed and used to operate the permanent WLAD GNSS station. The WLAD\_BM benchmark is located vertically below the GNSS antenna.

The height measurement between these points is possible thanks to the revision made in the roof and the concrete pole for mounting the antenna. Height difference between WLAD\_ARP and ECR\_RP points were determined using the GNSS technique (-0.1348 m) and geometric levelling (-0.1354 m). The obtained closure deviation of the measured closed levelling polygon with a length of 3.89 km is +1.35 mm, with an acceptable deviation of +/- 3.94 mm.

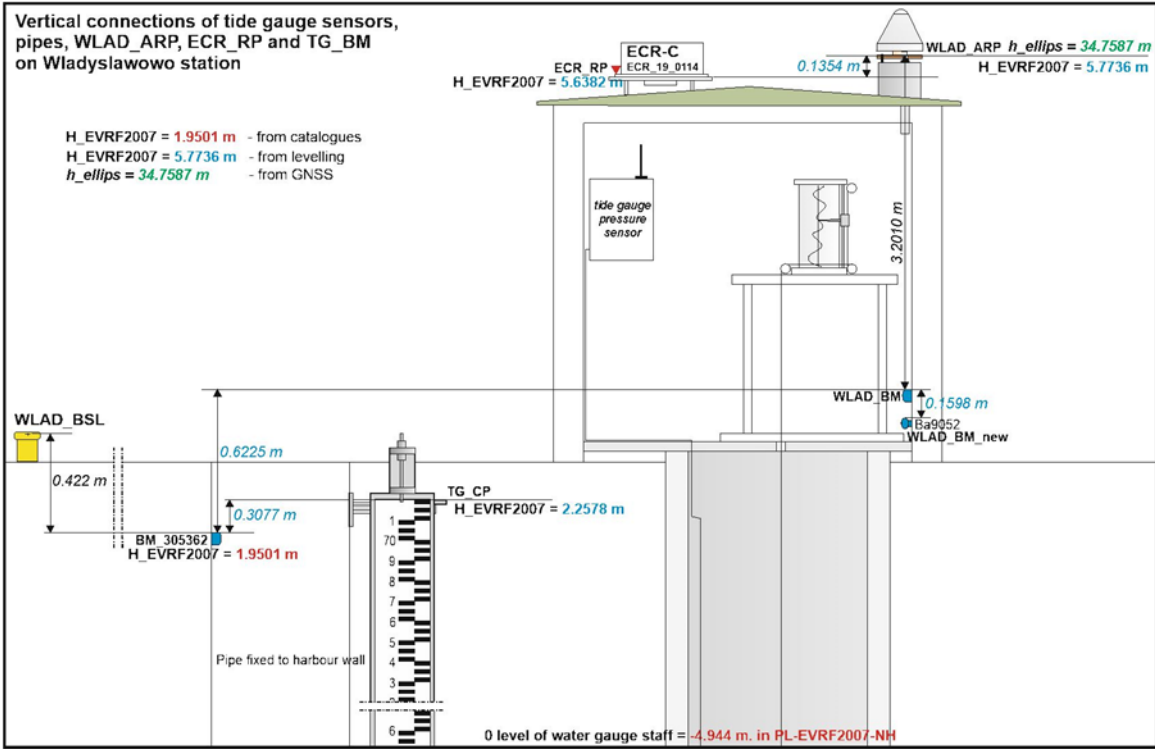


**Figure 7-17:** Vertical connections of primary benchmark of Władysławowo tide-gauge (BM305362), tide-gauge reference point (TG\_BM), reference benchmark of WLAD GNSS station (WLAD\_BM), reference point of GNSS antenna (WLAD\_ARP) and reference point of ECR-C transponder (ECR\_RP). On the left (in yellow) a historical marker of a GPS station used in the BSL campaigns (WLAD\_BSL), located several dozen meters from the tide-gauge.

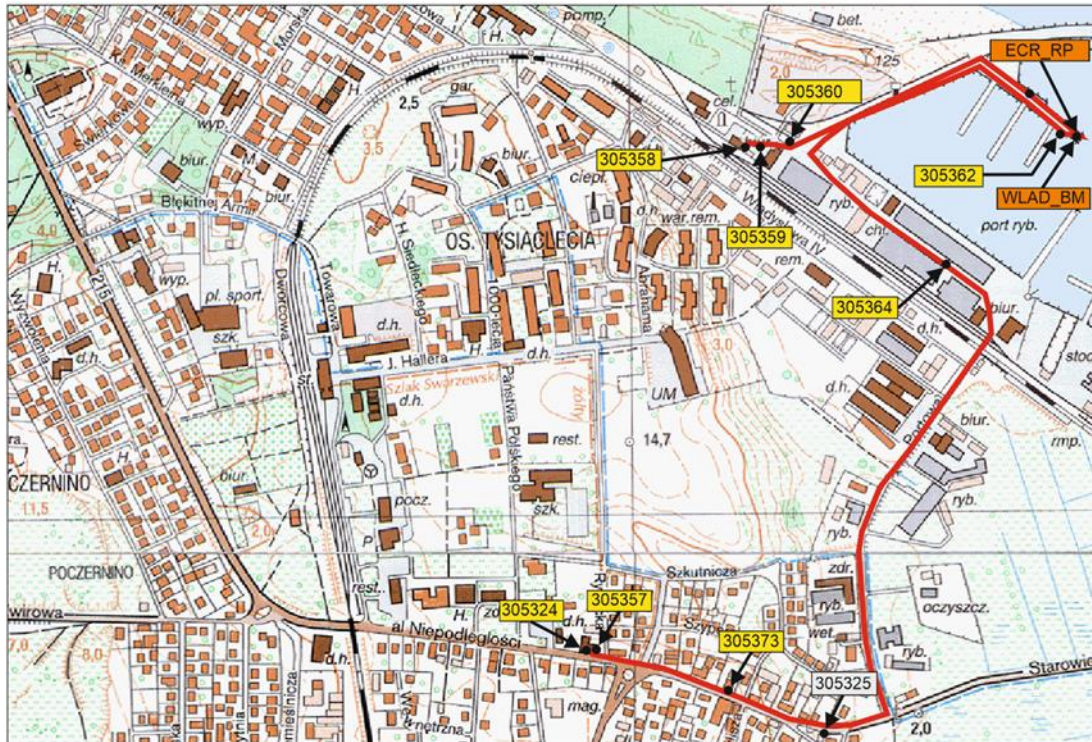
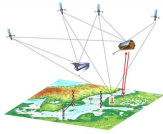


**Figure 7-18:** Levelling lines and selected benchmarks of the 1st order national vertical network, measured during measurements performed in September 10-11, 2020

Leba:

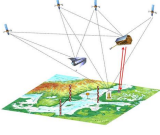


**Figure 7-19:** Map of the location of the measured points and benchmarks using the geometric levelling method in Leba on 2020-09-11 – 2020-09-18

## 7.4 Tide Gauge Data Analysis

The ECR transponders are mounted nearby seven tide gauge (TG) stations (Loksa, Emäsalo, Rauma, Leba, Wladyslawowo, Forsmark and Spikarna) in Estonia, Finland, Poland and Sweden. TG data analysis is based on the theoretical principles that are explained in section 6.4. In this chapter the used data and the results are analysed.

The TG data are recorded by the national tide gauge authorities of Estonia, Finland, Poland and Sweden. For preliminary analyses, the project requested the domestic TG data series for the time period 01.01.2020-31.07.2020, also relevant TG station documentation and meta-data. These include: definition of the TG station location, used sensor types, vertical datums, benchmarks, levelling information, maintenance, malfunctioning, etc. It appeared that all the participating tide gauge stations utilise automatic sea level detection sensors (e.g. pressure gauges, radars etc), see Table 7-12 for further details.

	<b>BALTIC+ Theme 5</b>  Geodetic SAR for Baltic Height System Unification and Baltic Sea Level Research	<b>Final Report</b> Doc. Nr: SAR-HSU-SR-0022 Issue: 1.1 Date: 07.07.2021 Page: 81 of 170
---	--	--

**Table 7-12:** Summary of participating TG stations

Tide gauge station	Location, national tide gauge agency	Tide gauge sensor type	Coordinates	Comments on the TG data series (see below an example)
Estonia Loksa	Southern coast of the Gulf of Finland  Estonian Environment Agency <a href="https://www.keskkonnaagentuur.ee/">https://www.keskkonnaagentuur.ee/</a>	modern pressure sensor,	59° 34' 58.8" 25° 42' 21.2"	TG readings are hourly averaged, corrected for: a) the sensor drift b) shift of the TGZ  TG station equipped with level staff for visual control readings
Finland Emäsalo	Northern coast of the Gulf of Finland  Finnish Meteorological Institute <a href="https://en.ilmatieteenlaitos.fi/">https://en.ilmatieteenlaitos.fi/</a>	Stilling well with float	60° 12' 20.8" 25° 37' 30.3"	<b>TGZ = staff reading 185.8 cm</b> TG readings refer to theoretical mean sea level. The conversion to N2000 in Emäsalo is +0.207 m. The TG readings are instantaneous, i.e. not hourly averaged. The hourly averaged data may be available for the final computations
Finland Rauma Ulko - Petäjäs	Eastern coast of the Gulf of Bothnia  Finnish Meteorological Institute <a href="https://en.ilmatieteenlaitos.fi/">https://en.ilmatieteenlaitos.fi/</a>	Stilling well with float	61° 08' 00.7" 21° 25' 33.0"	<b>TGZ = staff reading 150.5 cm</b> TG readings refer to theoretical mean sea level. The conversion to N2000 in Rauma is +0.119 m. The TG readings are instantaneous, i.e. not hourly averaged. The hourly averaged data may be available for the final computations
Sweden Forsmark	South-Western coast of the Gulf of Bothnia  Swedish Meteorological and Hydrological Institute (SMHI): <a href="http://www.smhi.se/">http://www.smhi.se/</a>	Two modern radar sensors.	62.3633° 17.5311°	TG readings are averaged, over 1-minute period every full hour. The hourly data are already in RH 2000.
Sweden Spikarna	Western coast of the Gulf of Bothnia SMHI: <a href="http://www.smhi.se/">http://www.smhi.se/</a>	Two modern radar sensors.	60.4085° 18.2109°	TG readings are averaged, over 1-minute period every full hour. The hourly data are already in RH 2000.
Poland Wladyslawo	Southern coast of the Baltic Sea, <b>Polish Institute of Meteorology and Water Management (IMGW-PIB)</b> in Gdynia <a href="https://www.imgw.pl/">https://www.imgw.pl/</a>	modern pressure sensor, modern float sensor	54° 47' 48.4" 18° 25' 07.4"	TG readings are hourly averaged, Initially not corrected (operational data). Checked by operator each day at 6am UTC. The hourly averaged and quality checked data were available for the final computations
Poland Leba	Southern coast of the Baltic Sea, <b>Polish Institute of Meteorology and Water Management IMGW-PIB</b> in Gdynia <a href="https://www.imgw.pl/">https://www.imgw.pl/</a>	modern pressure sensor, modern float sensor	54° 45' 48.2" 17° 33' 01.6"	TG readings are hourly averaged, Initially not corrected (operational data). Checked by operator each day at 6am UTC. The hourly averaged and quality checked data were available for the final computations

The data content and problematic quality issues were consulted with the respective national tide gauge authority. Relevantly, it was also identified whether the submitted TG data is „raw“ or is it corrected to account for certain phenomena, e.g. ocean and Earth tides.

The intention was to obtain hourly averaged sea level records for the time period 01.01.2020-31.07.2020. The advantage of the hourly TG data is that these contain no high frequency noise (i.e. sudden spikes in the time series), that usually is eliminated by the averaging procedure. However, these were not available in all the occasions, only the instantaneous ones. A sample of TG sea level fluctuations in an individual TG station (Loksa) is shown in Figure 7-20.

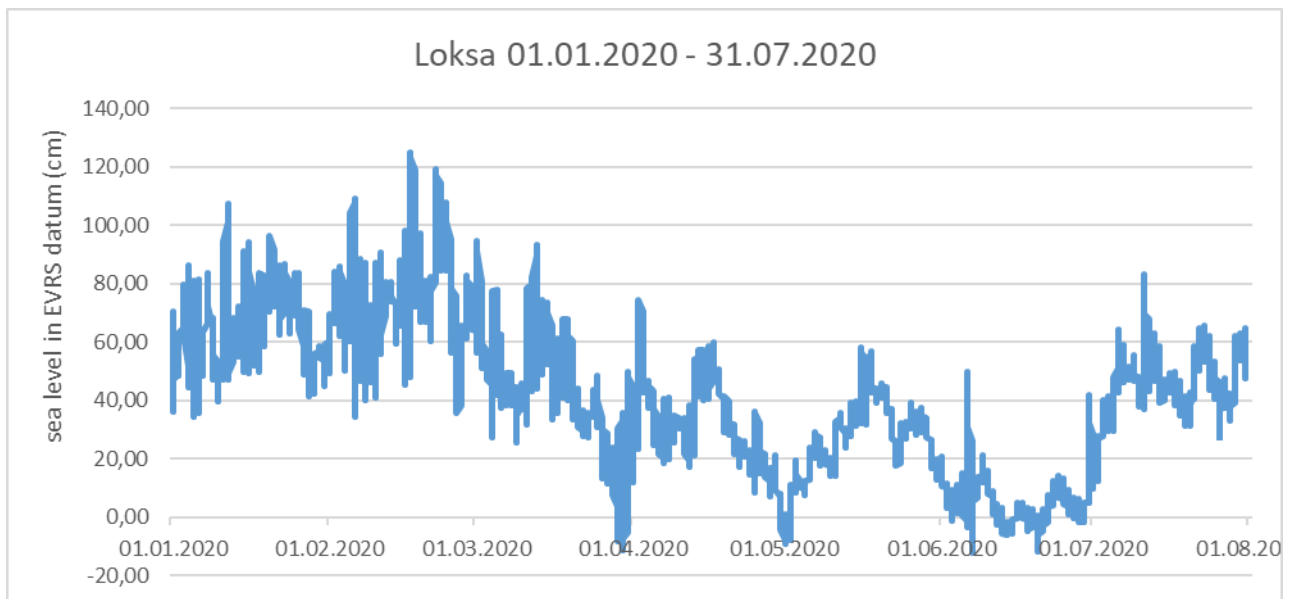
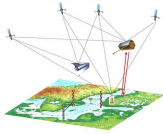


**Figure 7-20:** A sample of TG sea level fluctuations in the Loksa TG station for the time period 01.01.2020-31.07.2020

The tide gauge records were analysed for consistency and systematic distortions (that may occur due to external disturbances), in order to exclude unreliable records or low-quality observation data. Abrupt sea level changes (e.g. >10 cm over an hour) could be an indication of gross errors, such occasions were examined individually and verified with contemporary weather conditions. For instance, a few larger peaks at the sea level values were identified, see Figure 7-21, that illustrates an abrupt sea level rise in the Rauma TG station in Feb. 22.

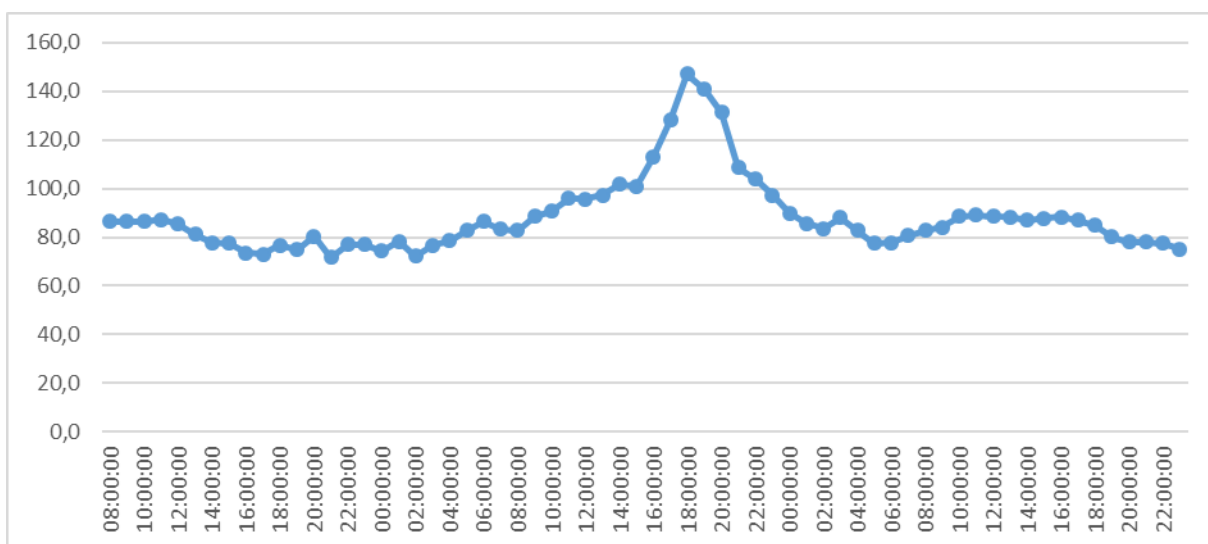


**Figure 7-21:** Rapid sea level rise in the Rauma TG station from 08.00 (UTC) 21/02/2020 up to 23:00 (UTC) 23.02.2020, with the highest peak at Feb 22 at 19:00 (UTC). The units of the vertical axis are cm.

The sea level in Rauma rises quite rapidly nearly one meter and drops back to where it started within some 8-10h period. It was confirmed that the sea level rise was generated by extreme meteorological conditions.

The data gaps (e.g. due to malfunctioning of instruments) in TG data series were identified, see Table 7-12. The standard deviation (STD) of the readings reflects the inner consistency (for the entire period, or seasonally) of the time series at each tide gauge station. Typically, the STD of the annual sea level series should remain within selected limit, whereas the larger STD is associated with the rougher sea conditions at individual TG station. The smaller STD may also reveal sea sheltered locations of certain tide gauges. The largest STD (0,253 m) is associated with the Loksa TG station, whereas the lowest STD of the tide gauge series are associated with both Polish TG stations (the corresponding STD values are 0.174 and 0.187 m).

The TG data series were used for computing the tentative (based on the 7 calendar months of observations only) mean sea level estimates for each TG station. The Gulf of Finland TG stations (Loksa and Emäsalo) at the opposite shores

showed good agreement, the average mean sea level was +40...+41 cm. In other words, the height difference between the mean sea levels at the opposite side of the gulf is almost zero. It appeared that during the time period in question (Jan-July) an upward sea level trend from west to east was identified in Gulf of Bothnia tide gauge stations. In other words, the sea level at the Finnish shore appeared to be about 7-8 cm higher than the sea level at the Swedish tide gauge stations.

The Rauma mean sea level (as of 30,5 cm) for the given time span (01.01.-31.7.2020) was confirmed by the adjacent Finnish TG stations Pori (+31 cm) and Turku (+33 cm). Intuitively thus, such a west-east directional upward tilt (and also higher than average sea level in the Gulf of Finland) could be due to prevailing (stronger and more frequent) westerly winds during the season in question.

Also examination of the closed hydrodynamic levelling loop Forsmark-Spikarna-Rauma-Forsmark yielded the zero value for the loop misclosure, see Table 7-13.

**Table 7-13:** Result of hydrodynamic levelling loop Forsmark-Spikarna-Rauma-Forsmark

Forsmark/Kobben	0,237	
		-0,014
Spikarna/Vinberget	0,223	
		0,087
Rauma	0,310	
		-0,073
Forsmark/Kobben	0,237	
<i>Loop misclosure</i>		0,000

The 3 cm mean sea level difference (+27 versus +30 cm) for the adjacent Polish stations could have some local coastal circulation related reason.

The national representatives also performed precise levelling for determining the ECR heights with respect to nearby levelling benchmarks. The numerical results of such levelling are summarized in Table 7-14. The details of such levelling are also documented in [AD-4].

**Table 7-14:** Summary of the TG and ECR levelling results, the mean sea level for the period 01.01.2020 – 31.07.2020, units in meters

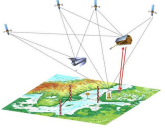
Tide gauge station National realisation of the EVRS Height datum	Tide gauge sensor type	Expected random noise of Tide Gauge readings [reference]	The levelled height (either the NW screw-top or the upper surface of the ECR cover plate) Units in m	Vertical distance between the upper surface of the cover (or NW bolt top!) and the lower boundary of the ECR baseplate Units in m	The reference height of the ECR (the lower boundary of the ECR baseplate!*)  H <sub>ECR</sub> height (in metres) in the national realisation of the EVRS Units in m	Average sea level height (in the EVRS datum) for the period 01.01.2020 – 31.07.2020 Units in m	Standard deviation of tide gauge time series 01.01.2020 – 31.07.2020 Units in m	Missing data/ percentage
Loksa, Estonia EH2000	modern pressure sensor	1 cm <sup>***</sup>	2,6568 (surface of the cover plate, NW corner)	- 0.0183	H <sub>ECR</sub> =2,6385	+0,410	0,253	0 N/A -> 0%
Emäsalo, Finland N2000	Stilling well with float	1 cm <sup>***</sup>	17,8400 (NW bolt top)	-0.0245	H <sub>ECR</sub> =17,8155 m	+0,401	0,250	31 N/A -> 0,6 %
Rauma, Finland N2000	Stilling well with float	1 cm <sup>***</sup>	5,032 (NW bolt top)	-0.0245	H <sub>ECR</sub> =5,007 m	+0,310	0,235	57 N/A -> 1,1 %
Forsmark, Sweden RH2000	Two modern radar sensors.	< 1 cm <sup>****</sup>	2,9786 (surface of the ECR cover plate, NE corner)	- 0.018** (estimated from the photo)	H <sub>ECR</sub> =2,9606 m (computed by TUT)	+0,237	0,222	0 N/A -> 0%
Spikarna, Sweden RH2000	Two modern radar sensors.	< 1 cm <sup>****</sup>	123,5413 (surface of the ECR cover plate, NE corner)	- 0.018** (estimated from the photo)	H <sub>ECR</sub> =123,5233 m (computed by TUT)	+0,223	0,236	0 N/A -> 0%
Władysławowo, Poland PL-EVRF2007-NH	modern pressure sensor, modern float sensor	1 cm <sup>***</sup>	N/A	N/A	H <sub>ECR</sub> =5,6382 m	+0,305	0,187	92 N/A -> 1,8 %
Łeba, Poland PL-EVRF2007-NH	modern pressure sensor, modern float sensor	1 cm <sup>***</sup>	N/A	N/A	H <sub>ECR</sub> =3,0510 m	+0,273	0,174	50 N/A -> 1,0 %

\* Recall that lower boundary of the ECR baseplate was agreed for the ECR vertical reference in Sopot in 2019, see also the project document: ECR Installation and Local Tie Survey, C. Gisinger  
 \*\* The Swedish levellings

\*\*\* Libusk, A., Ellmann, A., Köuts, T., Jürgenson, H. (2013): Precise Hydrodynamic Leveling by Using Pressure Gauges, Marine Geodesy, 36:2, 138-163 <http://dx.doi.org/10.1080/01490419.2013.771594>

\*\*\*\* Gobron, K.; de Viron, O.; Wöppelmann, G.; Poirier, É.; Ballu, V.; Van Camp, M. Assessment of Tide Gauge Biases and Precision by the Combination of Multiple Collocated Time Series. *J. Atmos. Oceanic Technol.* 2019, 36, 1983–1996.

For the consistency of the TG analysis it is requested that TG data is presented in same sea level datum. This was ensured by the national representatives. Also possible inconsistencies between the national vertical datums (Poland just recently switched from the obsolete Kronstadt vertical datum into new national realisation of the EVRS, denoted as PL-EVRF2007-NH) were considered in the TG processing and analysis.

	<b>BALTIC+ Theme 5</b>  Geodetic SAR for Baltic Height System Unification and Baltic Sea Level Research	<p style="text-align: right;">Final Report</p> Doc. Nr: SAR-HSU-SR-0022 Issue: 1.1 Date: 07.07.2021 Page: 84 of 170
---	--	--

Due to relatively short observation period the land uplift values were not considered at the tide gauge readings.

The TG instrumental drift can be an important issue that has to be taken under control through regular control readings from a nearby staff gauge. During the field checks the tide gauge sensor readings were compared to the visual tide gauge pole readings. No need for the drift correction was identified. Hence it is concluded that the TG readings are affected by the random noise only. The expected range of the random noise for specific gauge sensors is estimated in Table 7-14. These estimates can be used at the final computations

## 7.5 GOCE based Geoid Computation

### 7.5.1 Introduction

The evaluation of gravimetric quasigeoid models is made over two test areas. The north area covers basically the central and northern parts of the Baltic Sea, while the large area extends to include also the Polish tide gauges to the south. Below the results from the test computations outlined in Section 6.5 are presented and analysed. The final height anomalies for the tide gauges are also given.

As a parallel and independent action, CPK-PAN made an alternative computation of the Baltic Sea quasigeoid, aiming mainly to check the Polish quasigeoid. In these computations, which are still preliminary, only gravity data officially available to Poland/CBK-PAN were utilised. This is not the same data as was used for the computations presented in the current section. The corresponding height anomalies for the Polish tide gauges/EVRs are also presented in Table 7-18 and Table 8-25 below. These alternative Polish geoid computations are presented in Łyszkowicz et-al (2021).

### 7.5.2 Compilation of Gravity Data, GNSS/levelling and DEM

The first step was to compile gravity data covering the Baltic Sea area. From the beginning, the intention was to use as much as possible of the gravity data compiled and quality checked in the NKG2015 geoid model project (Ågren et al. 2016; Mårdla et al. 2017) and then to add marine gravity data collected in the FAMOS project. To these data, we would then add a suitable Polish dataset.

However, to facilitate the licensing efforts, it was decided to limit the NKG2015 gravity data to data owned by Sweden, Finland and Estonia (plus the NKG 1999 airborne campaign and a few open marine gravity datasets). The Polish colleagues then gave permission to use their gridded data in the NKG2015 database (publication 353 and 354) under condition that Poland/CBK-PAN get permission to use Swedish gravity data up to 57 degree latitude in the project, even though it turned out that Łyszkowicz et al. (2021) never used the Swedish data in their computation. The reason for this was that they wanted to use only data available without any restrictions to Poland/CBK-PAN. After that, all the new FAMOS marine gravity datasets available from Sweden, Finland and Estonia were added. All the above gravity observations cover the tide gauges/ECRs of the project with an overlap of more than 110 km in all directions. Finally, pseudo observations were generated by EIGEN-6C4 with 5'x5' resolution in areas without real gravity observations to cover a gravity (grid) area overlapping the large quasigeoid test area with  $\pm 2$  degrees in latitude and  $\pm 6$  degrees in longitude. The final gravity dataset for this gravity area as well as the large and north test areas are illustrated in Figure 7-22.

The NKG2015 and FAMOS gravity data are in the national gravity systems. For the most accurate gravity data on land, a transformation was made in the NKG2015 project to the zero permanent tide system and the postglacial land uplift epoch 2000.0. However, these corrections are small and hardly significant for geoid determination. All surface (free air) gravity anomalies were computed using the GRS80 normal gravity field (Moritz, 2000). As the atmospheric correction is applied differently in the two quasigeoid computation methods, the atmospheric correction is treated below together with the numerical tests of the methods.

To evaluate the quasigeoid models in a relative sense, NKG2015 GNSS/levelling data from Sweden, Finland and Estonia were used (cf. Figure 7-23 below). In the NKG2015 project, the GNSS heights above the ellipsoid in the national ETRS89 realizations were transformed to a common ETRS89 realization (ETRF2000) with postglacial land uplift epoch 2000.0. This was accomplished using the transformations derived in the NKG2008 GPS campaign project (Häkli et al. 2016). The final ETRF2000 coordinates were then transformed to ITRF2008 (Boucher and Altamimi 2011). The levelled normal heights are given in the respective national realization of EVRS (RH 2000, N 2000 and EH 2000), which means that they refer to the zero permanent tide system and postglacial land uplift epoch 2000.0 (Mårdla et al., 2017). Before the evaluation of gravimetric models, the GNSS ellipsoidal heights were transformed from non-tidal to zero permanent tide system (Mäkinen, 2008; Ekman, 1988). Note that the permanent tide and land uplift corrections are very significant for the GNSS/levelling observations.

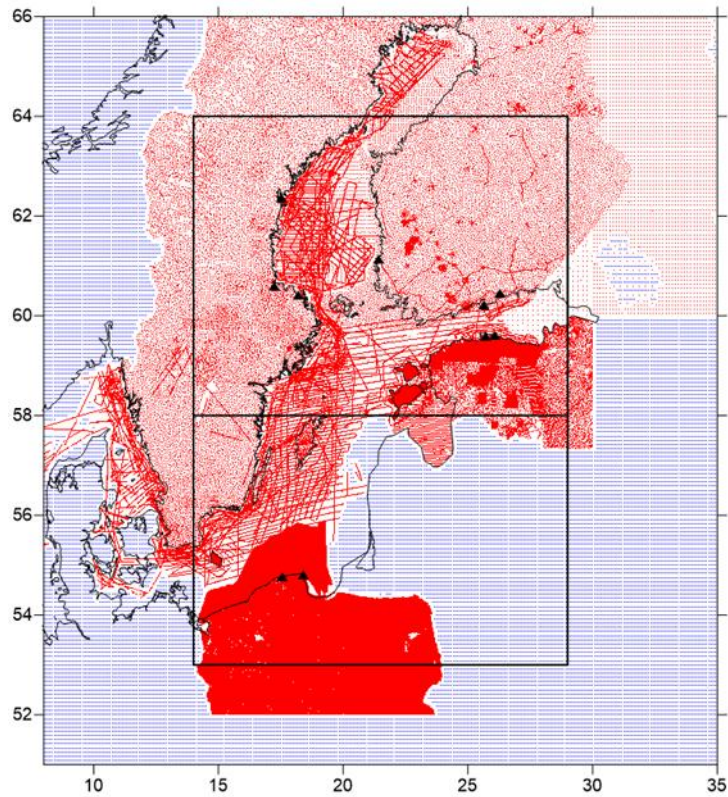


**Figure 7-22:** Gravity data selected to compute the gravimetric quasigeoid models (Table 7-15) over the gravity grid area. The data includes the gravity datasets of the NKG2015 project from Sweden, Finland and Estonia (plus some other open datasets), new FAMOS marine gravity data from the same countries and the Polish gravity data currently in the NKG2015 gravity database. Pseudo observations ( $5' \times 5'$ ) generated by EIGEN-6C4 are plotted as blue dots. The tide gauges/ECRs of the project are plotted as black triangles. The north and large quasigeoid test areas are also illustrated.

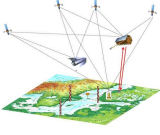
In order to compute topographic corrections, the NKG2015 DEM (called NKG\_DEM2014) was used over Sweden, Finland and Estonia. In Poland and areas with pseudo-observations, a DEM compiled by Heiner Denker (IfE) based on GTOPO and SRTM3 (below 60 degrees latitude) is utilised. The latter DEM was used as the starting point to create NKG\_DEM2014. The high accuracy national DEMs were then overlaid on top of this model to create NKG\_DEM2014 (Ågren et al. 2016).

### 7.5.3 Evaluation of regional Quasigeoid Determination Methods and GOCE based GGMs

As explained in section 6.5, two different regional quasigeoid determination methods are here evaluated together with two different GOCE based satellite-only GGMs, namely GO\_CONS\_GCF\_2\_DIR\_R6 (DIR\_R6) and GOCO06S, both with maximum degree 300 ( $M = 300$ ). In addition, the combined XGM2019 model with  $M=760$  is also tested for one of the methods (3D LSC). Note that XGM2019 is derived based on GOCO06S in the lower and medium degrees. The following combined ultra-high degree GGMs ( $M = 2190$ ) are also evaluated: EGM2008, EIGEN-6C4 and XGM2019e. See <http://icgem.gfz-potsdam.de> for more information and detailed references.

The regional quasigeoid determination methods under investigation are the following:

- The first method is Least squares modification of Stokes' formula with additive corrections (LSMSA or KTH method); see e.g. Sjöberg (1991), Ågren et al. (2009), Sjöberg and Bagherbandi (2017) and Märdla et al. (2017). The remove-compute-restore technique is here applied for gridding of the surface gravity anomaly. The RTM and GGM gravity anomaly effects are first removed from the surface gravity anomalies. The Residual Terrain Modelling (RTM) effect (Forsberg, 1984) is computed using the DEM in question (see above) averaged to  $0.0025 \times 0.0050$  degrees resolution (around  $250 \times 250$  meters). The residual surface gravity anomalies are then gridded using least squares collocation as implemented in Geogrid (Forsberg et al. 2008). After this, the RTM and GGM surface gravity anomaly effects are restored. This results in a surface gravity anomaly grid with  $0.01 \times 0.02$  degrees resolution. The LSMSA method is finally applied on this surface gravity anomaly grid using the same tuning as for the NKG2015 geoid model (Ågren et al. 2015, 2016; Märdla et al., 2017). The only difference is that the satellite only GGM and maximum degree  $M$  are different.

	<b>BALTIC+ Theme 5</b> Geodetic SAR for Baltic Height System Unification and Baltic Sea Level Research	<b>Final Report</b> Doc. Nr: SAR-HSU-SR-0022 Issue: 1.1 Date: 07.07.2021 Page: 86 of 170
---	--	--

- The second method is classical three-dimensional Least Squares Collocation (classical 3D LSC method) (Moritz 1980; Tscherning 2013) using the remove-compute-restore method with Residual Terrain Modelling (RTM) of topographic corrections (Forsberg 1984) and removing/restoring also the GGM. An empirical covariance function is first computed for the reduced gravity anomalies, to which an analytical Tscherning and Rapp (1974) function is fitted. This method is tested with the two satellite-only models mentioned above, but since this does not seem to give optimum results, the combined XGM2016 model with M=760 is also used. Note that this model is based on GOCO06S for the lower degrees. The same DEM as for the LSMSA computations averaged to the resolution (0.0025 x 0.0050 degrees) is utilised. The standard IAG atmospheric correction is used (Moritz, 2000).

Both the computation of regional quasigeoid models as well as the evaluation of ultra-high degree GGMs (like EGM2008) are made using the following zero-degree term, considering that GRS80 is used as normal gravity field in the gravimetric computations (cf. Heiskanen and Moritz, 1967, Eq. 2-182).

$$\zeta_P = \frac{(GM - GM_{GRS80})}{r_P \gamma_P} - \frac{(W_0 - U_{GRS80})}{\gamma_P} + \zeta_{\text{gravimetric, GRS 80, zero tide}}^{2-M^*} \quad (7.3)$$

This is the generalized Brun's formula in Eq. 2-178 and Eq. 2-182 in Heiskanen and Moritz (1967): Here  $GM$  is the current best estimate of GM ( $398\,600\,441.5 \times 10^6 \text{ m}^3\text{s}^{-2}$ ),  $GM_{GRS80}$  is the same quantity for GRS 80 ( $398\,600\,500 \times 10^6 \text{ m}^3\text{s}^{-2}$ ),  $r_P$  is the geocentric radius for the surface point  $P$  and  $\gamma_P$  is normal gravity at the telluroid. Furthermore,  $W_0$  is the selected potential of the geoid,  $U_{GRS80}$  is the normal potential of GRS80 and  $\zeta_{\text{gravimetric, GRS 80, zero tide}}^{2-M^*}$  is the gravimetric height anomaly from degree 2 to the Nyquist degree corresponding to the effective resolution of the model (or simply  $M$  for the ultra-high degree GGMs).

In the local quasigeoid computation part in the Geodetic SAR project, it has been agreed to use following standards (Gruber et al., 2020, Section 4),

- $W_0$  is selected to the value obtained in the NKG2015 geoid project ( $W_0 = 62\,636\,858.18 \text{ m}^2/\text{s}^2$ ).
- The zero permanent tide system is used.
- The postglacial land uplift epoch is taken as 2000.0 (except for the final model, where the mean epoch of the Geodetic SAR project is used, 2020.5. See below.)

Overall, seven gravimetric quasigeoid models were computed as summarised in Table 7-15. Note that the classical 3D LSC method is evaluated only for the north area. This limitation is due to that this method is extremely demanding computationally and it was considered enough to compare the 3D LSC and LSMSA methods over the north area.

In order to evaluate the GGM in the postglacial land uplift epoch 2000.0, two different strategies are tested. The first is used with DIR\_R6 and implies that the GGM is corrected using the Nordic land uplift model NKG2016LU (Vestøl et al. 2019). The second strategy is used with GOCO06S and implies that the available temporal variations of the potential coefficients (up to degree 120) are used to convert the coefficients from the reference epoch 2010.0 to 2000.0. This temporal model stems from the ITSG-Grace2018s model (Mayer-Gürr et al. 2018; Kvas et al. 2019) estimated using 162 months of GRACE data. The type of land uplift correction for the GGM is indicated in Table 7-15. See further below.

**Table 7-15:** Gravimetric quasigeoid models computed based on the gravity data in Figure 7-22. For the first 6 models, the land uplift corrections concern how the GGM is obtained at epoch 2000.0. The final solution (#7) is same as LSMSA 2 but with land uplift epoch 2020.5.

#	Model	Method	Area	GGM	Max. deg.	Land uplift epoch	Land uplift correction
1	LSMSA 1	LSMSA/KTH	Large	DIR_R6	300	2000.0	NKG2016LU
2	LSMSA 2	LSMSA/KTH	Large	GOCO06S	300	2000.0	GOCO06S (ITSG-GRACE2018s)
3	LSMSA 3	LSMSA/KTH	Large	GOCO06S	240	2000.0	GOCO06S (ITSG-GRACE2018s)
4	LSC 1	Classical 3D LSC	North	DIR_R6	300	2000.0	NKG2016LU
5	LSC 2	Classical 3D LSC	North	GOCO06S	300	2000.0	GOCO06S (ITSG-GRACE2018s)
6	LSC 3	Classical 3D LSC	North	XGM2019	760	2000.0	GOCO06S (ITSG-GRACE2018s)
7	LSMSA 4	LSMSA/KTH	Large	GOCO06S	300	2020.5	GOCO06S (ITSG-GRACE2018s)

#### 7.5.4 GNSS/levelling Evaluation of the Gravimetric Models and Combined EGMs

The relative quality of the gravimetric models in Table 7-15 and the combined GGMs with maximum degree 2190 (EGM2008, Eigen-6C4 and XGM2019e) are then evaluated using the GNSS/levelling datasets from Sweden, Finland and Estonia. Note that all evaluations are made in a consistent way using the postglacial land uplift 2000.0 and the zero

permanent tide system. Standard deviations obtained in the 1-parameter GNSS/levelling fits are presented in Table 7-16. The standard deviation for “All” refers to the common mean value of all the GNSS/levelling differences, while the standard deviations for the individual countries refer to the respective country mean values. The last column contains standard deviations after specific country offsets have been removed. The GNSS/levelling residuals after a common 1-parameter fit of the LSMSA 2 and XGM2019e models are plotted in Figure 7-23 and Figure 7-24.

The GNSS/levelling evaluation results clearly show that all the LSMSA models and the LSC 3 model have a very low relative uncertainty in the GNSS/levelling area. After removal of the individual country mean offsets, the standard deviations become as low as 0.013–0.015 m. Considering that these measures also contain errors in the GNSS and levelling observations, this is excellent. It can further be seen that the LSMSA and LSC 3 models are one step better than the ultra-high degree GGMs. The standard deviations are about half as large. It can further be seen that the LSC 1 and LSC 2 models computed using the satellite only GGMs DIR\_R6 and GOCO06S, respectively, have a significantly worse fit than the LSC 3 model (that utilizes the combined XGM2019 model with  $M=760$ ). It seems very difficult to apply 3D Least Squares Collocation with a satellite only GGM.

**Table 7-16:** Standard deviations from the GNSS/levelling 1-parameters fits.

Unit: m	Standard deviations in GNSS/levelling fit (1-parameter)				
Model	All	Estonia	Finland	Sweden	All after correction of country biases
LSMSA 1	0.0190	0.0122	0.0167	0.0144	0.0136
LSMSA 2	0.0188	0.0120	0.0156	0.0150	0.0135
LSMSA 3	0.0186	0.0119	0.0155	0.0147	0.0134
LSC 1	0.0237	0.0144	0.0237	0.0262	0.0206
LSC 2	0.0237	0.0146	0.0232	0.0262	0.0205
LSC 3	0.0202	0.0134	0.0143	0.0174	0.0150
NKG2015_zt	0.0204	0.0154	0.0175	0.0156	0.0157
EGM2008	0.0354	0.0359	0.0439	0.0221	0.0323
EIGEN-6C4	0.0320	0.0359	0.0304	0.0208	0.0303
XGM2019e	0.0369	0.0391	0.0270	0.0315	0.0351

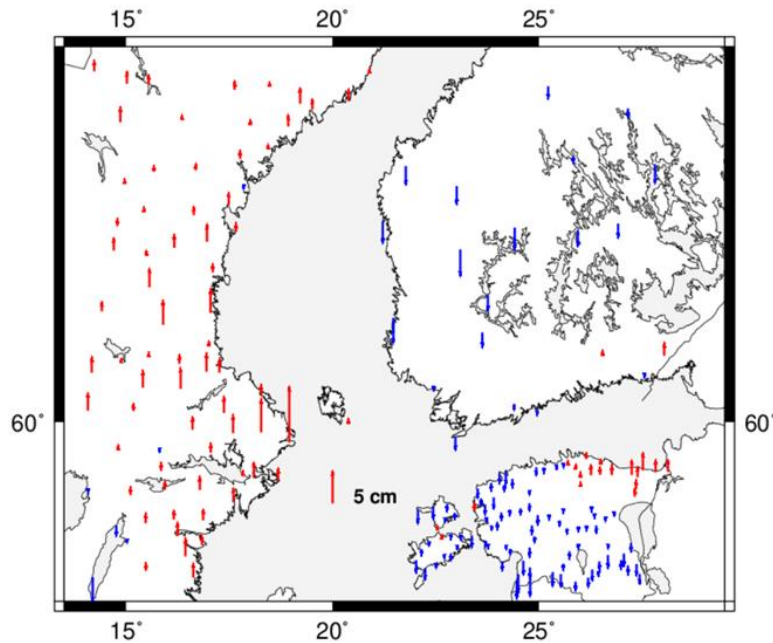


**Figure 7-23:** GNSS/levelling residuals from the 1-parameter fit of the LSMSA 2 model without corrections for specific country offsets (only one shift parameter estimated). Red arrows mean positive residuals, while blue means negative. The scale is given by the red arrow in the middle of the Baltic Sea

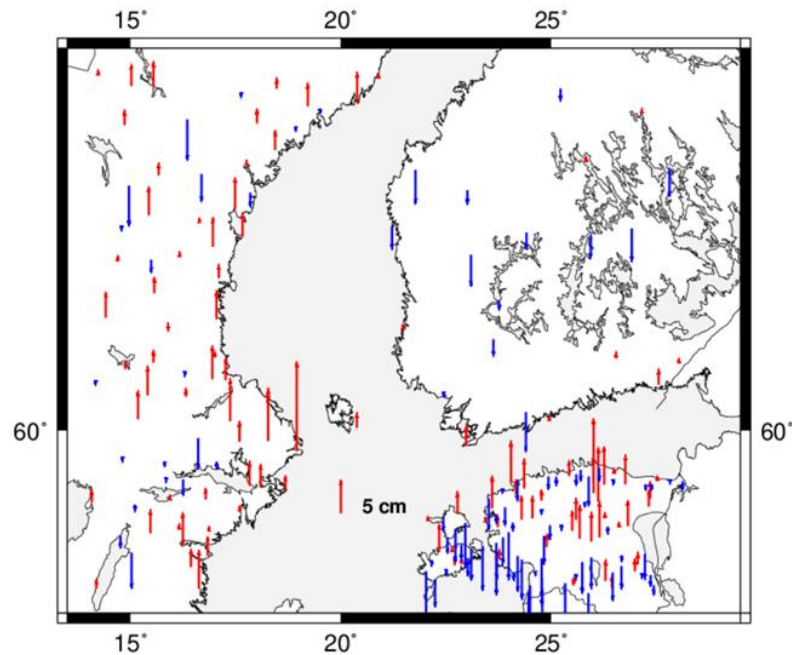


**Figure 7-24:** GNSS/levelling residuals from the 1-parameter fit of the XGM2019e model without corrections for country offsets (only one shift parameter estimated).

#### 7.5.5 Grid Comparisons

Statistics for the grid differences between all models and the LSMSA 2 model are presented in Table 7-17. The LSMSA 2 model is regarded as reference solution and finally selected as final solution in section 8.5.2. The difference between the LSC 3 and LSMSA 2 models are also illustrated in Figure 7-25. It should be stressed that these results are raw differences between models after computation using Eq. (7.3). No GNSS/levelling fit/transformation or other correction has been made.

**Table 7-17:** Statistics for the difference between the (grid) models in the large and north areas. Unit: m

Difference between models		Area	Mean	Min	Max	StdDev	RMS
LSMSA 1	LSMSA 2	Large	0.0005	-0.0100	0.0101	0.0033	0.0034
LSMSA 3	LSMSA 2	Large	-0.0001	-0.0037	0.0030	0.0010	0.0010
LSC 1	LSMSA 2	North	-0.0086	-0.0972	0.0852	0.0207	0.0224
LSC 2	LSMSA 2	North	-0.0123	-0.0879	0.0830	0.0191	0.0227
LSC 3	LSMSA 2	North	-0.0104	-0.1693	0.0242	0.0128	0.0165
NKG2015_zt	LSMSA 2	Large	0.0019	-0.1429	0.1253	0.0160	0.0161
EGM2008	LSMSA 2	Large	-0.0080	-0.2337	0.4257	0.0356	0.0356
EIGEN-6C4	LSMSA 2	Large	-0.0074	-0.1603	0.2967	0.0230	0.0242
XGM2019e	LSMSA 2	Large	-0.0069	-0.2190	0.1224	0.0266	0.0274
LSMSA 4	LSMSA 2	Large	0.0038	-0.0032	0.0094	0.0035	0.0051

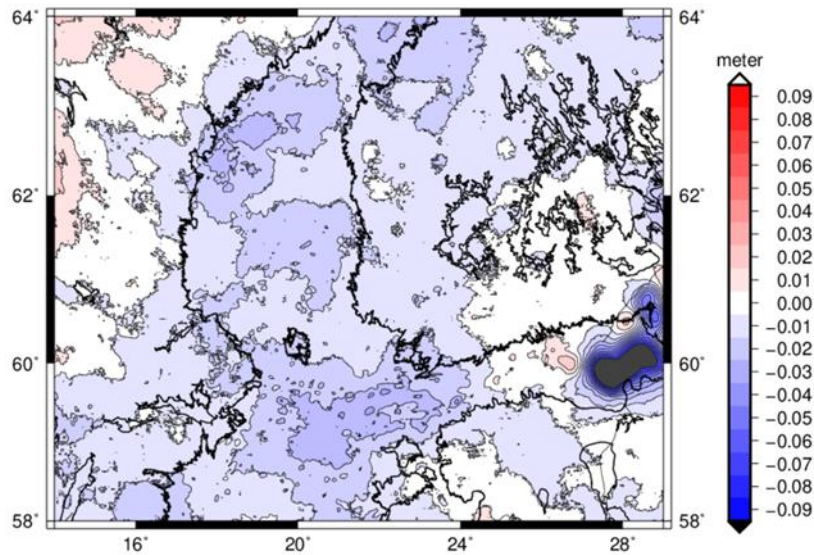


**Figure 7-25:** Illustration of the difference between the LSMSA 2 and LSC 3 models. Unit: m.

Here all the LSMSA models agree with each other on the few mm level. As these models have been computed in very much the same way, varying just the satellite only GGM and the maximum degree M, this is perhaps not too surprising. However, it is an important result that the difference between using DIR\_R6 or GOCO06S with the LSMSA method is so small. The RMS of the differences is only 3.4 mm and the fit to GNSS/levelling is almost the same (see Table 7-18). It can be concluded that it is arbitrary whether DIR\_R6 or GOCO06S is used for regional quasigeoid determination in this area.

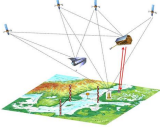
The RMS for the difference between the LSMSA and LSC models is significantly larger, also for the LSC 3 model with the best fit to GNSS/levelling (among the LSC models). However, the major part of the disagreement between LSC 3 and the LSMSA models occurs in the eastern part of the Gulf of Finland, where no real gravity data is available. The sparse red dots in this area in Figure 7-22 are synthetic observations adapted as a patch in the NKG2015 project (Märdla et al. 2017). It is clear from Figure 7-25 that the difference between the LSMSA and LSC 3 models is small in all other areas than the eastern Gulf of Finland.

#### 7.5.6 Point-wise Comparisons in the Tide Gauges/ECRs

The next step is to study all the quasigeoid models in the tide gauges/ECRs. The corresponding height anomalies are presented in Table 7-18. The patterns observed in the grid comparisons can mainly be observed also here. It can for instance be seen that the three ultra-high degree GGMs differ significantly more between each other than the LSMSA and LSC 3 models. The preliminary quasigeoid heights computed by Poland/CBK-PAN (Łyszkowicz et al, 2021) are also included in Table 7-18.

**Table 7-18:** Height anomalies from to the different models in each tide gauges/ECRs ( $W_0 = 62\,636\,858.18\text{ m}^2/\text{s}^2$ , zero permanent tide system, land uplift epoch 2000.0 – for the LSMSA and LSC models). The LSMSA 4 model is the same as LSMSA 2 but corrected to land uplift epoch 2020.5. The complementary Polish height anomalies (Łyszkowicz et al, 2021) are also presented for the Polish tide gauges/ECRs. in Unit: m.

Tide gauge/ ECR	Estonia		Finland			Sweden			Poland		
	Loksa	Vergi	Emäsalo	Lovisa	Rauma	Forsmark	Spikarna	Mårtsbo	Wladysl.	Rosewie	Leba
LSMSA 1	16.818	16.551	16.507	15.453	19.092	22.379	25.057	24.619	28.884	29.030	30.785
LSMSA 2	16.816	16.551	16.504	15.447	19.089	22.374	25.057	24.619	28.883	29.030	30.787
LSMSA 3	16.814	16.548	16.504	15.447	19.089	22.373	25.056	24.619	28.883	29.030	30.789
LSC 1	16.794	16.530	16.488	15.437	19.083	22.360	25.043	24.606			
LSC 2	16.789	16.526	16.483	15.432	19.080	22.351	25.039	24.604			
LSC 3	16.811	16.549	16.506	15.452	19.077	22.359	25.042	24.606			
NKG2015_zt	16.825	16.563	16.505	15.446	19.089	22.369	25.063	24.609	28.882	29.029	30.783
EGM2008	16.853	16.594	16.472	15.384	19.101	22.366	25.055	24.592	28.899	29.048	30.792
EIGEN-6C4	16.793	16.533	16.454	15.377	19.082	22.387	25.052	24.612	28.866	29.013	30.758
XGM2019e	16.811	16.571	16.534	15.441	19.042	22.387	25.030	24.605	28.877	29.032	30.742
Łyszkowicz et al. (2021)	-	-	-	-	-	-	-	-	28.831	28.976	30.717
LSMSA 4	16.821	16.555	16.509	15.453	19.096	22.381	25.065	24.627	28.883	29.030	30.787

	<b>BALTIC+ Theme 5</b>  Geodetic SAR for Baltic Height System Unification and Baltic Sea Level Research	<b>Final Report</b> Doc. Nr: SAR-HSU-SR-0022 Issue: 1.1 Date: 07.07.2021 Page: 90 of 170

## 7.6 Reference Frames and Joint Standards

A general description of the issues and procedures related to the product validation is provided in Sect. 6.6. This section summarizes the major issues that are considered for the validation of the different products derived from the various observation techniques such as geodetic SAR, GNSS, GOCE, terrestrial/airborne gravity data and tide gauges used for the determination of ellipsoidal and physical heights of tide gauge stations in the Baltic Sea region.

In order to get consistent results for the different geometric and gravimetric quantities generated within this project, the standards used for the data processing have been homogenized as much as possible. In this context, it has been considered that different standards are specified for the individual observation techniques (e.g., IGS- and EPN-Standards, SAR Standards, GOCE Standards, standards for geoid computations as well as for gravity and tide gauge data) which puts some constraints on the homogenization. Nevertheless, a high level of standardization was achieved by applying processing standards for the different geometric and gravimetric observations and the geophysical background models as close as possible according to the IERS Conventions 2010 (and its updates). For the transformation of 3-D Cartesian coordinates, it was specified to use the conventional GRS80 parameters within this project. According to the tide system, the gravimetric products, such as the satellite-only gravity field models, are given in the zero-tide system (in agreement with IAG resolution No. 16 of the 18th General Assembly 1983), whereas the geometric quantities such as the ITRF as well as the SAR and GPS results are given in the conventional tide free system. Thus, these different definitions of the tide system have been considered within the product validation by using the transformation formulae provided in Sect. 7 of the IERS Conventions 2010 (Petit and Luzum, 2010). As an important requirement for the final product validation the standards used for the generation of the different geometric and gravimetric quantities have been clearly documented. Thus, in case of any deviations regarding standards, transformations between different sets can be performed to get consistent results. More information is provided in the inventory of standards and conventions compiled by the GGOS Bureau of Products and Standards (Angermann et al., 2020).

In the context of reference frames, mainly the four following issues have been considered for the product validation:

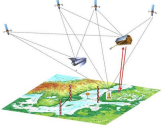
- (1) Transformation between ITRF and EPN results: For the validation of the GNSS positioning results with existing solutions of the global and regional permanent network (IGS, EPN) transformations between the ITRS and the European Terrestrial Reference System 89 (ETRS89) have been applied. As described in more detail in the Algorithm Theoretical Basis Document [AD-5], the transformation formulae allowing to link the ETRS89 to the ITRS, for both station positions and velocities, is given for example in Boucher and Altamimi (2011), Altamimi (2018) and at the EPN website: "[https://www.epncb.oma.be/\\_productsservices/coord\\_trans/](https://www.epncb.oma.be/_productsservices/coord_trans/)".
- (2) Non-linear station motions: As the ITRS realizations are primarily based on a linear model (station positions and constant velocities), non-linear motions are visible in the station position residuals, mostly in the height component caused by various effects such as neglected surface loading. These non-linear station motions may cause errors in the order of a few millimeters (or even more) when transforming the (regional) GNSS or SAR positioning solutions into the global reference frame. This effect can be considered in the validation procedure, e.g., by taking into account the periodic signals of the ITRF2014 results (available on request from IGN, Altamimi et al., 2016) or by analyzing the station position time series of the GNSS solutions.
- (3) Extrapolation of ITRF results: The transformation of GNSS and SAR station position solutions (e.g., estimated in 2020) into the ITRF requires an extrapolation over a time period of about 10 years, since the reference epoch of ITRF station positions is 2010.0. Thus, stable reference stations (with accurate velocities) have been selected for the transformations to minimize the impact of potential extrapolation errors on the validation results.
- (4) Time variability of CM vs. CF: According to the IERS Conventions, the ITRF origin follows the mean Earth center of mass (CM), averaged over the time span of SLR observations and modelled as a linear function in time. However, the time series of Satellite Laser Ranging (SLR) solutions provide valuable information for the time variability of CM versus the center of figure (CF). Both, the ITRF2014 (Altamimi et al., 2016) and the DTRF2014 (Seitz et al., 2016) provide an annual geocenter motion model which are available for the product validation. The corresponding amplitudes are 2.6 mm, 2.9 mm and 5.7 mm for tx, ty and tz, resp. (for ITRF2014) and 2.2 mm, 2.6 mm and 3.4 mm for tx, ty and tz, resp. (for DTRF2014). Furthermore, the results of the SLR multi-satellite solution of DGFITUM can be used for the product validation (Bloßfeld et al., 2015).

## 7.7 Height System Unification and Absolute Sea Level

The final step combines the various heights in order to determine absolute sea level heights at the selected tide gauge stations. This means results from the SAR positioning, the tide gauge data analysis and the geoid determination need to be combined. For this the formulas provided in section 6.7 need to be applied, which are repeated here for convenience (see equation (6.38) and adapted to perform the combination).

$$\begin{aligned}
 S^{TG}(t) &= h^{TG}(t) - N^{TG}(t) + z^{TG}(t) \\
 S^{TG}(t) &= h^{ECR}(t) + \Delta h_{ECR}^{TG}(t) - N^{TG}(t) + z^{TG}(t)
 \end{aligned}
 \tag{7.4}$$

where:  $t$                       Observation epoch

	<b>BALTIC+ Theme 5</b> Geodetic SAR for Baltic Height System Unification and Baltic Sea Level Research	<b>Final Report</b> Doc. Nr: SAR-HSU-SR-0022 Issue: 1.1 Date: 07.07.2021 Page: 91 of 170
---	--	--

- $z^{TG}(t)$  Tide gauge sea level height above tide gauge zero marker at epoch  $t$  (relative sea level)  
 $h^{TG}(t)$  Height of tide gauge zero marker above reference ellipsoid at epoch  $t$  (ellipsoidal height)  
 $h^{ECR}(t)$  Height of ECR reference point above ellipsoid at epoch  $t$  (ellipsoidal height)  
 $\Delta h_{ECR}^{TG}(t)$  Height difference from ECR reference point to tide gauge zero marker at epoch  $t$  (ellipsoidal height difference)  
 $N^{TG}(t)$  Height of reference equipotential surface above reference ellipsoid at tide gauge location at epoch  $t$  (geoid height)  
 $S^{TG}(t)$  Sea level height above reference equipotential surface at epoch  $t$  (absolute sea level height)

Physical heights at a tide gauge station referring to a unique reference equipotential surface at an epoch  $t$  and not considering the absolute or relative sea level, are computed by (6.39) and adapted accordingly:

$$\begin{aligned}
 H^{TG}(t) &= h^{TG}(t) - N^{TG}(t) \\
 H^{TG}(t) &= h^{ECR}(t) + \Delta h_{ECR}^{TG}(t) - N^{TG}(t)
 \end{aligned}
 \tag{7.5}$$

where:  $H^{TG}(t)$  Physical height of tide gauge zero marker above reference equipotential surface.

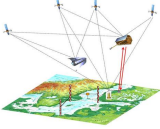
Results for some stations have been preliminary computed in order to validate the procedure. It still needs to be checked if the standards and conventions specified in chapter 7.6 are completely followed in the computations. Also time variable results are not considered yet meaning that only average values for a preliminary analysis time period are computed. Table 7-19 shows the preliminary absolute sea level and physical heights as they were computed so far from the different observation techniques (refer to sections 7.2 to 7.5). In addition to the quantities specified above, the local ellipsoidal height difference between the ECR reference point and the tide gauge zero marker is needed, as both stations in general are separated by decimetres to kilometres. The geoid height can be assumed to be identical within this area. Table 7-20 shows for some selected stations the observed height offsets between the ECR and co-located permanent GNSS stations and also differences between computed ellipsoidal heights (transferred from GNSS to ECRs) and ECRs observed heights (taken from Table 7-19, 2<sup>nd</sup> column) are shown.

**Table 7-19:** Collection of preliminary heights as determined by the ECR, Geoid and Tide Gauge for the selected stations and combination according to equations (7.4) and (7.5).

ECR Station	$h^{ECR}$ Ell. Height observed [m]	$N^{TG} = N^{ECR}$ Geoid Height [m]	$z^{TG}$ Tide Gauge [m]	TG zero wrt. EVRS [m]	$\Delta h_{ECR}^{TG}$ ECR to Tide Gauge [m]	$S^{TG}$ Absolute Sea Level [m]	$H^{TG}$ Physical Height [m]
Loksa	+20.075	+16.821	+0.410	0.000	-2.639	+1.025	+0.615
Emäsalo	+34.291	+16.509	+0.401	0.000	-17.816	+0.367	-0.034
Rauma	+24.082	+19.096	+0.310	0.000	-5.007	+0.289	-0.021
Forsmark/Kobben	+25.999	+22.381	+0.237	0.000	-2.961	+0.894	+0.657
Spikarna/Vinberget	+149.654	+25.065	+0.223	0.000	-123.523	+1.298	+1.066
Władysławowo	+34.639	+28.883	+5.249	-4.944	-10.582	+0.423	-4.826
Łeba	+34.390	+30.787	+0.273	0.000	-3.051	+0.825	+0.552

**Table 7-20:** Height Offset between ECR and nearby permanent GNSS Stations (last column shows the difference between the computed ECR height 6th column and the observed ECR height 7th column, copied from Table 7-19, 2<sup>nd</sup> column).

GNSS station (IGS Code)	Network	Connected ECR Station	$h^{GNSS}$ Ell. Height [m]	$\Delta h_{GNSS}^{ECR}$ GNSS to ECR [m]	$h^{ECR}$ Ell. Height computed [m]	$h^{ECR}$ Ell. Height observed [m]	$\Delta h^{ECR}$ computed - observed [m]
VERG	ESTPOS	Vergi	+30.067	-0.996	+29.071	+28.965	+0.106
WLAD	ASG-EUPOS	Władysławowo	+34.758	-0.135	+34.623	+34.639	-0.016
LEBI	Leica network	Łeba	+37.885	-3.932	+33.953	+34.390	-0.437

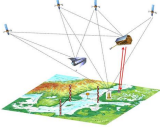
	<b>BALTIC+ Theme 5</b>  Geodetic SAR for Baltic Height System Unification and Baltic Sea Level Research	<b>Final Report</b> Doc. Nr: SAR-HSU-SR-0022 Issue: 1.1 Date: 07.07.2021 Page: 92 of 170
---	--	--

Validation of these results can be performed on signal and on error level. In principle one can perform an error propagation for the computed quantities in equations (7.4) and (7.5). When computing the absolute sea level, errors from the ECR ellipsoidal heights, the geoid heights, the tide gauge records and the local survey connecting the ECR to the tide gauge are contributing. The ECR height error is estimated to be at a level of 5 cm (preliminary estimate according to results shown in section 7.2). The geoid height error is estimated as 1.3 cm for the Swedish, Finnish and Estonian stations (refer to section 7.5) and 4 cm for the Polish stations. The tide gauge errors are assumed to be between 1 and 2 cm, while the local connection of the ECR to the tide gauge reference point shall be known with an accuracy of 1 cm or better. Regarding these preliminary numbers, we can assume that the main error source is the ECR ellipsoidal height, while the other components are marginal (assuming that the geoid error of the Polish stations will improve for the final solution). On signal level one can validate differences of physical heights of tide gauge stations (equation (7.5)) by comparison against conventional levelling observations. As explained this requires levelling results from the national authorities. Nevertheless, a first attempt, based on 7 months of averaged TG results, the ECR ellipsoidal heights and the geoid heights was made to verify the TG results. These results shall be regarded as preliminary and need to be checked in detail. Based on 7 months of data, ECRs ellipsoidal heights and normal heights at the tide gauge stations are used to compute the geoid heights at these stations. These computed geoid heights are compared to the results achieved from the geoid modelling shown in section 7.5. The results are shown in Table 7-21.

**Table 7-21:** ECR height comparisons with GNSS-levelling and dedicated SAR-HSU geoid model at the locations of participating TG stations

ECR Station (co-located to TG station)	$h^{ECR}$ Ell. Height observed [m]	$N^{ECR}$ Geoid Height [m]	$H_{EVRS}^{ECR}$ Normal height, [m]	$h^{ECR} - H_{EVRS}^{ECR}$ $= N_{geom}^{ECR}$ [m]	$N^{ECR} - N_{geom}^{ECR}$ [m]
Loksa	+20.075	+16.821	+2.639	+17.436	-0.615
Emäsalo	+34.291	+16,509	+17.816	+16.475	+0.034
Rauma	+24.082	+19,096	+5,007	+19,075	+0.021
Forsmark/Kobben	+25.999	+22.381	+2.961	+23.038	-0.657
Spikarna/Vinberget	+149.654	+25.065	+123.523	+26.131	-1.066
Władysławowo	+34.639	+28.883	+5.638	+29.001	-0.118
Łeba	+34.390	+30.787	+3.051	+31.339	-0.552

The differences between the GNSS and ECR derived ellipsoidal heights (Table 7-20) and the geoid height differences at the tide gauge stations (Table 7-21) show results between 1 cm and 1m. A majority of the differences is between 1 cm and 1 dm, which is a proof that the procedure is working at least at dm accuracy level. For some stations the differences are between several dm and a metre. These stations need to be checked for the final data analysis in more detail. It is very likely that there are made some wrong assumptions for the relative height differences between the GNSS and the ECR stations and the differences between the ECR and tide gauge stations.

	<b>BALTIC+ Theme 5</b>  Geodetic SAR for Baltic Height System Unification and Baltic Sea Level Research	<b>Final Report</b> Doc. Nr: SAR-HSU-SR-0022 Issue: 1.1 Date: 07.07.2021 Page: 93 of 170
---	--	--

## 8 DATA ANALYSES AND SCIENTIFIC ASSESSMENT

### 8.1 SAR Data Analysis and Value Adding

The aim of SAR data analysis and value adding was to support the selection and assessment of the ECR installations sites as well as the preparation of Sentinel-1 SAR measurement and corrections files serving the SAR positioning. The employed methods have been thoroughly validated, see the results shown in chapter 7.1, and the processing was successfully performed for all data acquired by Sentinel-1 in 2020 at the ECR installation sites.

#### 8.1.1 ECR Installations, Sentinel-1 Image Data and SAR Observations

The ECR installations were performed by the different project partners in 2020 in the January to June time frame. The latest installation at Vinberget took place in October. Logistics and obtaining the transmission licences were the main reasons for the different installation times which also affected operation times of the ECR network, see Table 8-1. Inspection of the on-site situation and careful analysis of Sentinel-1 SAR images were carried out prior to the installation in order to select locations favourable to both the SAR and on-ground site access. Once installed and configured, the operation proved fairly reliable with most ECRs, but three sites – Vergi, Loviisa, and DLR2 – experienced electronic failures and the ECR at Loksa site became damaged during a severe storm event flooding the area, see chapter 7.4. Therefore, only 8 out of 12 sites could be operated as planned.

Possible data acquisition with Sentinel-1 depends on the latitude, the site's location with respect to the Sentinel-1 ground track, and the coverage of the SAR instrument. The Sentinel-1 IW TOPS mode data covers a cross range of 250 km between 25° to 42° incidence angle (Bourbigot et al., 2015), and the higher the latitude the more overlapping tracks become available at a given site. For the mid-latitude ECR installations in Germany and Poland this yielded 3-4 repeat passes, whereas the more northerly sites in Finland and Sweden were covered by 5-6 repeat passes, see Table 8-1. Note that due to duty cycle limitation and data downlink constraints, Sentinel-1 does not acquire data for all available tracks over Europe and therefore some stations, e.g. Rauma, denote fewer passes than potentially available

**Table 8-1:** Summary on SAR data collected with the project's ECR network. Active periods are the times the ECRs operated successfully. Passes list the number of repeat pass geometries acquired by Sentinel-1 in ascending and descending orientation at a respective site. Sentinel-1 observations refer to the number of SAR images available in the catalogue whereas acquired observations list successful ECR activations with full performance signals in the SAR data. Signal strength summarizes the average peak power of the ECR signal (=  $\sigma_{0}$  integrated for 3dB peak width) along with corresponding standard deviations.

Station	Latitude [°]	Active Period mm/dd–mm/dd	Passes [#] (Asc / Desc)	Sentinel-1 Obs. [#]	Acquired Obs. [#]	Success Rate [%]	Signal Strength [dB]
Loksa	59.5826	02/14 – 09/12 12/28 – 12/31	3 / 2	171	164	95.61	87.58 ± 1.84
Vergi	59.6015	03/03 – 08/01 12/28 – 12/31	3 / 2	81	81	100.00	89.75 ± 2.68
Emäsalo	60.2037	01/23 – 12/31	3 / 2	222	185	83.33	89.85 ± 1.68
Loviisa	60.4407	02/01 – 10/20	2 / 2	132	106	80.30	87.87 ± 2.08
Rauma	61.1335	04/21 – 12/31	2 / 2	142	76	53.52	91.59 ± 1.52
Władysławowo	54.7968	03/20 – 12/31	2 / 2	164	142	85.59	89.24 ± 2.07
Łeba	54.7537	05/15 – 12/31	2 / 2	141	116	82.27	88.16 ± 0.95
Mårtsbo	60.5951	01/07 – 12/31	3 / 3	322	218	67.70	86.95 ± 2.58
Kobben	60.4099	06/01 – 12/31	2 / 2	160	154	96.25	88.33 ± 1.55
Vinberget	62.3739	10/01 – 12/31	2 / 3	57	57	100.00	88.51 ± 2.48
DLR2	48.0849	01/10 – 02/25 06/17 – 09/01	2 / 1	85	85	100.00	89.55 ± 2.00
DLR3	48.0879	01/10 – 12/31	2 / 1	177	177	100.00	90.54 ± 1.43



**Figure 8-1:** Time series of ECR signal peak power (=  $\sigma_0$  integrated for 3dB peak width). The red line marks the 81dB outlier threshold. Top: **Kobben**. Timing issues with the ECR clock led to a few missed activations but programmed resynchronization with GPS time quickly recovered the ECR after of such events. Bottom: **Emäsalo**. Missing activations for Sentinel-1B until reprogramming of the ECR for these additional data acquisitions.

Considering the different ECR operations times and the pass geometries served by Sentinel-1, a total amount of 1854 SAR observations would have been accessible to the ECR network. The number of acquired observations is 1561 which corresponds to an overall success rate of 84.2 percent. Table 8-1 shows detailed numbers for each station. Only very few observations were lost because of incorrect ECR activations or severe weather conditions that rendered the ECR signal unusable. The main reason why some ECRs contributed less data than possible was the programming of activation cycles with respect to Sentinel-1 operation plan, see examples in Figure 8-1. Until mid of May, only Sentinel-1A was operating in standard IW TOPS mode over the Baltic area while Sentinel-1B was acquiring wide area data for the seasonal sea ice monitoring campaign. Once both SAR sensors became available, several ECRs had to be reprogrammed, because initially programmed activation windows were limited to actual Sentinel-1 acquisitions to mitigate the risk of interference with other radio communication infrastructure. Reprogramming the ECR requires physical device access which for some locations meant more than 200 km of travel distance by the operators, prohibiting rapid on-site servicing. Therefore, about 15 percent of acquired data was missed by the ECRs, most prominently at Rauma site which could not be reprogrammed for Sentinel-1B.

Table 8-2 shows examples for the visibility of the ECRs in the analysed Sentinel-1 SAR data. All ECR installations provide a clearly visible point response which confirms good feasibility of the chosen installation sites. In particular, the installations close to coastline, e.g. Loksa, Vergi or Władysławowo, are very favourable sites because the surrounding water areas provide very dark backgrounds in SAR, rendering visible the details of the ECR signals. Accurate extraction of SAR timings from the point response requires only the visibility of an undistorted main peak, but the clean shapes and symmetries of the signals give confidence that in principle the novel ECR targets are behaving like well-established passive CR reference targets. The more challenging locations like Vinberget (surrounded by forest) or Rauma (industrial harbour area) also posed no problems for measuring the ECRs, thanks to the relatively strong signal return of the devices. The only ECR site that turned out to have limitations was Kobben. Because of concerns regarding radio interference with nearby military infrastructure, the installation had to be shielded by a meshed fence to prevent any signal amplification at low elevation angles [AD-4]. This fencing also caused interfering sidelobes in certain geometries, see Kobben ascending example in Table 8-2; Therefore only part of the observations acquired at Kobben could be used in the SAR positioning, see chapter 8.2.1.

In conclusion, the SAR data analysis preparing the ECR observations was performed very reliably and only few ECRs observations had to be marked unusable based on the imaging quality parameters. Further data assessment is provided in chapter 8.2, where these input data were screened in terms of the SAR positioning quality

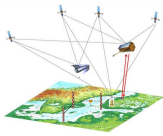
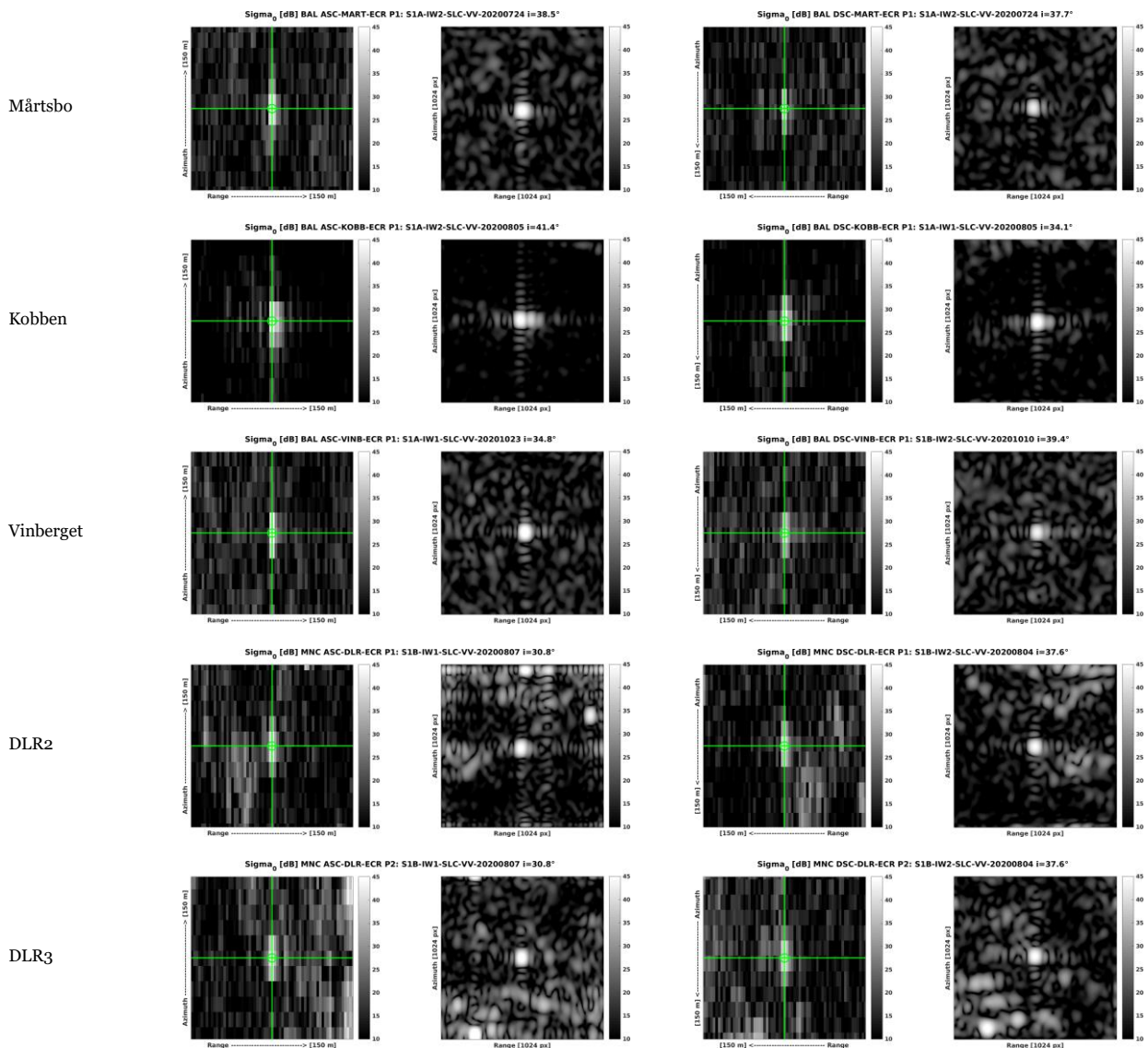
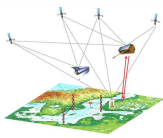


**Table 8-2:** Sentinel-1 SLC image samples showing the ECR point responses for ascending and descending IW TOPS data at the different installation sites. Images display the radar backscatter ( $\sigma_0$ ) in units of decibel. Left columns: original Sentinel-1 SLC SAR image samples showing an area of 150 m x 150m around ECR peak marked in green. Right columns: image areas of 32 x 32 pixels oversampled by a factor of 32 as generated by point target analysis to extract the ECR peak position

Station	Ascending Image Sample	Descending Image Sample
Loksa	<p><math>\sigma_0</math> [dB] BAL ASC-LOKS-ECR P1: S1A-IW1-SLC-VV-20200804 <math>i=30.5^\circ</math></p>	<p><math>\sigma_0</math> [dB] BAL DSC-LOKS-ECR P1: S1A-IW1-SLC-VV-20200728 <math>i=35.6^\circ</math></p>
Vergi	<p><math>\sigma_0</math> [dB] BAL ASC-VERG-ECR P1: S1B-IW2-SLC-VV-20200710 <math>i=39.3^\circ</math></p>	<p><math>\sigma_0</math> [dB] BAL DSC-VERG-ECR P1: S1B-IW2-SLC-VV-20200611 <math>i=41.2^\circ</math></p>
Emäsalo	<p><math>\sigma_0</math> [dB] BAL ASC-EMAE-ECR P1: S1A-IW3-SLC-VV-20200814 <math>i=44.8^\circ</math></p>	<p><math>\sigma_0</math> [dB] BAL DSC-EMAE-ECR P1: S1A-IW2-SLC-VV-20200704 <math>i=36.7^\circ</math></p>
Loviisa	<p><math>\sigma_0</math> [dB] BAL ASC-LOVI-ECR P1: S1A-IW2-SLC-VV-20200809 <math>i=40.9^\circ</math></p>	<p><math>\sigma_0</math> [dB] BAL DSC-LOVI-ECR P1: S1A-IW1-SLC-VV-20200728 <math>i=34.7^\circ</math></p>
Rauma	<p><math>\sigma_0</math> [dB] BAL ASC-RAUM-ECR P1: S1A-IW2-SLC-VV-20200620 <math>i=39.4^\circ</math></p>	<p><math>\sigma_0</math> [dB] BAL DSC-RAUM-ECR P1: S1A-IW1-SLC-VV-20200812 <math>i=31.1^\circ</math></p>
Władysławowo	<p><math>\sigma_0</math> [dB] BAL ASC-WLAD-ECR P1: S1B-IW1-SLC-VV-20200904 <math>i=35.3^\circ</math></p>	<p><math>\sigma_0</math> [dB] BAL DSC-WLAD-ECR P1: S1A-IW2-SLC-VV-20200819 <math>i=41.2^\circ</math></p>
Łeba	<p><math>\sigma_0</math> [dB] BAL ASC-LEBA-ECR P1: S1A-IW2-SLC-VV-20200717 <math>i=39.8^\circ</math></p>	<p><math>\sigma_0</math> [dB] BAL DSC-LEBA-ECR P1: S1A-IW2-SLC-VV-20200824 <math>i=36.7^\circ</math></p>



### 8.1.2 ECR SAR Observations Analysis

The SAR observation analysis discussed in this chapter is a continuation of the SAR data validation documented in chapter 7.1. With all SAR data prepared and the ECR delay calibrated, the SAR data and correction files (see chapter 9.1) were analysed for the overall SAR observation quality of the ECR network. The following steps were performed in order to assess ECR data quality:

- Computation of residuals from the surveyed ECR origin coordinates [AD-4] by applying the SAR data end-to-end validation methods (chapter 7.1.1).
- Removal of outliers from the residuals of each individual geometry using the median and a 95% confidence interval, assuming normal distribution.
- Estimation of average ECR offsets from the cleaned residuals of each geometry along with the 95% confidence interval using least-squares methods.
- Computation of the range and azimuth standard deviation for each set of residuals to quantify the single observation precision (1 sigma) of each geometry.

The results are visualized in Figure 8-2 and Figure 8-3 and the numbers are summarized in Table 8-3. The analysis was performed with the surveyed ECR origin coordinates corrected for the geometric ECR phase centre offsets specified for ascending and descending passes (see chapter 9.1). Consequently, the estimated offsets show mainly electronic delays of the ECRs, with additional bias contributions stemming from the orbit, the finite correction accuracy and the surveyed coordinates. The sum of additional bias is assumed with maximum 8 cm. A subset of ECRs with accurate coordinates

better than 4 cm was used to calibrate the electronic delays with an angular-dependent ECR delay model (see chapter 7.1.2), which is shown in Figure 8-2 as well.

Several conclusions can be drawn from these results. The SAR range observations of the ECRs generally have a high precision when considering only the individual geometries. For most of the data stacks, the range offsets are estimated with a precision of better than 4 cm (95% confidence), which also confirms that most of the detected differences among ECRs and geometries are significant. Only a few ECRs can provide relatively homogeneous data across all incidence angles, e.g., Emäsalo or Loksa, and there is low consistency among the different ECR delay patterns.

Despite being built to same specification and stemming from one manufacturing series, the ECR delays can vary between 1.2 m (Loksa, DLR2) and 3 meters (Loviisa). The lower precision of the Kobben results is caused by interference of the fencing which particularly affects the 34° ascending geometry. The lower precision of the DLR2 is due to the repaired electronics which changed the electronic characteristics of this device. The experimentally determined model can therefore remove the delay effects only within ±0.5 m and only for a limited number of ECRs. Moreover, absolute SAR positioning accuracy will be limited to decimetres if these systematic effects are not compensated for. Stations like DLR2, Loksa or Loviisa will perform worse because of their less common delay patterns.

The azimuth observations are much more consistent and seem less affected by the ECR electronic characteristics. The offsets are comparable to the results obtained with passive CR (chapter 7.1.2). The precision of azimuth bias estimation is limited to 15 cm (95% confidence) mainly because of the 20m azimuth image resolution. Considering this limited precision, the experimentally determined model can remove most of the systematic effects and an azimuth accuracy in the order of 20 cm is attainable.

The precision of a single ECR measurement in range generally varies between 5 to 10 cm (1 sigma), as shown in Figure 8-3 left. Again, the interfering fence at Kobben and the impact of the repaired electronics of DLR2 are visible in the results. The ECR measurements in azimuth show a typical standard deviation of 10 to 30 cm (1 sigma), see Figure 8-3 right, but there is a considerable difference between ascending and descending data. Such a difference is also visible in the range results. The reason for this behaviour is unclear but it is likely related to the ECR themselves because such results have not been reported so far with Sentinel-1 and passive reflectors (Schubert et al. 2017; Gisinger et al. 2021).

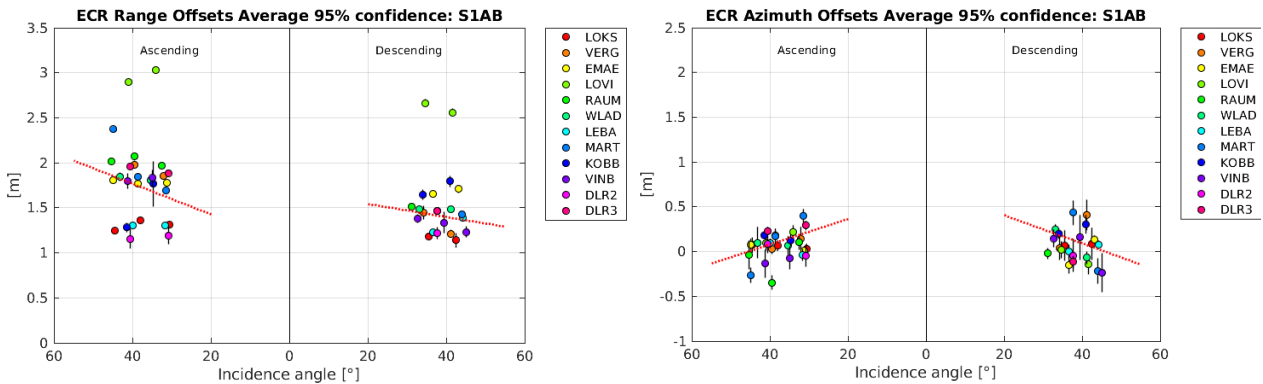


**Figure 8-2:** ECR offsets for the different pass geometries observed with the ECR network. Offsets estimated with least-squares adjustment from residuals of surveyed ECR positions [AD-4] and measured SAR data filtered for outliers. Range offset estimates per geometry (left) and azimuth offset estimates per geometry (right). Black bars show the 95% confidence intervals of the estimation results. Red lines show the angular-dependent ECR delay models as described in chapter 7.1.2.

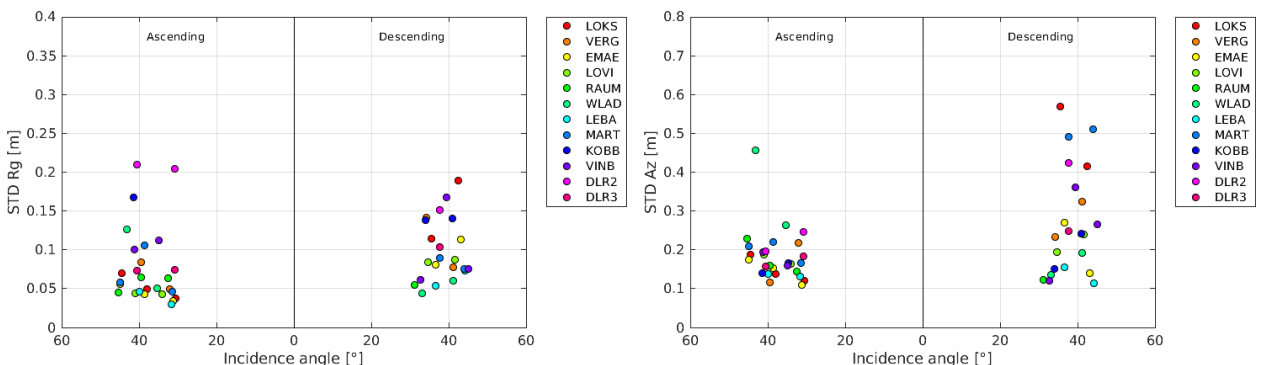


**Figure 8-3:** ECR SAR observation quality for the different pass geometries observed with the ECR network. Standard deviation of residuals derived from surveyed ECR positions [AD-4] and measured SAR data filtered for outliers. Standard deviation of range measurements per geometry (left) and standard deviations of azimuth measurements per geometry (right).

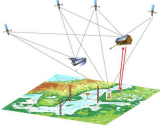
**Table 8-3:** Results of SAR observation quality show in Figure 8-2 and Figure 8-3. Numbers grouped by pass geometry and incidence angle of the SAR data acquired at the stations. Range and azimuth offsets estimated from residuals derived from surveyed ECR positions [AD-4] and measured SAR data filtered for outliers. The 95% confidence levels of the offset estimates are listed in adjacent columns. Standard deviations of the residuals denote the precision of single range and azimuth observations.

Station	Pass	Inc. Angle [°]	Obs. [#]	Rg Offset [m]	Offset 95% [m]	Rg STD [m]	Az Offset [m]	Offset 95% [m]	Az STD [m]
LOKS	ASC	30.6	22	1.311	0.017	0.038	0.032	0.055	0.121
LOKS	ASC	38.0	24	1.362	0.021	0.050	0.065	0.060	0.138
LOKS	ASC	44.5	22	1.243	0.032	0.070	0.072	0.085	0.188
LOKS	DSC	35.6	45	1.184	0.035	0.114	0.066	0.173	0.569
LOKS	DSC	42.4	23	1.140	0.084	0.189	0.085	0.184	0.415
VERG	ASC	32.1	14	1.850	0.030	0.050	0.144	0.130	0.217
VERG	ASC	39.4	19	1.979	0.041	0.084	0.032	0.058	0.116
VERG	DSC	34.2	16	1.444	0.078	0.141	0.037	0.128	0.232
VERG	DSC	41.2	17	1.214	0.041	0.077	0.411	0.171	0.324
EMAE	ASC	31.3	27	1.774	0.014	0.034	0.008	0.044	0.109
EMAE	ASC	38.5	33	1.770	0.015	0.043	0.177	0.055	0.153
EMAE	ASC	44.8	28	1.805	0.022	0.056	0.074	0.069	0.175
EMAE	DSC	36.7	34	1.653	0.029	0.081	-0.147	0.096	0.271
EMAE	DSC	43.3	33	1.707	0.041	0.113	0.134	0.050	0.139
LOVI	ASC	34.1	21	3.032	0.020	0.043	0.216	0.076	0.163
LOVI	ASC	40.9	24	2.898	0.019	0.044	0.092	0.081	0.188
LOVI	DSC	34.8	19	2.664	0.042	0.084	0.019	0.096	0.194
LOVI	DSC	41.5	21	2.559	0.040	0.087	-0.143	0.112	0.239
RAUM	ASC	32.5	16	1.970	0.035	0.064	0.101	0.079	0.143
RAUM	ASC	39.4	18	2.074	0.033	0.065	-0.348	0.082	0.159
RAUM	ASC	45.4	11	2.020	0.032	0.045	-0.035	0.162	0.229
RAUM	DSC	31.2	18	1.517	0.028	0.054	-0.020	0.063	0.123
WLAD	ASC	35.3	27	1.809	0.020	0.050	0.069	0.106	0.262
WLAD	ASC	43.1	30	1.846	0.048	0.126	0.099	0.173	0.455
WLAD	DSC	33.1	28	1.485	0.017	0.044	0.247	0.053	0.135
WLAD	DSC	41.2	30	1.482	0.023	0.060	-0.068	0.073	0.191
LEBA	ASC	31.5	18	1.302	0.015	0.029	-0.040	0.067	0.132
LEBA	ASC	39.8	27	1.308	0.018	0.046	0.091	0.056	0.138
LEBA	DSC	36.7	20	1.228	0.026	0.054	0.000	0.074	0.155
LEBA	DSC	44.2	27	1.385	0.029	0.073	0.077	0.046	0.113
MART	ASC	31.4	22	1.691	0.021	0.047	0.399	0.076	0.167
MART	ASC	38.6	27	1.843	0.043	0.106	0.172	0.089	0.221
MART	ASC	44.8	27	2.371	0.023	0.058	-0.266	0.084	0.209
MART	DSC	37.7	52	1.465	0.025	0.090	0.434	0.138	0.491
MART	DSC	44.0	52	1.429	0.021	0.075	-0.220	0.144	0.511
KOBB	ASC	34.7	27	1.767	0.250	0.620	0.122	0.067	0.165
KOBB	ASC	41.4	50	1.281	0.048	0.168	0.184	0.040	0.140
KOBB	DSC	34.1	27	1.646	0.056	0.138	0.199	0.061	0.151
KOBB	DSC	41.0	23	1.797	0.062	0.140	0.303	0.106	0.241
VINB	ASC	34.8	9	1.831	0.091	0.112	-0.072	0.130	0.159
VINB	ASC	41.2	9	1.796	0.082	0.101	-0.136	0.159	0.194
VINB	DSC	32.8	9	1.382	0.050	0.062	0.147	0.098	0.120
VINB	DSC	39.4	11	1.335	0.118	0.168	0.159	0.254	0.361
VINB	DSC	45.2	9	1.232	0.062	0.076	-0.239	0.216	0.266
DLR2	ASC	30.9	19	1.193	0.101	0.204	-0.047	0.122	0.246
DLR2	ASC	40.5	18	1.155	0.107	0.209	0.082	0.100	0.196
DLR2	DSC	37.6	23	1.219	0.067	0.152	-0.043	0.187	0.424
DLR3	ASC	30.8	50	1.888	0.021	0.074	0.294	0.053	0.184
DLR3	ASC	40.5	48	1.961	0.021	0.073	0.228	0.046	0.157
DLR3	DSC	37.6	50	1.464	0.030	0.104	-0.114	0.071	0.247

In summary, the attainable precision of Sentinel-1 SAR observations of ECR is largely equivalent to observations of passive CR but absolute accuracy is limited by the delay effects introduced by the active ECR electronics. The effects vary between the individual instruments, which makes an ensemble characterization impossible. In order to achieve better absolute accuracy and improve feasibility for SAR positioning, the ECR should be electronically characterized and calibrated by the manufacturer.

## 8.2 SAR Positioning

In this chapter the results of the SAR positioning of 12 ECR stations located in the Baltic sea region and at DLR in Oberpfaffenhofen are presented. The positions were acquired using the refined absolute positioning of the SAR processor

	<b>BALTIC+ Theme 5</b>  Geodetic SAR for Baltic Height System Unification and Baltic Sea Level Research	<b>Final Report</b> Doc. Nr: SAR-HSU-SR-0022 Issue: 1.1 Date: 07.07.2021 Page: 99 of 170
---	--	--

described in Gruber et al. (2020). The SAR observations are corrected for atmospheric, geodynamic and SAR systematic effects, such as phase center offset and electronic delay of the SAR-transponders. Depending on the station, the number of data takes (DTs) will vary due to different periods of operations and different latitudes and therefore different number of available incidence angles for the ECR transponders. The processor uses as input the resulting products from the SAR data analysis and value adding described in chapter 9.1.

At the ECR station Forsmark/Kobben there are some problematic observation days, namely 2020/08/17, 2020/10/28 and 2020/11/21. For each of these days there are two descending geometries, which indicate unrealistic incidence angles ( $>100^\circ$ ) which influence the results. As a consequence, these dates have to be flagged manually. One possibility is that the observations are faulty, which might be caused by the fence structure around the ECR (refer to Table 5-1). Another possibility is that the orbit information for these dates was corrupted. The reasons for this problem need to be further investigated.

In the following subchapter the positioning results using all available data from 2020 are presented. Later on, the positioning results for each station are discussed, taking different observation periods into account.

### 8.2.1 Results for complete Data Set of 2020

For each station the available data since the start of operation of an ECR until the end of 2020 was used. The results are presented for each station ordered according to the country they are located in. Table 8-4 shows an overview for all 12 Stations with their estimated coordinates and the estimation precision. As can be seen in Table 8-4, the precision (internal accuracy) varies between a few millimeters and one centimeter. The precision is fairly stable, even though the number of data takes vary over the stations. This independency is due to the fact that the estimator becomes already stable when more than 20 DT's per station are used.

Table 8-5 shows the same coordinates in ellipsoidal coordinates for the WGS-84 reference ellipsoid.

**Table 8-4:** Coordinate estimation results in ITRF2014 coordinates (X,Y,Z) using observations available in 2020 for all 12 stations at a given reference epoch (last column). The columns "sx", "sy", "sz" are the standard deviations in x, y and z direction. Additionally, the number of valid data takes (DTs) are given for azimuth (A) and range (R) and their respective number of excluded outliers. The sum of valid DTs and outliers gives the total number of available observations per station

Station	X [m]	Y [m]	Z [m]	sx [+m]	sy [+m]	sz [+m]	Valid DTs [#] A/R	Outlier A/R	Epoch
Loksa	2916918.1992	1404185.7317	5477094.4628	0.0077	0.0094	0.0091	160/163	4/1	2020.475
Vergi	2905540.0951	1423459.7267	5478169.9996	0.0021	0.0013	0.0016	66/77	15/4	2020.422
Emäsalo	2864912.1149	1374213.9082	5511818.0322	0.0008	0.0004	0.0007	181/165	4/20	2020.586
Loviisa	2828356.0091	1396893.4400	5524907.3447	0.002	0.001	0.0017	101/99	5/7	2020.508
Rauma	2873768.8399	1127721.2946	5562562.6038	0.0107	0.0104	0.0111	75/72	1/4	2020.656
Wladyslawowo	3496342.5690	1164349.6260	5188403.3155	0.0087	0.0052	0.0086	133/139	9/3	2020.639
Łeba	3517627.0472	1111458.0491	5185634.1701	0.0015	0.004	0.0028	116/109	0/7	2020.681
Mårtsbo	2998190.4082	931452.1659	5533398.1195	0.0005	0.0012	0.0008	206/194	12/24	2020.581
Kobben	2999000.5296	987780.2882	5523192.2752	0.0087	0.0049	0.0056	81/78	16/19	2020.586
Vinberget	2829284.2185	888154.4489	5628090.4310	0.0011	0.0002	0.0007	54/54	3/3	2020.852
DLR2	4186629.5251	835142.3027	4723656.7292	0.013	0.0118	0.017	83/71	2/14	2020.542
DLR3	4186415.7519	834943.2779	4723876.0869	0.0083	0.0099	0.0105	174/172	3/5	2020.517

**Table 8-5:** Coordinate estimation results in WGS-84 coordinates (Lon., Lat., Height) for all stations using all available observation in the year 2020. The coordinates are given in longitude, latitude and height with respect to the WGS-84 reference ellipsoid and the respective epoch. As in Table 1 the number of all available observations is the sum of valid DTs and outliers

Station	Lon [°]	Lat [°]	Height [m]	Valid DTs [#] A/R	Outlier A/R	Epoch
Loksa	25.7059	59.5826	20.0761	160/163	4/1	2020.475
Vergi	26.1008	59.6015	28.9661	66/77	15/4	2020.422
Emäsalo	25.6257	60.2037	34.2932	181/165	4/20	2020.586
Loviisa	26.2843	60.4408	46.8399	101/99	5/7	2020.508
Rauma	21.4260	61.1335	24.0824	75/72	1/4	2020.656
Władysławowo	18.4188	54.7968	34.6395	133/139	9/3	2020.639
Leba	17.5349	54.7537	34.3894	116/109	0/7	2020.681
Mårtsbo	17.2585	60.5951	75.4769	206/194	12/24	2020.581
Kobben	18.2303	60.4099	25.6586	81/78	16/19	2020.586
Vinberget	17.4279	62.3739	149.6544	54/54	3/3	2020.852
DLR2	11.2812	48.0849	626.6280	83/71	2/14	2020.542
DLR3	11.2791	48.0879	623.8140	174/172	3/5	2020.517

A more detailed view about the internal accuracy of the estimated ECR station coordinates is provided by the confidence ellipsoids in a local North-East-Up coordinate frame. Figure 8-4 shows the results for all stations in one figure, while Figure 8-5 shows the individual ellipsoids per station with adapted axes scaling. By this a more detailed view per station is possible. The confidence ellipsoids only spread over a couple of millimeters or few centimeter in the local reference frame (Figure 8-4 and Figure 8-5). The eccentricity of the ellipses is related to the ratio of observations taken in ascending and descending geometry. The more balanced the number of observations per geometry the more circular the confidence ellipse will become. The confidence ellipses in Figure 8-4 and Figure 8-5 are located around the estimated coordinates of each station.

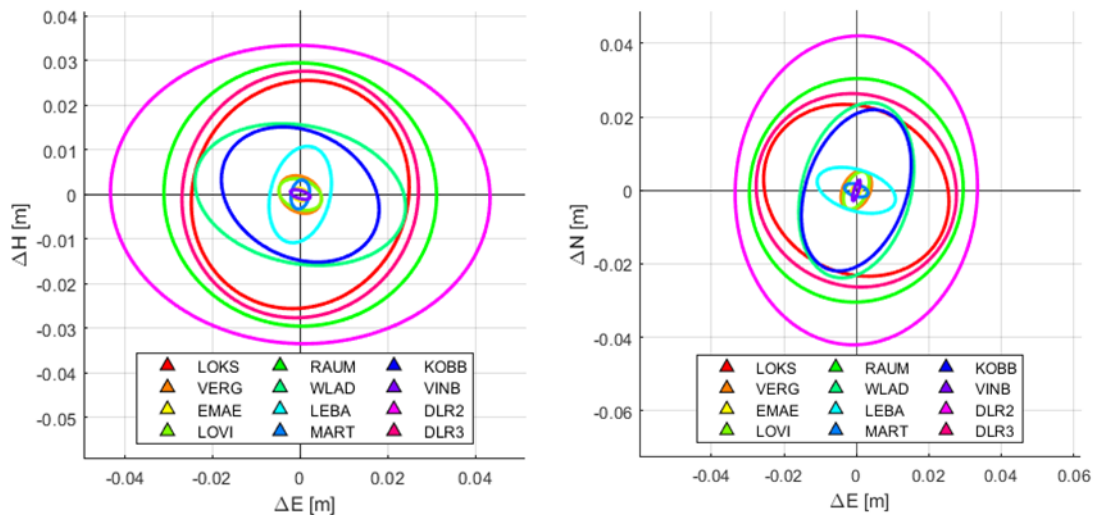


**Figure 8-4:** The confidence ellipsoids are presented for all 12 stations using all available observations in the year 2020. The confidence is shown in the local North, East (right image), and East, height (left image) coordinate frame with respect to the estimated coordinates.

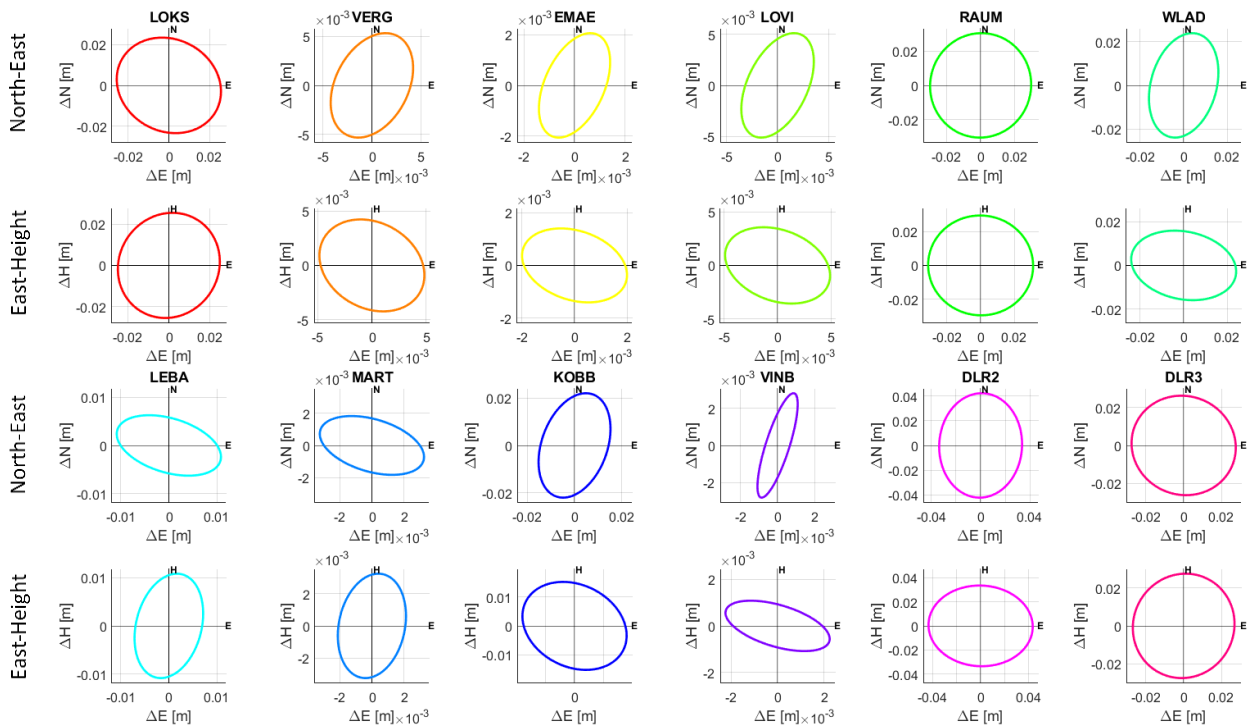
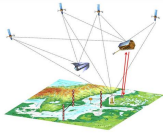


**Figure 8-5:** This figure shows the same confidence ellipses as in Figure 8-4 for all stations in the year 2020, just separated for each station. The first row shows the North-East [m] component and the second row the East-Height [m] component of the stations (from left to right) Loksa, Vergi, Emäsalo, Loviisa, Rauma, and Władysławowo. The third row displays North-East [m] and the fourth row the East-Height [m] component of the stations (from left to right) Łeba, Mårtsbo, Kobben, Vinberget, DLR2, and DLR3.

The confidence ellipses can also be presented with respect to reference coordinates as in Figure 8-6. Here, one can see that the absolute positioning can vary on a larger scale than the internal accuracies. More details on the obtained reference coordinates are given in [AD-4]. The absolute accuracy in height varies between centimeter offsets and a few decimeters. Large offsets in height such as at Loviisa and Łeba deviate from the other stations. On the other hand these stations differ from other stations also by having high absolute accuracies, looking at the horizontal offsets.

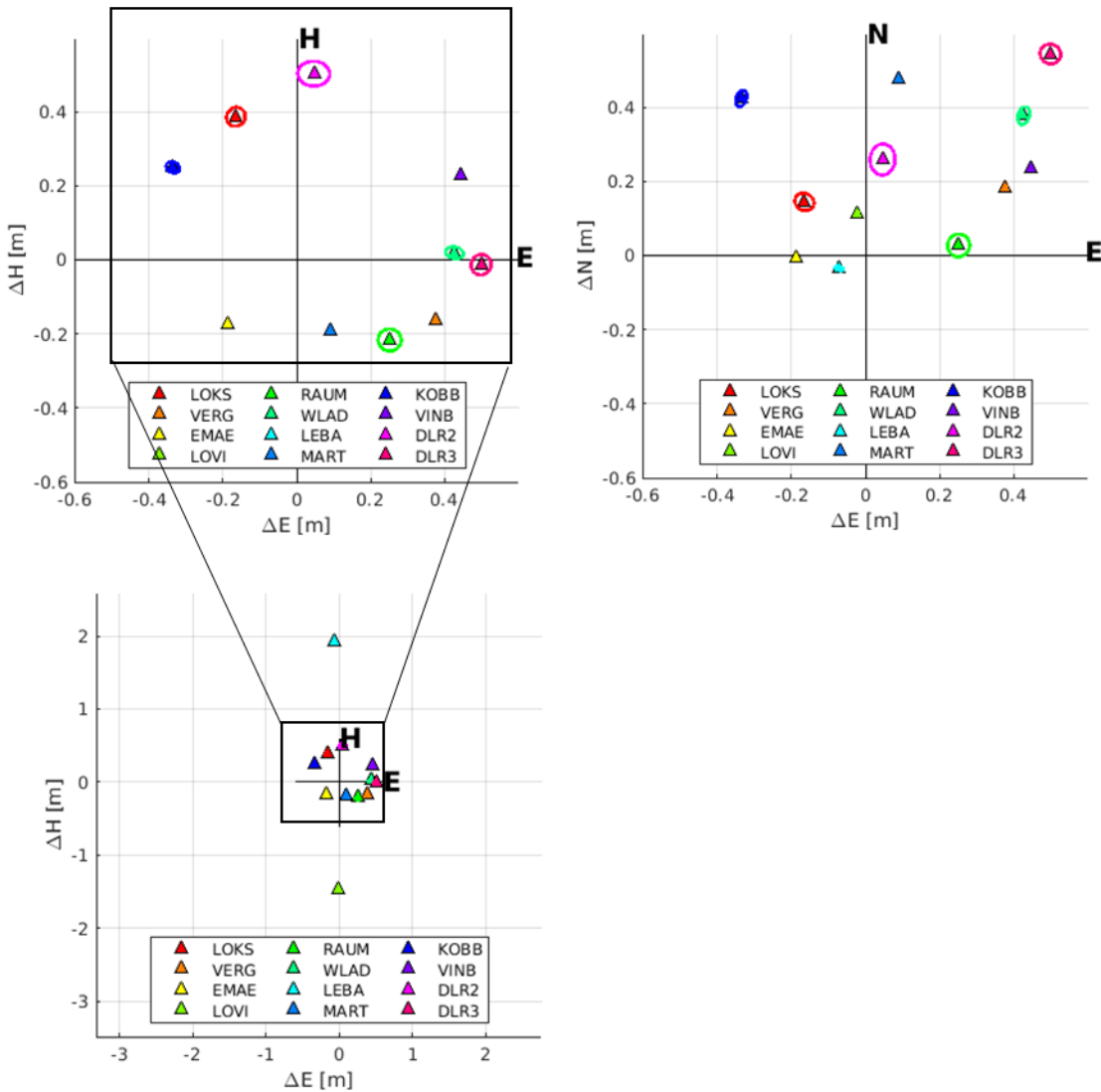
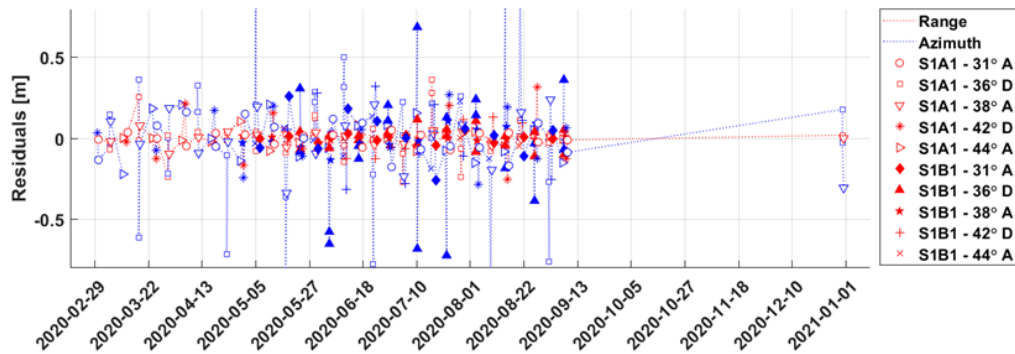
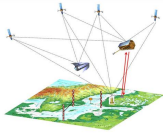


**Figure 8-6:** Error ellipsoids in local East Height (left), zoomed out local East-Height (bottom left), and local North East (right) coordinates of all ECR stations using all available observations from 2020. The position of the ellipses are given with respect to reference coordinates, previously measured by GNSS campaigns.

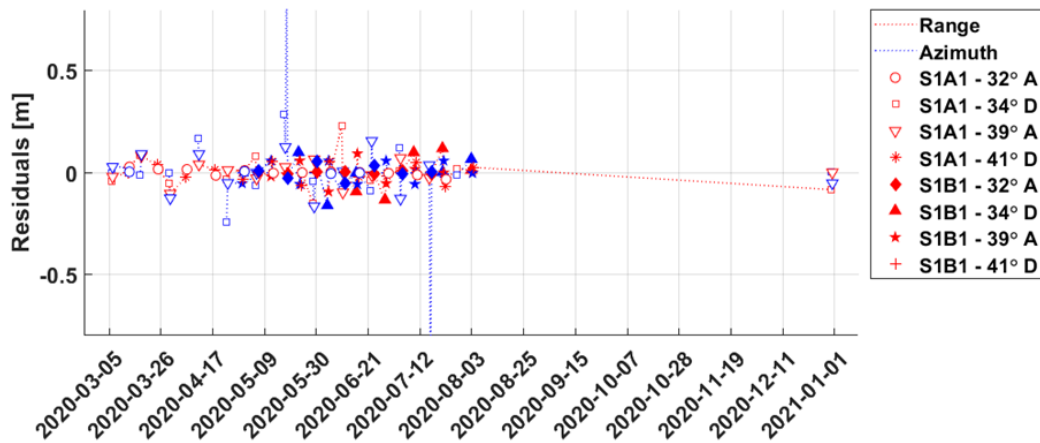
The following graphs show the residuals of valid data takes for each station with respect to the observation period. The residuals are expressed in meters by multiplying the observations residuals with the speed of light; for range observations; or the speed of the satellite; for azimuth observations. The residuals are computed after the refined absolute positioning is finished. This means that, flagged dates, gross outliers (larger residuals than half a pixel of sentinel 1 SAR-image) and outliers (3 $\sigma$ -median criterion) have been removed. Furthermore, a bias correction due to the systematic behaviour of residuals per incidence angle was applied.

Estonia (Loksa, Vergi)

The ECR located at Loksa performed well since the beginning of February until a flooding event in end of September that damaged the transponder. The transponder was repaired (missing observations in Figure 8-7 and reinstalled in the end of 2020. Vergi worked with very high internal accuracies until it experienced a malfunction too, as can be seen in missing observations between August and December in Figure 8-8.



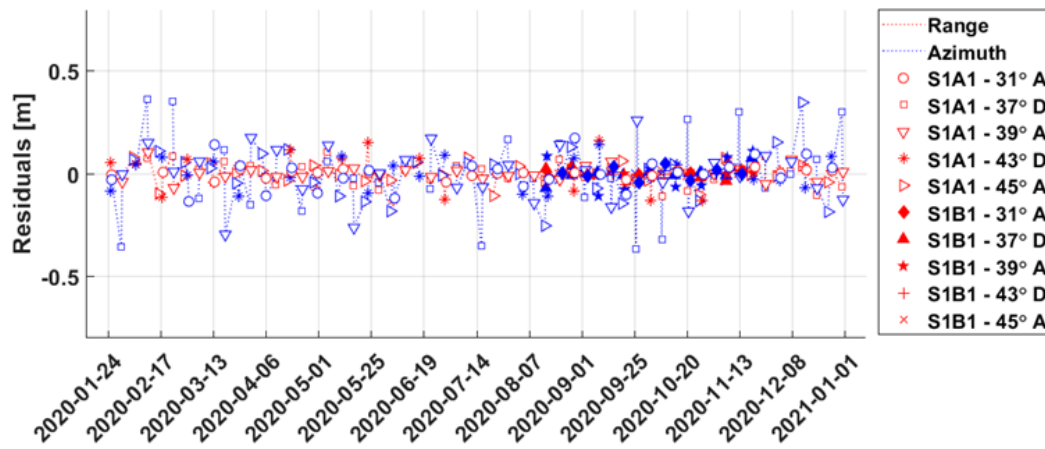
**Figure 8-7:** Residuals at the station **Loksa**. Range observations are coloured in red, the different symbols indicate different incidence angles. Azimuth observations are shown in blue, symbols indicate the same incidence angles as for the range observations.



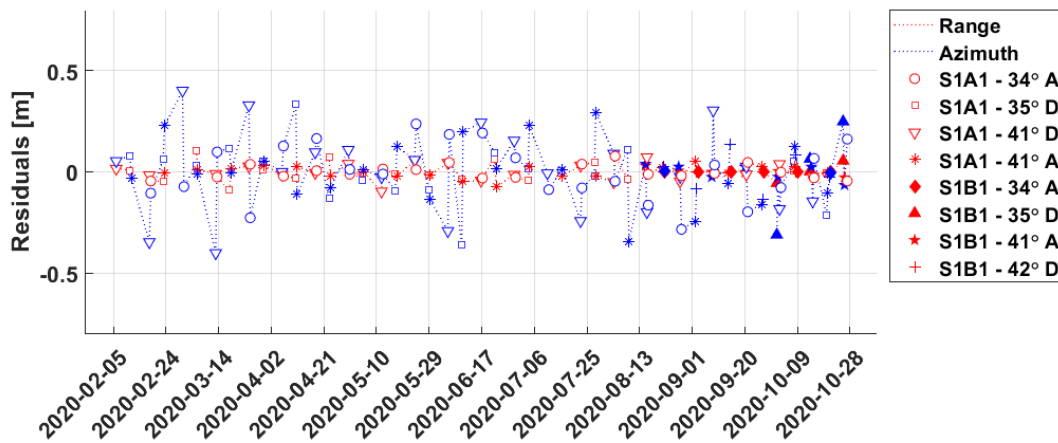
**Figure 8-8:** Residuals at the station **Vergi**. Range observations are coloured in red, the different symbols indicate different incidence angles. Azimuth observations are shown in blue, symbols indicate the same incidence angles as for the range observations.

Finland (Emäsalo, Loviisa, Rauma):

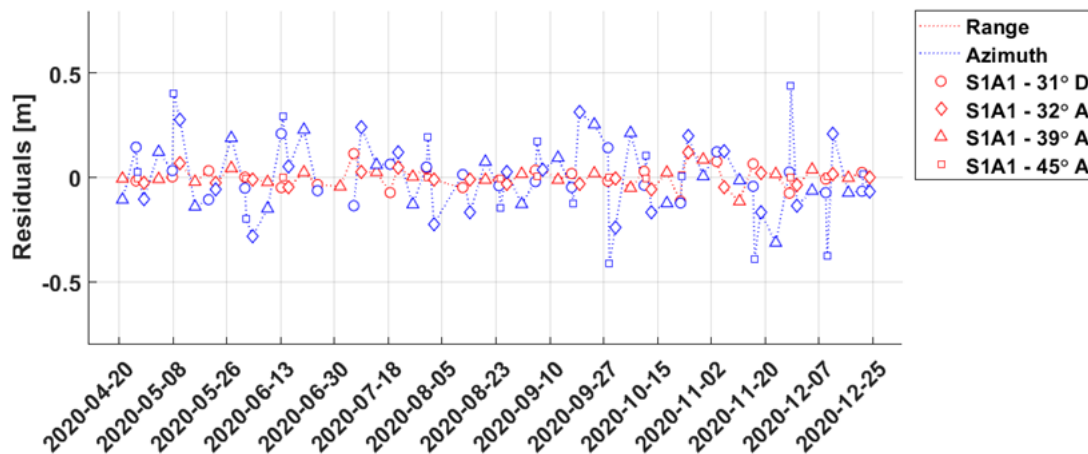
Emäsalo (Figure 8-9) and Loviisa (Figure 8-10) are one of the longest performing stations. They both perform stable and reach high internal accuracies. Rauma (Figure 8-11) has a shorter period of observations. For Rauma it was striking that here multiple gross outliers were present, which might have been caused by the metallic (container) surroundings at the location of the ECR (see Table 5-1).



**Figure 8-9:** Residuals at the station **Emäsalo**. Range observations are coloured in red, the different symbols indicate different incidence angles. Azimuth observations are shown in blue, symbols indicate the same incidence angles as for the range observations.



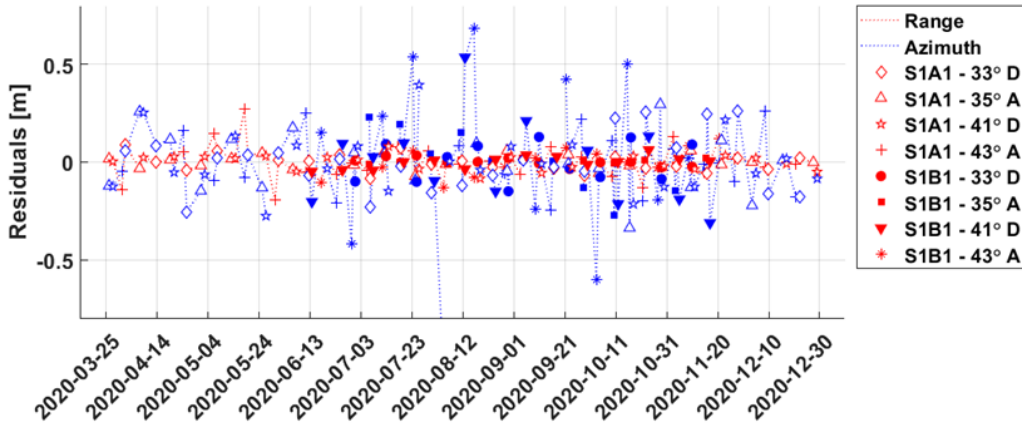
**Figure 8-10:** Residuals at the station **Loviisa**. Range observations are coloured in red, the different symbols indicate different incidence angles. Azimuth observations are shown in blue, symbols indicate the same incidence angles as for the range observations.



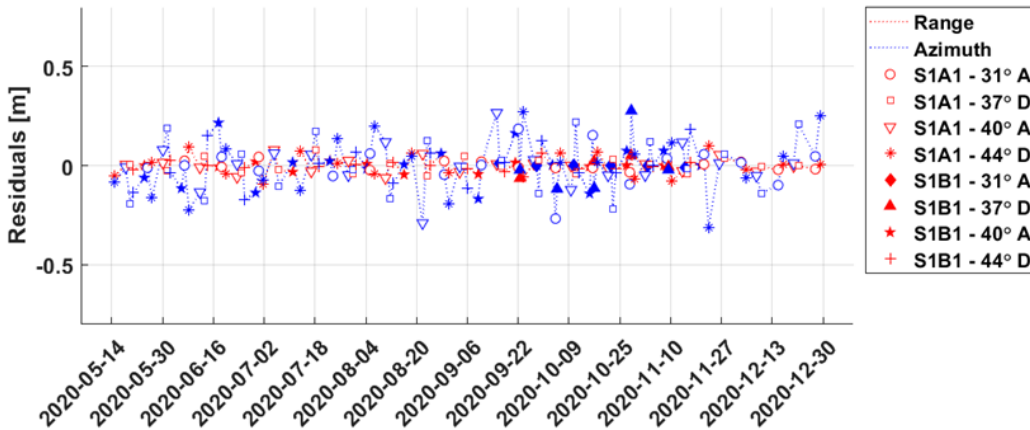
**Figure 8-11:** Residuals at the station **Rauma**. Range observations are coloured in red, the different symbols indicate different incidence angles. Azimuth observations are shown in blue, symbols indicate the same incidence angles as for the range observations.

Poland (Władysławowo, Łeba)

Władysławowo (Figure 8-12) and Łeba (Figure 8-13) perform nominally. They show stable residuals and internal accuracies of a few centimeters.



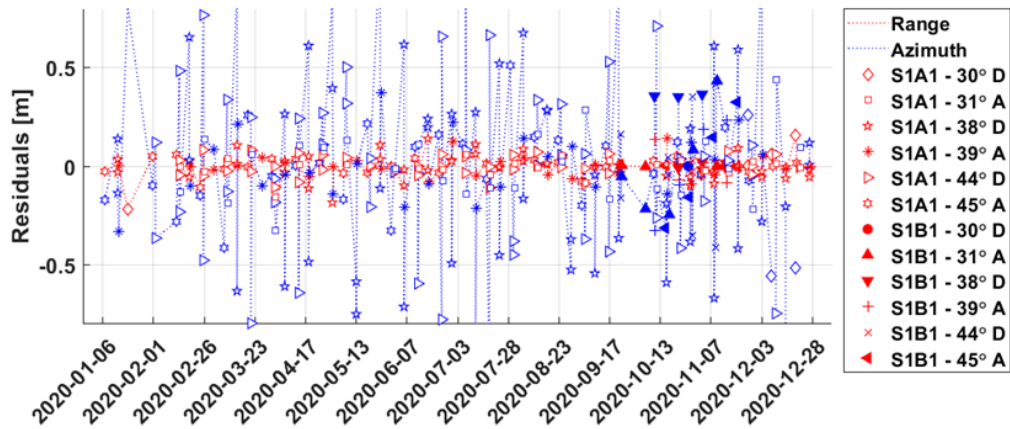
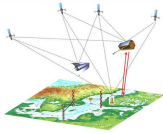
**Figure 8-12:** Residuals at the station **Władysławowo**. Range observations are coloured in red, the different symbols indicate different incidence angles. Azimuth observations are shown in blue, symbols indicate the same incidence angles as for the range observations.



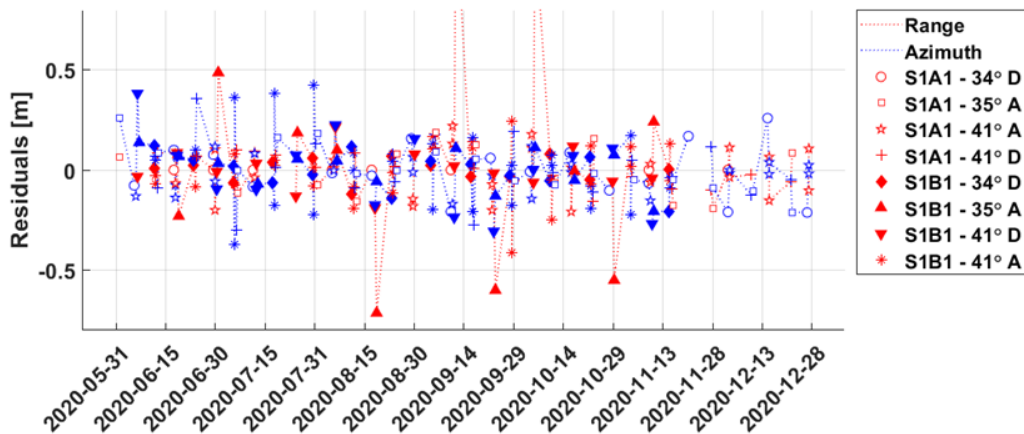
**Figure 8-13:** Residuals at the station **Łeba**. Range observations are coloured in red, the different symbols indicate different incidence angles. Azimuth observations are shown in blue, symbols indicate the same incidence angles as for the range observations.

Sweden (Mårtsbo, Forsmark/Kobben, Spikarna/Vinberget)

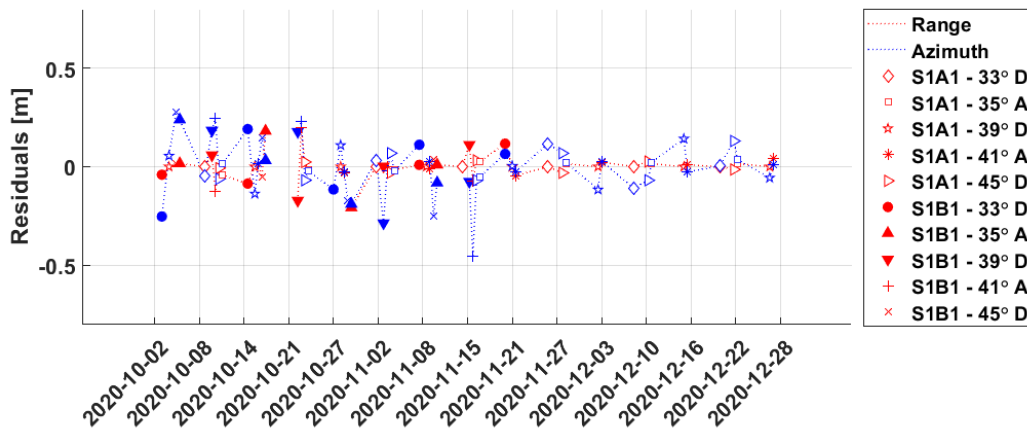
The ECR at Mårtsbo (Figure 8-14) belongs to the longest performing stations. It shows the smallest residuals in range and interestingly the large residuals in azimuth compared to other stations. Forsmark/Kobben (Figure 8-15) shows as only station some large residuals in the range geometry of 35° ascending. This might be related to the fence located around it. Additionally, there are some flagged observation dates due to invalid observations, as mentioned before. Spikarna/Vinberget (Figure 8-16), is one of the stations operating the shortest period of time. The few months of observations show stable and good performance.



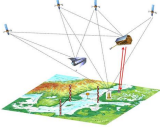
**Figure 8-14:** Residuals at the station **Mårtsbo**. Range observations are coloured in red, the different symbols indicate different incidence angles. Azimuth observations are shown in blue, symbols indicate the same incidence angles as for the range observations.



**Figure 8-15:** Residuals at the station **Forsmark/Kobben**. Range observations are coloured in red, the different symbols indicate different incidence angles. Azimuth observations are shown in blue, symbols indicate the same incidence angles as for the range observations.



**Figure 8-16:** Residuals at the station **Spikarna/Vinberget**. Range observations are coloured in red, the different symbols indicate different incidence angles. Azimuth observations are shown in blue, symbols indicate the same incidence angles as for the range observations.

	<b>BALTIC+ Theme 5</b> Geodetic SAR for Baltic Height System Unification and Baltic Sea Level Research	<b>Final Report</b> Doc. Nr: SAR-HSU-SR-0022 Issue: 1.1 Date: 07.07.2021 Page: 107 of 170
---	--	---

Germany (DLR2, DLR3)

One of the two ECRs located in Oberpfaffenhofen at DLR, DLR2 (Figure 8-17), had two malfunctions and has been repaired twice. For this station the performance changed over time, which leads to larger uncertainties in the location estimation. Additionally, there might be some corrupted dates aliasing into the solution as the performance decreased before the repair. The other ECR, DLR3 (Figure 8-18), has one of the longest periods of observation and performs stable.

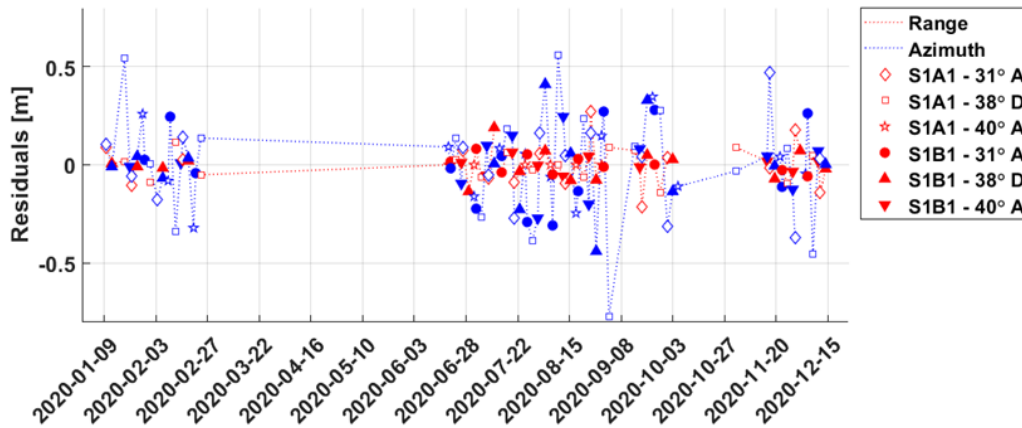


**Figure 8-17:** Residuals at the station **DLR2**. Range observations are coloured in red, the different symbols indicate different incidence angles. Azimuth observations are shown in blue, symbols indicate the same incidence angles as for the range observations.

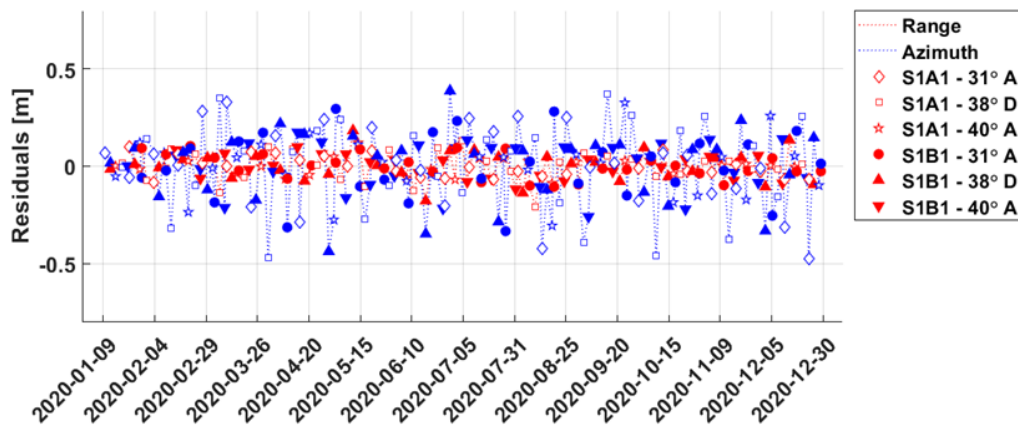


**Figure 8-18:** Residuals at the station **DLR3**. Range observations are coloured in red, the different symbols indicate different incidence angles. Azimuth observations are shown in blue, symbols indicate the same incidence angles as for the range observations.

8.2.2 Results for Data Subsets

In this chapter the performance of each station is shown taking different periods of observation into account for each solution. In the following the different temporal resolutions will be marked as monthly (1M), bimonthly (2M), trimonthly (3M) and every four months (4M). e.g. all data from March 2020 would be considered for a 1M solution, data from March and April for a 2M solution and so on. The mean date of the observation period is the epoch of the positioning result. The purpose of this analysis is twofold. First it is investigated what is the minimum number of observations to reach a stable positioning solution, and second it is investigated how stable the solutions are over time and if there is a chance to observe vertical land motion.

In chapter 7.2, it was shown that the SAR positioning stabilizes when more than 20 data takes (DT) (azimuth+range) are used. Figure 8-19 illustrates the behaviour of the standard deviations with respect to the number of data takes (DTs) for the different temporal resolutions at all stations. As can be seen the internal accuracies in terms of standard deviations further improves with increasing number of DTs, but reaches a limit where there is no further improvement achievable.

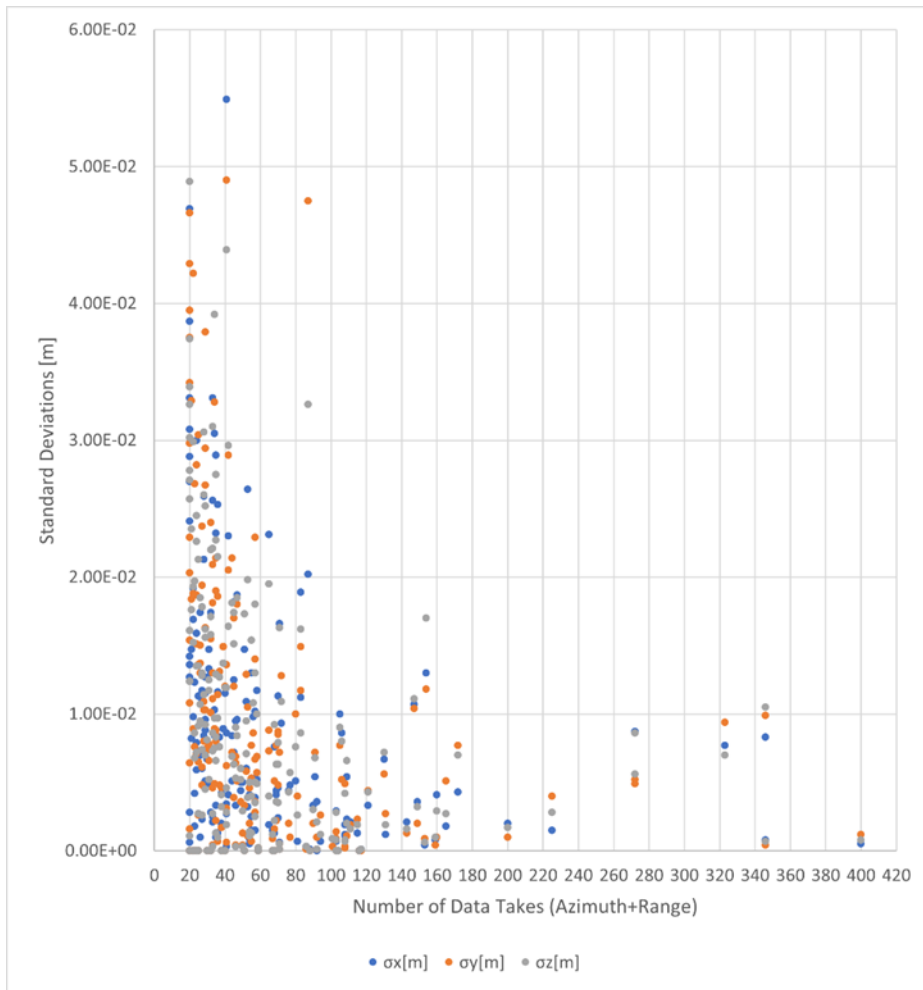
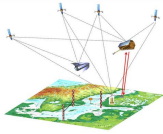
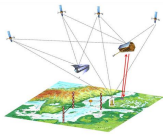


**Figure 8-19:** Standard Deviations of Absolute Positioning of all ECRs and all temporal resolutions (1M,2M,3M,4M, yearly) per number of data takes.

In the following figures the performance of each stations for different temporal resolutions (1M, 2M, 3M, and 4M) is shown. The confidence ellipsoids are located with respect to the given reference coordinates in the local North East Up reference frame. The different colours indicate the different temporal resolutions. Next to the ellipsoids the positioning offsets with respect to the reference coordinate in the local North, East Up frame are presented along their respective reference epoch in the figures. A detailed overview about the number of DTs used for each temporal resolution per station and the respectively achieved internal accuracies can be found for each station in the subsequent tables.

In general, one can observe the trend of increasing internal accuracies with increasing number of observations. 1M solutions tend to have larger standard deviations, larger confidence ellipsoids than their respective 2M, 3M or 4M solutions at the same station. 3M and 4M solutions perform for most stations as good as the solutions using all available observations.

For every SAR positioning solution, a linear correction was applied based on the trend of the nearest IGS station to shift the reference coordinates to the respective epochs of the SAR positioning. Therefore, the 1M and 2M solutions ideally should show a constant offset to their reference coordinates over time, if one assumes that the IGS station coordinate trends are applicable to the ECR stations as well. Any residual trend for the coordinate axes could imply that the IGS linear correction model doesn't reflect the reality good enough or that the uncertainty of the estimated ECR positions is too high to observe such trends. To evaluate this the root mean square (RMS) value for the 1M and 2M solution offsets was estimated. As can be seen in the figures, all stations show a RMS in all three directions (North, East, Up) between 5 to 20 centimetres, which is significantly above the IGS trend model at a level of 1-2 cm per year per coordinate axis.



Estonia (Loksa, Vergi)

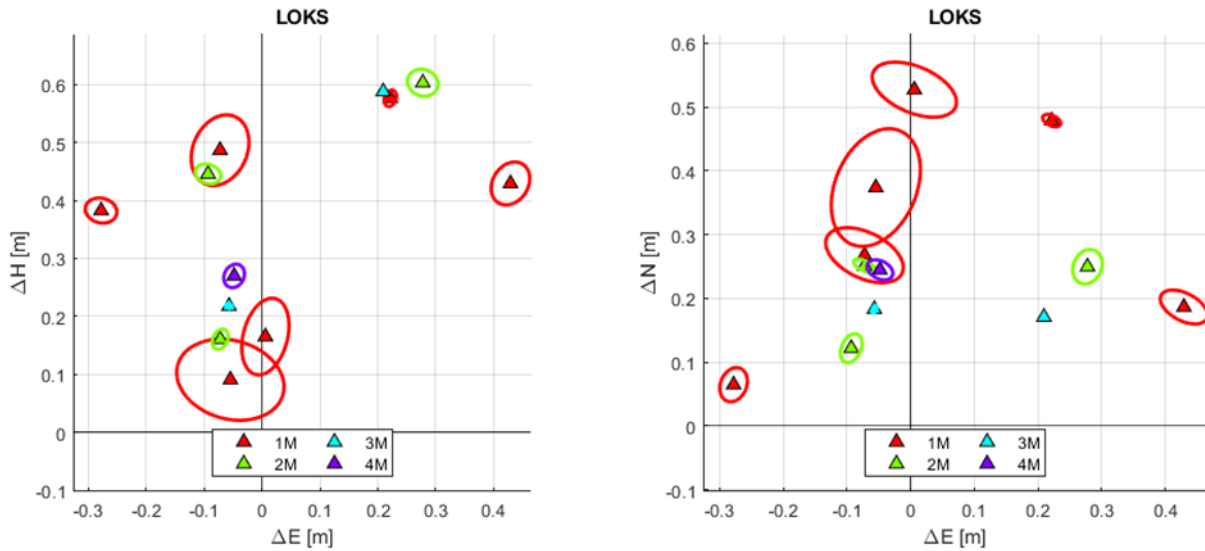


**Figure 8-20:** Error ellipsoids in local East Height (left) and local North East (right) coordinates of the ECR located at **Loksa** for the different temporal resolutions: monthly (1M), bi monthly (2M), trimonthly (3M), and every four months (4M) in the year 2020 at their respective reference epochs

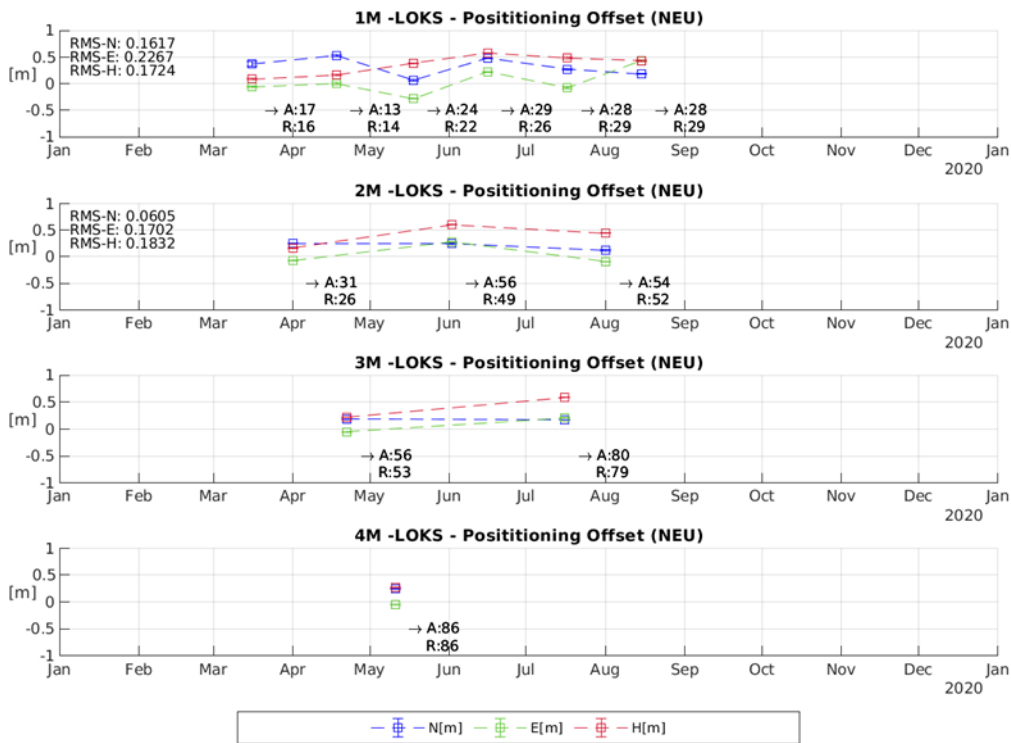


**Figure 8-21:** Positioning Offset of the ECR located at **Loksa** for the different temporal resolutions: monthly (1M), bi monthly (2M), trimonthly (3M), and every four months (4M) in the year 2020. The offsets are displayed in local North (blue), East (green), and Height (red) with respect to given reference coordinates from GNSS campaigns at the mean date of the observation period. For 1M and 2M the Root Mean Square (RMS) values are displayed in the top left corner of the respective graph. “A:” and “R:” beneath each solution indicate the number of data takes used in azimuth and range for the particular solution.

**Table 8-6:** Standard deviations for the cartesian x, y, z coordinate resulting from the SAR-Positioning for different temporal resolutions (1M, 2M, 3M,4M and all observations (--)) at **Loksa**. The number of data takes used in azimuth and range are shown in the columns DT's A and DT's R. Epoch refers to the mean date of the period of observation.

Temp Res.	$\sigma_x$ [m]	$\sigma_y$ [m]	$\sigma_z$ [m]	Epoch	DTs A	DTs R
1M	3.31E-02	2.09E-02	3.10E-02	2020.205	17	16
1M	1.17E-02	2.37E-02	1.30E-02	2020.295	13	14
1M	9.50E-03	6.90E-03	9.00E-03	2020.377	24	22
1M	2.50E-03	5.30E-03	4.00E-03	2020.456	29	26
1M	1.02E-02	2.29E-02	1.80E-02	2020.541	28	29
1M	5.30E-03	1.40E-02	1.30E-02	2020.620	28	29
2M	1.50E-03	6.70E-03	5.00E-03	2020.249	31	26
2M	1.00E-02	7.70E-03	9.00E-03	2020.418	56	49
2M	8.60E-03	5.20E-03	8.00E-03	2020.582	54	52
3M	2.30E-03	1.10E-03	2.00E-03	2020.306	56	53
3M	8.00E-04	4.00E-04	1.00E-03	2020.538	80	79
4M	4.30E-03	7.70E-03	7.00E-03	2020.358	86	86
--	7.70E-03	9.40E-03	7.00E-03	2020.473	160	163

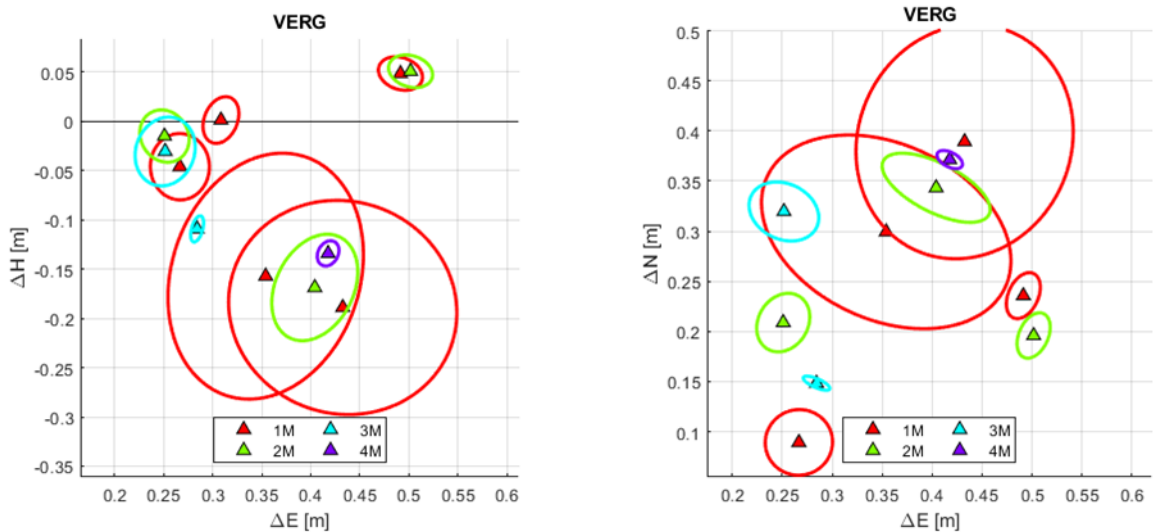


**Figure 8-22:** Error ellipsoids in local East Height (left) and local North East (right) coordinates of the ECR located at **Vergi** for the different temporal resolutions: monthly (1M), bi monthly (2M), trimonthly (3M) ,and every four months (4M) in the year 2020 at their respective reference epochs.

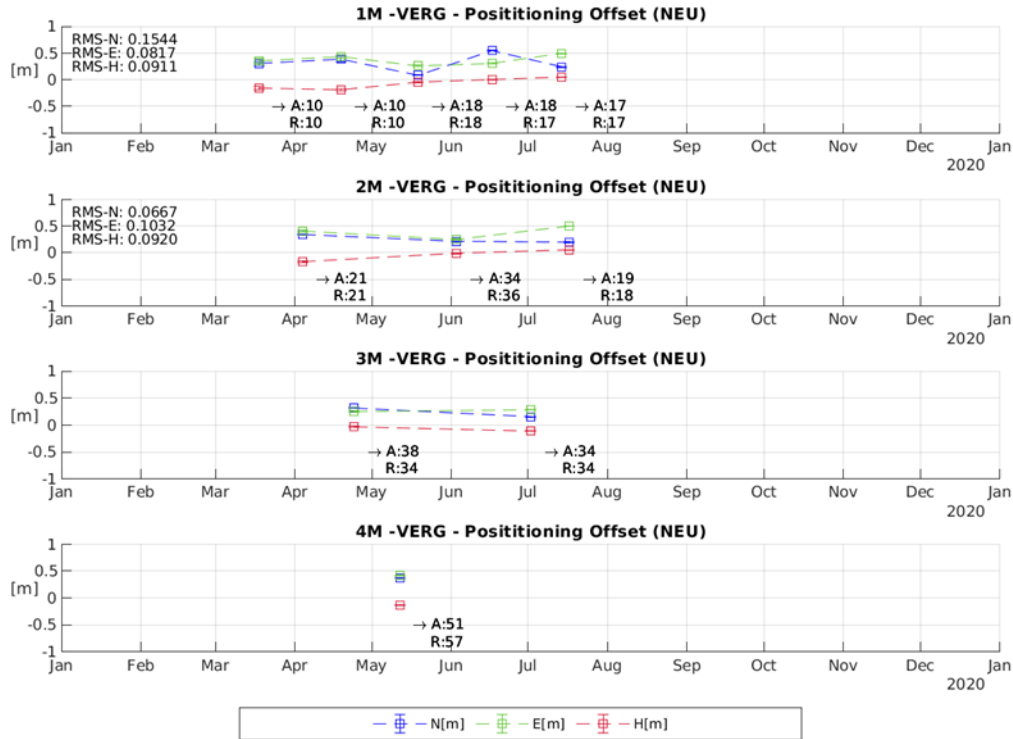
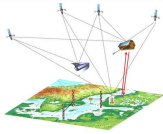


**Figure 8-23:** Positioning Offset of the ECR located at **Vergi** for the different temporal resolutions: monthly (1M), bi monthly (2M), trimonthly (3M), and every four months (4M) in the year 2020. The offsets are displayed in local North (blue), East (green), and Height (red) with respect to given reference coordinates from GNSS campaigns at the mean date of the observation period. For 1M and 2M the Root Mean Square (RMS) values are displayed in the top left corner of the respective graph. “A:” and “R:” beneath each solution indicate the number of data takes used in azimuth and range for the particular solution.

**Table 8-7:** Standard deviations for the cartesian x, y, z coordinate resulting from the SAR-Positioning for different temporal resolutions (1M, 2M, 3M, 4M and all observations (--)) at **Vergi**. The number of data takes used in azimuth and range are shown in the columns DT's A and DT's R. Epoch refers to the mean date of the period of observation.

Temp Res.	$\sigma_x$ [m]	$\sigma_y$ [m]	$\sigma_z$ [m]	Epoch	DTs A	DTs R
1M	2.70E-02	4.29E-02	3.26E-02	2020.210	10	10
1M	3.87E-02	3.42E-02	3.74E-02	2020.298	10	10
1M	1.16E-02	1.14E-02	9.70E-03	2020.380	18	18
1M	3.30E-03	8.80E-03	6.60E-03	2020.459	18	17
1M	8.40E-03	4.90E-03	7.50E-03	2020.533	17	17
2M	4.10E-03	2.05E-02	1.64E-02	2020.257	21	21
2M	1.13E-02	8.70E-03	7.90E-03	2020.421	34	36
2M	8.30E-03	4.80E-03	7.60E-03	2020.541	19	18
3M	9.30E-03	1.28E-02	1.09E-02	2020.311	38	34
3M	1.30E-03	5.10E-03	2.20E-03	2020.500	34	34
4M	1.90E-03	4.90E-03	4.20E-03	2020.361	51	57
--	2.10E-03	1.30E-03	1.60E-03	2020.421	66	77

**Finland (Emäsalo, Loviisa, Rauma):**

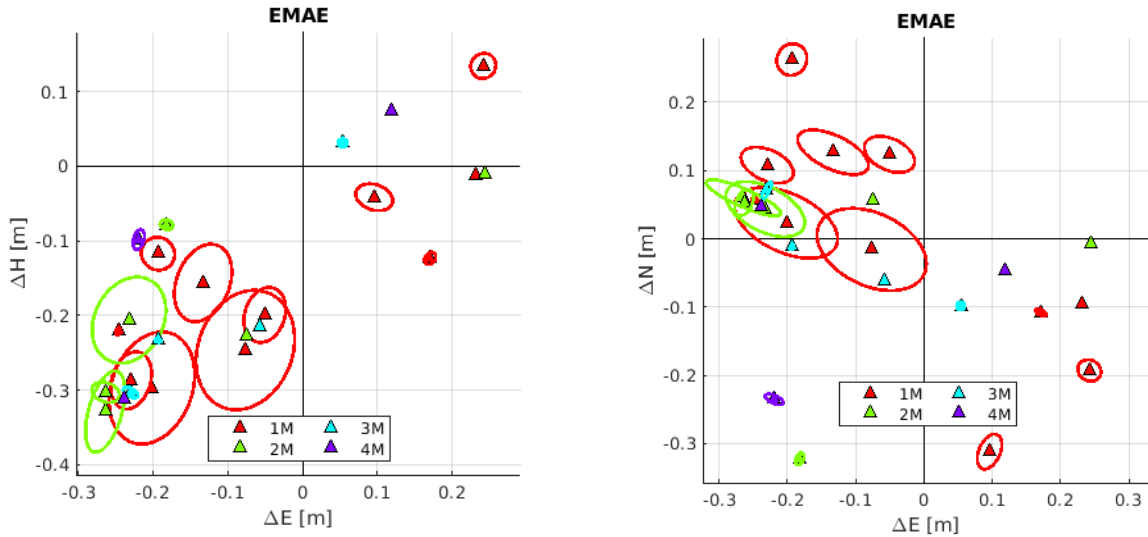


**Figure 8-24:** Error ellipsoids in local East Height (left) and local North East (right) coordinates of the ECR located at **Emäsalo** for the different temporal resolutions: monthly (1M), bi monthly (2M), trimonthly (3M), and every four months (4M) in the year 2020 at their respective reference epochs.

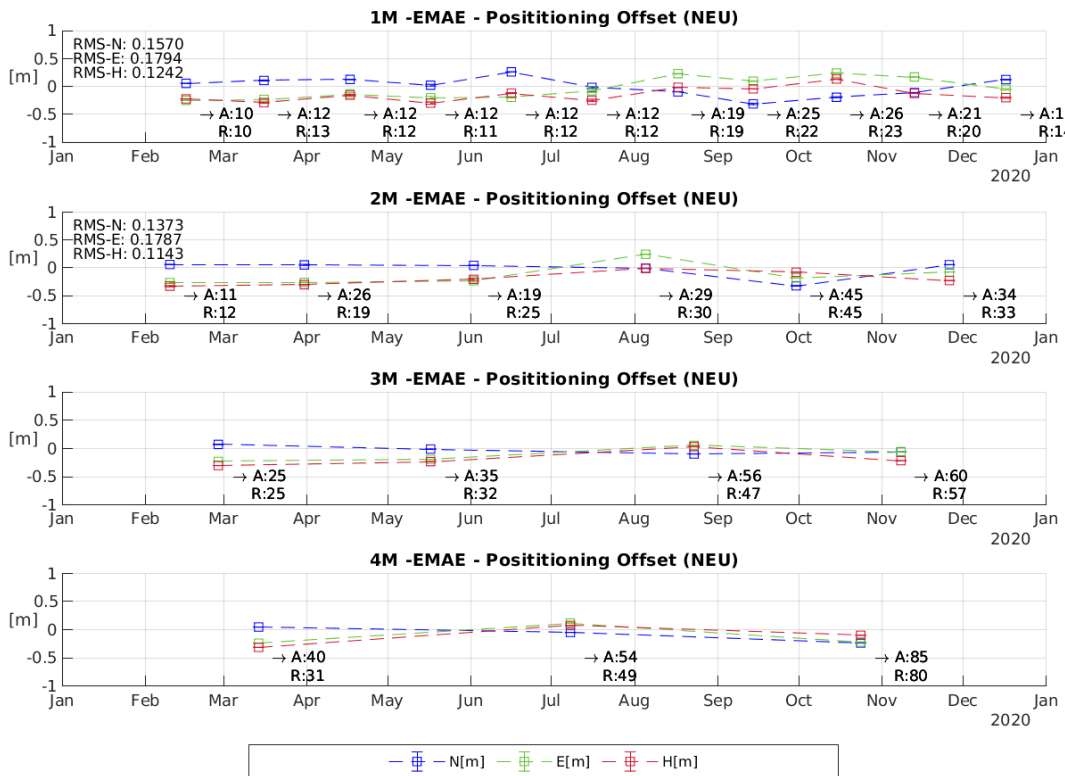


**Figure 8-25:** Positioning Offset of the ECR located at **Emäsalo** for the different temporal resolutions: monthly (1M), bi monthly (2M), trimonthly (3M), and every four months (4M) in the year 2020. The offsets are displayed in local North (blue), East (green), and Height (red) with respect to given reference coordinates from GNSS campaigns at the mean date of the observation period. For 1M and 2M the Root Mean Square (RMS) values are displayed in the top left corner of the respective graph. “A:” and “R:” beneath each solution indicate the number of data takes used in azimuth and range for the particular solution.

**Table 8-8:** Standard deviations for the cartesian x, y, z coordinate resulting from the SAR-Positioning for different temporal resolutions (1M, 2M, 3M,4M and all observations (--)) at **Emäsalo**. The number of data takes used in azimuth and range are shown in the columns DT's A and DT's R. Epoch refers to the mean date of the period of observation.

Temp Res.	$\sigma_x$ [m]	$\sigma_y$ [m]	$\sigma_z$ [m]	Epoch	DTs A	DTs R
1M	6.00E-04	1.60E-03	1.10E-03	2020.126	10	10
1M	6.90E-03	1.36E-02	9.10E-03	2020.205	12	13
1M	5.90E-03	1.87E-02	1.35E-02	2020.292	12	12
1M	1.23E-02	2.68E-02	1.97E-02	2020.374	12	11
1M	7.90E-03	7.10E-03	7.20E-03	2020.456	12	12
1M	1.59E-02	2.82E-02	2.26E-02	2020.538	12	12
1M	0.00E+00	0.00E+00	0.00E+00	2020.626	19	19
1M	9.60E-03	5.10E-03	8.40E-03	2020.702	25	22
1M	5.00E-03	6.00E-03	6.00E-03	2020.787	26	23
1M	3.00E-04	3.10E-03	2.80E-03	2020.866	21	20
1M	7.00E-03	1.30E-02	9.50E-03	2020.959	12	14
2M	1.80E-03	1.97E-02	8.60E-03	2020.109	11	12
2M	7.20E-03	3.90E-03	6.30E-03	2020.246	26	19
2M	8.40E-03	2.14E-02	1.81E-02	2020.418	19	25
2M	0.00E+00	0.00E+00	0.00E+00	2020.593	29	30
2M	3.30E-03	2.00E-03	3.00E-03	2020.746	45	45
2M	0.00E+00	0.00E+00	0.00E+00	2020.902	34	33
3M	5.00E-03	1.30E-03	2.90E-03	2020.158	25	25
3M	1.50E-03	9.00E-04	1.20E-03	2020.374	35	32
3M	2.00E-03	2.00E-03	2.20E-03	2020.642	56	47
3M	1.00E-04	0.00E+00	1.00E-04	2020.852	60	57
4M	1.00E-04	1.00E-04	1.00E-04	2020.199	40	31
4M	0.00E+00	0.00E+00	0.00E+00	2020.516	54	49
4M	1.80E-03	5.10E-03	2.70E-03	2020.811	85	80
--	8.00E-04	4.00E-04	7.00E-04	2020.585	181	165

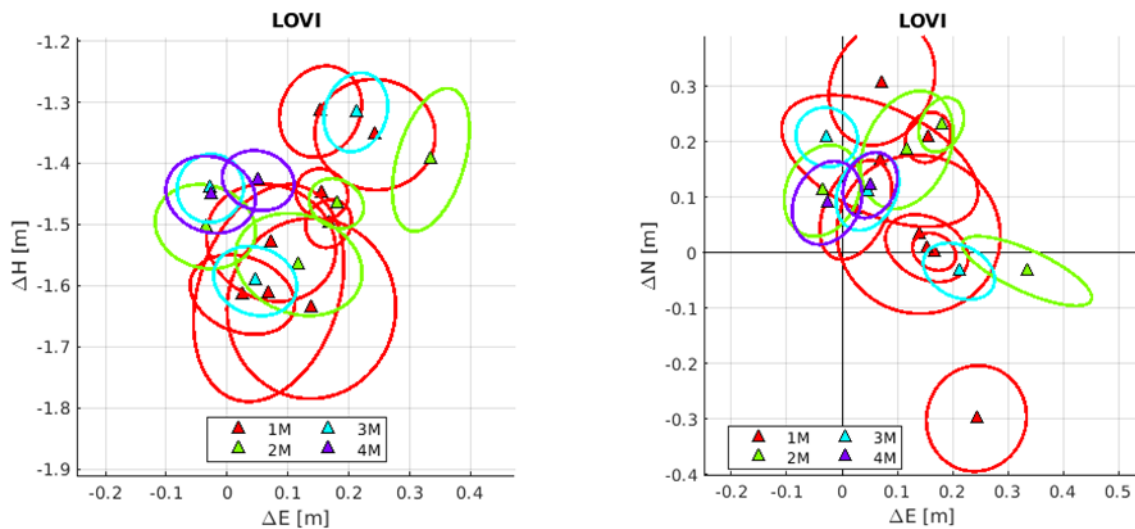


**Figure 8-26:** Error ellipsoids in local East Height (left) and local North East (right) coordinates of the ECR located at **Loviisa** for the different temporal resolutions: monthly (1M), bi monthly (2M), trimonthly (3M) ,and every four months (4M) in the year 2020 at their respective reference epochs.

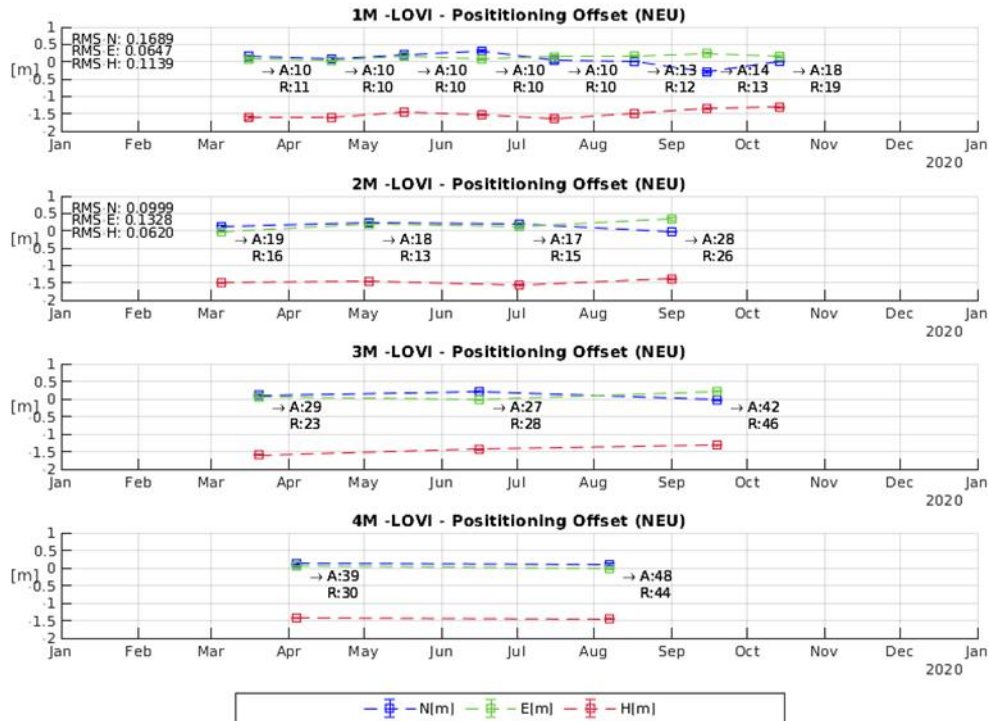
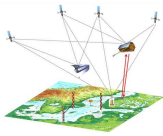


**Figure 8-27:** Positioning Offset (no Bias Corrections applied) of the ECR located at **Loviisa** for the different temporal resolutions: monthly (1M), bi monthly (2M), trimonthly (3M), and every four months (4M) in the year 2020. The offsets are displayed in local North (blue), East (green), and Height (red) with respect to given reference coordinates from GNSS campaigns at the mean date of the observation period. For 1M and 2M the Root Mean Square (RMS) values are displayed in the top left corner of the respective graph. “A:” and “R:” beneath each solution indicate the number of data takes used in azimuth and range for the particular solution.

**Table 8-9:** Standard deviations (no Bias Corrections applied) for the cartesian x, y, z coordinate resulting from the SAR-Positioning for different temporal resolutions (1M, 2M, 3M, 4M and all observations (—)) at **Loviisa**. The number of data takes used in azimuth and range are shown in the columns DT's A and DT's R. Epoch refers to the mean date of the period of observation.

Temp Res.	ox[m]	oy[m]	oz[m]	Epoch	DTs A	DTs R
1M	2.83E-02	6.24E-02	4.06E-02	2020.205	10	11
1M	3.16E-02	1.75E-02	2.72E-02	2020.295	10	10
1M	1.56E-02	1.26E-02	1.34E-02	2020.374	10	10
1M	3.80E-02	2.90E-02	3.35E-02	2020.459	10	10
1M	4.65E-02	4.80E-02	4.40E-02	2020.538	10	10
1M	9.70E-03	1.37E-02	1.30E-02	2020.626	13	12
1M	3.16E-02	2.99E-02	3.35E-02	2020.705	14	13
1M	1.71E-02	2.70E-02	2.39E-02	2020.784	18	19
2M	2.94E-02	2.18E-02	2.81E-02	2020.175	19	16
2M	1.82E-02	1.26E-02	1.45E-02	2020.336	18	13
2M	3.85E-02	2.52E-02	3.49E-02	2020.500	17	15
2M	9.30E-03	4.50E-02	2.20E-02	2020.667	28	26
3M	2.60E-02	1.78E-02	2.34E-02	2020.216	29	23
3M	1.80E-02	1.96E-02	1.91E-02	2020.456	27	28
3M	1.56E-02	2.40E-02	1.86E-02	2020.716	42	46
4M	2.17E-02	1.59E-02	2.06E-02	2020.257	39	30
4M	2.79E-02	2.05E-02	2.55E-02	2020.598	48	44
--	1.73E-02	1.42E-02	1.67E-02	2020.505	101	99

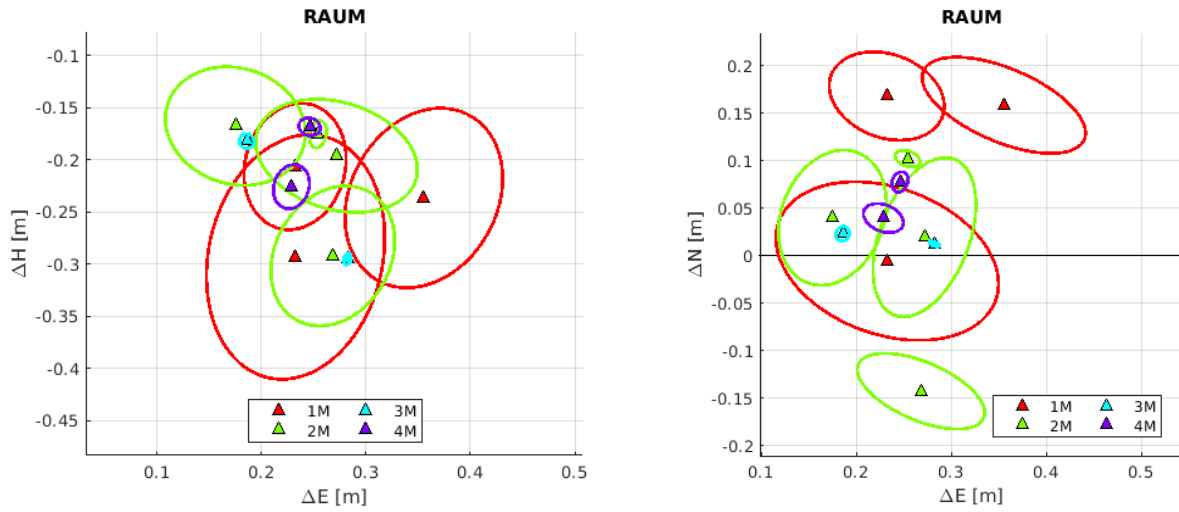
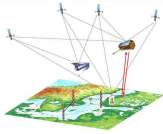


**Figure 8-28:** Error ellipsoids (no Bias Corrections applied) in local East Height (left) and local North East (right) coordinates of the ECR located at **Rauma** for the different temporal resolutions: monthly (1M), bi monthly (2M), trimonthly (3M), and every four months (4M) in the year 2020 at their respective reference epochs.

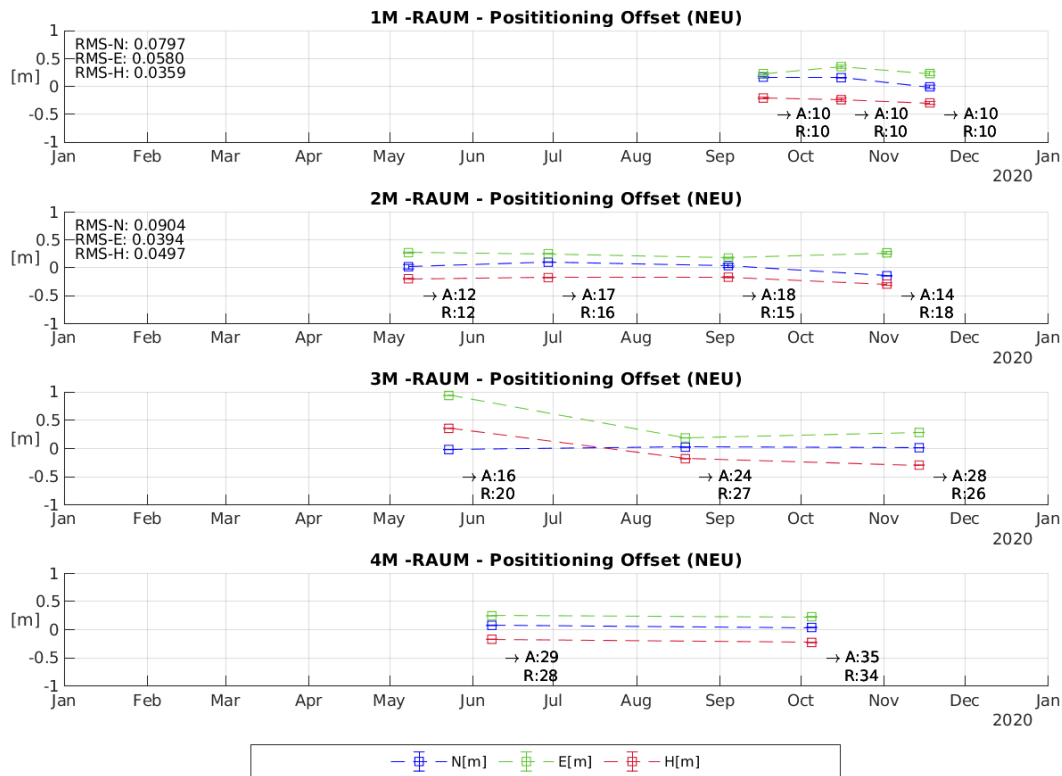


**Figure 8-29:** Positioning Offset of the ECR located at **Rauma** for the different temporal resolutions: monthly (1M), bi monthly (2M), trimonthly (3M), and every four months (4M) in the year 2020. The offsets are displayed in local North (blue), East (green), and Height (red) with respect to given reference coordinates from GNSS campaigns at the mean date of the observation period. For 1M and 2M the Root Mean Square (RMS) values are displayed in the top left corner of the respective graph. “A:” and “R:” beneath each solution indicate the number of data takes used in azimuth and range for the particular solution.

**Table 8-10:** Standard deviations for the cartesian x, y, z coordinate resulting from the SAR-Positioning for different temporal resolutions (1M, 2M, 3M,4M and all observations (--)) at **Rauma**. The number of data takes used in azimuth and range are shown in the columns DT's A and DT's R. Epoch refers to the mean date of the period of observation.

Temp Res.	$\sigma_x$ [m]	$\sigma_y$ [m]	$\sigma_z$ [m]	Epoch	DTs A	DTs R
1M	1.36E-02	2.03E-02	1.61E-02	2020.710	10	10
1M	2.80E-03	2.98E-02	2.71E-02	2020.790	10	10
1M	2.41E-02	3.95E-02	2.78E-02	2020.880	10	10
2M	3.00E-02	1.51E-02	2.45E-02	2020.350	12	12
2M	2.70E-03	4.60E-03	2.70E-03	2020.492	17	16
2M	2.56E-02	1.81E-02	2.21E-02	2020.675	18	15
2M	2.80E-03	2.40E-02	2.20E-02	2020.836	14	18
3M	1.30E-03	7.00E-04	1.00E-03	2020.391	16	20
3M	2.80E-03	2.40E-03	2.30E-03	2020.631	24	27
3M	5.00E-04	2.00E-03	1.40E-03	2020.869	28	26
4M	3.90E-03	2.80E-03	3.50E-03	2020.434	29	28
4M	4.40E-03	7.70E-03	6.30E-03	2020.760	35	34
--	1.07E-02	1.04E-02	1.11E-02	2020.653	75	72

Poland (Władysławowo, Łeba)

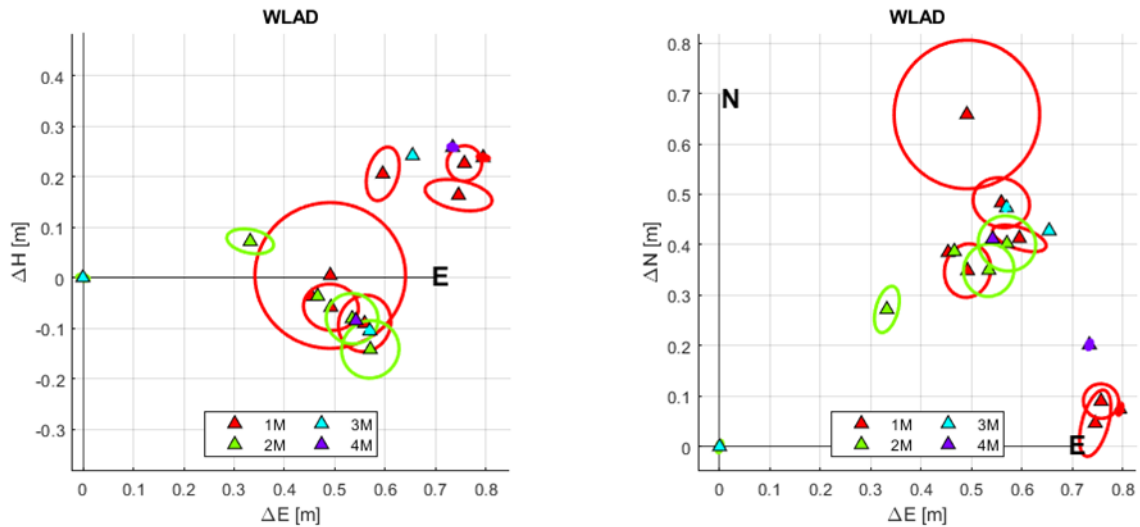


**Figure 8-30:** Error ellipsoids in local East Height (left) and local North East (right) coordinates of the ECR located at **Władysławowo** for the different temporal resolutions: monthly (1M), bi monthly (2M), trimonthly (3M), and every four months (4M) in the year 2020 at their respective reference epochs.

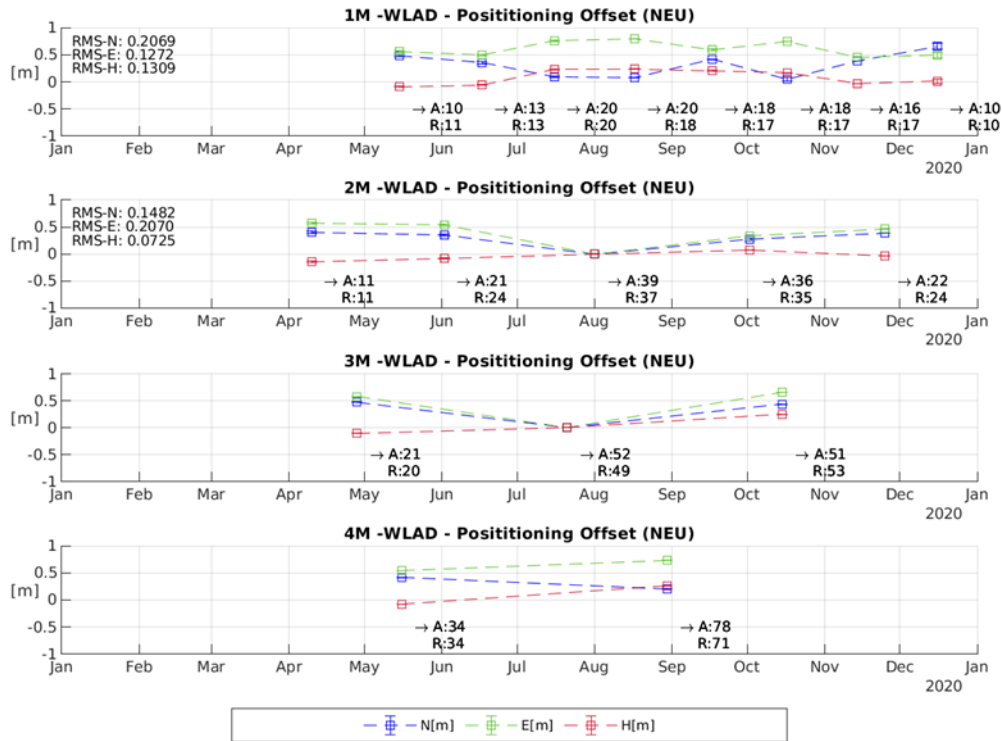


**Figure 8-31:** Positioning Offset of the ECR located at **Wladyslawowo** for the different temporal resolutions: monthly (1M), bi monthly (2M), trimonthly (3M), and every four months (4M) in the year 2020. The offsets are displayed in local North (blue), East (green), and Height (red) with respect to given reference coordinates from GNSS campaigns at the mean date of the observation period. For 1M and 2M the Root Mean Square (RMS) values are displayed in the top left corner of the respective graph. “A:” and “R:” beneath each solution indicate the number of data takes used in azimuth and range for the particular solution.

**Table 8-11:** Standard deviations for the cartesian x, y, z coordinate resulting from the SAR-Positioning for different temporal resolutions (1M, 2M, 3M, 4M and all observations (—)) at **Wladyslawowo**. The number of data takes used in azimuth and range are shown in the columns DT’s A and DT’s R. Epoch refers to the mean date of the period of observation.

Temp Res.	$\sigma_x$ [m]	$\sigma_y$ [m]	$\sigma_z$ [m]	Epoch	DTs A	DTs R
1M	1.47E-02	1.84E-02	1.76E-02	2020.369	10	11
1M	1.74E-02	1.50E-02	1.85E-02	2020.459	13	13
1M	1.15E-02	1.20E-02	1.19E-02	2020.538	20	20
1M	4.20E-03	1.70E-03	4.10E-03	2020.626	20	18
1M	1.30E-03	1.90E-02	1.29E-02	2020.710	18	17
1M	2.32E-02	8.00E-03	2.27E-02	2020.792	18	17
1M	3.00E-04	4.00E-04	3.00E-04	2020.869	16	17
1M	4.69E-02	4.66E-02	4.89E-02	2020.956	10	10
2M	1.69E-02	1.88E-02	1.93E-02	2020.273	11	11
2M	1.82E-02	1.70E-02	1.74E-02	2020.418	21	24
2M	4.40E-03	2.00E-03	4.30E-03	2020.582	39	37
2M	1.66E-02	7.20E-03	1.63E-02	2020.751	36	35
2M	3.00E-04	4.00E-04	3.00E-04	2020.899	22	24
3M	2.70E-03	6.00E-04	1.90E-03	2020.322	21	20
3M	9.00E-04	3.00E-04	9.00E-04	2020.552	52	49
3M	0.00E+00	0.00E+00	0.00E+00	2020.787	51	53
4M	0.00E+00	0.00E+00	0.00E+00	2020.372	34	34
4M	3.60E-03	2.00E-03	3.20E-03	2020.661	78	71
—	8.70E-03	5.20E-03	8.60E-03	2020.637	133	139

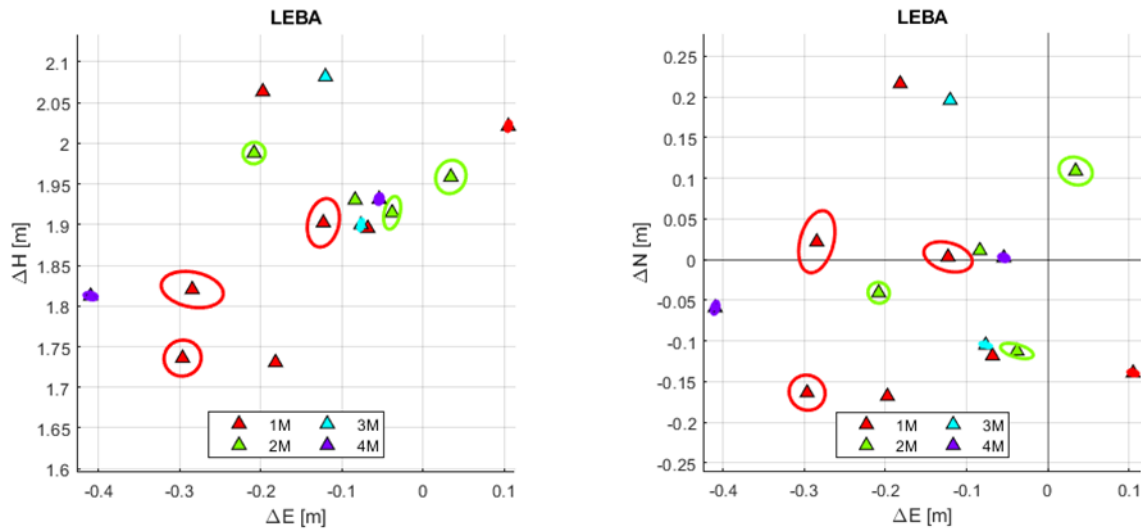
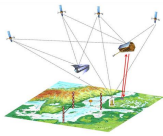


**Figure 8-32:** Error ellipsoids in local East Height (left) and local North East (right) coordinates of the ECR located at **Leba** for the different temporal resolutions: monthly (1M), bi monthly (2M), trimonthly (3M), and every four months (4M) in the year 2020 at their respective reference epochs:

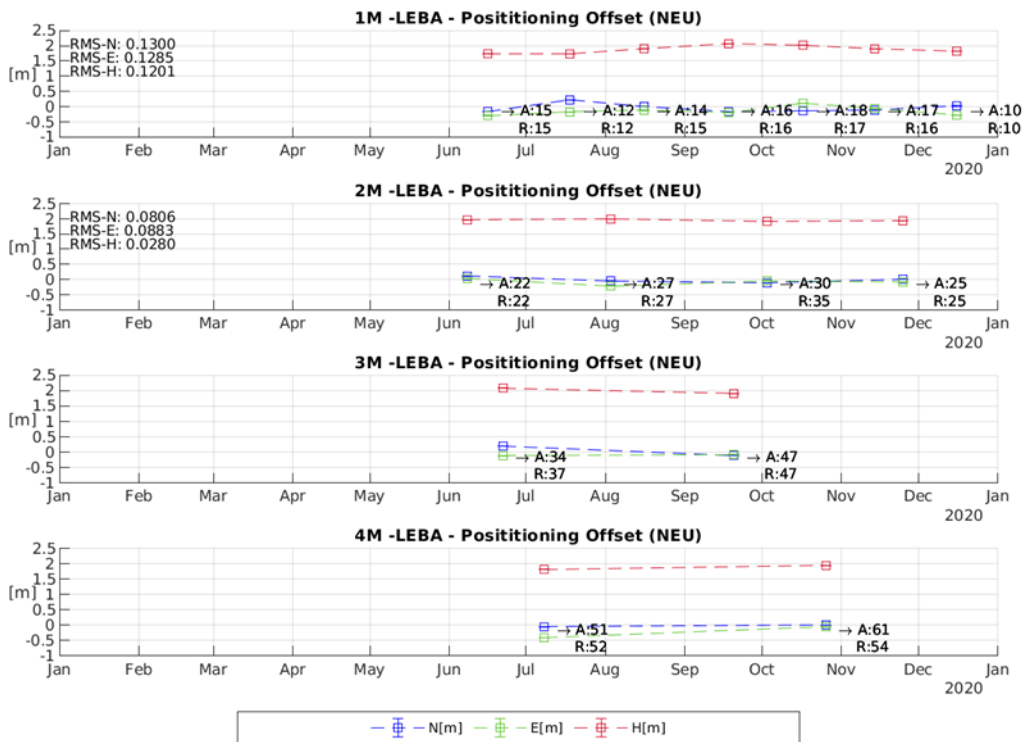


**Figure 8-33:** Positioning Offset of the ECR located at **Leba** for the different temporal resolutions: monthly (1M), bi monthly (2M), trimonthly (3M), and every four months (4M) in the year 2020. The offsets are displayed in local North (blue), East (green), and Height (red) with respect to given reference coordinates from GNSS campaigns at the mean date of the observation period. For 1M and 2M the Root Mean Square (RMS) values are displayed in the top left corner of the respective graph. “A:” and “R:” beneath each solution indicate the number of data takes used in azimuth and range for the particular solution.

**Table 8-12:** Standard deviations for the cartesian x, y, z coordinate resulting from the SAR-Positioning for different temporal resolutions (1M, 2M, 3M,4M and all observations (--)) at **Leba**. The number of data takes used in azimuth and range are shown in the columns DT's A and DT's R. Epoch refers to the mean date of the period of observation.

Temp Res.	$\sigma_x$ [m]	$\sigma_y$ [m]	$\sigma_z$ [m]	Epoch	DTs A	DTs R
1M	6.70E-03	7.50E-03	8.10E-03	2020.456	15	15
1M	0.00E+00	0.00E+00	0.00E+00	2020.544	12	12
1M	5.10E-03	1.03E-02	7.00E-03	2020.623	14	15
1M	0.00E+00	0.00E+00	0.00E+00	2020.713	16	16
1M	1.00E-03	2.20E-03	1.30E-03	2020.792	18	17
1M	3.00E-04	4.00E-04	3.00E-04	2020.869	17	16
1M	1.27E-02	6.40E-03	1.24E-02	2020.956	10	10
2M	5.10E-03	7.20E-03	6.90E-03	2020.434	22	22
2M	4.10E-03	4.60E-03	5.00E-03	2020.587	27	27
2M	1.90E-03	7.30E-03	4.00E-03	2020.754	30	35
2M	3.00E-04	4.00E-04	3.00E-04	2020.899	25	25
3M	6.00E-04	5.00E-04	5.00E-04	2020.473	34	37
3M	7.00E-04	2.60E-03	1.20E-03	2020.719	47	47
4M	2.90E-03	1.40E-03	2.80E-03	2020.516	51	52
4M	1.30E-03	2.30E-03	1.90E-03	2020.817	61	54
--	1.50E-03	4.00E-03	2.80E-03	2020.680	116	109

Sweden (Mårtsbo, Forsmark/Kobben, Spikarna/Vinberget)

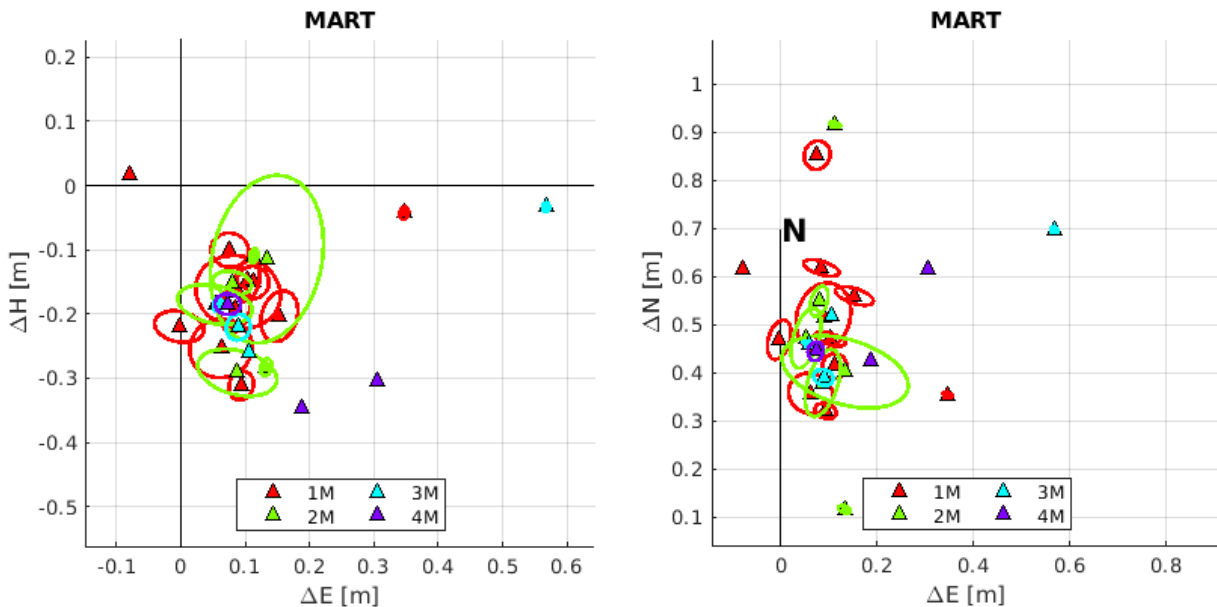


**Figure 8-34:** Error ellipsoids in local East Height (left) and local North East (right) coordinates of the ECR located at **Mårtsbo** for the different temporal resolutions: monthly (1M), bi monthly (2M), trimonthly (3M) ,and every four months (4M) in the year 2020 at their respective reference epochs.

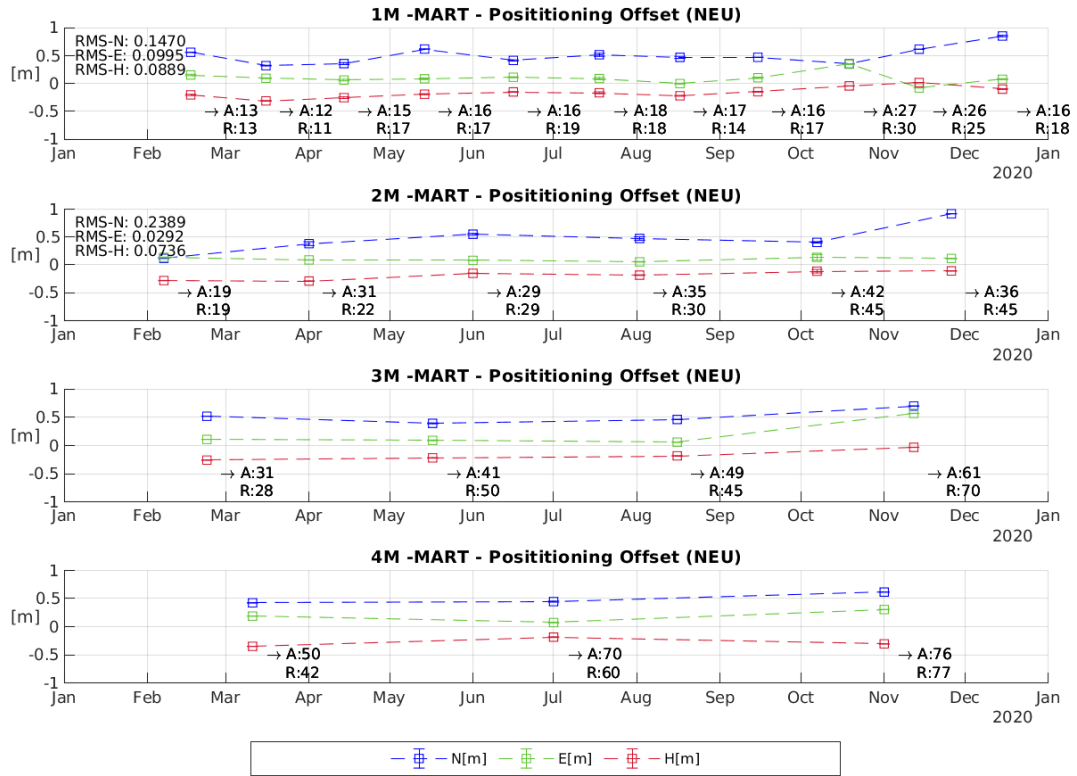
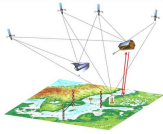


**Figure 8-35:** Positioning Offset of the ECR located at **Mårtsbo** for the different temporal resolutions: monthly (1M), bi monthly (2M), trimonthly (3M), and every four months (4M) in the year 2020. The offsets are displayed in local North (blue), East (green), and Height (red) with respect to given reference coordinates from GNSS campaigns at the mean date of the observation period. For 1M and 2M the Root Mean Square (RMS) values are displayed in the top left corner of the respective graph. “A:” and “R:” beneath each solution indicate the number of data takes used in azimuth and range for the particular solution.

**Table 8-13:** Standard deviations for the cartesian x, y, z coordinate resulting from the SAR-Positioning for different temporal resolutions (1M, 2M, 3M,4M and all observations (--)) at **Mårtsbo**. The number of data takes used in azimuth and range are shown in the columns DT's A and DT's R. Epoch refers to the mean date of the period of observation.

Temp Res.	$\sigma_x$ [m]	$\sigma_y$ [m]	$\sigma_z$ [m]	Epoch	DTs A	DTs R
1M	1.00E-03	1.37E-02	1.07E-02	2020.128	13	13
1M	4.20E-03	7.60E-03	6.80E-03	2020.205	12	11
1M	1.30E-02	1.55E-02	1.71E-02	2020.284	15	17
1M	2.50E-03	1.30E-02	8.60E-03	2020.366	16	17
1M	8.80E-03	8.40E-03	8.30E-03	2020.456	16	19
1M	2.53E-02	1.86E-02	2.15E-02	2020.544	18	18
1M	1.47E-02	7.40E-03	1.25E-02	2020.626	17	14
1M	2.10E-03	1.11E-02	7.30E-03	2020.705	16	17
1M	1.50E-03	3.60E-03	2.50E-03	2020.798	27	30
1M	0.00E+00	0.00E+00	0.00E+00	2020.869	26	25
1M	1.03E-02	8.90E-03	9.70E-03	2020.954	16	18
2M	2.00E-03	4.60E-03	3.20E-03	2020.101	19	19
2M	2.64E-02	1.05E-02	1.98E-02	2020.249	31	22
2M	1.17E-02	5.70E-03	1.00E-02	2020.415	29	29
2M	2.31E-02	8.80E-03	1.95E-02	2020.585	35	30
2M	2.02E-02	4.75E-02	3.26E-02	2020.765	42	45
2M	7.00E-04	4.00E-03	2.60E-03	2020.902	36	45
3M	1.00E-04	2.00E-04	2.00E-04	2020.145	31	28
3M	5.40E-03	7.20E-03	6.80E-03	2020.374	41	50
3M	7.00E-04	4.00E-03	2.60E-03	2020.623	49	45
3M	1.20E-03	2.70E-03	1.90E-03	2020.863	61	70
4M	0.00E+00	1.00E-04	1.00E-04	2020.191	50	42
4M	6.70E-03	5.60E-03	7.20E-03	2020.497	70	60
4M	4.00E-04	9.00E-04	6.00E-04	2020.833	76	77
--	5.00E-04	1.20E-03	8.00E-04	2020.577	206	194

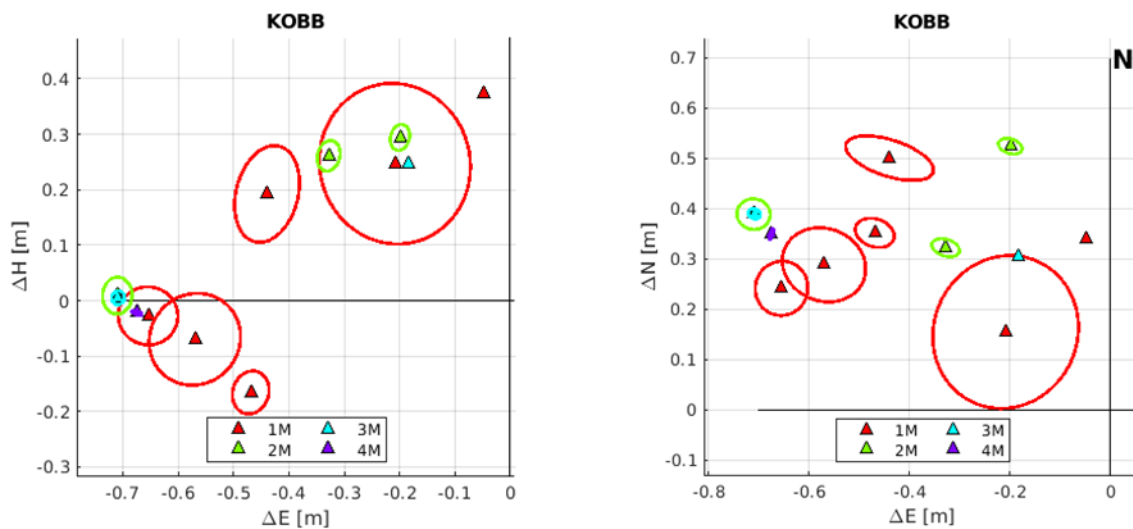


**Figure 8-36:** Error ellipsoids (no Bias Corrections applied) in local East Height (left) and local North East (right) coordinates of the ECR located at **Forsmark/Kobben** for the different temporal resolutions: monthly (1M), bi monthly (2M), trimonthly (3M), and every four months (4M) in the year 2020 at their respective reference epochs.

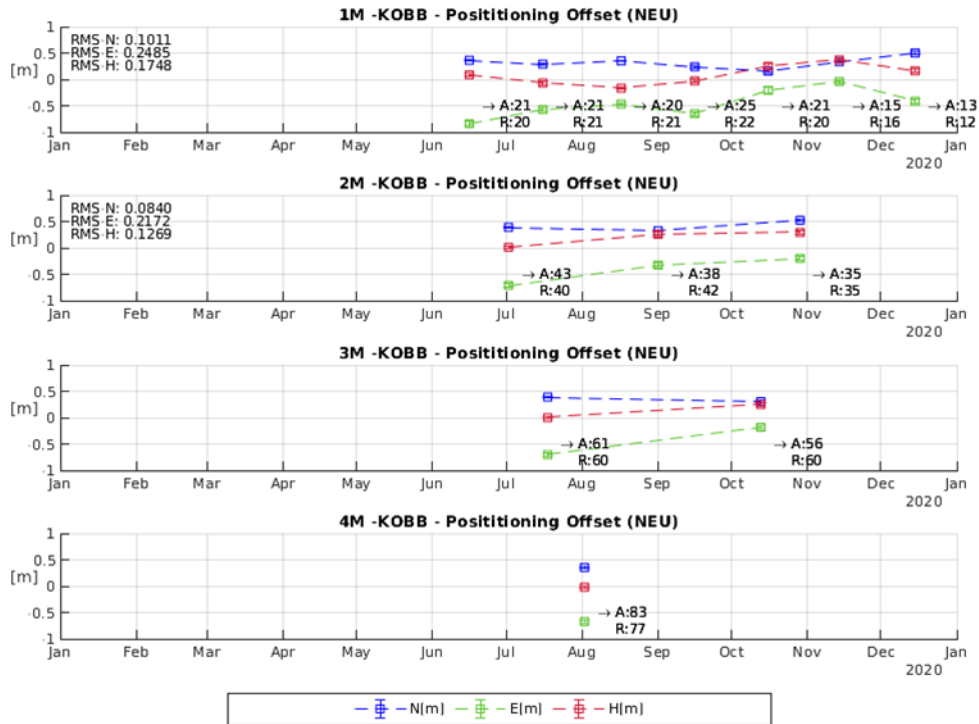
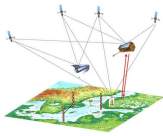


**Figure 8-37:** Positioning Offset (no Bias Corrections applied) of the ECR located at **Forsmark/Kobben** for the different temporal resolutions: monthly (1M), bi monthly (2M), trimonthly (3M), and every four months (4M) in the year 2020. The offsets are displayed in local North (blue), East (green), and Height (red) with respect to given reference coordinates from GNSS campaigns at the mean date of the observation period. For 1M and 2M the Root Mean Square (RMS) values are displayed in the top left corner of the respective graph. “A:” and “R:” beneath each solution indicate the number of data takes used in azimuth and range for the particular solution.

**Table 8-14:** Standard deviations (no Bias Corrections applied) for the cartesian x, y, z coordinate resulting from the SAR-Positioning for different temporal resolutions (1M, 2M, 3M, 4M and all observations (--) at **Forsmark/Kobben**. The number of data takes used in azimuth and range are shown in the columns DT's A and DT's R. Epoch refers to the mean date of the period of observation.

Temp Res.	$\sigma_x$ [m]	$\sigma_y$ [m]	$\sigma_z$ [m]	Epoch	DTs A	DTs R
1M	0.032000	0.033700	0.021800	2020.456	21	20
1M	0.023000	0.028900	0.029600	2020.538	21	21
1M	0.012000	0.020500	0.016800	2020.626	20	21
1M	0.028500	0.031100	0.029900	2020.708	25	22
1M	0.054900	0.049000	0.043900	2020.790	21	20
1M	0.016700	0.030500	0.023400	2020.869	15	16
1M	0.030700	0.041200	0.035000	2020.954	13	12
2M	0.028900	0.029800	0.018200	2020.500	43	40
2M	0.021300	0.051300	0.041000	2020.667	38	42
2M	0.031800	0.030000	0.026700	2020.825	35	35
3M	0.025200	0.026200	0.016200	2020.544	61	60
3M	0.033900	0.029000	0.028800	2020.781	56	60
4M	0.024100	0.025700	0.019000	2020.585	83	77
--	0.020800	0.035200	0.030000	2020.686	142	130

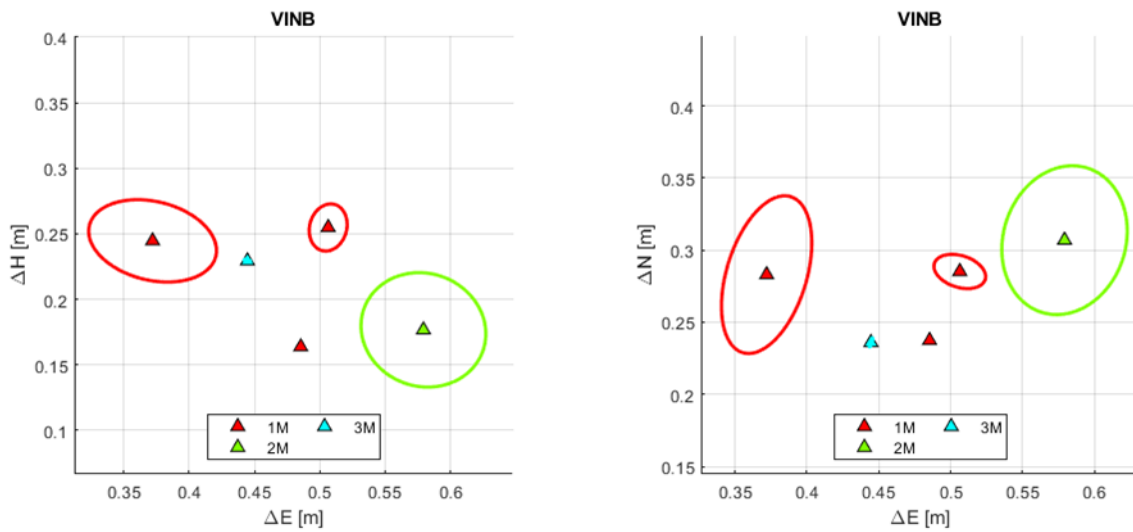


**Figure 8-38:** Error ellipsoids in local East Height (left) and local North East (right) coordinates of the ECR located at **Spikarna/Vinberget** for the different temporal resolutions: monthly (1M), bi monthly (2M), trimonthly (3M), and every four months (4M) in the year 2020 at their respective reference epochs.

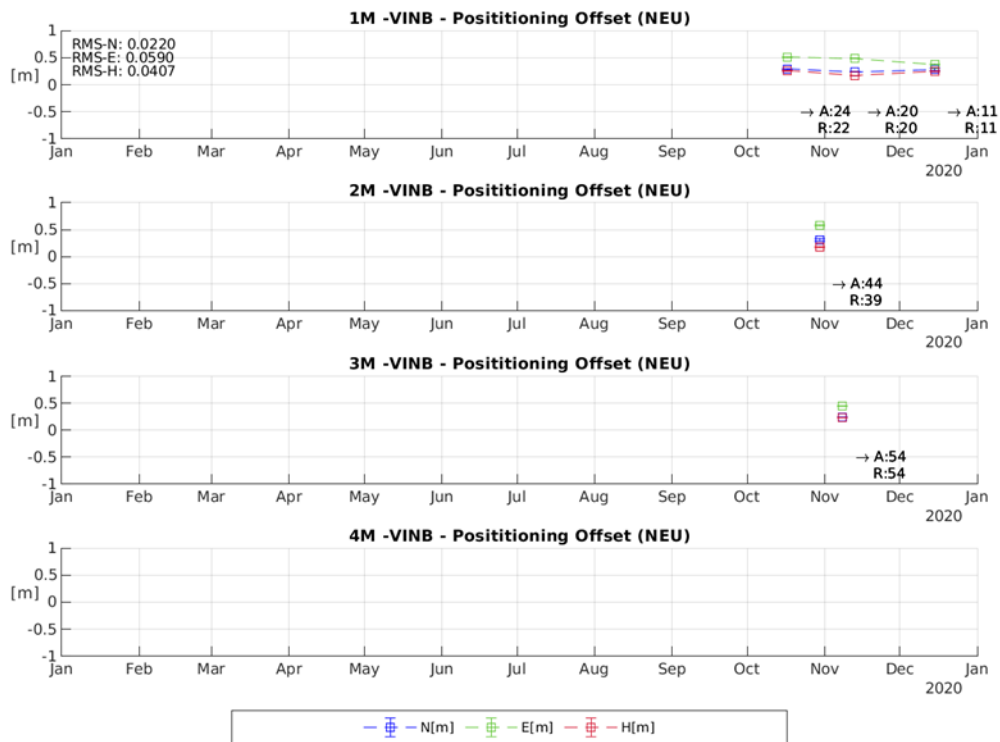
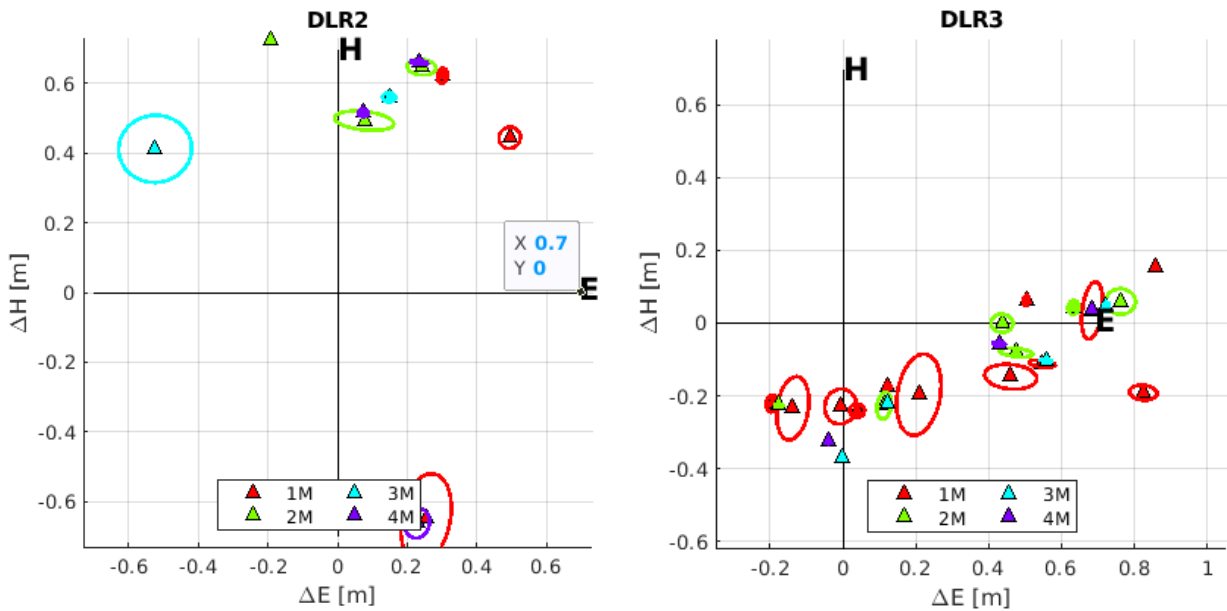


**Figure 8-39:** Positioning Offset of the ECR located at **Spikarna/Vinberget** for the different temporal resolutions: monthly (1M), bi monthly (2M), trimonthly (3M), and every four months (4M) in the year 2020. The offsets are displayed in local North (blue), East (green), and Height (red) with respect to given reference coordinates from GNSS campaigns at the mean date of the observation period. For 1M and 2M the Root Mean Square (RMS) values are displayed in the top left corner of the respective graph. "A:" and "R:" beneath each solution indicate the number of data takes used in azimuth and range for the particular solution.

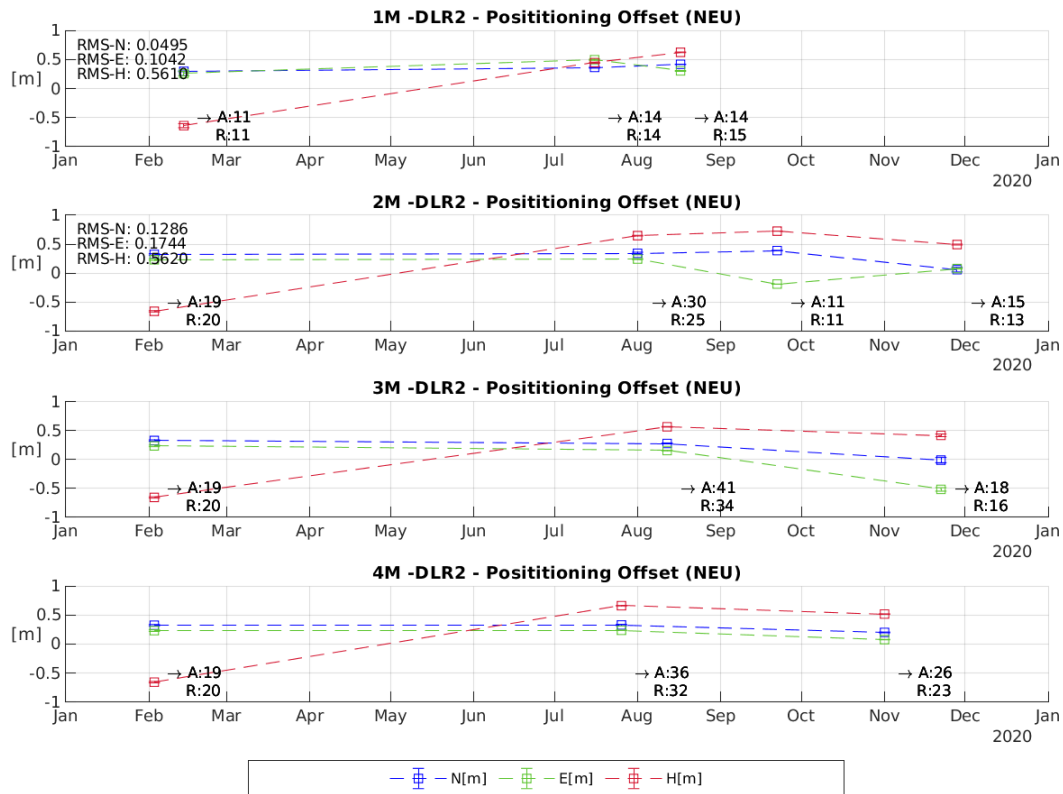
**Table 8-15:** Standard deviations for the cartesian x, y, z coordinate resulting from the SAR-Positioning for different temporal resolutions (1M, 2M, 3M,4M and all observations (--)) at **Spikarna/Vinberget**. The number of data takes used in azimuth and range are shown in the columns DT's A and DT's R. Epoch refers to the mean date of the period of observation.

Temp Res.	$\sigma_x$ [m]	$\sigma_y$ [m]	$\sigma_z$ [m]	Epoch	DTs A	DTs R
1M	3.30E-03	6.40E-03	5.30E-03	2020.792	24	22
1M	0.00E+00	0.00E+00	0.00E+00	2020.866	20	20
1M	1.92E-02	8.90E-03	1.52E-02	2020.954	11	11
2M	1.89E-02	1.49E-02	1.62E-02	2020.828	44	39
3M	1.20E-03	3.00E-04	8.00E-04	2020.852	54	54
--	1.10E-03	2.00E-04	7.00E-04	2020.852	54	54

Germany (DLR2, DLR3)



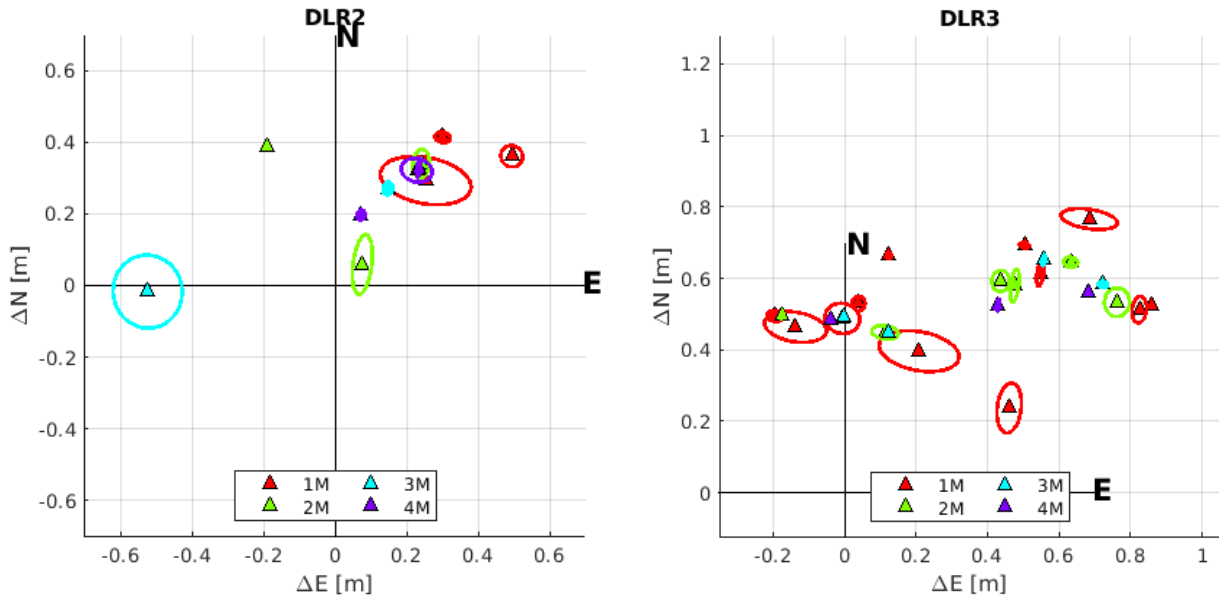
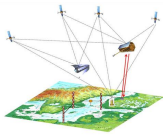
**Figure 8-40:** Error ellipsoids in local East Height (left) and local North East (right) coordinates of the ECR located at **DLR2** for the different temporal resolutions: monthly (1M), bi monthly (2M), trimonthly (3M) ,and every four months (4M) in the year 2020 at their respective reference epochs.



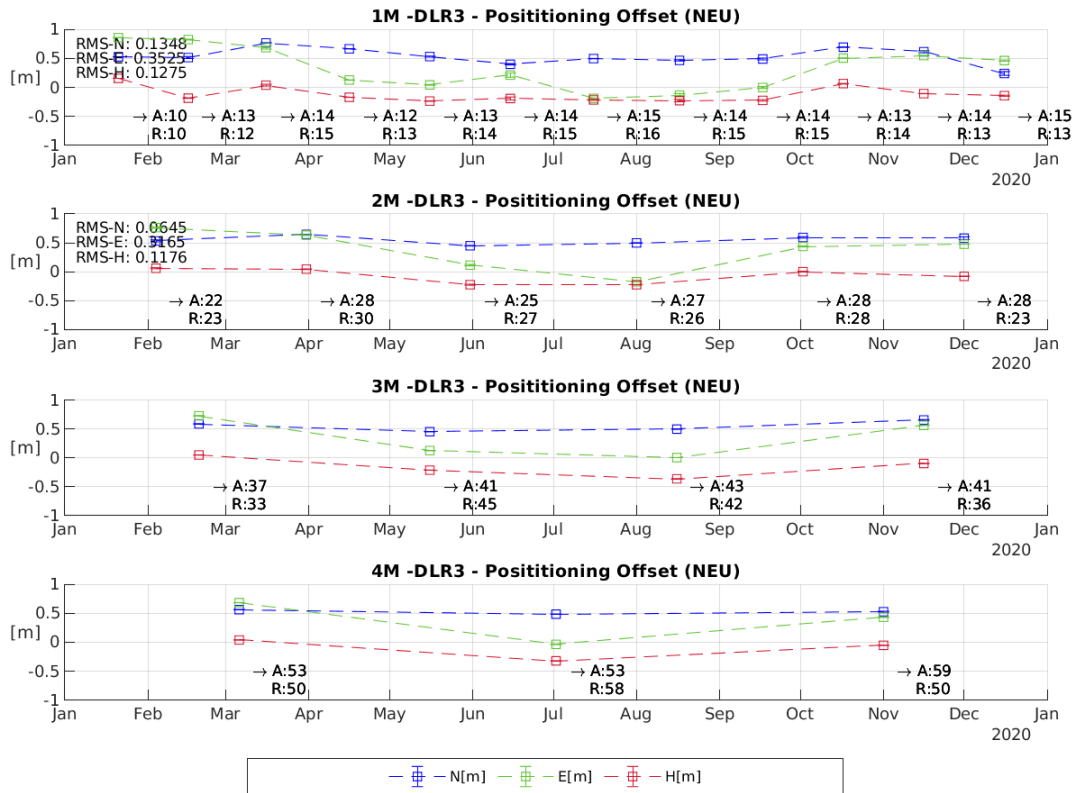
**Figure 8-41:** Positioning Offset of the ECR located at **DLR2** for the different temporal resolutions: monthly (1M), bi monthly (2M), trimonthly (3M), and every four months (4M) in the year 2020. The offsets are displayed in local North (blue), East (green), and Height (red) with respect to given reference coordinates from GNSS campaigns at the mean date of the observation period. For 1M and 2M the Root Mean Square (RMS) values are displayed in the top left corner of the respective graph. “A:” and “R:” beneath each solution indicate the number of data takes used in azimuth and range for the particular solution.

**Table 8-16:** Standard deviations for the cartesian x, y, z coordinate resulting from the SAR-Positioning for different temporal resolutions (1M, 2M, 3M, 4M and all observations (--)) at **DLR2**. The number of data takes used in azimuth and range are shown in the columns DT’s A and DT’s R. Epoch refers to the mean date of the period of observation.

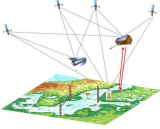
Temp Res.	$\sigma_x$ [m]	$\sigma_y$ [m]	$\sigma_z$ [m]	Epoch	DTs A	DTs R
1M	9.80E-03	4.22E-02	2.99E-02	2020.120	11	11
1M	8.40E-03	1.03E-02	1.14E-02	2020.538	14	14
1M	5.00E-03	7.20E-03	4.50E-03	2020.626	14	15
2M	8.90E-03	1.49E-02	1.37E-02	2020.090	19	20
2M	1.30E-02	7.70E-03	1.54E-02	2020.582	30	25
2M	0.00E+00	0.00E+00	0.00E+00	2020.724	11	11
2M	2.59E-02	8.00E-03	3.06E-02	2020.907	15	13
3M	8.90E-03	1.49E-02	1.37E-02	2020.090	19	20
3M	6.00E-03	4.60E-03	6.70E-03	2020.612	41	34
3M	3.05E-02	3.28E-02	3.92E-02	2020.891	18	16
4M	8.90E-03	1.49E-02	1.37E-02	2020.090	19	20
4M	7.60E-03	1.60E-03	9.20E-03	2020.566	36	32
4M	4.40E-03	3.60E-03	5.20E-03	2020.833	26	23
--	1.30E-02	1.18E-02	1.70E-02	2020.538	83	71



**Figure 8-42:** Error ellipsoids in local East Height (left) and local North East (right) coordinates of the ECR located at **DLR3** for the different temporal resolutions: monthly (1M), bi monthly (2M), trimonthly (3M) ,and every four months (4M) in the year 2020 at their respective reference epochs.



**Figure 8-43:** Positioning Offset of the ECR located at **DLR3** for the different temporal resolutions: monthly (1M), bi monthly (2M), trimonthly (3M), and every four months (4M) in the year 2020. The offsets are displayed in local North (blue), East (green), and Height (red) with respect to given reference coordinates from GNSS campaigns at the mean date of the observation period. For 1M and 2M the Root Mean Square (RMS) values are displayed in the top left corner of the respective graph. "A:" and "R:" beneath each solution indicate the number of data takes used in azimuth and range for the particular solution.

	<b>BALTIC+ Theme 5</b>  Geodetic SAR for Baltic Height System Unification and Baltic Sea Level Research	<b>Final Report</b> Doc. Nr: SAR-HSU-SR-0022 Issue: 1.1 Date: 07.07.2021 Page: 127 of 170
---	--	---

**Table 8-17:** Standard deviations for the cartesian x, y, z coordinate resulting from the SAR-Positioning for different temporal resolutions (1M, 2M, 3M,4M and all observations (--) at **DLR3**. The number of data takes used in azimuth and range are shown in the columns DT's A and DT's R. Epoch refers to the mean date of the period of observation.

Temp Res.	$\sigma_x$ [m]	$\sigma_y$ [m]	$\sigma_z$ [m]	Epoch	DTs A	DTs R
1M	0.00E+00	0.00E+00	0.00E+00	2020.055	10	10
1M	1.13E-02	6.50E-03	1.35E-02	2020.126	13	12
1M	8.80E-03	2.67E-02	9.20E-03	2020.205	14	15
1M	2.70E-03	2.60E-03	2.70E-03	2020.290	12	13
1M	6.00E-03	6.10E-03	7.40E-03	2020.372	13	14
1M	9.60E-03	3.79E-02	2.52E-02	2020.454	14	15
1M	4.90E-03	7.80E-03	5.20E-03	2020.538	15	16
1M	1.15E-02	2.94E-02	1.62E-02	2020.626	14	15
1M	1.27E-02	1.63E-02	1.56E-02	2020.710	14	15
1M	2.30E-03	4.80E-03	2.60E-03	2020.792	13	14
1M	1.10E-02	2.60E-03	1.28E-02	2020.874	14	13
1M	2.13E-02	1.09E-02	2.60E-02	2020.956	15	13
2M	1.25E-02	1.20E-02	1.51E-02	2020.093	22	23
2M	5.20E-03	6.90E-03	4.90E-03	2020.246	28	30
2M	6.00E-03	1.29E-02	7.10E-03	2020.413	25	27
2M	3.20E-03	1.10E-03	3.90E-03	2020.582	27	26
2M	9.80E-03	8.60E-03	1.08E-02	2020.751	28	28
2M	1.47E-02	3.30E-03	1.73E-02	2020.915	28	23
3M	2.40E-03	4.80E-03	3.50E-03	2020.137	37	33
3M	3.00E-04	1.00E-04	3.00E-04	2020.372	41	45
3M	1.10E-03	4.00E-04	1.20E-03	2020.623	43	42
3M	4.80E-03	1.00E-03	5.70E-03	2020.874	41	36
4M	7.00E-04	9.00E-04	8.00E-04	2020.178	53	50
4M	2.10E-03	1.90E-03	1.60E-03	2020.500	53	58
4M	5.40E-03	1.10E-03	6.60E-03	2020.833	59	50
--	8.30E-03	9.90E-03	1.05E-02	2020.514	174	172

### 8.2.3 Conclusions from SAR Positioning Results

From the positioning results for all ECR stations by processing all available SAR observations from year 2020 some conclusions can be drawn. These conclusions need to be considered for any future data analyses of this kind.

First of all, the ECR's seem to perform not equally, meaning that for example electronic delays could differ significantly for each ECR. For the SAR positioning in this project, it was assumed that the delay is determined from the average coordinate differences for a few reference stations and then applied to all ECR's during processing (see section 7.1.2). Positioning result show that, as long as there is an uncertainty about a common electronic behaviour of the ECRs, each ECR shall be calibrated at a reference station, before it is installed at a designated observation point. In case ECRs perform similar with this respect, then a representative electronic delay from a few ECRs at reference stations can be computed. Varying electronic delays per ECR strongly influence the absolute coordinate accuracy rather than the internal estimate of the position accuracy.

When looking at systematic effects, one always has to keep in mind to take care of the different viewing geometries due to different incidence angles. To use both ascending and descending orbit observations the phase centre correction has to be applied, as the phase centre differs by several decimetres in the positioning depending on the incidence angle.

Currently outlier detection is split in two steps i.e., gross outliers (half pixel resolution of Sentinel-1) and outliers (3-sigma criteria per incidence angle) are treated separately. Additionally, observations are flagged, where precise orbit information seems to be insufficient accurate. Optionally, also single data points can also be flagged manually, if required. Outlier detection is critical to the positioning performance and need to be done very carefully.

Monthly observations is the shortest time interval of observations in order to reach realistic positing results. Most ECR stations only gather 10 valid range and 10 valid azimuth observations over a period of one month, which is the minimum for a stable performance of the positioning processor. The higher the latitude the more observations within a month are possible. This needs to be considered for possible applications of the SAR positioning technique. Table 8-18 shows RMS of the positioning results for all stations and their 1M and 2M positioning solutions. DLR2 is excluded, because its performance changed significantly after each repair. One can see that when looking at the height component that the RMS behaves different for every station and varies between 0.035 meter and 0.174 meter for the 1 M solutions with a

mean of 0.11 meter. For the 2M solution the RMS improves in the mean to 0.09 meter. This shows that with increased number of observation the positioning becomes more stable for most stations. A longer period of observation, would allow a comparison with 3M and 4M solutions and might be helpful for further analysis. But after all, monthly and bimonthly solutions still vary on a decimetre level with respect to each other.

**Table 8-18:** This table shows the root mean square (rms) values of the one-monthly (1M) and bi-monthly (2M) solutions of each station. Loviisa and Kobben, where computed without bias correction, due to computational issues for single observation intervals. DLR2 is excluded in the table as its performance significantly changed after each repair of the transponder.

Station	1M RMS			2 RMS		
	dN [m]	dE [m]	dH [m]	dN [m]	dE [m]	dH [m]
LOKS	0.1617	0.2267	0.1724	0.0605	0.1702	0.1832
VERG	0.1544	0.0817	0.0911	0.0667	0.1032	0.0920
EMAE	0.1570	0.1794	0.1242	0.1373	0.1787	0.1143
LOVI	0.1689	0.0647	0.1139	0.0999	0.1328	0.0620
RAUM	0.0797	0.0580	0.0359	0.0904	0.0394	0.0497
WLAD	0.2069	0.1272	0.1309	0.1482	0.2070	0.0725
LEBA	0.1300	0.1285	0.1201	0.0806	0.0883	0.0280
MART	0.1470	0.0995	0.0889	0.2389	0.0292	0.0736
KOBB	0.1011	0.2485	0.1748	0.0840	0.2172	0.1269
VINB	0.0220	0.0549	0.0407	-	-	-
DLR3	0.1348	0.3525	0.1275	0.0645	0.3165	0.1176
<b>Mean:</b>	0.1330	0.1474	0.1109	0.1071	0.1483	0.0920
<b>Min:</b>	0.0220	0.0549	0.0359	0.0605	0.0292	0.0280
<b>Max:</b>	0.2069	0.3525	0.1748	0.2389	0.3165	0.1832
<b>Median:</b>	0.1470	0.1272	0.1201	0.0872	0.1515	0.0828
					No Bias Correction	

After repair of an ECR, one has to evaluate, if a station can be regarded as the same station or if its performance changed significantly and it has to be treated as a “new” independent station.

There are observation periods for which the processor does not converge for a positioning result even with sufficient number of data takes. Therefore, the positioning is terminated providing unreliable results. The bias correction in general helps to reach convergence for the position solution, but for a few stations (LOVI and KOBB) and only single observation intervals the bias correction even deteriorates the achieved solution. Therefore for these two stations solutions without the bias correction were computed (see Table 8-18).

As a promising result of this study it can be stated that positioning exhibits high internal accuracies. The internal accuracies for the solutions using all stations vary between few centimetres down to millimetres in the local North, East, Height reference frame. This implies, that having a continuous observation period with good data coverage, relative coordinate variations can be observed on bi-monthly (monthly, under optimal conditions) time intervals with a few centimetres accuracy. For absolute positions a well calibrated and long term stable instrument is needed, which is not the case for the ECRs used during the study.

### 8.3 GNSS Positioning

Twelve GNSS stations near ECR-C and/or Tide-Gauge stations were involved in the Baltic+ project. Data processing was performed in accordance with the presented assumptions, which are described in detail in chapter 6.3 and 7.3. The processing of daily observations was performed as daily network solutions in the Bernese GNSS Software ver. 5.2 in the double-difference mode (DD method). As the reference frame the ITRF2014 was used, in which all IGS global products are available for the calculations: precise orbits, the Earth's rotation parameters and the corrections of GNSS satellite clocks. The study covered the entire period of 2020. The daily network solutions are related to the middle of the development period of each daily session. Based on these solutions, time series of X, Y, Z Cartesian coordinates covering the entire year 2020 were generated. From these series, for the purposes of the project, time series of B, L, h geodetic coordinates were then created, related to the GRS-80 geocentric ellipsoid. The graphs below present the B, L, h time series for the designated GNSS stations.

#### 8.3.1 Time series of GNSS stations coordinates

Figure 8-44 to Figure 8-55 show the resulting coordinate time series for the GNSS stations specified in Table 7-10.

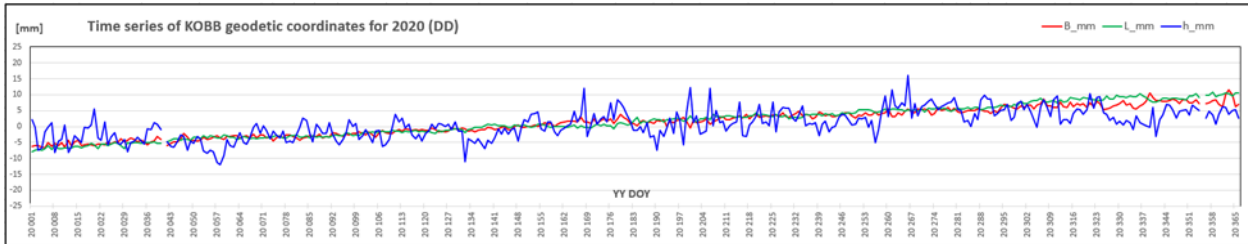
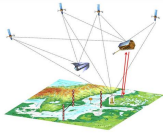


Figure 8-44: Time series of KOBB GNSS station, Sweden for 2020 (DD)

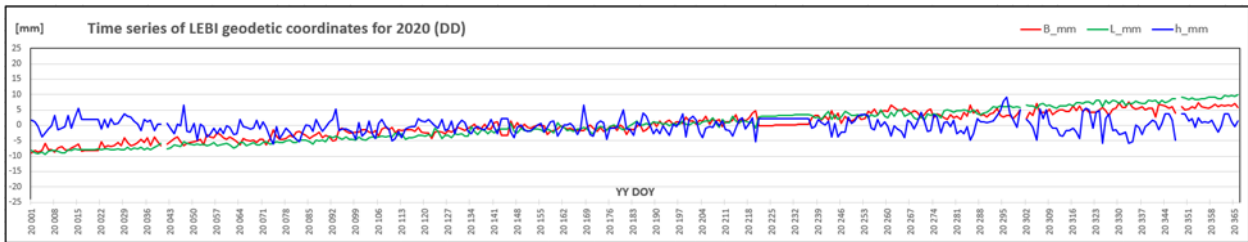


Figure 8-45: Time series of LEBI GNSS station, Poland for 2020 (DD)

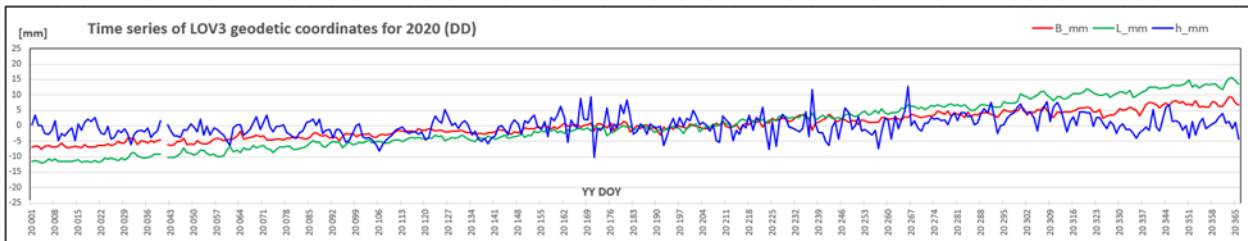


Figure 8-46: Time series of LOV3 GNSS station, Finland for 2020 (DD)

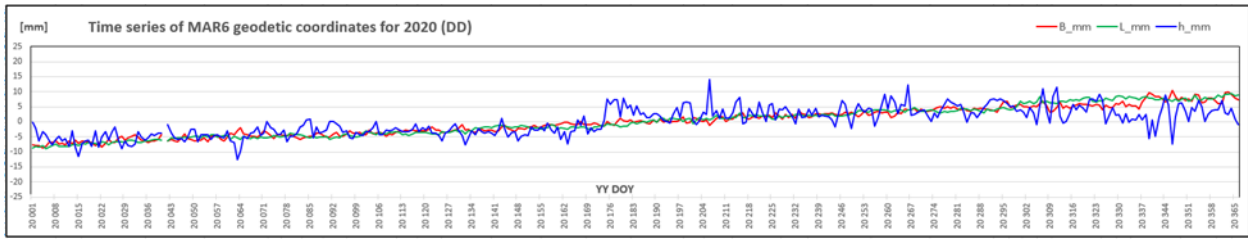


Figure 8-47: Time series of MAR6 GNSS station, Sweden for 2020 (DD)

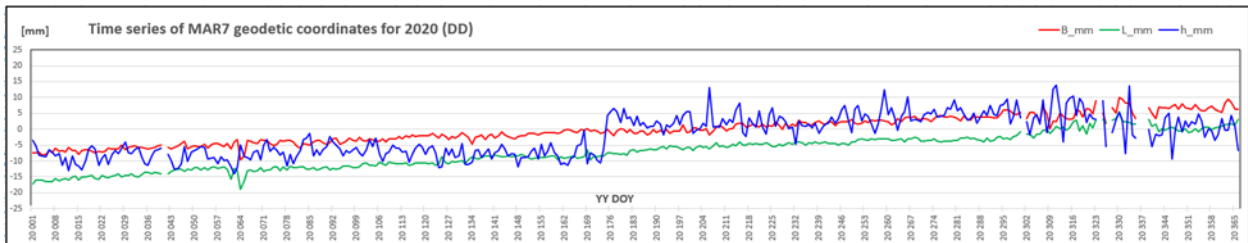


Figure 8-48: Time series of MAR7 GNSS station, Sweden for 2020 (DD)

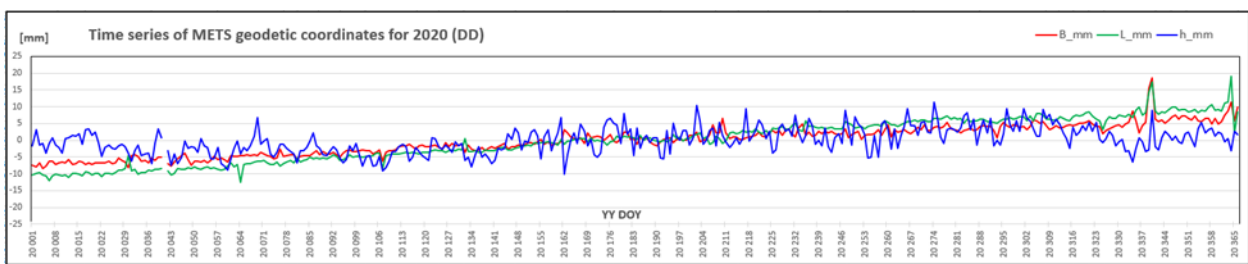


Figure 8-49: Time series of METS GNSS station, Finland for 2020 (DD)

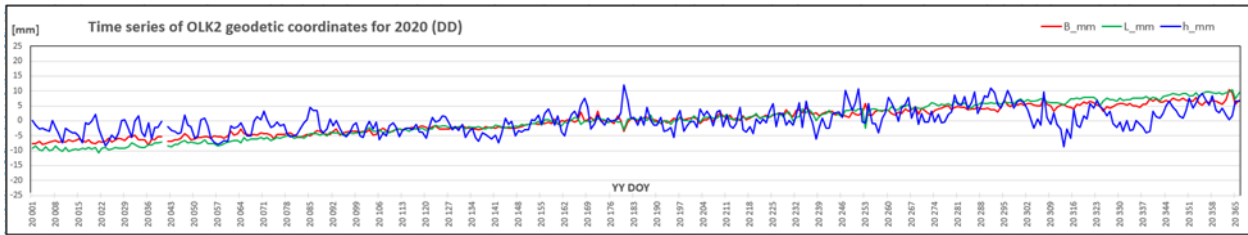
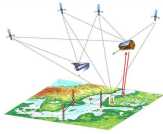


Figure 8-50: Time series of OLK2 GNSS station, Finland for 2020 (DD)

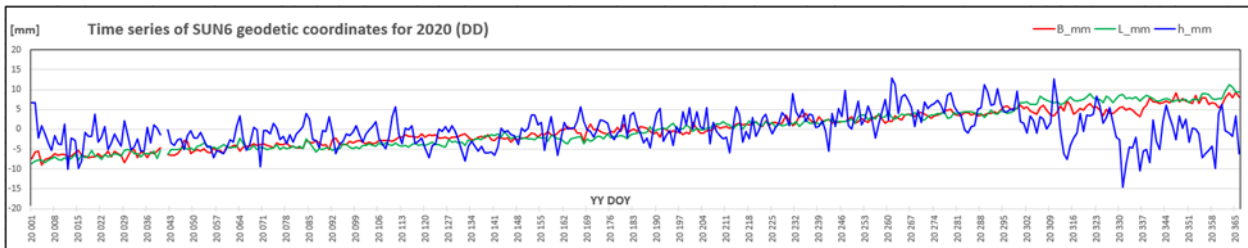


Figure 8-51: Time series of SUN6 GNSS station, Sweden for 2020 (DD)

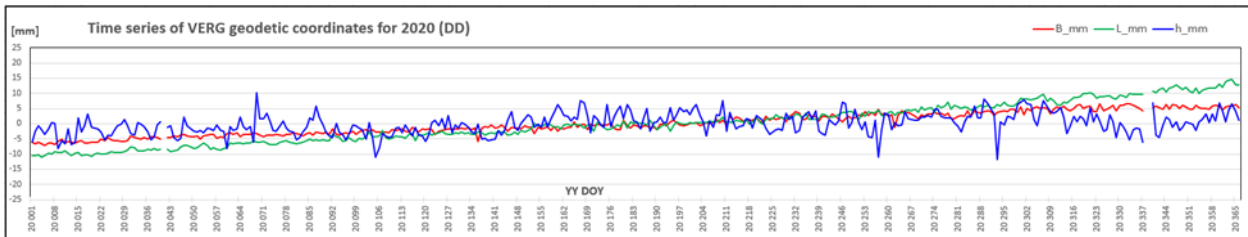


Figure 8-52: Time series of VERG GNSS station, Estonia for 2020 (DD)

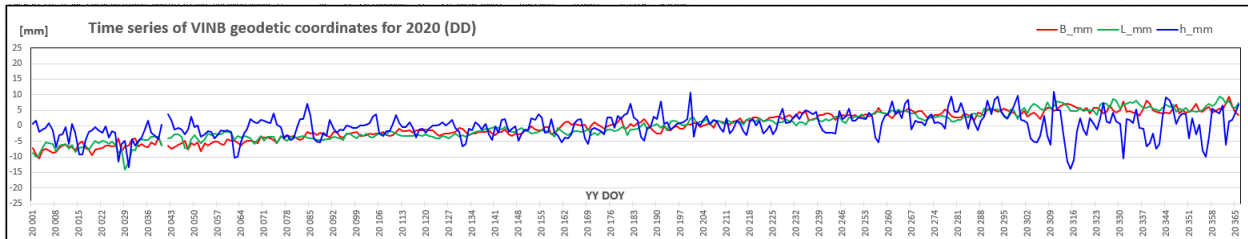


Figure 8-53: Time series of VINB GNSS station, Sweden for 2020 (DD)

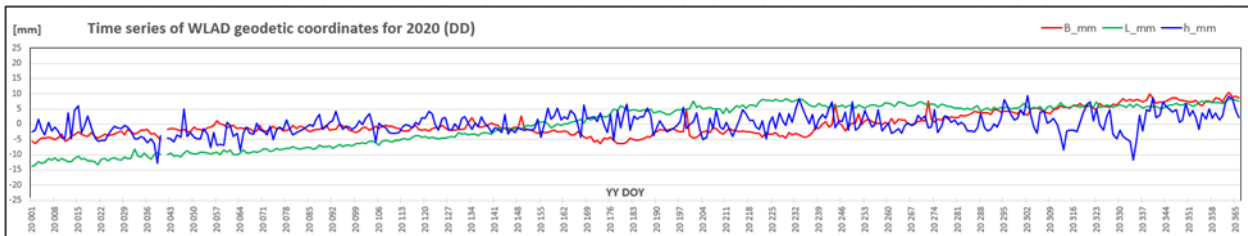
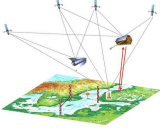


Figure 8-54: Time series of WLAD GNSS station, Poland for 2020 (DD)



Figure 8-55: Time series of OBE4 GNSS station, Germany for 2020 (DD)

	<b>BALTIC+ Theme 5</b> Geodetic SAR for Baltic Height System Unification and Baltic Sea Level Research	<b>Final Report</b> Doc. Nr: SAR-HSU-SR-0022 Issue: 1.1 Date: 07.07.2021 Page: 131 of 170
---	--	---

The above graphs clearly show horizontal displacements of stations caused by the movement of continental tectonic plates and trends in vertical movements at stations located in the Gulf of Bothnia. Due to the fact that the period of data processing is too short (covering only one full year), it is not possible to accurately determine the values of linear trends, and periodic terms (annual, semi-annual) from the prepared time series of station coordinates. For this purpose, the best way seems to be to use the values from the kinematic model that sufficiently well describes the dominant movements in the studied region, common to the reduction of data from all observational techniques used in the project.

### 8.3.2 Coordinate Solutions (Double Differences)

The final coordinate solutions for all stations are summarized in Table 8-19 in terms of 3D Cartesian Coordinates in ITRF2014 for epoch 2020.50 and in Table 8-20 in terms of geodetic coordinates referred to the GRS-80 ellipsoid.

**Table 8-19:** GNSS stations Cartesian coordinates X, Y, Z in ITRF2014 ep. 2020.50 (from period 2020-01-01 to 2020-12-31), solution from DD method)

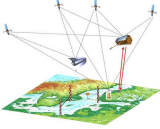
GNSS Station	X [m]	RMS_X [m]	Y [m]	RMS_Y [m]	Z [m]	RMS_Z [m]
KOBB	2999027.7298	0.00021	987782.3846	0.00021	5523181.1153	0.00029
LEBI	3517620.3301	0.00024	1111450.7279	0.00022	5185644.5355	0.00016
LOV3	2828365.3809	0.00029	1396873.0632	0.00024	5524911.1908	0.00021
MAR6	2998189.2025	0.00021	931451.9993	0.00022	5533398.8890	0.00030
MAR7	2998198.2440	0.00032	931450.1204	0.00034	5533393.0470	0.00040
METS	2892570.5193	0.00028	1311843.6629	0.00025	5512634.2765	0.00025
OBE4	4186704.2723	0.00041	834903.7135	0.00032	4723664.8948	0.00051
OLK2	2866981.0690	0.00025	1129669.0080	0.00023	5565665.8738	0.00027
SUN6	2838910.7948	0.00025	903817.4135	0.00020	5620661.3520	0.00025
VERG	2905540.9537	0.00028	1423460.0474	0.00025	5478170.7432	0.00021
VINB	2829293.3126	0.00024	888151.5179	0.00018	5628086.9713	0.00023
WLAD	3496344.4823	0.00022	1164350.4435	0.00034	5188401.9976	0.00021

**Table 8-20:** GNSS stations geodetic coordinates (Latitude, Longitude and height) in ITRF2014 ep. 2020.50 (from period 2020-01-01 to 2020-12-31) referred to GRS-80 ellipsoid. Solution from DD method

GNSS Station	Latitude	Longitude	Height [m]
KOBB	60 24' 34.7071241"	18 13' 48.7385491"	29.0345
LEBI	54 45' 13.5924082"	17 32' 05.2766327"	37.8856
LOV3	60 26' 26.7772467"	26 17' 01.8398188"	49.8794
MAR6	60 35' 42.5249405"	17 15' 30.7135007"	75.5578
MAR7	60 35' 42.2049598"	17 15' 30.4194686"	74.4363
METS	60 13' 02.9063735"	24 23' 43.1731888"	94.6596
OBE4	48 05' 05.3021161"	11 16' 40.2923939"	650.4974
OLK2	61 11' 27.6950545"	21 30' 20.8716050"	39.4473
SUN6	62 13' 56.9355602"	17 39' 35.2557055"	32.5199
VERG	59 36' 05.3630848"	26 06' 02.8751830"	30.0692
VINB	62 22' 25.7385998"	17 25' 39.8752536"	150.2055
WLAD	54 47' 48.3411213"	18 25' 07.5270042"	34.7580

### 8.3.3 Coordinate Solutions (Precise Point Positioning)

For the purpose of comparing the results calculated by the DD method and for the verification and interpretation of the effects in the height component observed at several GNSS stations, an additional study was made using the Precise Point Positioning (PPP) method. This method is slightly less accurate than the DD method, but at the same time it is free from the influence of the selection of the reference station network on the coordinates of the determined stations. The results in Cartesian and ellipsoidal coordinates are summarized in Table 8-21.

	<b>BALTIC+ Theme 5</b>  Geodetic SAR for Baltic Height System Unification and Baltic Sea Level Research	<b>Final Report</b> Doc. Nr: SAR-HSU-SR-0022 Issue: 1.1 Date: 07.07.2021 Page: 132 of 170
---	--	---

**Table 8-21:** GNSS stations Cartesian coordinates X, Y, Z and geodetic B, L, h (GRS-80 ellipsoid) in ITRF2014 ep. 2020.50 (from period 2020-01-01 to 2020-12-31), solution from PPP (GPS+GLONAS) method.

STAT	X [m]	RMS_X	Y [m]	RMS_Y	Z [m]	RMS_Z	Latitude	Longitude	height
KOBB	2999027.7306	0.0018	987782.3851	0.0011	5523181.1170	0.0031	60 24' 34.7071688"	18 25' 48.7386750"	29.0372
LEBI	3517620.3306	0.0022	1111450.7284	0.0012	5185644.5363	0.0031	54 45' 13.5924119"	17 32' 05.2766485"	37.8865
LOV3	2828365.3812	0.0018	1396873.0647	0.0012	5524911.1922	0.0031	60 26' 26.7772441"	26 17' 01.8398950"	49.8810
MAR6	2998189.2026	0.0019	931452.0001	0.0011	5533398.8892	0.0033	60 35' 42.5249338"	17 15' 30.7135526"	75.5582
MAR7	2998198.2443	0.0019	931450.1222	0.0011	5533393.0507	0.0033	60 35' 42.2049647"	17 15' 30.4194928"	74.4376
METS	2892570.5197	0.0022	1311843.6635	0.0014	5512634.2777	0.0041	60 13' 02.9063752"	24 23' 43.1732121"	94.6609
OBE4	4186704.2707	0.0033	834903.7165	0.0014	4723664.8956	0.0035	48 05' 05.3021248"	11 16' 40.2924958"	650.4980
OLK2	2866981.0688	0.0018	1129669.0096	0.0011	5565665.8768	0.0032	61 11' 27.6950582"	21 30' 20.8716282"	39.4492
SUN6	2838910.7953	0.0018	903817.4138	0.0011	5620661.3532	0.0033	62 13' 56.9355617"	17 39' 35.2557147"	32.5211
WERG	2905540.9547	0.0018	1423460.0488	0.0012	5478170.7462	0.0032	59 36' 05.3630936"	26 06' 02.8752336"	30.0725
VINB	2829293.3135	0.0015	888151.5185	0.0009	5628086.9733	0.0027	62 22' 25.7385992"	17 25' 39.8752693"	150.2078
WLAD	3496344.4833	0.0023	1164350.4446	0.0012	5188401.9992	0.0032	54 47' 48.3411160"	18 25' 07.5270407"	34.7601
WLAD*	3496344.4843	0.0029	1164350.4449	0.0015	5188401.9996	0.0041	54 47' 48.3410969"	18 25' 07.5270434"	34.7611

The differences between the two methods finally are shown in Table 8-22.

**Table 8-22:** Differences of calculated heights of GNSS stations using DD and PPP methods (averaged values for ep. 2020.50)

	PPP (GPS+GLONAS) solution	DD (GPS) solution	PPP-DD
Station	h [m]	h [m]	dh [m]
KOBB	29.0372	29.0345	0.0027
LEBI	37.8865	37.8856	0.0009
LOV3	49.8810	49.8794	0.0016
MAR6	75.5582	75.5578	0.0004
MAR7	74.4376	74.4363	0.0013
METS	94.6609	94.6596	0.0013
OBE4	650.4980	650.4974	0.0006
OLK2	39.4492	39.4473	0.0019
SUN6	32.5211	32.5199	0.0012
WERG	30.0725	30.0692	0.0033
VINB	150.2078	150.2055	0.0023
WLAD	34.7601	34.7580	0.0021
WLAD*	34.7611	34.7580	0.0030

During the entire period covering the development of data from GNSS stations (in 2020), neither the receiver, the antenna nor the antenna cable were replaced at any station. Only on four stations (see Table 7-11, marked in blue) the receiver's firmware was updated. Based on the analysis of site-log files of individual stations and the headers of the RINEX files, these changes took place on the following stations in the following epochs:

Station MAR7: 2020-06-17 DOY:169 – firmware ver. 5.43 was changed on v.5.45

Station LOV3: 2020-01-01 DOY:001 - firmware ver. 3.7.7, 2020-09-10 DOY:254 – firmware ver.4.0.00

Station OBE4: 2020-01-01 DOY:001 v.3.7.6, 2020-03-13 DOY:073 v.3.7.9, 2020-11-10 DOY:315 v.3.7.10

Station SUN6: 2020-01-01 DOY:001 v.5.43, 2020-06-16 DOY:168 v.5.45

Station VERG: 2020-01-01 DOY:001 v.4.31-6.712, 2020-04-02 DOY:093 v.4.31-6.713

Examples for the coordinate time series with both methods are shown in Figure 8-56, Figure 8-57 and Figure 8-58.

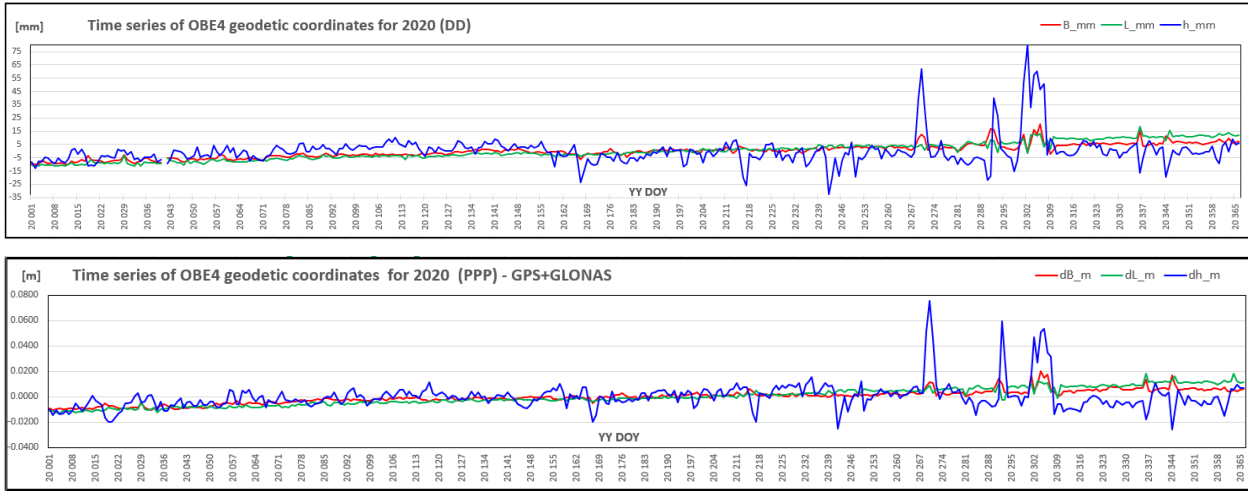
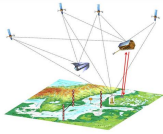


**Figure 8-56:** Time series of OBE4 GNSS station, Germany for 2020: from DD (only GPS - top) and PPP (GPS+GLONAS - bottom). On above figure we can see very similar patterns for both methods: DD network solution and PPP – independent solution for each station. There is no time coincidence between the periods of outliers and the periods of firmware updates. The most likely cause disturbances seem to be at the station, occurring during this period, affecting the quality of observation.

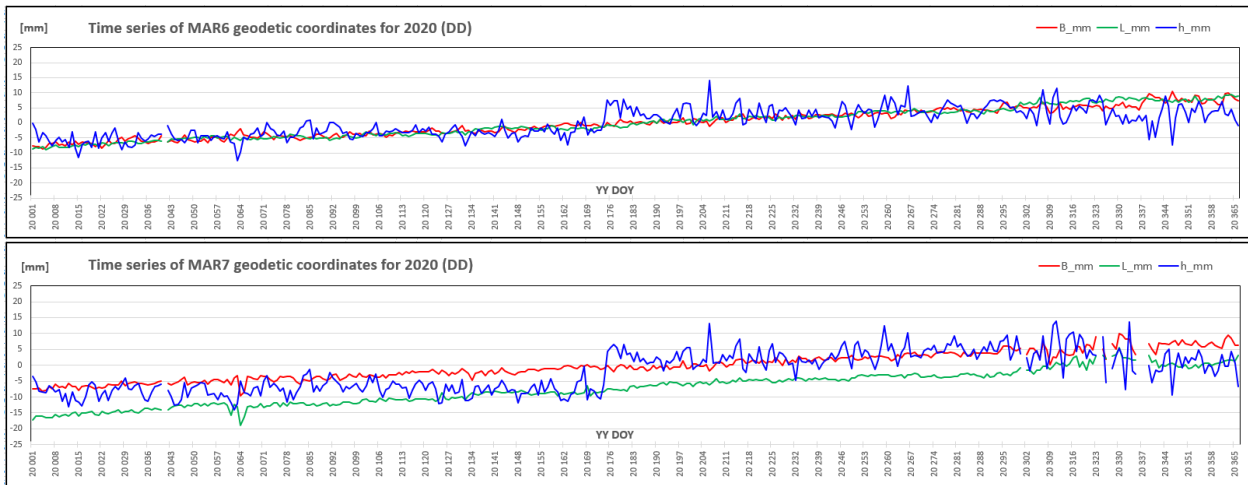


**Figure 8-57:** During the 2 days period, since 2020-06-21 (2020:DOY173) to 2020-06-23 (2020:DOY175) antenna height was changed about 10-12 mm. At the same time, a very similar effect occurred (also only in the height component) at the neighbouring station MAR6, where no hardware, software or antenna height changes were made during this period. Firmware update was made only on MAR7 station on 2020:DOY169 – four days before the vertical effect.

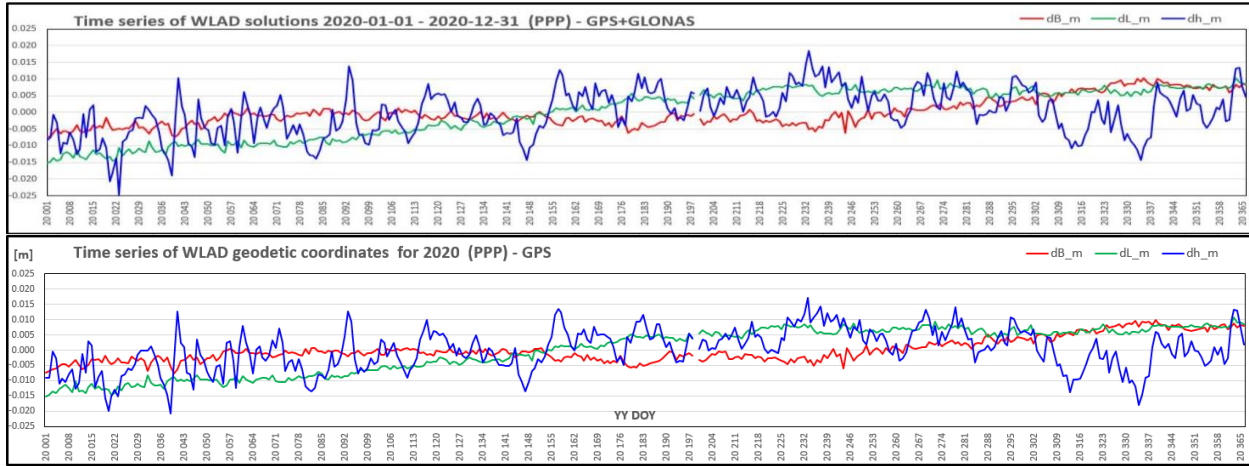
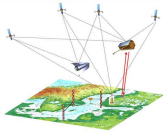


**Figure 8-58:** Example for WLAD station of time series from PPP method using GPS+GLONAS (top) and only GPS (bottom) observations. We can see very similar pattern for both solutions. GPS+GLONAS solutions have slightly smaller errors compared to GPS only solutions. In both solutions, annual oscillations in low amplitude horizontal components are also visible, characteristic for WLAD station.

## 8.4 Tide Gauge Data Analysis

The ECR transponders were mounted at seven tide gauge (TG) stations (Loksa, Emäsalo, Rauma, Leba, Wladyslawowo, Forsmark and Spikarna) in Estonia, Finland, Poland and Sweden (see Figure 5-1). All the participating tide gauge stations utilise automatic sea level detection. These tide gauges are connected to national height network in order to monitor and predict adequately the sea level fluctuations and oceanographic processes, as well as vertical land motions (VLM) along the entire shore of respective countries. All the participating countries are using the European Vertical Reference System (EVRS), that is referred to the Normaal Amsterdam Peil (NAP). The time epoch for the vertical datum is 2000.0.

The project team requested the corresponding national TG authorities to deliver TG data series for the year 2020, also relevant TG station documentation and metadata. These include: definition of the TG station location, used sensor types, datums, bench-marks, levelling information, maintenance, malfunctioning, etc. It is also of interest to identify whether the submitted TG data is „raw“ or is it corrected to account for certain phenomena, e.g. ocean and Earth tides, inverse barometric correction. It appeared that the all the tide gauge data in the study are un-normalized, i.e. presenting the actual hourly sea level heights at the tide gauge stations. The VLM estimates (reaching up to 9 mm/year) were either embedded in the TG records (Sweden) or accounted for separately (Estonia, Finland, Poland). All TG metadata and the connection to the national vertical network are described in Table 7-12 and Table 8-23.

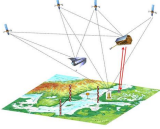
In order to filter out data blunders the tide gauge series were statistically analysed by the project team. The initial TG time series were quality checked in several tests for identifying gross errors and systematic biases. For the removal of gross errors the sea values to be studied (e.g. visually or using numerical constraints). The occasional data jumps (defined as a single reading differing from its adjacent readings by some threshold, due to sea vessels manoeuvring close to TG station) were identified, studied and eliminated. Abrupt sea level changes (e.g. >10 cm over an hour) could be an indication of gross errors, such occasions need to be examined individually and verified with contemporary weather conditions. The detected gross errors were eliminated from the further analysis. Such a revision led to coherent time series for all the participating tide gauges.

The data gaps (e.g. due to malfunctioning of instruments) in TG data series also occurred. These were identified. The standard deviation (STD) of the readings reflects the inner consistency (for the entire period, or seasonally) of the time series at each tide gauge station. Typically, the STD of the annual sea level series remained within 2 dm whereas the larger STD is associated with the rougher sea conditions at individual TG station. The smaller STD revealed sea sheltered locations of certain tide gauges.

The data series is used for computing the mean sea level estimates for each TG station. The averaged (over the given time period – one year) readings  $\bar{R}_A$  and  $\bar{R}_B$  correspond to the MSL at Station A and B, respectively, i.e.

$$\bar{R} = \frac{1}{n} \sum_{i=1}^{n=i_{\max}} R(t_i) + d(t_i) \quad (8.1)$$

where  $R(t_i)$  is the reading at the  $i$ -th time-epoch of measurements ( $t_i$ ) and  $d(t_i)$  denotes relevant corrections (e.g. due to drift of pressure sensors, for a more extended discussion see the TG data analysis section above) at the same instant. The

	<b>BALTIC+ Theme 5</b> Geodetic SAR for Baltic Height System Unification and Baltic Sea Level Research	<b>Final Report</b> Doc. Nr: SAR-HSU-SR-0022 Issue: 1.1 Date: 07.07.2021 Page: 135 of 170
---	--	---

corresponding numerical values are presented in Table 8-24. Table 8-24 also contains estimates of expected random noise of Tide Gauge readings, that is based on the technological capabilities of the used tide gauge sensor types. This can also be considered as an attempt for assigning appropriate weights to the TG measurements/data.

#### 8.4.1 Tide Gauge Data Time Series

The intention was to obtain hourly averaged sea level records for the time period 01.01.2020-31.12.2020. The advantage of the hourly TG data is that these contain no high frequency noise (i.e. sudden spikes in the time series), that usually is eliminated by the averaging procedure. However, these were not available in all the occasions, only the instantaneous ones. The hourly averaged tide gauge records became available in March 2021, after the tide gauge authorities quality check the data series for the preceding year. The graphs of sea level variations in participating countries are shown in the following Figure 8-59 to Figure 8-65.

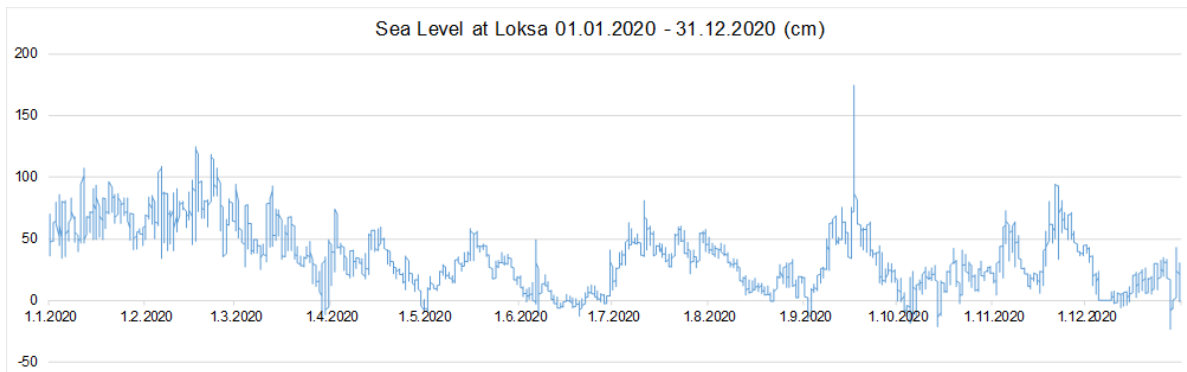


**Figure 8-59:** Tide Gauge Sea Level Time Series for Loksa, Estonia for year 2020

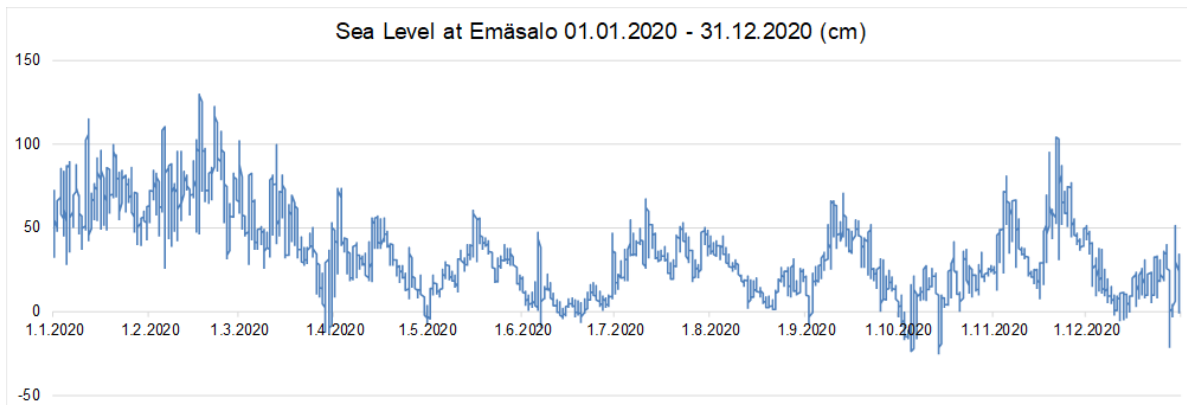


**Figure 8-60:** Tide Gauge Sea Level Time Series for Emäsalo, Finland for year 2020

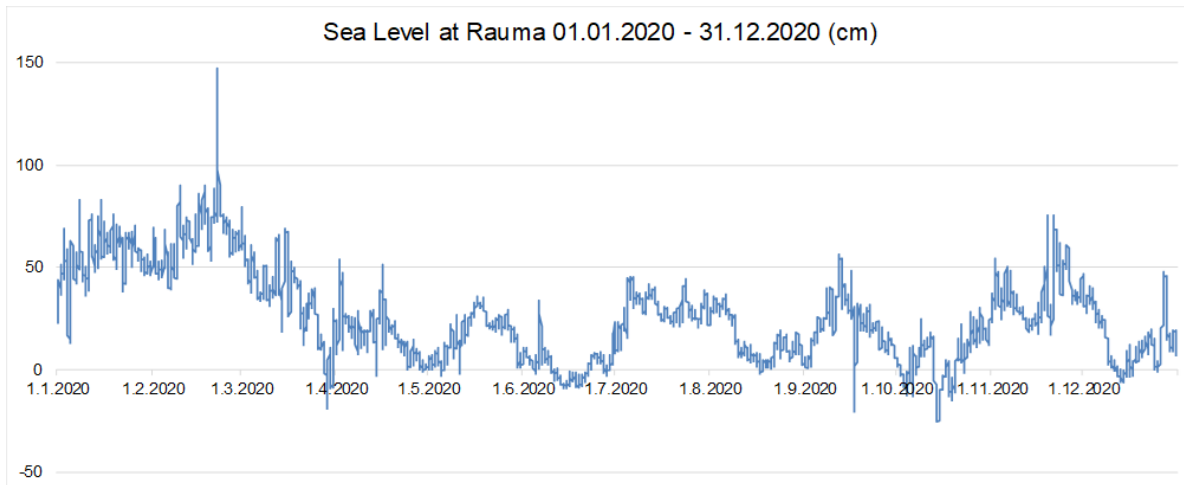
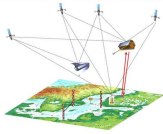


**Figure 8-61:** Tide Gauge Sea Level Time Series for Rauma, Finland for year 2020

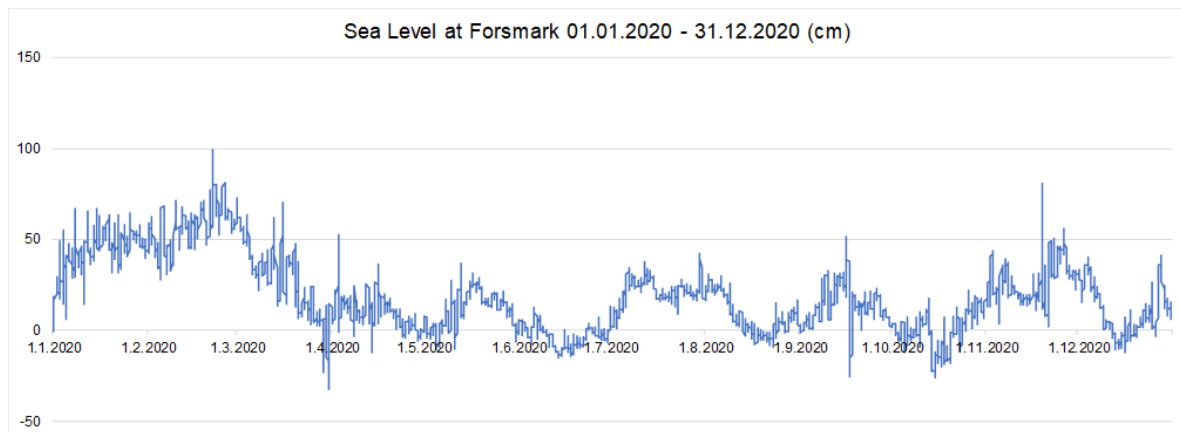


**Figure 8-62:** Tide Gauge Sea Level Time Series for Forsmark/Kobben, Sweden for year 2020

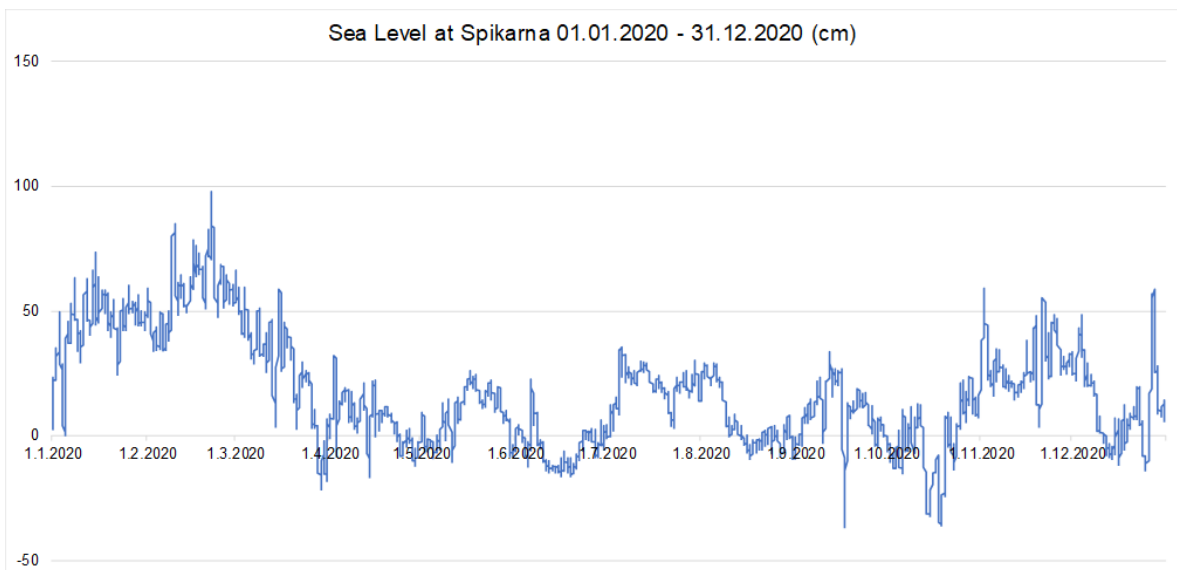


**Figure 8-63:** Tide Gauge Sea Level Time Series for Spikarna/Vinberget, Sweden for year 2020

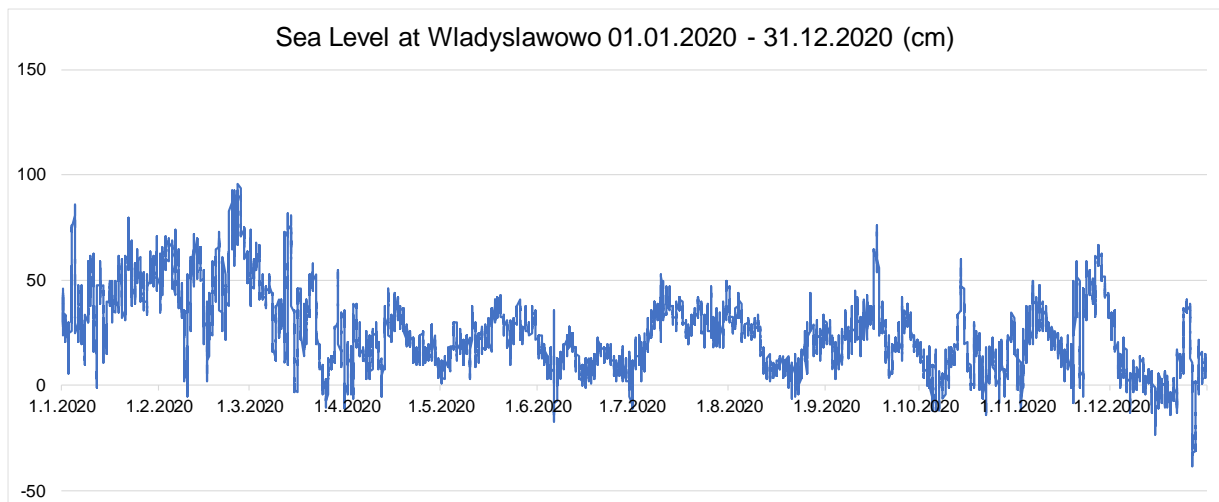
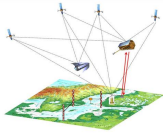


**Figure 8-64:** Tide Gauge Sea Level Time Series for Wladyslawowo, Poland for year 2020

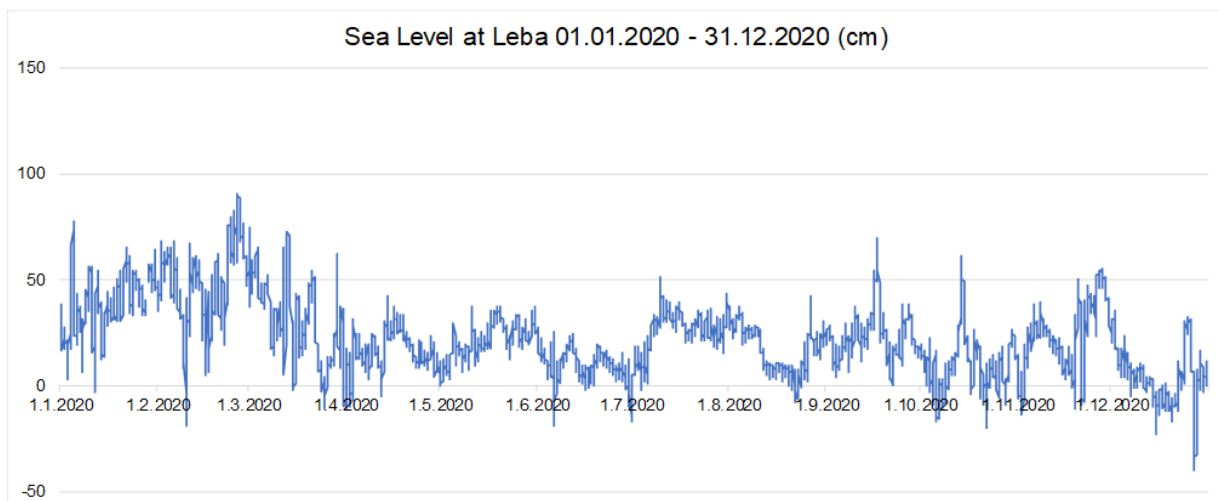


**Figure 8-65:** Tide Gauge Sea Level Time Series for Leba, Poland for year 2020

The tide gauge records were analysed for consistency and systematic distortions (that may occur due to external disturbances), in order to exclude unreliable records or low-quality observation data. Abrupt sea level changes (e.g. >10 cm over an hour) could be an indication of gross errors, such occasions were examined individually and verified with contemporary weather conditions. For instance, a few larger peaks at the sea level values were identified and confirmed, see Figure 8-66 that illustrates an abrupt sea level rise in the Lokska TG station in September 17-18.

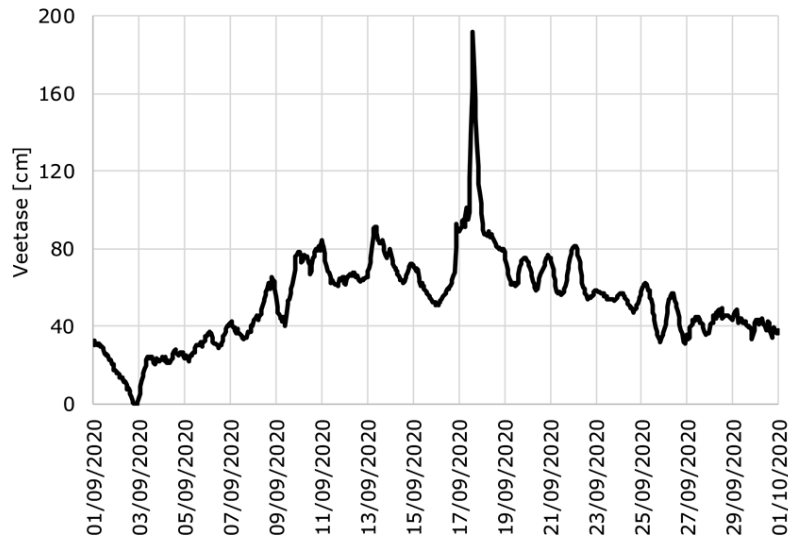


**Figure 8-66:** Rapid sea level rise in the Loksa Tide Gauge station in Sept 17-18 The units of the vertical axis are cm.

The sea level in Loksa rises quite rapidly nearly more than one meter and drops back to where it started within some 8-10h period. It was confirmed that the sea level rise was generated by extreme meteorological conditions.

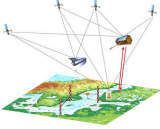
The data gaps (e.g. due to malfunctioning of instruments) in TG data series were identified, see Table 7-12 and Table 8-23. The standard deviation (STD) of the readings reflects the inner consistency (for the entire period, or seasonally) of the time series at each tide gauge station. Typically, the STD of the annual sea level series should remain within selected limit, whereas the larger STD is associated with the rougher sea conditions at individual TG station. The smaller STD may also reveal sea sheltered locations of certain tide gauges. The largest STD (0,245 m) is associated with the Loksa TG station, whereas the lowest STD of the tide gauge series are associated with both Polish TG stations (the corresponding STD values are 0.173 and 0.186 m).

#### 8.4.2 Levelling Connection of Tide Gauges to ECRs

The national authorities also performed precise levelling for determining the ECR heights with respect to nearby tide gauge levelling benchmarks. The numerical results of such levelling are summarized in Table 8-23 and Table 8-24. The details of such levelling are also documented in the Electronic Corner Reflector Station Description document [AD-4].

**Table 8-23:** Summary of tide gauge station levelling benchmarks (for station information see table Table 7-12)

Tide gauge station	Height datum, epoch	Vertical Land motion [mm/year] Source	TG benchmark (connected to national levelling Network) TGBM  TGBM's height (EVRS) /  Approximate distance between TGBM and TG	Heights (EVRS) of: tide gauge contact point (CP)/ vertical distance T (from CP to TGZ)/ the actual height of the of the TG zero (TGZ)	Levelled height (EVRS) of the ECR (reference surface)
Estonia Loksa	EH2000 (the Estonian realization of EVRS), epoch 2000.0	Abs= 3.1 Lev= 2.7 NKG2016LU	BM 73-094-90101 <a href="https://www.maaamet.ee/rr/geo/?refnr_id=205878">https://www.maaamet.ee/rr/geo/?refnr_id=205878</a>  $H_{TGBM} = 3.495$ m (EH2000/EVRS) Distance ~ 0,3 km	$H_{CP} = 2.168$ m  $T = 2.16$ m  $H_{TGZ} = +0.008$ m = correction to the tide gauge records	$H_{ECR} = 2,638$ m
Finland Emäsalo	N2000 (the Finnish realization of EVRS), epoch 2000.0	Abs = 3.8 Lev = 3.4 NKG2016LU	BM 13406 <a href="https://www.maanmittauslaitos.fi/en/research/publications/fgi-series/fgi-publications">https://www.maanmittauslaitos.fi/en/research/publications/fgi-series/fgi-publications</a> No. 139  $H_{TGBM} = 3.193$ m (N2000/EVRS) Distance = 55.35 m	$H_{CP} = 2.689$ m	$H_{ECR} = 17.816$ m
Finland Rauma Ulko - Petäjäs	N2000, epoch 2000.0	Abs = 7.3 Lev = 6.8 NKG2016LU	BM 92403 <a href="https://www.maanmittauslaitos.fi/en/research/publications/fgi-series/fgi-publications">https://www.maanmittauslaitos.fi/en/research/publications/fgi-series/fgi-publications</a> No. 139  $H_{TGBM} = 2.703$ m (N2000/EVRS) Distance = 7.43 m	$H_{CP} = 1.605$ m	$H_{ECR} = 5.007$ m

	<b>BALTIC+ Theme 5</b>		<b>Final Report</b>		
	Geodetic SAR for Baltic Height System Unification and Baltic Sea Level Research		Doc. Nr:	SAR-HSU-SR-0022	
		Issue:	1.1		
		Date:	07.07.2021		
		Page:	139 of 170		

Sweden Forsmark / Kobben	RH 2000 (the Swedish realization of EVRS), epoch 2000.0	Abs = 6.5 NKG2016LU	N/A	N/A	$H_{ECR} =$ 2.9606
Sweden Spikarna / Vinberget	RH 2000, epoch 2000.0	Abs = 9.0 NKG2016LU	N/A	N/A	$H_{ECR} =$ 123.5233
Poland Wladysla- wowo	PL- EVRF2007- NH, epoch 2007.0	~1.5 mm/year (ASG-EUPOS time series analysis)	TGBM 30530062 $H_{TGBM} = 1.9501$ m (PL-EVRF2007-NH /EVRS) Distance ~ 14 m	$H_{CP} = 2.2578$ m (EVRS). It corrensponds to 7.200 m reading of Tide Gauge staff	$H_{ECR} = 5,638$ 2 m (PL- EVRF2007- NH (the Polish realization of EVRS))
Poland Leba	PL- EVRF2007- NH, epoch 2007.0	N/A	TGBM 30430019 $H_{TGBM} = 2.0083$ m (PL-EVRF2007-NH /EVRS) Distance ~ 400 m TG 30430022 $H_{TGBM} = 2.1443$ m (PL-KRON86-NH /EVRS) Distance ~ 80 m	$H_{CP} = 2.2750$ m (EVRS). It corrensponds to 7.200 m reading of Tide Gauge staff	$H_{ECR} = 3,049$ 1 m (PL- EVRF2007- NH)

Table 8-23 also contains also interconnections (e.g local ties by precise levelling, GNSS) between the tide gauges and geodetic infrastructure. Figure 6-10 depicts inter-relations in between the tide gauge zero (TGZ), contact point (CP) and tide gauge benchmark TGBM.

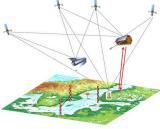
The geometrical levelling was conducted for determining the height of the reference boundary of the ECR transponder, which is the lower (horizontal) boundary of the ECR baseplate, see Figure 8-67.



**Figure 8-67:** Reference boundary of the ECR transponder (the lower horizontal boundary of the ECR baseplate)

For the consistency of the TG analysis it is requested that TG data is presented in same sea level datum. Also possible inconsistencies between the national vertical datums (Poland just recently switched from the obsolete Kronstadt vertical datum into new national realisation of the EVRS, denoted as PL-EVRF2007-NH) were considered in the TG processing and analysis. Due to relatively short observation period the land uplift values (see Table 8-23) were not considered at the tide gauge readings.

The TG instrumental drift can be an important issue that which has to be taken under control through regular control readings from a nearby staff gauge. During the field checks the tide gauge sensor readings were compared to the visual tide gauge pole readings. No need for the drift correction was identified. Hence it is concluded that the TG readings are affected by the random noise only. The expected range of the random noise for specific gauge sensors is estimated in Table 8-24. These estimates can be used at the final computations

	<b>BALTIC+ Theme 5</b> Geodetic SAR for Baltic Height System Unification and Baltic Sea Level Research	<b>Final Report</b> Doc. Nr: SAR-HSU-SR-0022 Issue: 1.1 Date: 07.07.2021 Page: 140 of 170
---	--	---

**Table 8-24:** Summary of the TG and ECR levelling results, the mean sea level for the period 01.01.2020 – 31.12.2020

Tide gauge station National realisation of the EVRS Height datum	Expected random noise of TG readings	Levelling height (either the NW screw-top or the upper surface of the ECR cover plate) [m]	Vertical distance between upper surface of cover (or NW bolt top!) and lower boundary of ECR baseplate [m]	Reference height of ECR (lower boundary of the ECR baseplate!*)  H <sub>ECR</sub> height [m] in national realisation of the EVRS height datum	Average sea level height (in EVRS datum) for the period 01.01.2020 – 31.12.2020 [m]	Standard deviation of tide gauge time series 01.01.2020 – 31.12.2020 [m]	Missing data [%]
Loksa, Estonia EH2000	1 cm <sup>***</sup>	2,6568 (surface of the cover plate, NW corner)	- 0.0183	H <sub>ECR</sub> =2,6385	+0,343	0,245	107 N/A - > 1,2%
Emäsalo, Finland N2000	1 cm <sup>***</sup>	17.8400 (NW bolt top)	-0.0245	H <sub>ECR</sub> =17.8155 m	+0,338	0,238	31 N/A -> 0,6 %
Rauma, Finland N2000	1 cm <sup>***</sup>	5.032 (NW bolt top)	-0.0245	H <sub>ECR</sub> =5.0075 m	+0,258	0,216	57 N/A -> 1,1 %
Forsmark/ Kobben, Sweden RH2000	< 1 cm <sup>****</sup>	2,9786 (surface of the ECR cover plate, NE corner)	- 0.018 <sup>**</sup> (estimated from the photo)	H <sub>ECR</sub> =2.9606 m (computed by TUT)	+0,188	0,200	0 N/A - > 0%
Spikarna/ Vinberget, Sweden RH2000	< 1 cm <sup>****</sup>	123,5413 (surface of the ECR cover plate, NE corner)	- 0.018 <sup>**</sup> (estimated from the photo)	H <sub>ECR</sub> =123.5233 m (computed by TUT)	+0,175	0,215	0 N/A - > 0%
Wladyslawowo , Poland PL-EVRF2007-NH	1 cm <sup>***</sup>	Levelling and GNSS measurements were performed to the ECR_RP point.	Levelling and GNSS measurements were performed to the ECR_RP point.	H <sub>ECR</sub> =5,6382 m	+0,253	0,186	16 N/A -> 0,2 %
Leba, Poland PL-EVRF2007-NH	1 cm <sup>***</sup>	Levelling and GNSS measurements were performed to the ECR_RP point.	Levelling and GNSS measurements were performed to the ECR_RP point.	H <sub>ECR</sub> =3,0491 m	+0,224	0,173	24 N/A -> 0,3 %

\*Recall that lower boundary of the ECR baseplate was agreed for the ECR vertical reference in Sopot in 2019, see also [AD-4]

\*\*The Swedish levellings

\*\*\* Liibusk, A., Ellmann, A., Kõuts, T.; Jürgenson, H. (2013): Precise Hydrodynamic Leveling by Using Pressure Gauges, Marine Geodesy, 36:2, 138-163  
<http://dx.doi.org/10.1080/01490419.2013.771594>

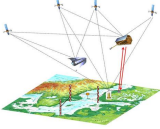
\*\*\*\* Gobron, K.; de Viron, O.; Wöppelmann, G.; Poirier, É.; Ballu, V.; Van Camp, M. Assessment of Tide Gauge Biases and Precision by the Combination of Multiple Collocated Time Series. J. Atmos. Ocean. Technol. 2019, 36, 1983–1996.

### 8.4.3 Mean Sea Level Estimates for Tide Gauges

The TG data series were used for computing the annual mean sea level estimates for each TG station in the common EVRS. Table 8-24 summarizes the average sea level height (in EVRS datum) for the period 01.01.2020 to 31.12.2020.

The Gulf of Finland TG stations (Loksa and Emäsalo) at the opposite shores showed good agreement, the average mean sea level was +34 cm. In other words, the height difference between the mean sea levels at the opposite side of the gulf is almost zero. It appeared that during the time period in question an upward sea level trend from west to east was identified in Gulf of Bothnia tide gauge stations. In other words, the sea level at the Finnish shore appeared to be about 7-8 cm higher than the sea level at the Swedish tide gauge stations.

The Rauma mean sea level (as of +26 cm) for the given time span (01.01.-31.12.2020) was confirmed by the adjacent Finnish TG stations Pori and Turku. Intuitively thus, such a west-east directional upward tilt (and also higher than average sea level in the Gulf of Finland) could be due to prevailing (stronger and more frequent) westerly winds during the season in question.

	<b>BALTIC+ Theme 5</b>  Geodetic SAR for Baltic Height System Unification and Baltic Sea Level Research	<b>Final Report</b> Doc. Nr: SAR-HSU-SR-0022 Issue: 1.1 Date: 07.07.2021 Page: 141 of 170
---	--	---

The 3 cm mean sea level difference (+22 versus +25 cm) for the adjacent Polish stations could have some local coastal circulation related reason.

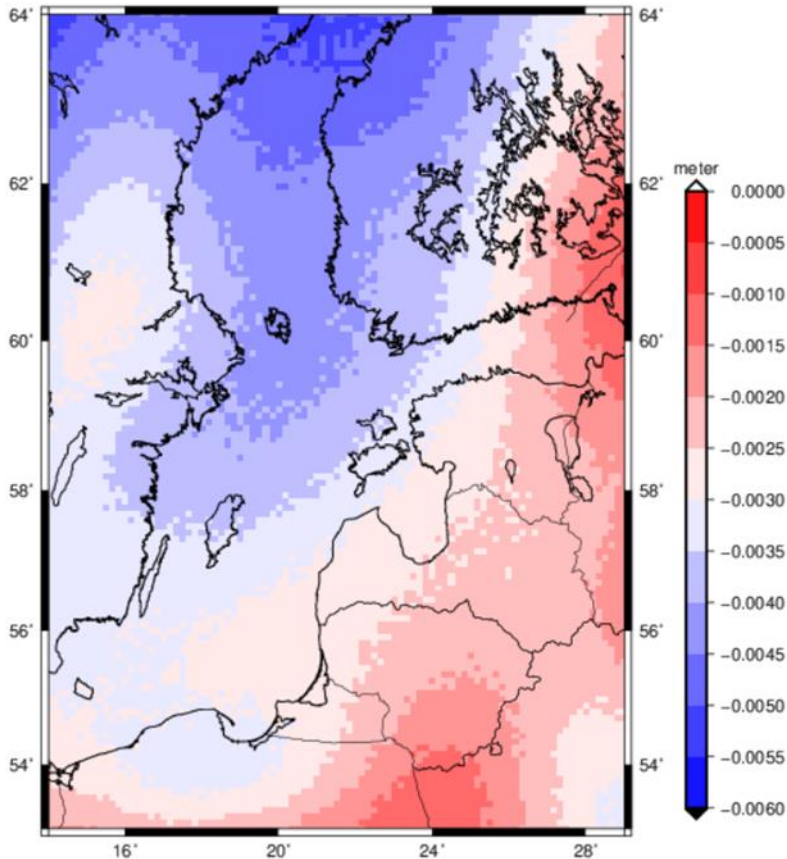
## 8.5 GOCE Based Geoid Computation

### 8.5.1 Postglacial Land Uplift Correction to epoch 2020.5

The LSMSA and LSC geoid models computed in Section 7.5 (Table 7-15) refers (approximately) to postglacial land uplift epoch 2000.0, which is in accordance with the conventions stated in Subsection 7.5.3. This is also the case for the NKG2015 geoid model. The final quasigeoid model for the project, however, should refer to the mean epoch of the Geodetic SAR project (~2020.5). We therefore have to apply a correction the mean epoch 2020.5.

The conversion from 2000.0 to 2020.5 was made using the temporal variation model for the spherical harmonic coefficients up to degree 120 from GOCO06S/ITSG-Grace2018s (Mayer-Gürr et al. 2018; Kvas et al. 2019). This land uplift correction strategy was then compared with the geoid uplift for 20.5 years modelled by NKG2016LU (Vestøl et al., 2019). The geoid rise model for NKG2016LU was computed by 1D Glacial Isostatic Adjustment (GIA) modelling under several assumptions (Vestøl et al., 2019). The height anomaly difference between the two strategies is illustrated in Figure 8-68 for the large test area.

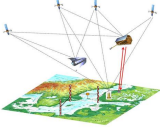
The height anomaly difference between the two land uplift correction strategies for 20.5 years lies between 0 and -0.006 m with a mean around -0.003 m. As the zero of the geoid rise of the NKG2016LU model is not so well defined, depending on several assumptions, we prefer to use the GOCO06S/ITSG-GRACE2018S strategy for the final LSMSA 4 model.



**Figure 8-68:** Difference between the land uplift correction of the height anomaly computed using the temporal spherical harmonic model of GOCO06S/ITSG-Grace2018s and the geoid rise of the NKG2016LU model. Unit: m

### 8.5.2 Final (Quasi-)Geoid Heights in the Tide Gauges/ECRs

Based on the results in Section 7.5, it is not possible to say which one of the LSMSA 1, LSMSA 2, LSMSA 3 and LSC 3 geoid models that is best. They agree very well with each other and have about the same fit to GNSS/levelling. We pick, therefore, rather arbitrarily the LSMSA 2 model, which is then converted to the project mean epoch 2020.5 by the land

	<b>BALTIC+ Theme 5</b>  Geodetic SAR for Baltic Height System Unification and Baltic Sea Level Research	<b>Final Report</b> Doc. Nr: SAR-HSU-SR-0022 Issue: 1.1 Date: 07.07.2021 Page: 142 of 170
---	--	---

uplift correction described above, resulting in what we called the LSMSA 4 model in Section 7.5. The final geoid heights in the Swedish, Finnish and Estonian tide gauges are given by this LSMSA 4 model; see Table 8-25 below.

As can be judged from the comparison to GNSS/levelling, the standard uncertainty of the LSMSA 4 geoid heights in Sweden, Finland and Estonia is estimated to be approximately 0.010 m in a relative sense. As can be seen in Table 7-16, the GNSS/levelling fit standard deviation after correction of country biases is 0.013–0.015 m. Considering that there are also errors in the GNSS ellipsoidal heights and in the levelled heights, 0.010 m should be a reasonable estimate (for the Swedish, Finnish and Estonian geoid heights).

In order to get consistent geoid heights for the whole project, the quasigeoid model LSMSA 4 is selected also for the Polish stations. For these stations, however, the uncertainty should be somewhat higher.

**Table 8-25:** (Version 2) Final (Quasi)Geoid Heights in the Tide Gauges/ECRs. LSMSA 4 for all stations. Unit: m.

Estonia		Finland			Sweden			Poland		
Loksa	Vergi	Emäsalo	Lovisa	Rauma	Forsmark	Spikarna	Mårtsbo	Wladysl.	Rosewie	Leba
16.821	16.555	16.509	15.453	19.096	22.381	25.065	24.627	28.883	29.030	30.787

### 8.5.3 Time Series of GOCE Based Geoid Heights

The time variation of the geoid heights is very small. The geoid velocities are below 0.6 mm/year for all the included tide gauges for both NKG2016LU (Vestøl et al., 2019) and GOC06S/ITSG-Grace2018s (Mayer-Gürr et al. 2018; Kvas et al. 2019). This means that the time variation within the project year 2020 is well below 1 mm for all the tide gauges. The final geoid height time series for the tide gauges can thus be taken as the constant values in Table 8-25 (for epoch 2020.5).

## 8.6 Reference Frames and Joint Standards

Within this project, different observations such as SAR, GNSS, GOCE, terrestrial/airborne gravity data and tide gauges are combined for the determination of ellipsoidal and physical heights at tide gauge stations. In order to ensure consistent results for the different products, it is essential that any differences regarding the underlying reference frames and inconsistencies with respect to the implemented standards and models must be taken properly into account. The issues that need to be considered in this context and the procedures related to the product validation are described in Sect. 6.6 and 7.6. In this section, the results of the assessment of the different geometric and gravimetric products with respect to the implemented models, standards and the underlying reference frames are summarized.

The standards and models used for the processing of the different observations used within this project are applied accordingly with the IERS Conventions 2010 (Petit and Luzum, 2010). In addition, technique-specific processing standards were applied for the individual observation techniques (e.g., IGS- and EPN-Standards, SAR Standards, GOCE Standards, standards for gravity and tide gauge data). The fact that the SAR and GNSS results are given in the conventional tide-free system, whereas the gravimetric products are expressed in the tide-free system has been taken into account by applying the transformation formulae provided in Sect. 7 of the IERS Conventions 2010. Another important issue are the very significant land uplift corrections due to postglacial rebound in the Baltic Sea region, which are also consistently applied. Since the general processing standards and models are applied closely to the IERS Conventions 2010, there are no further significant error sources regarding standards and conventions which need to be considered for the combination of the different observation types. For the transformation between 3-D Cartesian coordinates and ellipsoidal coordinates it was specified that the conventional GRS80 parameters are to be used within this project.

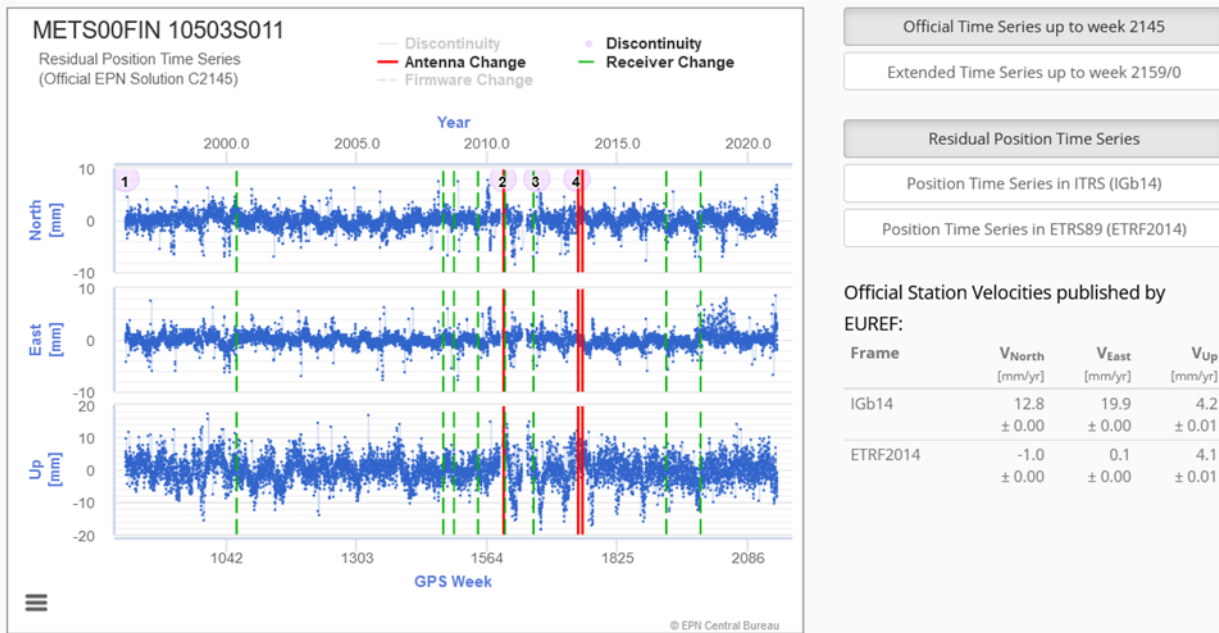
Concerning the underlying reference frames, the GNSS and SAR results are expressed in the ITRF2014, whereas the GOCE results refer to ITRF2008. The transformation parameters between both frames are rather small (max. 2.4 mm for T3) and thus they don't need to be taken into account within this project (see Table 8-26). The values are taken from the ITRF2014 publication (Altamimi et al, 2016, see also the IGN website at [https://itrf.ign.fr/ITRF\\_solutions/2014/](https://itrf.ign.fr/ITRF_solutions/2014/)).

**Table 8-26:** Transformation parameters at epoch 2010.0 and their rates from ITRF2014 to ITRF2008 (ITRF2008 minus ITRF2014) [Source: IGN website [https://itrf.ign.fr/ITRF\\_solutions/2014/](https://itrf.ign.fr/ITRF_solutions/2014/)]

	T1	T2	T3	D	R1	R2	R3
	mm	mm	mm	10-9	mas	mas	mas
	1.6	1.9	2.4	-0.02	0.000	0.000	0.000
+/-	0.2	0.1	0.1	0.02	0.006	0.006	0.006
<b>Rates</b>	0.0	0.0	-0.1	0.03	0.000	0.000	0.000
+/-	0.2	0.1	0.1	0.02	0.006	0.006	0.006

For the validation of the GNSS results, transformations between the ITRF2014 station positions and velocities and the results of the EUREF Permanent Network (EPN) given in the ETRS89 have been performed. The transformation formulae are published for example in Boucher and Altamimi (2011) and Altamimi (2018). Furthermore, for these transformations a web-based tool is available at the EPN website: [http://epncb.oma.be/productsservices/coord\\_trans/](http://epncb.oma.be/productsservices/coord_trans/)

The GNSS network stations in the Baltic Sea region were processed together with about 10 to 15 IGS/EPN stations which are used for the datum definition of the regional network in the ITRF2014. For the processing of the GNSS solutions, the ITRF2014 station coordinates (given at the epoch 2010.0) were extrapolated over a time span of about 10 years to the observation epoch (in the year 2020) by using the ITRF2014 station velocities. To minimize the errors caused by the required extrapolation of station coordinates, stable reference stations with a long observation time span have been selected for the realization of the geodetic datum. As an example, Figure 8-69 shows the time series of the IGS/EPN station Metsahovi in Finland which has been taken from the EPN website <https://www.epncb.oma.be/productsservices/timeseries/>. The observation time series of about 25 years indicates a high long-term stability, so that the extrapolation of station coordinates from epoch 2010.0 to the year 2020 can be performed with a sufficient accuracy. The vertical station velocity of about 4 mm/yr with respect to ETRF2014 and IGB14 reference frames can be well explained by postglacial uplift.

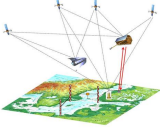


**Figure 8-69:** Residual position time series of GNSS station Metsahovi in Finland [Source: EPN website at <https://www.epncb.oma.be/productsservices/timeseries/>]

In context with the extrapolation of station positions and the transformation of GNSS and SAR solutions into ITRF2014, also possible non-linear station motions may affect the results. As shown for example in Figure 8-69, the amplitudes of the annual signals are mostly in the range of a few millimeters only, and thus they can be neglected in the framework of this project. However, if higher accuracies are required, the annual signals of all the ITRF2014 stations are available on request from IGN in Paris, so that the non-linear signals can be considered for the extrapolation of station positions and for the transformation of GNSS and SAR solutions into ITRF2014.

Furthermore, in principle the time variability of the center of mass (CM) versus the center of figure (CF) is an issue which has to be considered within this project, since the geometric quantities are expressed in the CF frame, whereas the gravimetric quantities refer to CM. The ITRF2014 provides an annual geocenter model with amplitudes of 2.6 mm, 2.9 mm and 5.7 mm for the x-, y- and z-component, respectively. So, in principle these corrections could be applied for the combination of geometric and gravimetric observations, but with respect to the current accuracy level of the obtained SAR positions the geocenter variations can be neglected.

In summary, for the combination of the different geometric and gravimetric quantities a correct treatment of the permanent tide and a consistent correction of postglacial uplift is essential to achieve consistent results within this project. Regarding the extrapolation of ITRF2014 station positions, stable reference stations need to be selected, to ensure that a linear propagation models provides sufficient accurate results. The transformation parameters between ITRF2014 and ITR2008 as well as the geocenter variations can be neglected within this project, as the effects are much below the centimeter level. The same holds for non-linear motions in station positions. However, if GNSS solutions

	<b>BALTIC+ Theme 5</b> Geodetic SAR for Baltic Height System Unification and Baltic Sea Level Research	<b>Final Report</b> Doc. Nr: SAR-HSU-SR-0022 Issue: 1.1 Date: 07.07.2021 Page: 144 of 170
---	--	---

computed in the ITRF2014 are compared with EPN results, the transformation formulae between the ITRS and ETRS89 need to be applied, since the effect is about 75 cm for observations in the year 2020.

## 8.7 Height System Unification and Absolute Sea Level

### 8.7.1 Absolute Height Experiments

In this chapter the results of the individual observations techniques in terms of heights are summarized for the static case. Static here means that average values over the observation period of the year 2020 are considered disregarding sub-annual variations of heights. The reason for this is that when combining all observation data sets, the error always is driven by the worst component. As shown in chapters 8.1 and 8.2 the weakest point at this stage is the accuracy of the SAR positions, which in average is at a level of a decimetre (see Table 8-18). Therefore, at this stage it doesn't make sense to compute the time variable absolute sea level. Mean values for all observed and computed heights above the reference ellipsoid GRS80 or the tide gauge zero marker for the stations of the Baltic Sea test network are summarized in Table 8-27.

**Table 8-27:** Summary of observed ellipsoidal, geoid and tide gauge heights at Balti Sea network. All heights represent mean values averaged over the observation period in year 2020.

ECR Station	Local Tie	$h^{ECR}$ Ellipsoidal Height [m]	$N^{TG} = N^{ECR}$ Geoid Height [m]	$z^{TG}$ Tide Gauge [m]	$h^{GNSS}$ Ellipsoidal Height [m]
<b>Władysławowo</b>	Tide Gauge, GNSS	+34.640	+28.883	+0.253	+34.758
<b>Leba</b>	Tide Gauge, GNSS	+34.389	30.787	+0.224	+37.886
<b>Vergi</b>	GNSS	+28.966	+16.555	n/a	+30.069
<b>Loksa</b>	Tide Gauge	+20.076	+16.821	+0.343	n/a
<b>Emäsalo</b>	Tide Gauge	+34.293	+16.509	+0.338	n/a
<b>Loviisa</b>	GNSS	+46.840	15.453	n/a	+49.879
<b>Rauma</b>	Tide Gauge	+24.082	+19.096	+0.258	n/a
<b>Forsmark/ Kobben</b>	Tide Gauge	+25.659	+22.381	+0.188	n/a
<b>Mårtsbo</b>	GNSS	+75.477	+24.627	n/a	+75.558
<b>Spikarna/ Vinberget</b>	Tide Gauge, GNSS	+149.654	+25.065	+0.175	+150.206

where:

$h^{ECR}$  Height of ECR reference point above GRS80 ellipsoid (refer to Table 8-5).

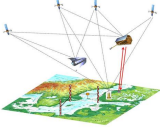
$N^{TG}$  Height of reference equipotential surface above GRS80 reference ellipsoid at tide gauge location (refer to Table 8-25)

$N^{ECR}$  Height of reference equipotential surface above GRS80 reference ellipsoid at ECR location (refer to Table 8-25)

$z^{TG}$  Tide gauge sea level height above tide gauge zero marker in EVRF (refer to Table 8-24)

$h^{GNSS}$  Height of GNSS station above GRS80 reference ellipsoid (refer to Table 8-20)

In order to connect the ECR reference point either to the tide gauge zero marker and the GNSS reference point conventional spirit levelling has been done. The results of the local ties are summarized in Table 8-28.

	<b>BALTIC+ Theme 5</b> Geodetic SAR for Baltic Height System Unification and Baltic Sea Level Research	Final Report Doc. Nr: SAR-HSU-SR-0022 Issue: 1.1 Date: 07.07.2021 Page: 145 of 170
---	--	--

**Table 8-28:** Levelled height differences between ECR reference point and tide gauge or GNSS reference points.

ECR Station	Local Tie	$\Delta h_{ECR}^{TG}$ ECR to Tide Gauge [m]	$\Delta h_{GNSS}^{ECR}$ GNSS to ECR [m]
<b>Wladyslawowo</b>	Tide Gauge	-5.638	n/a
<b>Wladyslawowo</b>	GNSS	n/a	-0.135
<b>Leba</b>	Tide Gauge	-3.049	n/a
<b>Leba</b>	GNSS	n/a	-3.932
<b>Vergi</b>	GNSS	n/a	-0.996
<b>Loksa</b>	Tide Gauge	-2.639	n/a
<b>Emäsalo</b>	Tide Gauge	-17.816	n/a
<b>Loviisa</b>	GNSS	n/a	-3.574
<b>Rauma</b>	Tide Gauge	-5.007	n/a
<b>Forsmark/ Kobben</b>	Tide Gauge	-2.961	n/a
<b>Mårtsbo</b>	GNSS	n/a	-0.032
<b>Spikarna/ Vinberget</b>	Tide Gauge	-123.523	n/a
<b>Spikarna/ Vinberget</b>	GNSS	n/a	-0.998

where:

$\Delta h_{ECR}^{TG}$  Levelled height difference from ECR reference point to tide gauge zero marker in (ellipsoidal height difference) (refer to Table 8-24)

$\Delta h_{GNSS}^{ECR}$  Levelled height difference from GNSS reference point to ECR reference point (ellipsoidal height difference) (refer to [AD-4], chapter Table 7-3 and Table 7-20).

For the ECR stations co-located to a permanent GNSS station the resulting heights can be directly compared by applying the relative height difference between the GNSS antenna reference point and the ECR reference point. This is an indicator about the absolute performance of the SAR positioning technique. Table 8-29 (right column) shows the results of this comparison. It can be identified that the absolute height differences between the 2 techniques are varying and that no ultimate conclusion can be drawn from this comparison. While three stations exhibit good to reasonable agreement between the GNSS and the ECR height results at decimetre level or below, for three other stations the GNSS versus ECR height differences are at a level of several decimetres to half a meter. As one can assume that the GNSS derived heights are accurate at a level of a few centimetres, the ECR derived heights are the main driver for the absolute performance results. Regarding the reason why some ECR positioning results are better than others there is no unique answer. For the station Spikarna/Vinberget the reason could be that the observation time series is relatively short, but for the stations in Loviisa and Leba the raw observation data series seem to be good and that no indicator about possible problems can be identified (see chapter 8.1 and chapter 8.2).

**Table 8-29:** Comparison of SAR positioning at ECR stations to co-located permanent GNSS station results.

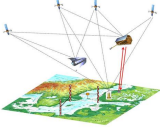
ECR Station	$h^{GNSS}$ Ellipsoidal Height [m]	$\Delta h_{GNSS}^{ECR}$ GNSS to ECR [m]	$h_{comp}^{ECR}$ Ell. Height computed [m]	$h^{ECR}$ Ell. Height observed [m]	$\Delta h^{ECR}$ computed - observed [m]
<b>Wladyslawowo</b>	+34.758	-0.135	+34.623	+34.640	-0.017
<b>Leba</b>	+37.886	-3.932	+33.954	+34.389	-0.435
<b>Vergi</b>	+30.069	-0.996	+29.073	+28.966	+0.107
<b>Loviisa</b>	+49.879	-3.574	+46.305	+46.840	-0.535
<b>Mårtsbo</b>	+75.558	-0.032	+75.526	+75.477	+0.049
<b>Spikarna/ Vinberget</b>	+150.206	-0.998	+149.208	+149.654	-0.446

Average physical heights (for the year 2020) of tide gauge stations referring to a unique reference equipotential surface and not considering the absolute or relative sea level, are computed by the following formula (refer to equation (7.5) in chapter 7.7).

$$H^{TG} = h^{ECR} + \Delta h_{ECR}^{TG} - N^{TG} \quad (8.2)$$

where:  $H^{TG}$  Physical height of tide gauge zero marker above reference equipotential surface.

From the ECR stations co-located to a tide gauge station the resulting physical heights of the tide gauge zero markers above the reference equipotential surface (GOC-based geoid) are computed with equation (8.2) (Table 8-30, right column). As all tide gauge zero markers are already provided in the EVRS, meaning, that in the ideal case this height for

	<b>BALTIC+ Theme 5</b> Geodetic SAR for Baltic Height System Unification and Baltic Sea Level Research	<b>Final Report</b> Doc. Nr: SAR-HSU-SR-0022 Issue: 1.1 Date: 07.07.2021 Page: 146 of 170
---	--	---

all stations shall be zero, any deviation from zero can be interpreted as a performance indicator for the involved quantities and here mainly the performance of the SAR positioning. The results show that some stations seem to provide very good results with only a few centimetres offset, while other stations exhibit an offset of several decimetres up to a meter. Regarding the results presented in chapter 8.1 (Table 8-3) and chapter 8.2 (Figure 8-6 to Figure 8-18) there seems to be some correlation of the physical height results with the SAR observation quality, the SAR residuals and the length of the SAR observation time series. For example, the stations Emäsalo and Rauma have a better performance than some other stations. The time series of Spikarna/Vinberget is very short and therefore the uncertainty probably is significantly larger. For the stations Władysławowo, Łeba, Loksa and Forsmark/Kobben there is a larger variability in the SAR observation quality, which could be the reason for higher uncertainties. At this point it is difficult to provide a complete assessment of the results as no single reason can be identified.

**Table 8-30:** Results for physical heights of tide gauge stations (right column) applying equation (8.2).

<b>ECR Station</b>	$h^{ECR}$ <b>Ell. Height [m]</b>	$\Delta h_{ECR}^{TG}$ <b>ECR to Tide Gauge [m]</b>	$N^{TG}$ <b>Geoid Height [m]</b>	$H^{TG}$ <b>Physical Height [m]</b>
<b>Władysławowo</b>	+34.640	-5.638	+28.883	+0.119
<b>Łeba</b>	+34.389	-3.049	+30.787	+0.553
<b>Loksa</b>	+20.076	-2.639	+16.821	+0.616
<b>Emäsalo</b>	+34.293	-17.816	+16.509	-0.032
<b>Rauma</b>	+24.082	-5.007	+19.096	-0.021
<b>Forsmark/ Kobben</b>	+25.659	-2.961	+22.381	+0.317
<b>Spikarna/ Vinberget</b>	+149.654	-123.523	+25.065	+1.066

From the tide gauge physical height it is then easy to compute absolute the sea level height by adding the averaged tide gauge records using equation (8.3). The results are shown in Table 8-31. These results contain the full uncertainty of the physical heights of the tide gauge stations as they were computed with equation (8.2). Therefore, all what has been said related to these results also apply to the absolute sea level heights and no further conclusions can be drawn.

$$S^{TG} = h^{ECR} + \Delta h_{ECR}^{TG} - N^{TG} + z^{TG} = H^{TG} + z^{TG} \quad (8.3)$$

where:  $S^{TG}$  Sea level height above reference equipotential surface at epoch t (absolute sea level height)

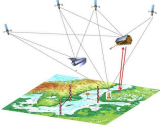
**Table 8-31:** Results for absolute sea level heights at tide gauge stations

<b>ECR Station</b>	$H^{TG}$ <b>Physical Height [m]</b>	$z^{TG}$ <b>Tide Gauge [m]</b>	$S^{TG}$ <b>Absolute Sea Level [m]</b>
<b>Władysławowo</b>	+0.119	+0.253	+0.372
<b>Łeba</b>	+0.553	+0.224	+0.777
<b>Loksa</b>	+0.616	+0.343	+0.959
<b>Emäsalo</b>	-0.032	+0.338	+0.306
<b>Rauma</b>	-0.021	+0.258	+0.237
<b>Forsmark/ Kobben</b>	+0.317	+0.188	+0.505
<b>Spikarna/ Vinberget</b>	+1.066	+0.175	+1.241

In chapter 5.2 experiments have been defined in order to link tide gauge stations to the permanent GNSS network via the ECR stations. Even if the performance of the ECR positioning results do not meet the expectations in terms of accuracy an attempt is made to compute the results for these experiments. The meaning of the results might be questionable as from the analysis of the individual station performances shown in Table 8-29 and Table 8-30 it is obvious that the ECR heights are within an accuracy level of a few centimetres up to a meter. These uncertainties are fully propagated to the results of the experiments shown in the following.

### 8.7.2 Baseline (Relative Height) Experiments:

Relative height differences are compared between GNSS or tide gauge stations and those observed with the ECR's. There are several of such baselines available, which can be observed over long or short distances. For the relative comparisons between station A and station B the following formulas are applied. All numbers are taken from Table 8-27 and Table 8-28.

	<b>BALTIC+ Theme 5</b> Geodetic SAR for Baltic Height System Unification and Baltic Sea Level Research	<b>Final Report</b> Doc. Nr: SAR-HSU-SR-0022 Issue: 1.1 Date: 07.07.2021 Page: 147 of 170
---	--	---

$$\begin{aligned}
 \Delta h^{GNSS} &= h^{GNSS-B} - h^{GNSS-A} \\
 \Delta h^{ECR} &= \left( h^{ECR-B} - \Delta h_{GNSS-B}^{ECR-B} \right) - \left( h^{ECR-A} - \Delta h_{GNSS-A}^{ECR-A} \right) \\
 \Delta \Delta h^{GNSS-ECR} &= \Delta h^{GNSS} - \Delta h^{ECR}
 \end{aligned} \tag{8.4}$$

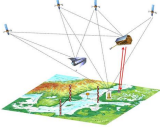
**Table 8-32:** Relative height differences between ECR stations at the Baltic sea and between co-located GNSS stations. GNSS height differences and ECR height differences transferred to the GNSS reference markers are computed according equation (8.4).

Station A	Station B	$\Delta h^{GNSS}$ Ell. Height Difference [m]	$\Delta h^{ECR}$ Ell. Height Difference [m]	$\Delta \Delta h^{GNSS-ECR}$ Difference Ell. Height Diff. [m]
Władysławowo	Łeba	+3.128	+3.546	-0.418
Władysławowo	Vergi	-4.689	-4.813	+0.124
Władysławowo	Loviisa	+15.121	+15.639	-0.518
Władysławowo	Mårtsbo	+40.800	+40.734	+0.066
Władysławowo	Spikarna/Vinberget	+115.448	+115.877	-0.429
Łeba	Vergi	-7.817	-8.359	+0.542
Łeba	Loviisa	+11.993	+12.093	-0.100
Łeba	Mårtsbo	+37.672	+37.188	+0.484
Łeba	Spikarna/Vinberget	+112.320	+112.331	-0.011
Vergi	Loviisa	+19.810	+20.452	-0.642
Vergi	Mårtsbo	+45.489	+45.547	-0.058
Vergi	Spikarna/Vinberget	+120.137	+120.690	-0.553
Loviisa	Mårtsbo	+25.679	+25.095	+0.584
Loviisa	Spikarna/Vinberget	+100.327	+100.238	+0.089
Mårtsbo	Spikarna/Vinberget	+74.648	+75.143	-0.495

The results of the baseline comparisons again show a diverse behaviour. Basically, the differences between GNSS and ECR observed height differences vary between a few centimetres and some decimetres. For stations, which exhibit a large absolute offset (see Table 8-29, stations Łeba, Loviisa, Spikarna/ Vinberget) the differential height error between these stations becomes small (below a decimetre), while the differential error between one of these stations with the other stations becomes significantly larger. This indicates, that there is a systematic height offset in the ECR positioning results with the same sign, as it is also shown in the absolute comparisons in Table 8-29. The reason for this is yet unknown. Similar for the stations, which exhibit a small absolute offset (see Table 8-29, stations Władysławowo, Vergi, Mårtsbo) the differential height error between these stations becomes also small (below a decimetre).

Finally, as another relative height experiment the sea level at tide gauge stations can be compared. For the relative comparisons between tide gauge station A and station B the following formulas are applied. All numbers are taken from Table 8-31.

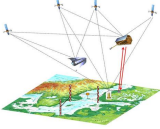
$$\begin{aligned}
 \Delta z^{TG} &= z^{TG-B} - z^{TG-A} \\
 \Delta S^{TG} &= S^{TG-B} - S^{TG-A} \\
 \Delta \Delta S^{TG} &= \Delta z^{TG} - \Delta S^{TG}
 \end{aligned} \tag{8.5}$$

	<b>BALTIC+ Theme 5</b> Geodetic SAR for Baltic Height System Unification and Baltic Sea Level Research	Final Report Doc. Nr: SAR-HSU-SR-0022 Issue: 1.1 Date: 07.07.2021 Page: 148 of 170
---	--	--

**Table 8-33:** Relative height differences between ECR stations at the Baltic sea and between co-located tide gauge stations. Tide gauge height differences and ECR height differences transferred to the tide gauge reference markers are computed according equation (8.5).

Station A	Station B	$\Delta z^{TG}$ Tide Gauge Height Difference [m]	$\Delta S^{TG}$ Absolute Sea Level Height Difference [m]	$\Delta\Delta S^{TG}$ Difference Sea Level Difference [m]
Władysławowo	Łeba	-0.029	+0.405	-0.434
Władysławowo	Loksa	+0.090	+0.587	-0.497
Władysławowo	Emäsalo	+0.085	-0.066	+0.151
Władysławowo	Rauma	+0.005	-0.135	+0.140
Władysławowo	Forsmark/Kobben	-0.065	+0.133	-0.198
Władysławowo	Spikarna/Vinberget	-0.078	+0.869	-0.947
Łeba	Loksa	+0.119	+0.182	-0.063
Łeba	Emäsalo	+0.114	-0.471	+0.585
Łeba	Rauma	+0.034	-0.540	+0.574
Łeba	Forsmark/Kobben	-0.036	-0.272	+0.236
Łeba	Spikarna/Vinberget	-0.049	+0.464	-0.513
Loksa	Emäsalo	-0.005	-0.653	+0.648
Loksa	Rauma	-0.085	-0.722	+0.637
Loksa	Forsmark/Kobben	-0.155	-0.454	+0.299
Loksa	Spikarna/Vinberget	-0.168	+0.282	-0.450
Emäsalo	Rauma	-0.080	-0.069	-0.011
Emäsalo	Forsmark/Kobben	-0.150	+0.199	-0.349
Emäsalo	Spikarna/Vinberget	-0.163	+0.935	-1.098
Rauma	Forsmark/Kobben	-0.070	+0.268	-0.338
Rauma	Spikarna/Vinberget	-0.083	+1.004	-1.087
Forsmark/Kobben	Spikarna/Vinberget	-0.013	+0.736	-0.749

The results from the tide gauge baseline differences show in most cases large differences. Right now, it seems that only three ECR stations with good performance and linked to a tide gauge are available. These are the stations in Władysławowo (see also comment above for GNSS comparisons), Emäsalo and Rauma, where differences up to a decimetre can be achieved. There is also a good agreement between Łeba and Loksa, which probably is due to similar systematic offsets at both stations (see again comment above for GNSS comparisons).

	<b>BALTIC+ Theme 5</b>  Geodetic SAR for Baltic Height System Unification and Baltic Sea Level Research	<b>Final Report</b> Doc. Nr: SAR-HSU-SR-0022 Issue: 1.1 Date: 07.07.2021 Page: 149 of 170
---	--	---

## 9 PRODUCTS AND DATA SETS

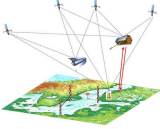
This chapter provides a brief description of the experimental products generated by the project and the content of these products (including the format).

### 9.1 SAR Data and Corrections

From the SAR data analysis and value adding processor the products summarized in Table 9-1 are generated. The detailed content and format of these products are described in Table 9-2 to Table 9-9.

**Table 9-1:** Summary of SAR Data Analysis and Value Adding Products

<b>Product Acronym</b>	<b>Product Title</b>	<b>Product Description</b>	<b>Processing Module</b>
PTA-RES	Extracted Target Locations	The files contain the extracted target range and azimuth location(s) from point target analysis. Multiple targets may be summarized in one file as noted by the header. Data blocks are repeated for each target.	SAR Data Analysis
PTA-OBS	SAR Raw Measurements	The observation file is generated from the point target analysis file (PTA-RES). Processor specific corrections are applied to range and azimuth during file generation, representing the raw SAR measurements. Multiple targets may be summarized in one file. Data blocks for different targets are placed side by side organized by dates. If a target is unavailable or detected an outlier (low SCR), the entries are set to 9. Note on SWST: differential corrections are applied if the SWST became updated in the S-1 SAR processor, i.e. range measurements based on previous configurations are corrected in order to match the latest value applied in processing.	SAR Data Analysis
COR-TD	Tropospheric Delays	The tropospheric correction files are generated from PTA-OBS and VMF3. Tropospheric delays are stored as 1-way path delay in units of meters. In order to apply them to the range observations, they need to be scaled by $2/c$ , with $c$ denoting speed of light in vacuum. Multiple targets may be summarized in one file. Data blocks for different targets are placed side by side organized by dates. If a target is unavailable or detected an outlier (low SCR), the entries are set to 9.	SAR Data Analysis
COR-ID	Ionospheric Delay	The ionospheric correction files are generated from PTA-OBS and IGS-TEC. Ionospheric delays are stored as 1-way path delay in units of meters. In order to apply them to the range observations, they need to be scaled by $2/c$ , with $c$ denoting speed of light in vacuum. Multiple targets may be summarized in one file. Data blocks for different targets are placed side by side organized by dates. If a target is unavailable or detected an outlier (low SCR), the entries are set to 9.	SAR Data Analysis
COR-GC	Geodynamic Corrections	The geodynamic effects are computed from PTA-OBS and IERS-2010, following the definitions of the ITRF as outlined in the IERS conventions (version 2010, chapter 7, displacements of reference points). The cumulative impact on range and azimuth are stored in the correction file. The range corrections are available in units of meters 1-way. In order to apply them to the range observations, they need to be scaled by $2/c$ , with $c$ denoting speed of light in vacuum. The azimuth corrections are in units of seconds and can be used as is. The following geodynamic corrections are comprised in values list in the file: Solid Earth tidal deformations caused by Sun & Moon, Ocean loading stemming from water mass redistribution by tides weighing on the coastlines using the FES2004 tidal model, Atmospheric pressure loading induced by diurnal heating of the atmosphere (S1 and S2 components), Rotational deformation due to polar motion, Ocean pole tide loading, Secular trends as inferred from nearby IGS reference site located on same tectonic plate. Multiple targets may be summarized in one file. Data blocks for different targets are placed side by side organized by dates. If a target is unavailable or detected an outlier (low SCR), the entries are set to 9.	SAR Data Analysis
COR-SC	Sentinel-1 Systematic	Sensor specific calibration constants (S1A, S1B) are stored in dedicated calibration files. The numbers need to be applied to the raw	SAR Data Analysis

	<b>BALTIC+ Theme 5</b> Geodetic SAR for Baltic Height System Unification and Baltic Sea Level Research	<b>Final Report</b> Doc. Nr: SAR-HSU-SR-0022 Issue: 1.1 Date: 07.07.2021 Page: 150 of 170
---	--	---

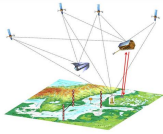
	Effects Corrections	range and azimuth observations to ensure unbiased observations. The numbers primarily account for SAR payload internal signal delays and have been inferred from S1A and S1B measurements of the long term stable corner reflector installed at Metsähovi geodetic observatory	
COR-EC1	ECR Antenna Geometric Phase Center Location Correction	The different locations of ECR antennas as well as the signal delay introduced by ECR electronics have to be taken into account. Depending on the orbit geometry, the phase center of the ECR is shifted with respect to the estimated position. This offset is added as a correction to the observations as a function of the incidence angle. (Note: Phase Center variation maps are not yet available for the ECRs. Therefore, this data file is not available as a result of the project).	SAR Data Analysis
COR-EC2	ECR Electronic Delay Correction	The ECR electronics causes a signal delay which has to be corrected in the SAR measurements. The effect was calibrated with a set of reference ECR, yielding a model that describes the delay as a function of orbit geometry and incidence angle. The model is evaluated for each acquisition and the results are stored the in dedicated correction files as described below.	SAR Data Analysis

**Table 9-2:** Detailed description of product PTA-RES

<b>File Name</b>	
<ID>_PTA_Result.txt	<ID> = <AAA_BBB_XXXX_YYY_ZZZZ> [AAA] = BAL: Baltic Sea; [AAA] = MNC: Munich [BBB] = ASC: Ascending; [BBB] = DSC: Descending [XXXX] = Station Location Acronym (3 or 4 Letters) [YYY] = Reflector Acronym; ECR: Electronic Corner Reflector; CR: Corner Reflector [ZZZZ] = ECR Number or CR Station Acronym
<b>Header</b>	
NR OF SC :	Number of targets included in file
COORDINATES XYZ ITRF14 [m] :	List of approximate target coordinates in the ITRF14; XYZ in meters
Results SC ## : #	Number of extractions available for target ###
<b>Data Block Columns Description (repeated per epoch)</b>	
Col 01 = S_ID	Satellite ID for given acquisition, 4 digits, e.g. S1A1, S1B1, ...
Col 02 to 04 = YYYY MM DD	Date of given acquisition, year, day, month
Col. 05 = t [SOD UTC]	Time of closest approach (azimuth) as seconds of day referring to UTC
Col. 06 = tau [s 2-way]	Signal round trip time (range) at zero Doppler, seconds
Col. 07 = PPower [dB]	Peak power as sigma0 integrated for 3dB peak width, decibel
Col. 08 = BPower [dB]	Background power inferred from the 4 quadrants surrounding the peak and scaled to 3dB peak area, decibel
Col. 09 = SCR [dB]	Signal-to-clutter ratio; difference of PPower minus BPower, decibel
Col. 10 = Rres [m]	Range resolution inferred from 3dB peak width
Col. 11 = Ares [m]	Azimuth resolution inferred from 3dB peak width
Col. 12 = sR [m]	Theoretical PTA standard deviation in range as inferred from SCR and Rres
Col. 13 = sA [m]	Theoretical PTA standard deviation in azimuth as inferred from SCR and Ares
Col. 14 = S	Number of the sub-swath containing the target location, e.g. 1 --> IW1, 2 --> IW2
Col. 15 = B	Number of the burst containing the target location, e.g. 1 --> Burst 1, ...
Col. 16 = tPX [px]	Target azimuth location inside image in units of pixels; in case of burst modes, it means w.r.t. the burst
Col. 17 = tauPX [px]	Target range location inside image in units of pixels; in case of burst modes, it means w.r.t. the burst
Col. 18 = BAC [s]	Correction for bistatic azimuth effects not considered in the S-1 SAR image processor, seconds
Col. 19 = AFMC [s]	Correction for azimuth FM-rate mismatch shifts still present in S-1 SAR images, seconds
Col. 20 = DRC [s]	Correction for Doppler shifts in the range pulses, seconds two-way
Col. 21 = IPFv	Version of the S-1 SAR processor that processed the S-1 SAR image
Col. 22 = SWST [s 2-way]	Sampling window start time bias applied by the S-1 SAR processor during image generation, seconds two-way

**Table 9-3:** Detailed description of product PTA-OBS

<b>File Name</b>	
<ID>_SAR_Observations.cfg	<ID> = <AAA_BBB_XXXX_YYY_ZZZZ> [AAA] = BAL: Baltic Sea; [AAA] = MNC: Munich [BBB] = ASC: Ascending; [BBB] = DSC: Descending [XXXX] = Station Location Acronym (3 or 4 Letters) [YYY] = Reflector Acronym; ECR: Electronic Corner Reflector; CR: Corner Reflector [ZZZZ] = ECR Number or CR Station Acronym
<b>Header</b>	
IGS GNSS RX TS : [XXXX]	Optional list of IGS stations that can be used to correct the tropospheric delay, [XXXX] = 4 digit IGS IDs



**BALTIC+ Theme 5**  
Geodetic SAR for Baltic Height System  
Unification and Baltic Sea Level Research

Final Report  
Doc. Nr: SAR-HSU-SR-0022  
Issue: 1.1  
Date: 07.07.2021  
Page: 151 of 170

IGS GNSS RX IS : [XXXX]	Optional list of IGS stations that can be used to correct the ionospheric delay, [XXXX] = 4 digit IGS IDs
NR OF SC :	Number of targets included in file
COORDINATES XYZ ITRF14 [m] :	List of approximate target coordinates in the ITRF14; XYZ in meters
<b>Data Block Columns Description (repeated per epoch)</b>	
Col 01 = S_ID	Satellite ID for given acquisition, 4 digits, e.g. S1A1, S1B1, ...
Col 02-04 = YYYY MM DD	Date of given acquisition, year, day, month
Col 05 = AZIMUTH [SOD UTC]	Target 1 time of closest approach (azimuth); corrected for BAC & AFMC; seconds of day referring to UTC
Col 06 = RANGE [s]	Target 1 signal round trip time (range) at zero Doppler; corrected for DRC (& SWST); seconds two-way
Col 07 = AZIMUTH [SOD UTC]	Target 2 time of closest approach (azimuth); corrected for BAC & AFMC; seconds of day referring to UTC
Col 08 = RANGE [s]	Target 2 signal round trip time (range) at zero Doppler; corrected for DRC (& SWST); seconds two-way
...	Target 3 ...

**Table 9-4:** Detailed description of product COR-TD

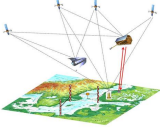
<b>File Name</b>	
<ID>_D_Troposphere.txt	<ID> = <AAA_BBB_XXXX_YYY_ZZZZ> [AAA] = BAL: Baltic Sea; [AAA] = MNC: Munich [BBB] = ASC: Ascending; [BBB] = DSC: Descending [XXXX] = Station Location Acronym (3 or 4 Letters) [YYY] = Reflector Acronym; ECR: Electronic Corner Reflector; CR: Corner Reflector [ZZZZ] = ECR Number or CR Station Acronym
<b>Header</b>	
NR OF SC :	Number of targets for which corrections are included in file
<b>Data Block Columns Description (repeated per epoch)</b>	
Col 01 = ID	Satellite ID for given acquisition, 4 digits, e.g. S1A1, S1B1, ...
Col 02-04 = YYYY MM DD	Date of given acquisition, year, day, month
Col 05 = SOD UTC	Target 1 time of closest approach (azimuth) as seconds of day referring to UTC
Col 06 = d_tro [m]	Target 1 tropospheric delay in units of meters, one-way
Col 07 = s_d_tro [+m]	Target 1 standard deviation of tropospheric delay if provided by underlying method; meters
Col 08 = SOD UTC	Target 2 time of closest approach (azimuth) as seconds of day referring to UTC
Col 09 = d_tro [m]	Target 2 tropospheric delay in units of meters, one-way
Col 10 = s_d_tro [+m]	Target 2 standard deviation of tropospheric delay if provided by underlying method; meters
...	Target 3 ...

**Table 9-5:** Detailed description of product COR-ID

<b>File Name</b>	
<ID>_D_Ionosphere.txt	<ID> = <AAA_BBB_XXXX_YYY_ZZZZ> [AAA] = BAL: Baltic Sea; [AAA] = MNC: Munich [BBB] = ASC: Ascending; [BBB] = DSC: Descending [XXXX] = Station Location Acronym (3 or 4 Letters) [YYY] = Reflector Acronym; ECR: Electronic Corner Reflector; CR: Corner Reflector [ZZZZ] = ECR Number or CR Station Acronym
<b>Header</b>	
NR OF SC :	Number of targets for which corrections are included in file
<b>Data Block Columns Description (repeated per epoch)</b>	
Col 01 = ID	Satellite ID for given acquisition, 4 digits, e.g. S1A1, S1B1, ...
Col 02-04 = YYYY MM DD	Date of given acquisition, year, day, month
Col 05 = SOD UTC	Target 1 time of closest approach (azimuth) as seconds of day referring to UTC
Col 06 = d_iono [m]	Target 1 ionospheric delay in units of meters, one-way
Col 07 = s_d_iono [+m]	Target 1 standard deviation of ionospheric delay if provided by underlying method; meters
Col 08 = SOD UTC	Target 2 time of closest approach (azimuth) as seconds of day referring to UTC
Col 09 = d_tro [m]	Target 2 ionospheric delay in units of meters, one-way
Col 10 = s_d_tro [+m]	Target 2 standard deviation of ionospheric delay if provided by underlying method; meters
...	Target 3 ...

**Table 9-6:** Detailed description of product COR-GC

<b>File Name</b>	
<ID>_D_Geodynamics.txt	<ID> = <AAA_BBB_XXXX_YYY_ZZZZ> [AAA] = BAL: Baltic Sea; [AAA] = MNC: Munich [BBB] = ASC: Ascending; [BBB] = DSC: Descending [XXXX] = Station Location Acronym (3 or 4 Letters) [YYY] = Reflector Acronym; ECR: Electronic Corner Reflector; CR: Corner Reflector [ZZZZ] = ECR Number or CR Station Acronym
<b>Header</b>	
NR of SC :	Number of targets for which corrections are included in file
ITRF Epoch YYYY MM DD :	Fixed to 2020 01 01; the ITRF epoch for which the secular trends are corrected for in the measurements.

	<b>BALTIC+ Theme 5</b> Geodetic SAR for Baltic Height System Unification and Baltic Sea Level Research	<b>Final Report</b> Doc. Nr: SAR-HSU-SR-0022 Issue: 1.1 Date: 07.07.2021 Page: 152 of 170
---	--	---

Nearest IGS Stations :	IGS 4 digits Station ID which was used to compute the trend
ITRF Velocity VxVyVz [m/y] :	IGS site velocity vector as given in the ITRF solution in meters per year
<b>Data Block Columns Description (repeated per epoch)</b>	
Col 01 = ID	Satellite ID for given acquisition, 4 digits, e.g. S1A1, S1B1, ...
Col 02-04 = YYYY MM DD	Date of given acquisition, year, day, month
Col 05 = SOD UTC	Target 1 time of closest approach (azimuth) as seconds of day referring to UTC
Col 06 = d_geod_R [m]	Target 1 cumulative displacement effects in range in units of meters, one-way
Col 07 = d_geod_A [s]	Target 1 cumulative displacement effects in azimuth in units of seconds
Col 08 = SOD UTC	Target 2 time of closest approach (azimuth) as seconds of day referring to UTC
Col 09 = d_geod_R [m]	Target 2 cumulative displacement effects in range in units of meters, one-way
Col 10 = d_geod_A [s]	Target 2 cumulative displacement effects in azimuth in units of seconds
...	Target 3 ...

**Table 9-7:** Detailed description of product COR-SC

<b>File Name</b>	
D_Sys <ID> IFT.txt	<ID> = S1A or S1B (for Sentinel-1A or 1B respectively)
<b>Data Block Columns Description</b>	
Col 01 = Azimuth_delay [s]	Azimuth calibration constant in units of seconds
Col 02 = Range_delay [s]	Slant range calibration constant in units of seconds, 2-way

**Table 9-8:** Detailed description of product COR-EC1. Data file is not available, check note in Table 9-1.

<b>File Name</b>	
<ID>_D_Phasecenter.txt	<ID> = <AAA_BBB_XXXX_YYY_ZZZZ> [AAA] = BAL: Baltic Sea; [AAA] = MNC: Munich [BBB] = ASC: Ascending; [BBB] = DSC: Descending [XXXX] = Station Location Acronym (3 or 4 Letters) [YYY] = Reflector Acronym; ECR: Electronic Corner Reflector [ZZZZ] = ECR Number
<b>Header</b>	
NR of SC :	Number of targets for which corrections are included in file
<b>Data Block Columns Description (repeated per epoch)</b>	
Col 01 = ID	Satellite ID for given acquisition, 4 digits, e.g. S1A1, S1B1, ...
Col 02-04 = YYYY MM DD	Date of given acquisition, year, day, month
Col 05 = SOD UTC	Target 1 time of closest approach (azimuth) as seconds of day referring to UTC
Col 06 = d_ECR_R [m]	Target 1 geometric phase center offset effects in range in units of meters, one-way
Col 07 = d_ECR_A [s]	Target 1 geometric phase center offset effects in azimuth in units of seconds

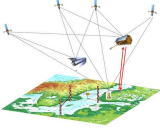
**Table 9-9:** Detailed description of product COR-EC2

<b>File Name</b>	
<ID>_D_ECR_Delay.txt	<ID> = <AAA_BBB_XXXX_YYY_ZZZZ> [AAA] = BAL: Baltic Sea; [AAA] = MNC: Munich [BBB] = ASC: Ascending; [BBB] = DSC: Descending [XXXX] = Station Location Acronym (3 or 4 Letters) [YYY] = Reflector Acronym; ECR: Electronic Corner Reflector [ZZZZ] = ECR Number
<b>Header</b>	
NR of SC :	Number of targets for which corrections are included in file
<b>Data Block Columns Description (repeated per epoch)</b>	
Col 01 = ID	Satellite ID for given acquisition, 4 digits, e.g. S1A1, S1B1, ...
Col 02-04 = YYYY MM DD	Date of given acquisition, year, day, month
Col 05 = SOD UTC	Target 1 time of closest approach (azimuth) as seconds of day referring to UTC
Col 06 = d_ECR_R [m]	Target 1 ECR electronic delay impact on range in units of meters, one-way
Col 07 = d_ECR_A [s]	Target 1 ECR electronic delay impact on azimuth in units of seconds

## 9.2 SAR Geometric Positions

The results of the SAR Positioning include the X, Y, Z target coordinates in ITRF2014, the uncertainties  $\sigma_x, \sigma_y, \sigma_z, \sigma_{xy}, \sigma_{xz}, \sigma_{yz}$ , derived from the variance-covariance matrix  $\Sigma(\hat{x})$ , the confidence ellipsoid, which can be obtained by performing eigenvalue and eigenvector decomposition of  $\Sigma(\hat{x})$  scaled to a 95% confidence level as described in (Gisinger et al. 2017), in case external reference coordinates for the same target are also available (e.g. from a terrestrial survey), the  $\Delta X_{x,y,z}$  coordinate differences, the range and azimuth standard deviations  $\sigma_r$  and  $\sigma_a$ , provided by the variance component estimation and the observation residuals.

From the SAR positioning processor the products summarized in Table 9-10 are generated. The detailed content and format of these products are described in Table 9-11 and Table 9-12.

	<b>BALTIC+ Theme 5</b>  Geodetic SAR for Baltic Height System Unification and Baltic Sea Level Research	<b>Final Report</b> Doc. Nr: SAR-HSU-SR-0022 Issue: 1.1 Date: 07.07.2021 Page: 153 of 170
---	--	---

**Table 9-10:** Summary of SAR Positioning Products

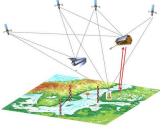
Product Acronym	Product Title	Product Description	Processing Module
SAR-POS	SAR Positioning Solution	Time series of coordinates of the SAR target as X, Y, Z coordinates in the ITRF2014 and uncertainties $\sigma_x, \sigma_y, \sigma_z, \sigma_{xy}, \sigma_{xz}, \sigma_{yz}$ , derived from the variance-covariance matrix $\Sigma(\hat{x})$ . Confidence ellipsoid from eigenvalue and eigenvector decomposition of $\Sigma(\hat{x})$ scaled to a 95% confidence level. In case external reference coordinates for the same target are also available (e.g. from a terrestrial survey), the $\Delta X_{x,y,z}$ coordinate differences are computed.	SAR Positioning
SAR-OBS	SAR Observation Residuals	Time series of range and azimuth standard deviations $\sigma_r$ and $\sigma_a$ , provided by the variance component estimation and observation residuals.	SAR Positioning

**Table 9-11:** Detailed description of product SAR-POS

File Name	
<ID>_<temp_res>_summary_results.txt.	<ID> = <AAA BBBB XXXX YYY ZZZZ> [AAA] = BAL: Baltic Sea; [AAA] = MNC: Munich [BBBB] = AS__: Ascending; [BBBB] = DS__: Descending; [BBBB] = ASDS: Ascending and Descending [XXXX] = Station Location Acronym (3 or 4 Letters) [YYY] = Reflector Acronym; ECR: Electronic Corner Reflector; CR: Corner Reflector [ZZZZ] = ECR Number or CR Station Acronym <temp_res>=Temporal resolution of Observation intervals (e.g. 1M, 2M, 3M, 4M, All). "All" means average solution with all data
Header	
<XXXX> - <BBBB>	[XXXX] = Station Location Acronym (3 or 4 Letters) [BBBB] = AS__: Ascending; [BBBB] = DS__: Descending, [BBBB] = ASDS: Ascending and Descending
<Temporal Resolution> time series	<temp_res>=Temporal resolution of Observation intervals (e.g. 1M, 2M, 3M, 4M, All). "All" means average solution with all available data.
Reference Epoch ITRF14	Reference epoch of the reference Coordinates yyyy mm dd
Coordinates XYZ ITRF14 [m] :	List of reference target coordinates in the ITRF14; XYZ in meters
ITRF Epoch YYYY MM DD :	Fixed to 2020 01 01; the ITRF epoch for which the secular trends are corrected for in the measurements.
Nearest IGS Stations :	IGS 4 digits Station ID which was used to compute the trend
ITRF Velocity VxVyVz [m/y] :	IGS site velocity vector as given in the ITRF solution in meters per year
Data Block Columns Description (repeated per temporal interval)	
Col 01 = Solution Epoch [YYYY MM DD]	Epoch of the Solution yyyy mm dd <temp_res>-mean date
Col 02 = DTs_A[#]	Number of valid data takes in azimuth
Col 03 = DTs_R[#]	Number of valid data takes in range
Col 04 = X[m]	Target X coordinate in ITRF14 in meters
Col 05 = Y[m]	Target Y coordinate in ITRF14 in meters
Col 06 = Z[m]	Target Z coordinate in ITRF14 in meters
Col 07-09 = { s_x [+m], s_y [+m], s_z [+m] }	Standard deviations $\sigma_x, \sigma_y, \sigma_z$ from variance-covariance matrix $\Sigma(\hat{x})$ ITRF14
Col 10-12 = { s_xy [m <sup>2</sup> ], s_xz [m <sup>2</sup> ], s_yz [m <sup>2</sup> ] }	Covariance $\sigma_{xy}, \sigma_{xz}, \sigma_{yz}$ , from variance-covariance matrix $\Sigma(\hat{x})$ ITRF14
Col 13-21 = { Eig_V1(N); Eig_V1(E), Eig_V1(H); Eig_V2(N); Eig_V2(E), Eig_V2(H); Eig_V3(N); Eig_V3(E), Eig_V3(H) }	Three Eigenvectors from $\Sigma(\hat{x})$ decomposition in Local reference frame with North East, Height components
Col 22-24 = { Eig_a1[m], Eig_a2[m], Eig_a3[m] }	Three Eigenvalues from $\Sigma(\hat{x})$ decomposition of the respective Eigenvectors
Col 25-27 = { dX[m], dY[m], dZ[m] }	the $\Delta X_{x,y,z}$ coordinate differences to reference coordinates ITRF14
Col 28-30 = { dN[m], dE[m], dH[m] }	the $\Delta X_{N,E,H}$ coordinate differences to reference coordinates in local frame (North, East, Up)
Col 31-33 = { s_N [+m], s_E [+m], s_H [+m] }	Confidence intervals $\sigma_N, \sigma_E, \sigma_H$ from variance-covariance matrix $\Sigma(\hat{x})$ in local frame (North, East, Up)

**Table 9-12:** Detailed description of product SAR-OBS

File Name
-----------

	<b>BALTIC+ Theme 5</b>  Geodetic SAR for Baltic Height System Unification and Baltic Sea Level Research	<b>Final Report</b> Doc. Nr: SAR-HSU-SR-0022 Issue: 1.1 Date: 07.07.2021 Page: 154 of 170
---	--	---

<ID>_<temp_res>_Observation_summary_Quality_Statistics.txt.	<ID> = <AAA_BBBB_XXXX_YYY_ZZZZ> [AAA] = BAL: Baltic Sea; [AAA] = MNC: Munich [BBBB] = AS_: Ascending; [BBBB] = DS_: Descending; [BBBB] = ASDS: Ascending and Descending [XXXX] = Station Location Acronym (3 or 4 Letters) [YYY] = Reflector Acronym; ECR: Electronic Corner Reflector; CR: Corner Reflector [ZZZZ] = ECR Number or CR Station Acronym <temp_res>=Temporal resolution of Observation intervals (e.g. 1M, 2M, 3M, 4M, All). "All" means average solution with all available data.
<b>Header</b>	
<XXXX> - <BBBB>	[XXXX] = Station Location Acronym (3 or 4 Letters) [BBBB] = AS_: Ascending; [BBBB] = DS_: Descending; [BBBB] = ASDS: Ascending and Descending
<Temporal Resolution> time series	<temp_res>=Temporal resolution of Observation intervals (e.g. 1M, 2M, 3M, 4M, All). "All" means average solution with all available data.
Reference Epoch ITRF14	Reference epoch of the reference Coordinates yyyy mm dd
Coordinates XYZ ITRF14 [m] :	List of reference target coordinates in the ITRF14; XYZ in meters
<b>Data Block Columns Description</b>	
Col 01 = Solution Epoch [YYYY MM DD]	Epoch of the Solution yyyy mm dd <temp_res>-mean date
Col 02 = Input DTs [#]	Number of Observation dates inputted in the processor
Col 03 = Valid DTs_A[#]	Number of valid data takes in azimuth
Col 04 = Valid DTs_R[#]	Number of valid data takes in range
Col 05 = s_o^2	Variance unit weight
Col 06 - (5+ #in_angle) = sR [+·m]	Standard deviation $\sigma_r$ in range direction per incidence angle (#in_angle=number of incidence angles)
Col (6+ #in_angle) -(5+2* #in_angle) = sA [+·m]	Standard deviation $\sigma_a$ in azimuth direction per incidence angle (#in_angle=number of incidence angles)

### 9.3 GNSS Geometric Positions

From the GNSS positioning processor the products summarized in Table 9-13 are generated. The detailed content and format of these product is described in Table 9-14.

**Table 9-13:** Summary of GNSS Positioning Products

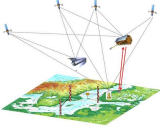
Product Acronym	Product Title	Product Description	Processing Module
GNSS-POS	GNSS Positioning Solution	Time series of coordinates of the GNSS stations as X, Y, Z coordinates in the ITRF2014 and uncertainties.	GNSS Positioning

**Table 9-14:** Detailed description of product GNSS-POS

<b>File Name</b>	
<ID>_GNSS_coordinates.txt.	<ID> = <AAA> [AAA] = BAL: Baltic Sea Network
<b>Header</b>	
Data Period: <Temporal Coverage>	<temporal Coverage>=Temporal coverage of observation intervals [yyyy mm dd - yyyy mm dd] = averaging period
Reference Ellipsoid:	Name of reference ellipsoid for geographic coordinates
<b>Data Description</b>	
Col 01 = Station Location Acronym (3 or 4 Letters)	GNSS station acronym
Col 02 = Solution Epoch [YYYY.XX]	Epoch of the Solution yyyy.xx - mean date in decimal year
Col 03 = X[m]	X coordinate in ITRF14 in meters
Col 04 = Y[m]	Y coordinate in ITRF14 in meters
Col 05 = Z[m]	Z coordinate in ITRF14 in meters
Col 06 = RMS_X [m]	RMS of X coordinate
Col 07 = RMS_Y [m]	RMS of Y coordinate
Col 08 = RMS_Z [m]	RMS of Z coordinate
Col 09 = Latitude [dd mm ss]	Latitude wrt. reference ellipsoid in [dd mm ss]
Col 10 = Longitude [dd mm ss]	Longitude wrt. reference ellipsoid in [dd mm ss]
Col 11 = Height [m]	Height above reference ellipsoid in [m]

### 9.4 Tide Gauge Sea Surface Heights

From the tide gauge data analysis processor the products summarized in Table 9-15 are generated. The detailed content and format of these product is described in Table 9-16.

	<b>BALTIC+ Theme 5</b>  Geodetic SAR for Baltic Height System Unification and Baltic Sea Level Research	<b>Final Report</b> Doc. Nr: SAR-HSU-SR-0022 Issue: 1.1 Date: 07.07.2021 Page: 155 of 170
---	--	---

**Table 9-15:** Summary of Tide Gauge Data Analysis Products

Product Acronym	Product Title	Product Description	Processing Module
TG-SSH	Corrected Sea Surface Height at Tide Gauge Stations	Time series of corrected sea surface heights observed at tide gauges with respect to the tide gauge benchmark with hourly temporal resolution.	Tide Gauge Data Analysis

**Table 9-16:** Detailed description of product TG-SSH

<b>File Name</b>	
<ID> _Tide_Gauge_heights.txt.	<ID> = <AAA> [AAA] = BAL: Baltic Sea Network
<b>Header</b>	
Data Period: <Temporal Coverage>	<temporal Coverage>=Temporal coverage of observation intervals [yyyy mm dd – yyyy mm dd] = averaging period
Reference Height:	Height Reference System
<b>Data Description</b>	
Col 01 = Tide Gauge Name	Name of tide gauge station
Col 02 = Solution Epoch [YYYY.XX]	Epoch of the Solution yyyy.xx - mean date in decimal year
Col 03 = Tide Gauge Height [m]	Average sea level height in meters
Col 04 = Standard Deviation of Tide Gauge Height [m]	Standard deviation of tide gauge time series

## 9.5 GOCE Geoid Heights

From the geoid processor the products summarized in Table 9-17 are generated. The detailed content and format of these product is described in Table 9-18.

**Table 9-17:** Summary of Geoid Products

Product Acronym	Product Title	Product Description	Processing Module
GEO-HGT	Geoid Heights	Geoid heights with mean epoch 2020.5 for the tide gauge stations	GOCE based Geoid Computation

**Table 9-18:** Detailed description of product GEO-HGT

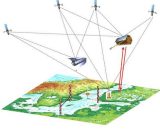
<b>File Name</b>	
<ID> _Geoid_heights.txt.	<ID> = <AAA> [AAA] = BAL: Baltic Sea Network
<b>Header</b>	
Data Period: <Temporal Coverage>	<temporal Coverage>=Temporal coverage of observation interval [yyyy mm dd – yyyy mm dd] = averaging period
Reference Ellipsoid:	Reference Ellipsoid (Normal Potential Field)
<b>Data Description</b>	
Col 01 = Station Name	Name of station
Col 02 = Solution Epoch [YYYY.XX]	Epoch of the Solution yyyy.xx - mean date in decimal year
Col 03 = Geoid Height [m]	Geoid height above reference ellipsoid in meters

## 9.6 Unified Heights and Absolute Sea Level

From the unified heights and absolute sea level processor the products summarized in Table 9-19 are generated. The detailed content and format of these products is described in Table 9-20 and Table 9-21.

**Table 9-19:** Summary of final heights and sea level products

Product Acronym	Product Title	Product Description	Processing Module
TG-HGT	Tide Gauge Heights	Time series of unified physical heights of tide gauge stations.	Height System Unification and Absolute Sea Level Heights

	<b>BALTIC+ Theme 5</b> Geodetic SAR for Baltic Height System Unification and Baltic Sea Level Research	<b>Final Report</b> Doc. Nr: SAR-HSU-SR-0022 Issue: 1.1 Date: 07.07.2021 Page: 156 of 170
---	--	---

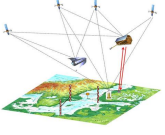
SL-ABS	Absolute Sea Level Heights	Time series of absolute sea level heights of tide gauge stations involved in the project.	Height System Unification and Absolute Sea Level Heights
--------	----------------------------	---	--

**Table 9-20:** Detailed description of product TG-HGT

<b>File Name</b>	
<ID> _Physical_heights.txt.	<ID> = <AAA> [AAA] = BAL: Baltic Sea Network
<b>Header</b>	
Data Period: <Temporal Coverage>	<temporal Coverage>=Temporal coverage of observation interval [yyyy mm dd – yyyy mm dd] = averaging period
Reference Height System:	Reference Height System (Geoid Solution)
<b>Data Description</b>	
Col 01 = Station Name	Name of station
Col 02 = Solution Epoch [YYYY.XX]	Epoch of the Solution yyyy.xx - mean date in decimal year
Col 03 = Physical Height [m]	Physical height above geoid in meters

**Table 9-21:** Detailed description of product SL-ABS

<b>File Name</b>	
<ID> _Absolute_Sea_Level_heights.txt.	<ID> = <AAA> [AAA] = BAL: Baltic Sea Network
<b>Header</b>	
Data Period: <Temporal Coverage>	<temporal Coverage>=Temporal coverage of observation interval [yyyy mm dd – yyyy mm dd] = averaging period
Reference Height System:	Reference Height System (Geoid Solution)
<b>Data Description</b>	
Col 01 = Station Name	Name of station
Col 02 = Solution Epoch [YYYY.XX]	Epoch of the Solution yyyy.xx - mean date in decimal year
Col 03 = Geoid Height [m]	Absolute sea level height above geoid in meters

	<p style="text-align: center;"><b>BALTIC+ Theme 5</b></p> <p style="text-align: center;">Geodetic SAR for Baltic Height System Unification and Baltic Sea Level Research</p>	<p style="text-align: right;">Final Report</p> <p>Doc. Nr: SAR-HSU-SR-0022</p> <p>Issue: 1.1</p> <p>Date: 07.07.2021</p> <p>Page: 157 of 170</p>
---	--	--

## 10 IMPACT ASSESSMENT

This chapter summarizes the achieved results in context with the project goal namely, to compute absolute sea level heights and to enable height unification in the Baltic Sea area. All details about the developed methodology, the experimental sets and the computed products are provided in the detailed documentation. First, the experiences made with electronic corner reflectors as a new observation tool to determine and monitor geometric positions are summarized. Here specifically experiences with their operability and calibration are provided, which could have impact on the further development of such instruments. Then, the results obtained by the SAR data analysis and positioning technique are critically assessed in terms of internal and external uncertainties and specific features to be considered for optimally exploit this data. A short assessment about the other observations and data necessary to determine the absolute sea level follows, while finally, the results obtained after combination of all data are critically reflected and a trade-off between the project goals and the achieved results is performed.

### 10.1 Electronic Corner Reflectors

#### 10.1.1 ECR Operability

The project team all together purchased 12 electronic corner reflectors (ECRs) from MetaSensing in order to setup a test network in the Baltic Sea area and in order to perform calibration activities at the DLR site in Oberpfaffenhofen, Germany. All transponders were purchased from institutional funds and devoted to this project. One of the key elements of the performed project was the first usage of commercial off-the-shelf active radar transponders, in geodetic field applications. The installations were carried out with durable mountings and permanent power supplies to ensure reliable operations in the harsh environmental conditions of the Baltic sea area. Considerable efforts were made to survey the local ties of co-located GNSS stations and tide gauges where available and to integrate the ECRs into the national levelling networks where possible [AD-4].

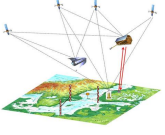
Based on our experience with transponders installed in different locations since 2019, here we list some of the problems/issues and some points that needs more work.

Compared to well-established passive Corner Reflectors (CRs) with 1.5m edge length, the equivalent ECR showed considerable advantages regarding transport, ease of installation and strength of backscattered signal for both ascending and descending tracks. Comparable passive infrastructure would have required two CRs at each of the twelve stations and more elaborate mounting solutions to support the bulky and heavy reflectors. Distribution of CR would also have required more advanced logistics as normal cars are not feasible for transporting such large reflectors. With the small and relatively lightweight ECRs, attachments could be made to existing infrastructures, e.g., the masts supporting GNSS antennas, or new platforms could be set up with reasonable efforts [AD-4]. However, because they are electronic devices and are active types, there are some disadvantages/problems as well relative to passive CRs.

The ECR system works by collecting signal from a passing satellite radar, amplifying this signal, and sending it back in the direction from which it came. In this way, it acts like a standard satellite corner reflector, but uses active technology, i.e. it is powered and it amplifies the radar signal electronically. Standard corner reflectors at these wavelengths are often several meters large; therefore, the active parts of the ECR allow for the advantage of being much smaller (half a meter) than a passive system (di Meo et al, 2019).

At its core, the ECR is meant to do one thing: determine satellite overpass times from user-programmed activation window, check the current time against these given times, and turn on the amplifiers at the given times. However, in practice, it is a more complicated system than that. It must do all of this independently, meaning it must have a microcontroller inside. It must keep time accurately in all weather conditions, meaning it has a GPS receiver inside to synchronize time data from the GPS network. It needs its own power supply that can recharge itself for the duration of the activities, and these batteries must also work in all weather conditions. And it must be able to communicate with the user, requiring a dedicated user interface (GUI) to allow the user to send satellite overpass times and check the status of the system. The ECR-C instrument can work with any C-band satellite radar operating in the bandwidth of the CAT, such as RADARSAT or Sentinel satellites. For right looking satellite missions, like Sentinel-1 and RADARSAT, the ECR can be used both in ascending and descending orbits (di Meo et al, 2019).

In summary, the ECR from MetaSensing is designed such that it shall be able to operate without the need of on-site user interaction and with energy supply either by connecting it to the electrical power supply at a station or, if not available, by charging the batteries with solar panels. The project team operated the ECRs from late 2019 until now and made a lot of experiences, which led to the remarks below. Some instruments were installed later in the year 2020 due to local constraints, some ECRs needed to be sent back for repair and some of them needed additional on-site maintenance due to various reasons, but mainly related to Software issues. The following remarks also can be regarded as recommendations for future development and use of ECRs. Specifically, the use in remote not easy accessible areas with strong weather conditions shall not be considered with the current ECR version, as the instruments exhibited several issues avoiding continuous operation.

	<b>BALTIC+ Theme 5</b>  <b>Geodetic SAR for Baltic Height System Unification and Baltic Sea Level Research</b>	<b>Final Report</b> <b>Doc. Nr: SAR-HSU-SR-0022</b> <b>Issue: 1.1</b> <b>Date: 07.07.2021</b> <b>Page: 158 of 170</b>
---	--	---

## ECR System Design and Operations

Configuration of the ECR activations for the Sentinel-1 passes was relatively straightforward but the ease of use in setting up device communication and uploading pass information could be improved. Once the configuration was set, most ECRs operated quite reliably and independently during the project's 1-year data acquisition period. In one case it was not possible to modify the old satellite configurations, activation times, etc. and every time someone had to go the field and change it. This feature was added in one of the firmware update, which were needed to be installed during the project. Passive targets would have required more maintenance as they are prone to fill up with debris, water or snow, which disturbs the SAR observations.

However, the experience gathered with the ECR installations also shows that consistent long-term operation of ECRs in the demanding environment of the Baltic sea region is not possible with the present ECR design. Three devices failed within 3-8 months because of damaged electronics, likely caused by deteriorated sealing of the ECR housings. After one year in the field, the other ECRs also showed signs of such sealing damage and it is unlikely that they would have sustained long-term operation. Small issues were also discovered with the time keeping of the ECRs, which can yield corrupted dates, leading to missed activations. Frequent resynchronization with GPS allows the devices to recover from such states, but this should be fixed for more robust operations.

ECRs, as they are today, and especially construction and housing of the model used in this pilot project, seem to be unreliable when considering their sustained operation duration. It means that construction of this model must be improved a lot to ensure that they are usable in real conditions for years without regular major maintenance.

A major concern is the on/off switch of the "first generation" ECRs (the ones with dark grey cover), as any passer-by can simply turn off the system. Note that the newer cover design has a key switch instead, which is a significantly better option.

If Wi-Fi is not an option at the ECR site and logfiles are needed, then these must be acquired at the site. The ECR has a currently running logfile and the previous logfile; the file memory limit is 245 KB. Once the currently running logfile reaches the limit, the previous logfile is deleted and replaced with the now filled logfile (this is then the new previous logfile). A new file is then started. Depending on the ECR setup, this requires visiting the site roughly once every 30–50 days.

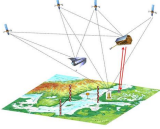
Access to transponders remotely was not easy and there were several issues with internet connection. Old fashion 2G sim cards can be inserted only by the Metasensing at the time of the order, or afterward by returning the transponder to the company. Even so, 2G sim cards provide very slow connection and takes longer time for firmware update, logbook download, etc. Instead of using internal 2G sim cards, at some stations 4G-routers were installed near the ECRs to provide the WIFI network for the transponder and access it remotely. So far, this solution worked very well. For one ECR, the GPS failed to sync the time. The ECR also tried to connect to the web to sync the time, but something went wrong, and a clock drift of 2592000 seconds was observed.

Sometimes, during the time synchronization scheduled in the ECR using built-in GPS receiver, the attempt limit is exceeded and the switch to time synchronization from the NTP server takes place. In such a scenario, regardless of the firmware version (these problems have occurred since the first tests of the device), the ECR synchronizes to the date shifted forward by exactly one month (Figure 10-1). This makes it impossible to wake up for the next programmed, observing session' and the only way to restore functionality so far is to perform a 'soft-reset'. It is possible, for example, via a USB connection and a remote computer (the case of the Władysławowo station). When communication is available only through the web-browser interface via Wi-Fi, there is practically no such functionality (the case of the station in Łeba). Then, to force a reset, we perform the firmware upgrade procedure (with forced restart function) and then re-program the flight, synchronization and reporting times, which is a quite dangerous operation, that may result in the loss of control over the device.

In one case the ECR stopped working for about 10 days (23 Sept.-5 Oct.) and no record in the log file was stored and no WIFI to access the device remotely was possible. A restart at the place (by on/off switch) was necessary and the ECR started working again.

Since the receipt of purchased ECR-C instruments in autumn 2019, the firmware update has been performed many times in order to eliminate the problems with the functioning of the instruments noticed during the tests and to improve their functionality. In the last available firmware version (v. 3.0.3.) installed for example on two Polish stations in September 2020 it is now possible to download the log files, define Sentinel-1 satellite flight times, epochs of time synchronization using the built-in GPS receiver and generating reports via the web-browser interface of the instruments. Unfortunately, the device reset feature is not available in this version. This causes problems with remote communication with the instrument via Wi-Fi, which periodically 'freezes'. 'Hanging' of Wi-Fi networks, as extensive field experience has shown, often does not require direct operator intervention in the field. In most cases, it was enough to perform the so-called 'soft-reset', which is currently only possible from the level of the ECR GUI configuration program installed on Windows system or Terminal software, using special dedicated commands. This, however, requires a permanent connection to the PC via the USB port. Not every target location of the ECR-C transponder installation enables the implementation of such a hardware configuration in the field. In Poland, it is carried out only at the station in Władysławowo.

As the ECRs are not easy to operate an improved user support is required. There is no website available to follow news related to ECR operations, to get updated software and firmware or read frequently asked questions for ECR operations.

	<b>BALTIC+ Theme 5</b>  <b>Geodetic SAR for Baltic Height System Unification and Baltic Sea Level Research</b>	<b>Final Report</b> <b>Doc. Nr: SAR-HSU-SR-0022</b> <b>Issue: 1.1</b> <b>Date: 07.07.2021</b> <b>Page: 159 of 170</b>
---	--	---

For any problem and information, MetaSensing had to be contacted. Since these are new devices in the market, there are some unknown parameters unknown about how they function in long run. These are for example: How long is the internal battery life in practice under cold weather conditions? Aging of the flash memory that hosts firmware, configurations, log files? Aging and damage to electronic parts (e.g. 4 internal antennas)? Are there phase center variations (PCV) and offsets and are they stable and identical for all ECRs (see below)? Is there any signal delay inside the transponder and is it an individual delay or the same for all transponders (see below)? Do these transponders have the same performance for both ascending and descending observations?

```

Heap free: 118736 [B]; Up-Time: 23 days & 4 Hours;
2020.10.05 11:30:00 [GPS] #1: 1,1,20201004233047.000,54.753652,17.534905,-2.500,0
.35,89.0,1,,0.8,1.1,0.8,,11,10,,42,,
2020.10.05 11:30:00 [GPS] module activated for UTC time update
2020.10.05 11:30:00 [FW_UPDATE] Firmware version check failed, got HTTP response
code:-1
2020.10.05 11:30:01 [GPS] #2: 1,0,20201005113002.000,,,,,0.00,0.0,0,,,,,12,0,,,,,
2020.10.05 11:30:02 [GPS] check_gps_status(): Attempt #1 of clock sync via GPS
2020.10.05 11:30:03 [GPS] check_gps_status(): Attempt #2 of clock sync via GPS
2020.10.05 11:30:05 [GPS] check_gps_status(): Attempt #3 of clock sync via GPS
2020.10.05 11:30:06 [GPS] check_gps_status(): Attempt #4 of clock sync via GPS
2020.10.05 11:30:07 [GPS] check_gps_status(): Attempt #5 of clock sync via GPS
2020.10.05 11:30:13 [GPS] check_gps_status(): Attempt #10 of clock sync via GPS
2020.11.05 11:30:14 [NTP] trying retrieve time from a time server (NTP)
2020.11.05 11:30:14 [NTP] Clock drift detected:2678400 [s]
2020.11.05 11:30:14 [NTP] ECR time updated via NTP Server! (GPS module turned
off)
2020.11.05 11:30:14 [GPS] check_gps_status(): Attempt #1 of clock sync via GPS
2020.11.05 11:30:14 [ALIVE] V_bat: 90% (13.28 [V]); Temp: 17 [Celsius]; RH: 69%;
Heap free: 117920 [B]; Up-Time: 54 days & 4 Hours;
2020.11.05 11:30:15 [ACT] Activation ON; Orbit:ASC; Pol.:V; Durat.:1200 [s]
2020.11.05 11:30:16 [ACT] Activation OFF (Scheduled)
2020.11.05 11:30:16 [ACT] Next scheduled Act.:2020/11/08 16:25:00; id:2;
De-Act:2020/11/08 16:45:00; id:3;
2020.11.05 11:30:16 [STATUS] New periodic Status Report scheduled:2020/11/05
11:45:00; id:4
2020.11.05 11:30:16 [ACT] Next scheduled Act.:2020/11/08 16:25:00; id:2;
De-Act:2020/11/08 16:45:00; id:3;
2020.11.05 11:30:16 [STATUS] New periodic Status Report scheduled:2020/11/05
11:45:00; id:4
2020.11.05 11:30:16 [GPS] New periodic GPS timer update scheduled:2020/11/05
23:30:00; id:5
2020.11.05 11:30:18 [STATUS-REP] Sent to
UART:UART:12006884000005FA3E249305A64E3FFFE418C477C425B03BD0C131145D705
2020.11.05 11:45:00 [STATUS] New periodic Status Report scheduled:2020/11/05
23:45:00; id:4
2020.11.05 11:45:00 [STATUS-REP] Sent to
UART:UART:12006884000005FA3E5BC305A64E3FFFE418C477C425B03BD0C131145F306
2020.11.05 12:30:14 [ALIVE] V_bat: 90% (13.27 [V]); Temp: 17 [Celsius]; RH: 69%;
Heap free: 118732 [B]; Up-Time: 54 days & 5 Hours;
2020.11.05 13:30:14 [ALIVE] V_bat: 90% (13.28 [V]); Temp: 17 [Celsius]; RH: 69%;
Heap free: 118736 [B]; Up-Time: 54 days & 6 Hours;

```

**Figure 10-1:** Log-file time synchronization problem with GPS at Władysławowo station

### Sealing of ECRs

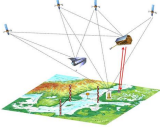
The sealing of the ECRs is a major concern (at least for the “first generation” ECRs – the ones with dark grey cover). Namely the cover consists of two components: the cover itself and a frame that keeps the cover in its place. These two components are connected/sealed by a silicone line. This silicone line, however, degrades during the operation of the ECRs, especially in harsher weather conditions. Elastic sealing insulation running around the plastic ECR-C cover is probably also not sufficiently resistant to UV radiation (after a few months, noticeable cracks appeared on ECRs). Once the silicone line has degraded enough, humidity can get inside the system, as the silicone line is essentially the only protection against this. It seems that due to the design of the cover and the frame, the humidity cannot leave the system and collects within as water (there have been a few reports of significant amount of water inside the ECRs). Humidity in the system then dampens the signal and eventually damages the electronics.

From reports of users of ECRs, it can be assumed that the problems of excess humidity within the system are connected to the occasional slow degradation of the ECRs’ signal strength. Such a degradation seems to occur over a few weeks, until the signal of the ECR is no longer visible from SAR images. This means that it is necessary to regularly assess the integrity of the cover (i.e., the state of the silicone line that connects the cover with the frame), as the damage to the silicone line may lead to eventual failure of the ECR system. This also means that the currently available ECRs (at least for the current project) are not capable of long-term self-sufficient operation, as they need regular visitations.

The “newer generation” ECRs have a cover that consists of a single component. Furthermore, there is a rubbery layer between the cover and the bottom plate. These improvements in the design suggest that the newer models may be more resistant to humidity. Unfortunately, so far there is no data to support this assumption.

### Power Supply

Power supply is needed for such transponders, either by solar panels or direct connection to power grid. Most ECRs were installed close to a permanent GNSS stations which had already electricity. The ECR power supply may be a cause for

	<b>BALTIC+ Theme 5</b>  Geodetic SAR for Baltic Height System Unification and Baltic Sea Level Research	<b>Final Report</b> Doc. Nr: SAR-HSU-SR-0022 Issue: 1.1 Date: 07.07.2021 Page: 160 of 170
---	--	---

problems in case no electricity is available and the solar panel and batteries need to be used. In the best-case scenario, the batteries last roughly 3 to 4 days without any external power supply. A short blackout should thus not cause any problems, however, a longer blackout may. Once the batteries are empty and there is no external power supply to charge these, the low voltage level of the batteries may trigger a safety mechanism that does not allow charging via AC (depending on the conditions, this may happen a few days to a few weeks after the batteries are discharged). This means that the only way to charge batteries is via a solar panel. Note, however, that a solar panel and an AC power cable should not be used at the same time for charging. Once the system is kickstarted with a solar panel, the safety mechanism should disable automatically. This means that it should be possible to charge the batteries via AC again. For one of the ECRs it happened that both batteries died and that it couldn't be turned on even by external power connection. In this case, charging one of the batteries by a solar panel, sent quickly by MetaSensing on request, helped to reactivate the internal batteries.

Such a safety mechanism suggests that a solar panel power supply could be a better option, as in case of a blackout (e.g., due to snow cover on the panel) the system is capable of kickstarting itself again. This is not an option with the AC power supply, as the system is incapable of starting again after a longer blackout (once the battery safety mechanism is triggered).

### Radio Frequency License

As the ECRs are active senders radio frequency permissions from the national authorities are needed to operate them. The procedure varies from country to country, as well the fees to be paid for the permission. During years, the permission fees will not be an insignificant cost. Depending on the place, also permission from military may be needed. This needs to be considered in case one plans to install a network of these instruments.

Negotiations with telecommunication authorities in the different countries were complicated by the lack of detailed ECR radio specifications from the manufacturer, which in some cases slowed down installations or sites had to be relocated. For instance, an installation was originally planned at Metsähovi geodetic station but was moved to Rauma because of concerns about possible radio-interference raised by the operators of the near-by radio telescope. In Sweden, getting permissions for installing such active radar reflectors took a long time. The permission period is limited (ends at end of 2021) and need to be extended again in case ECR operations will continue.

#### 10.1.2 ECR Calibration

Because the ECR is an active electronic instrument, an initial calibration after fabrication by the manufacturer is advised in order to correct for possible system delays. Ideally, this calibration should be identical for all ECRs of the same design. From the results obtained during the project there are indicators that each ECR somehow has its own characteristics and individual calibration sessions need to be performed.

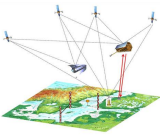
Regarding the SAR measurements with Sentinel-1, the ECR electronic delay characteristics turned out to be less controllable than anticipated. While the typical precisions of  $\pm 0.08\text{m}$  in range and of  $\pm 0.25\text{m}$  in azimuth are generally on-par with observations of passive CRs analyzed for comparison, the absolute accuracy of ECR measurements is only in the order of  $0.5\text{m}$ . The limitation comes from the delays introduced by the active ECR electronics which was found to vary significantly between  $1.2\text{m}$  and  $3\text{m}$  for different pass geometries and different devices. This was not expected as all ECRs are from the same batch and were built with identical components, which were supposed to show comparable electronic characteristics. The delay calibration determined with our SAR measurements could only partly compensate for this behavior. In order to improve the SAR measurements and achieve same stability and accuracy as with passive CRs, the ECRs should be investigated by the manufacturer and if possible calibrated in laboratories to determine their individual electronic characteristics.

In particular, differences of computed versus observed ellipsoidal heights seem to vary from near-zero to several decimetres between different ECRs. The height difference between GNSS and ECR has been determined with different (independent) measurements, and the height difference can be considered as reliable. Equally, there seems to be big variations between tide gauge geoid comparison, from 1-2 cm at Rauma and Emäsalo, up to 60 cm at Forsmark/Kobben and Loksa. This cannot be a problem of the geoid model, which we know to be consistent within a few cm. The only reason probably is related to insufficient calibration of individual instruments. During this short pilot project, it was not possible to evaluate the long-term stability of the ECRs, but such a big difference between ECRs make them useless in this kind of height determination without developing a reliable calibration for offsets and temporal variability monitoring.

## 10.2 SAR Data Processing and Positioning

For the majority of the selected installation sites the ECRs could be placed at locations with low background noise and the signals were very reliably detected in the acquired Sentinel-1 SAR image data. But even in more difficult environments like towers surrounded by forests or harbour areas with lots of additional signals, the ECRs remained clearly visible. This flexibility along with the small dimensions is a strong advantage of these active devices.

This is confirmed exemplarily by the situation in Władysławowo, Poland. Initial concerns related to the use of images with reflections in the range of radio waves emitted by the Sentinel-1A/B satellites in the area of the Władysławowo port were not confirmed by the obtained quality of reflected signals, which formed the basis for the Geodetic-SAR studies in the project. This location of the active transponder installation confirmed that they can work effectively and efficiently in

	<b>BALTIC+ Theme 5</b> Geodetic SAR for Baltic Height System Unification and Baltic Sea Level Research	<b>Final Report</b> Doc. Nr: SAR-HSU-SR-0022 Issue: 1.1 Date: 07.07.2021 Page: 161 of 170
---	--	---

typical conditions prevailing in most seaports, where tide-gauge stations are most often installed. Figure 10-2 below shows the obtained reflections from ECR-C instruments in the surroundings of the strongly ‘noisy’ fishing boats in the Władysławowo harbour (top) and in the meteorological garden in Łeba (bottom) surrounded by large green areas.

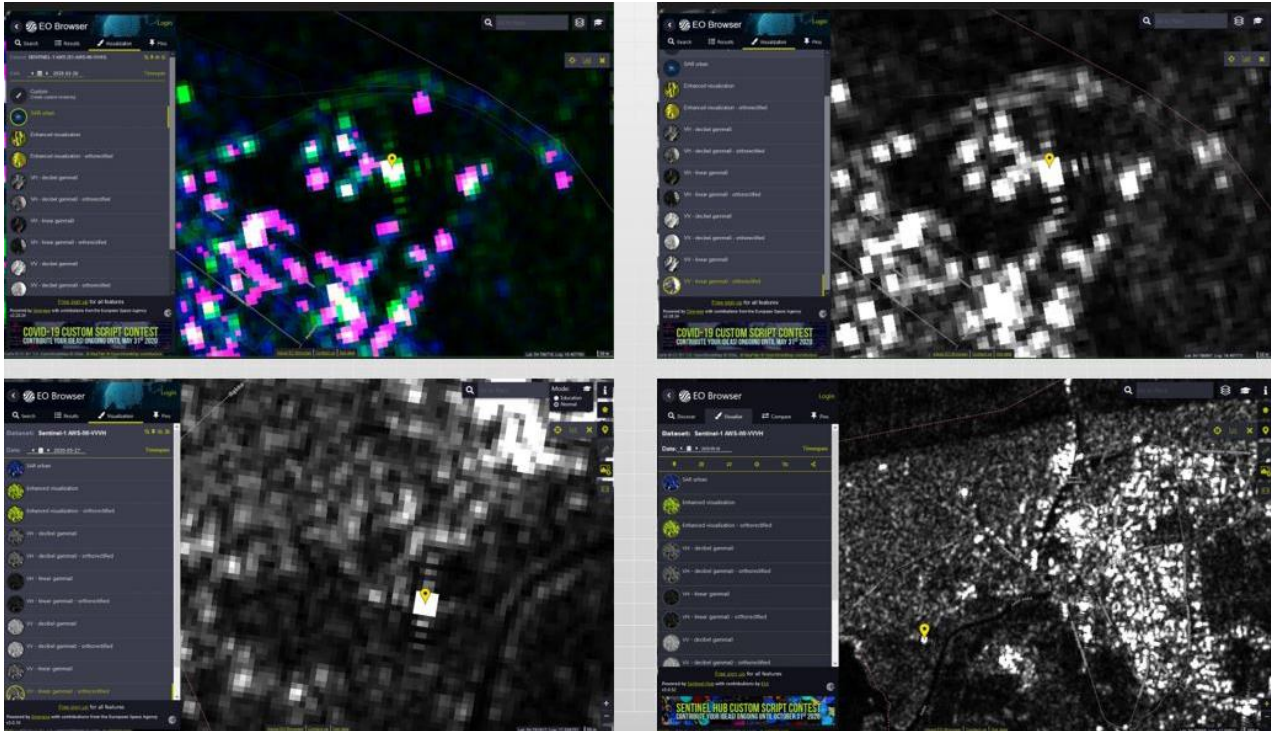


**Figure 10-2:** Preliminary analyses of the quality of the reflected signals at both stations were performed (Władysławowo - top row, Łeba - bottom row)

From the positioning results for all ECR stations by processing all available SAR observations from year 2020 the following observations could be made.

First of all, the ECR’s seem to perform not equally, meaning that for example electronic delays could differ significantly for each ECR. For the SAR positioning in this project, it was assumed that the delay is determined from the average coordinate differences for a few reference stations and then applied to all ECR’s during processing. Positioning result show that, as long as there is an uncertainty about a common electronic behaviour of the ECRs, each ECR shall be calibrated at a reference station, before it is installed at a designated observation point. In case ECRs perform similar with this respect, then a representative electronic delay from a few ECRs at reference stations can be computed. Varying electronic delays per ECR strongly influence the absolute coordinate accuracy rather than the internal estimate of the position accuracy).

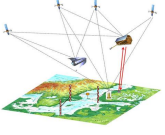
When looking at systematic effects, one always has to keep in mind to take care of the different viewing geometries due to different incidence angles. To use both ascending and descending orbit observations the phase centre correction has to be applied, as the phase centre differs by several decimetres in the positioning depending on the incidence angle.

Currently, outlier detection is split in two steps i.e., gross outliers (half pixel resolution of Sentinel-1) and outliers (3-sigma criteria per incidence angle) are treated separately. Additionally, observations are flagged, where precise orbit information seems to be insufficient accurate. Optionally, also single data points can also be flagged manually, if required. Outlier detection is critical to the positioning performance and need to be done very carefully.

Monthly solutions are the shortest time interval of observations in order to reach realistic positing results. Most ECR stations only gather 10 valid range and 10 valid azimuth observations over a period of one month, which is the minimum for a stable performance of the positioning processor. The higher the latitude the more observations within a month are possible. This needs to be considered for possible applications of the SAR positioning technique. With more observations the positioning becomes more stable for most stations.

After repair of an ECR, one has to evaluate, if a station can be regarded as the same station or if its performance changed significantly and it has to be treated as a “new” independent station.

There are observation periods for which the processor does not converge for a positing result even with sufficient number of data takes. Therefore, the positioning is terminated providing unreliable results. The bias correction in general helps to reach convergence for the position solution, but for a few stations and specific observation intervals the bias correction even deteriorates the achieved solution.

	<b>BALTIC+ Theme 5</b>  Geodetic SAR for Baltic Height System Unification and Baltic Sea Level Research	<b>Final Report</b> Doc. Nr: SAR-HSU-SR-0022 Issue: 1.1 Date: 07.07.2021 Page: 162 of 170
---	--	---

As a promising result of this study it can be stated that SAR positioning exhibits high internal accuracies. The internal accuracies for the solutions across all stations vary between few centimetres down to millimetres in the local North, East, Height reference frame. This implies, that having a continuous observation period with good data coverage, relative coordinate variations can be observed on bi-monthly (monthly, under optimal conditions) time intervals with a few centimetres accuracy. For absolute positions a well calibrated and long term stable instrument is needed, which is not the case for the ECRs used during the study.

For future work, the behavior of the ECRs needs to be investigated for a possible impact of temperature variations to the positioning results (e.g. influencing the electronic delay) and for individual instrument performance variations resulting in an improved bias correction. It needs to be investigated if the electronic delay has impact on the variances of the SAR positioning results and if a time dependent delay (e.g. due to temperature variations) causes these variances. Furthermore, the SAR positioning processor can be improved by analyzing situations where no convergence is achieved and by identifying optimal relative weights between range and azimuth observations.

### 10.3 GNSS, Tide Gauge and Geoid

#### 10.3.1 GNSS Data Processing

GNSS data processing was performed in accordance with the assumptions, which are described in detail in [AD-2] and 7.3. The processing of daily observations was performed as daily network solutions in the Bernese GNSS Software ver. 5.2 in the double-difference mode (DD method). As the reference frame the ITRF2014 was used, in which all IGS global products are available for the calculations: precise orbits, the Earth's rotation parameters and the corrections of GNSS satellite clocks. The study covered the entire period of 2020. The daily network solutions are related to the middle of the development period of each daily session. Based on these solutions, time series of X, Y, Z Cartesian coordinates covering the entire year 2020 were generated. From these series, for the purposes of the project, time series of B, L, h geodetic coordinates were then created, related to the GRS-80 geocentric ellipsoid. The final average coordinate solutions for all stations are computed as 3D Cartesian Coordinates in ITRF2014 and as ellipsoidal coordinates referred to the GRS80 ellipsoid for epoch 2020.50.

The processing followed the well established procedures without any difficulties. All data either from the GNSS network defined for this project were available either from open access services or were provided by the project partners in case national reference stations are included. The internal accuracy of the determined coordinates is at sub mm level, which by far is sufficient to reach the envisaged goals of this project.

#### 10.3.2 Tide Gauge Data Analysis

The developed methodology is based on the existing tide gauge processing approaches. The resulting annual mean sea level estimates are comparable to other concurrent tide gauge processing approaches. This study focused on ensuring the consistency of the participating TG time series. This was achieved by a rigorous conversion into the common vertical datum and accounting for the vertical land motion.

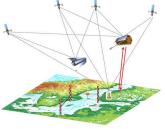
The participating tide gauge records are mostly affected by the used sensor technologies. In this study the following sensor technologies were used: stilling well with float, modern pressure, float and radar sensors. These all assured 1 cm accuracy for the resulting tide gauge records. However, also the sea state affects the accuracy of readings.

The internal and absolute consistency/integrity of the tide gauge records has often been overlooked in the current and past studies. It is shown now, that consistency (e.g. reduction to the same time epoch, a common vertical datum, removal of land-uplift effects, tide gauge connections with national geodetic infrastructure a) is essential for achieving the geodetic (sub-dm, cm-range?) accuracy for a rigorous validation and usage of new and emerging space technologies.

The higher than average quality of the Baltic Sea tide gauge records (in conjunction with the other techniques tested within the present study) could be beneficial for sister disciplines, such as oceanology, coastal and offshore engineering. The methodology developed in the Baltic Sea region can be applied in other parts of the world.

#### 10.3.3 Regional Geoid Determination

Several regional geoid models applying different procedures were computed. They all agree very well with each other and have about the same fit to GNSS/levelling. Finally, one model was picked, which then was converted to the project mean epoch 2020.5 by applying the land uplift correction computed from the temporal variation model for the spherical harmonic coefficients up to degree 120 from GOCO06S/ITSG-Grace2018s (Mayer-Gürr et al. 2018; Kvas et al. 2019). As can be judged from the comparison to GNSS/levelling, the standard uncertainty of the geoid heights in Sweden, Finland and Estonia is estimated to be approximately 0.010 m in a relative sense. For the Polish stations, the uncertainty is a bit higher, because for this area only an older gravity data set was available. Due to regulations of the data owners, a more recent updated data set could not be made available to the project team. Nevertheless, the impact is marginal and only affects the quality of the Polish geoid heights by an increase of uncertainty of less than a centimetre. Regarding the impact on the final results of the project, the accuracy obtained from the geoid modelling by far is sufficient. More important is that all data are processed with the same standards and conventions in order to keep compatibility with the other

	<b>BALTIC+ Theme 5</b>  Geodetic SAR for Baltic Height System Unification and Baltic Sea Level Research	<p style="text-align: right;">Final Report</p> Doc. Nr: SAR-HSU-SR-0022 Issue: 1.1 Date: 07.07.2021 Page: 163 of 170
---	--	---

observations. This has been carefully addressed and no systematic effects from the geoid modelling on the final results are to be expected.

It also shall be mentioned that the time variation of the geoid heights is very small. The geoid velocities are below 0.6 mm/year for all the included tide gauges. This means that the time variation within the project year 2020 is well below 1 mm for all the tide gauges. The final geoid height time series for the tide gauges can thus be taken as the constant values for epoch 2020.5.

## 10.4 Data Combination

### 10.4.1 Reference Frames and Standards

For the combination of the different geometric and gravimetric quantities a correct treatment of the permanent tide and a consistent correction of postglacial uplift is essential to achieve consistent results within this project. Regarding the extrapolation of ITRF2014 station positions, stable reference frame stations need to be selected, to ensure that a linear propagation models provides sufficient accurate results. The transformation parameters between ITRF2014 and ITR2008 as well as the geocenter variations can be neglected within this project, as the effects are much below the centimeter level. The same holds for non-linear motions in station positions. However, if GNSS solutions computed in the ITRF2014 are compared with EPN results, the transformation formulae between the ITRS and ETRS89 need to be applied, since the effect is about 75 cm for observations in the year 2020. All these items have been carefully considered when processing the individual data sets. In conclusion no systematic effects related to references frames and processing standards shall be present in the unified heights and absolute sea level results.

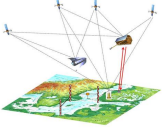
### 10.4.2 Unified Heights and Absolute Sea Level

The results of the individual observations techniques in terms of heights are combined for the static case. Static here means that average values over the observation period of the year 2020 are considered disregarding sub-annual variations of heights. The reason for this is that when combining all observation data sets, the error always is driven by the worst component. As identified in the previous chapters, the weakest point at this stage is the accuracy of the SAR positions, which in average is at a level of a decimetre (for a few good stations). Therefore, at this stage it doesn't make sense to compute the time variable absolute sea level.

For the ECR stations co-located to a permanent GNSS station the resulting heights can be directly compared by taking into account the local tie measurements. By this, the absolute performance of the SAR positioning technique can be quantified. As the results are varying no ultimate conclusion can be drawn from this comparison. While three stations exhibit good to reasonable agreement between the GNSS and the ECR height results at decimetre level or below, for three other stations the GNSS versus ECR height differences are at a level of several decimetres up to half a meter. Regarding the reason why some ECR positioning results are better than others there is no unique answer. It is assumed that several of the issues mentioned in section 10.1 are responsible for this. A major problem could be related to insufficient electronic calibration of the ECRs and/or possible instabilities of the calibration parameters.

From the ECR stations co-located to a tide gauge station the resulting physical heights of the tide gauge zero markers above the reference equipotential surface (GOC-based geoid) are computed. As all tide gauge zero markers are already provided in the EVRS, meaning, that in the ideal case this height for all stations shall be zero, any deviation from zero can be interpreted as a performance indicator for the involved quantities and here mainly the performance of the SAR positioning. The results show that some stations seem to provide very good results with only a few centimetres offset, while other stations exhibit an offset of several decimetres up to a meter. These results need to be further analysed together with the performance of the individual ECR stations and also with respect to the length of the data time series. Regarding the results there seems to be some correlation of the physical height results with the SAR observation quality, the SAR residuals and the length of the SAR observation time series. At this point it is difficult to provide a complete assessment of the results as no single reason can be identified, before the ECR calibration performance can be checked in detail. Derived absolute sea level heights contain the full uncertainty of the physical heights of the tide gauge stations as they were computed. Therefore, all what has been said above also applies to the absolute sea level heights and no further conclusions can be drawn.

For the experiments which have been defined in order to link tide gauge stations to the permanent GNSS network via the ECR stations, baseline height differences between ECRs collocated to GNSS stations and between ECRs collocated to tide gauge stations are computed. The results of the baseline comparisons again show a diverse behaviour. Basically, the differences between GNSS and ECR observed height differences vary between a few centimetres and some decimetres. For stations, which exhibit a large absolute offset the differential height error between these stations becomes small (below a decimetre), while the differential error between one of these stations with the other stations becomes significantly larger. This indicates, that there is a systematic height offset in the ECR positioning results with the same sign, as it is also shown in the absolute comparisons. The reason for this is yet unknown. Similar the for stations, which exhibit a small absolute offset the differential height error between these stations becomes also small (below a decimetre). The results from the tide gauge baseline differences show in most cases large differences. Right now, it seems that only two ECR stations with good performance and linked to a tide gauge are available, where differences up to a decimetre can be achieved. There is also a good agreement between two stations with similar systematic offsets at both stations.

	<b>BALTIC+ Theme 5</b>  Geodetic SAR for Baltic Height System Unification and Baltic Sea Level Research	<b>Final Report</b> Doc. Nr: SAR-HSU-SR-0022 Issue: 1.1 Date: 07.07.2021 Page: 164 of 170
---	--	---

This could hint towards a better relative performance if absolute errors can be eliminated by differentiation. This only is true if the absolute calibration is stable in time, which is a bit unsure when looking to all results obtained from the SAR positioning.

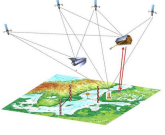
## 10.5 Summary and Outlook

The project gave a good overview on possibilities of geodetic SAR, possible applications and also good experience to work within such applications. Some of the technical difficulties in the beginning delaying the start of the project, but foremost the COVID-19 pandemic caused a lot on final outcome of the project. Some field campaigns, but especially all joint tasks and meetings suffered on that. As the scientific point of view, the project gave only a moderate outcome. However, it clearly showed the potential of the method, way to develop technique in the future, and a lot of information how to improve in the future projects. As such, it fulfilled the goals one may expect with such a new technique. ECRs can give additional information for areas of no previous observations, but cannot replace current positioning techniques. In wider perspective, the number of observations is very small comparing to GNSS observations. Currently, together with hardware issues, it might be the reason to not use geodetic SAR in geodetic applications as independent measurement technique, it could be useful as a supporting technique collocated with GNSS stations. The design of the ECRs needs to be improved in order to enable remote unmanned operations in harsh environmental conditions. Specifically, the calibration and characterization of the electronics needs to be improved heavily before these instruments can meet geodetic accuracy requirements.

It also was identified that ECRs are not suitable to observe temporal coordinate variations with shorter temporal resolution than a month. But they can be used for observations of large movement (>decimeter/month) in areas with critical slopes undergoing landslides, for volcanos and fast subsidence e.g. dolines or cave collapses. Additionally, they might be applicable for determining absolute reference coordinates to fix the orientation of SAR interferometry. Unfortunately, passive corner reflectors were not able to test and compare with ECRs more thoroughly within the project. However, there are quite much experiences of those elsewhere. For its future works, for example FGI ended up to order passive corner reflectors, 1.5 m side of a cube, for FinnRef permanent GNSS stations. This opens new possibilities for comparisons between active and passive reflectors for the purpose of SAR positioning.

The project team learned about these new geodetic devices, and the Geodetic SAR project was the first step to add such electronic corner reflectors to geodetic infrastructure and co-locate them with other geodetic instruments/benchmarks. Having such transponders co-located with GNSS (for example) can provide additional data for local deformation monitoring at the site, 3D absolute positioning and atmospheric studies and can be compared with GNSS data and time series in long run. In addition, such reflectors as artificial persistent scatterers (PS) co-located with GNSS permanent stations can be useful for future calibration of the European ground motion service (EGMS) products and to transform the deformation maps and rates into a global reference frame.

Within the project a very valuable data set has been compiled, which offers the possibility to enhance methods and procedures in order to develop the SAR positioning technique towards operability. The data set will be publicly available and can attract new users to develop processing strategies and to investigate new possible applications for the SAR positioning technique.

	<b>BALTIC+ Theme 5</b>  Geodetic SAR for Baltic Height System Unification and Baltic Sea Level Research	<b>Final Report</b> Doc. Nr: SAR-HSU-SR-0022 Issue: 1.1 Date: 07.07.2021 Page: 165 of 170
---	--	---

## 11 SCIENTIFIC ROADMAP

### 11.1 Assessment of Project Results

#### 11.1.1 Results versus Objectives Trade-Off

As described basically three scientific challenges have been identified, which were addressed by the project. A trade-off analysis for these goals versus the achieved results is done in the following paragraphs.

#### **Connection of tide gauge and GNSS stations by means of ECRs**

The overarching goal was to connect tide gauge markers with the GNSS network geometrically in order to determine the relative vertical motion and to correct the tide gauge readings. The idea was to use the geodetic SAR positioning technique for the time with Sentinel-1 data for this purpose. A test network in the Baltic Sea area has been defined and 10 stations (either tide gauges or permanent GNSS stations) were equipped with so-called electronic corner reflectors (ECRs) as a new observation technique providing continuous positioning results. By this technique a relatively simple way to acquire systematically geometric coordinates at tide gauge stations could be implemented.

The stations were carefully selected in order to ensure good operability (infrastructure and local support) and to setup meaningful experiments. This led to a network with stations in 4 Baltic Sea countries namely, Poland, Estonia, Finland and Sweden. In addition, two ECRs were installed at the DLR location in Oberpfaffenhofen, Germany in order to support calibration activities. At the beginning of the project, there were some delays in delivery of the purchased ECRs mainly due to delays in the manufacturing process. This caused a delay of a few months with the installation of some ECRs at the selected stations. In addition, the effort to acquire radio frequency licenses for operating the active ECRs in the different countries took significantly longer as expected. Finally, for some stations the access during the winter period was not easy and therefore the installation of a few ECRs was not possible before spring 2020. For all these reasons the full operational network was only available for about four months in 2020. Nevertheless, 6 out of the 10 ECRs were operational for 9 months or more in 2020 and delivered valuable observations in order to investigate their performance. But, due to the relatively short observation period, it became very early clear, that observing vertical land motion will not be possible due to the small signal amplitude and the short observation time series. Therefore, the project team concentrated to assess the overall performance of the geodetic SAR positioning technique using the new ECRs.

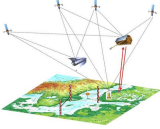
The geodetic SAR positioning requires basically three main processing steps. First, the SAR image analysis extracts the ECR target coordinates in terms of ranges and azimuth per radar (Sentinel-1) acquisition. Second, the required environmental, geophysical and instrumental corrections are determined and prepared for each observation. And third, the complete information from the previous steps is used to determine absolute 3-dimensional coordinates by an iterative analysis scheme applying the SAR Range-Doppler equations. In order to estimate the performance of these steps internal quality measures like observation residuals and errors estimates from a least squares process are analysed. From the results it could be identified that the general internal performance meets the expectations. In other words, from the results it could be concluded that the procedure is working and that average 3D coordinates can be determined with SAR data from Sentinel-1 with the expected accuracy. For some stations a slightly reduced performance was identified, which most likely is linked to nearby artificial reflectors, which reduced the quality of the retrieved image coordinates. This just points out the necessity to carefully select the installation site for the ECRs.

In order to link the ECRs with the tide gauge station or the permanent GNSS station a local survey (tie) between both stations is needed. For each station such a survey has been performed by the project team applying standard geodetic techniques. The results of these surveys indicate that the requirements to keep centimetre accuracy can be easily kept.

To summarize, from the internal quality estimates of the SAR image analysis and the 3D positioning the results look promising and accuracies at a level of 1 to 2 centimetres per coordinate axis could be achieved.

#### **Regional Geoid Determination for Absolute Heights**

In order to determine absolute sea level heights at the tide gauge stations, which are referring to a common equipotential surface, a regional geoid is needed. The computational approach for this regional geoid has to fulfil all corresponding requirements, namely, to use a common global gravity field model as baseline, and to refine the geoid for the tide gauge stations by using local gravity data around the station with a radius of at least 100 km. For the stations at the Baltic Sea a very dense and precise gravity data set is available, which was used for this purpose. The only critical item about local gravity data is the data access, as these data in many cases are restricted and are not publicly available. Luckily, the Nordic Geodetic Commission (NKG) is working since many years on the Baltic Sea geoid and therefore has access to such data covering most of the stations used in this project. Only for the two Polish stations some newly available gravity data could not be used, due to data restrictions, but it turned out that the available data was dense and good enough to compute the geoid heights with an accuracy level of 1 to 2 centimetres. In conclusion one can state that this goal was completely achieved.

	<b>BALTIC+ Theme 5</b>  <b>Geodetic SAR for Baltic Height System Unification and Baltic Sea Level Research</b>	<b>Final Report</b> <b>Doc. Nr: SAR-HSU-SR-0022</b> <b>Issue: 1.1</b> <b>Date: 07.07.2021</b> <b>Page: 166 of 170</b>
---	--	---

## Joint Analysis and Absolute Heights

For the combination of geometric heights, determined from the GNSS and SAR positioning techniques with the gravimetric geoid height one has to guarantee consistency of reference frames and processing standards. This was carefully analysed from the beginning and standards have been fixed prior to the data analysis in order to ensure this compatibility. The same holds for the tide gauge readings (relative sea level observations), which needed to be processed according to pre-defined standards.

In order to estimate the absolute performance of the SAR positioning using the ECRs, different kind of height combinations were done. First, for the ECR stations co-located to a permanent GNSS station geometric heights could be compared when applying the relative height difference between the GNSS antenna reference point and the ECR reference point, which was determined by local surveys. This is an indicator about the absolute performance of the SAR positioning technique. There are 6 stations in the Baltic Sea area enabling such a comparison. From the results one can identify a relative large variation of the obtained height differences in the range of a few centimetres up to half a meter. As one can assume that the GNSS derived heights are accurate at a level of a few centimetres, the ECR derived heights are the main driver for the absolute performance results. Regarding the reason why some ECR positioning results are better than others there is no unique answer. Sometimes the reason could be that the observation time series is relatively short, but for other stations the raw observation data series seem to be good and there is no indicator about possible data problems. This result points towards a possible ECR station dependent problem and it is assumed that electronic delays could play a major role. This also is confirmed by a detailed analysis at the calibration station in Oberpfaffenhofen, where a longer data time series and also a passive standard corner reflector is available for comparison. For more details about this problem it is referred to the following section.

A similar test could be performed for the tide gauge stations when computing the physical heights of the tide gauge zero marker above the common reference equipotential surface. As all tide gauge zero markers are already provided in a joint vertical reference system, any deviation from zero can be interpreted as a performance indicator for the involved quantities and here mainly the performance of the SAR positioning. The results show that 3 out of 7 stations seem to provide very good results with only a few centimetres up to one decimetre offset, while the 4 other stations exhibit an offset of several decimetres up to a meter. When analysing these results together with performance of the individual ECR stations and also with respect to the length of the data time series there seems to be some correlation with the SAR observation quality, the SAR residuals and the length of the SAR observation time series. As for the GNSS station comparison it is difficult to provide a complete assessment of the results as no single reason can be identified. Again, internal and varying electronic delays most likely are the main reason for the large variations in the differences.

Regarding all the results, at this point, the goal to use ECRs for observing and monitoring geometric heights of tide gauge stations could not be achieved yet. As the project team is convinced that technical reasons related to the ECRs are the major cause of problems, these need to be solved first, before they can be used operationally. Nevertheless, it shall be pointed out that SAR as a positioning tool is promising, but that active reflectors need to be characterized and calibrated extremely good before they can be used for this purpose. Standard corner reflectors are no alternative as their installation and maintenance also requires significant effort and they are quite large and not easy to install, e.g. close to a tide gauge station. In this case a permanent GNSS receiver could be the only alternative with the disadvantage that the maintenance of such a station also is costly and that very good communication channels are required in order to download the data continuously. So, from a system point of view, ECRs would be much easier to handle as all data in principle are acquired via the SAR images and no local data need to be downloaded.

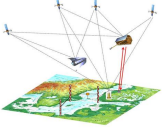
### 11.1.2 Observation System Weaknesses

In this chapter the identified major weaknesses of the ECR instruments and their operability are summarized. These were experienced during the study period and probably prevented the study team to obtain conclusive results, even if some results are very promising and indicate that an accuracy of a few centimetres is feasible. All other elements as the geoid heights, the tide gauge readings, and the GNSS coordinates, meet the requirements and can be used for an absolute sea level observing system.

#### ECR Calibration

As the ECR is an active electronic instrument, after fabrication an initial calibration by the manufacturer is required in order to correct for possible system delays. This calibration should be identical for all ECRs of the same design. From the results obtained during the project there are indicators that each ECR somehow has its own life and individual calibration sessions would need to be performed.

Regarding the SAR measurements with Sentinel-1, the ECR electronic delay characteristics turned out to be less controllable than anticipated. While the typical precisions in range and azimuth are generally on-par with observations of passive CRs analysed for comparison, the absolute accuracy of ECR measurements is only in the order of 0.5m. The limitation comes from the delays introduced by the active ECR electronics which was found to vary significantly between 1.2m and 3m for different pass geometries and different devices. This was not expected as all ECRs are from the same batch and were built with identical components, which were supposed to show comparable electronic characteristics. The delay calibration determined with our SAR measurements could only partly compensate for this behaviour. In order to improve the SAR measurements and achieve same stability and accuracy as with passive CRs, the ECRs should be

	<b>BALTIC+ Theme 5</b>  Geodetic SAR for Baltic Height System Unification and Baltic Sea Level Research	<b>Final Report</b> Doc. Nr: SAR-HSU-SR-0022 Issue: 1.1 Date: 07.07.2021 Page: 167 of 170
---	--	---

investigated by the manufacturer and if possible calibrated in laboratories to determine their individual electronic characteristics.

Differences of computed versus observed ellipsoidal heights vary from near-zero to several decimetres for different ECRs. The reason probably is related to insufficient calibration of individual instruments. During this short pilot project, it was not possible to evaluate the long-term stability of the ECRs, but such a big difference between ECRs make them useless in this kind of height determination without developing a reliable calibration for offsets and temporal variability monitoring. A long-term calibration is required in order to identify if there is a time dependency of the calibration parameters or the internal delays.

### ECR Operations

The experiences gathered with the ECR installations show that consistent long-term operation of ECRs in the demanding environment of the Baltic sea region is not possible with the present ECR design. Three devices failed within 3 to 8 months because of damaged electronics, likely caused by deteriorated sealing of the ECR housings. After one year in the field, the other ECRs also showed signs of such sealing damage and it is unlikely that they would have sustained long-term operation. The silicone line used as sealing degrades during the operation of the ECRs, especially in harsher weather conditions. Elastic sealing insulation running around the plastic ECR-C cover is probably also not sufficiently resistant to UV radiation (after a few months, noticeable cracks appeared on ECRs). Once the silicone line has degraded enough, humidity can get inside the system, as the silicone line is essentially the only protection against this. It seems that due to the design of the cover and the frame, the humidity cannot leave the system and collects within as water. Humidity in the system then damages the electronics. The “newer generation” ECRs have a cover that consists of a single component. Furthermore, there is a rubbery layer between the cover and the bottom plate. These improvements in the design suggest that the newer models may be more resistant to humidity. Unfortunately, so far there is no data to support this assumption.

Power supply is needed for such transponders, either by solar panels or direct connection to the electric network. Most ECRs were installed close to a permanent GNSS stations which had already access to electricity. The ECR power supply may be a cause for problems in case no electricity is available and the solar panel and batteries need to be used. In the best-case scenario, the batteries last roughly 3 to 4 days without any external power supply. A short blackout should thus not cause any problems, however, a longer blackout may. Once the batteries are empty and there is no external power supply to charge these, the low voltage level of the batteries may trigger a safety mechanism that does not allow charging via AC (depending on the conditions, this may happen a few days to a few weeks after the batteries are discharged). This means that the only way to charge batteries is via a solar panel. Note, however, that a solar panel and an AC power cable should not be used at the same time for charging.

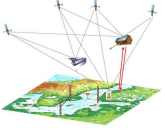
ECRs, as they are today, and especially construction and housing of the model used in this pilot project, seem to be unreliable when considering their durability. It means that construction of this model must be improved a lot to ensure that they are usable in real conditions for years without regular major maintenance. If Wi-Fi is not an option at the ECR site and logfiles are needed, then these must be acquired at the site. Access to transponders remotely was not easy and there were several issues with internet connection. Old fashion 2G sim cards can be inserted only by the Metasensing at the time of the order, or afterward by returning the transponder to the company. Even so, 2G sim cards provide very slow connection and takes longer time for firmware update, logbook download, etc. Instead of using internal 2G sim cards, at some stations 4G-routers were installed near the ECRs to provide the WIFI network for the transponder and access it remotely. So far, this solution worked very well. For one ECR GPS failed to sync the time.

Sometimes, during the time synchronization scheduled in the ECR using built-in GPS receiver, the attempt limit is exceeded and the switch to time synchronization from the NTP server takes place. In such a scenario, regardless of the firmware version, the ECR synchronizes to the date shifted forward by exactly one month. This makes it impossible to wake up for the next programmed, observing session’ and the only way to restore functionality so far is to perform a ‘soft-reset’. It is possible, for example, via a USB connection and a remote computer. When communication is available only through the web-browser interface via Wi-Fi, there is practically no such functionality. Then, to force a reset, a firmware upgrade procedure needed to be performed (with forced restart function) and then re-program the flight, synchronization and reporting times, which is a quite dangerous operation, that may result in the loss of control over the device.

The examples shown above indicate that some improvements need to be implemented in the ECR design before they can be used as an operational observing system.

## 11.2 Recommendations for Future Activities

To use ECRs as a new tool to perform continuous, unmanned and precise geometric positioning with Sentinel-1 is promising, but requires significant improvements related to calibration and operations (see above). Here some recommendations are provided what would be needed to improve the operability of ECRs and for what kind of applications this new system might be a promising technique if the hardware issues can be solved.

	<b>BALTIC+ Theme 5</b>  Geodetic SAR for Baltic Height System Unification and Baltic Sea Level Research	<b>Final Report</b> Doc. Nr: SAR-HSU-SR-0022 Issue: 1.1 Date: 07.07.2021 Page: 168 of 170
---	--	---

### 11.2.1 Recommendations towards an Operational System

The design of the ECR devices has to be revised by the manufacturer. Improvement of housing for long-term operations and revision of firmware for more reliable operations (specifically the timing issue) as well as the power supply system is required. Most crucial is an a-priori delay characterization of the ECRs electronic delay patterns for homogenous accuracy of SAR range observations at the 5 cm level.

A proper documentation of ECR radio signal characteristics by the manufacturer is needed in order to ease access to operation permission with radio-communication authorities. Such documentation should also be supported by ESA to encourage the installation and operation of Sentinel-1 ground infrastructure.

A more direct data access to Sentinel-1 image data is needed for such type of monitoring services. The access to data via the Sentinel-1 science hub API was reliable enough for science purposes but a monitoring service processing the Sentinel-1 SAR data of large amount of ECRs would require more stable continuous data access.

Development of operational software that can be used by partners wishing to contribute to a possible service shall be envisaged. This is especially needed for the SAR data component. Ready-to-use software is required to allow ECR operators the provision ECR SAR data measurement files that contribute to a common service (comparable to GNSS RINEX data).

Consolidated data format for product exchange shall be developed. Established formats exist for GNSS, but not for SAR, geoid heights, or tide gauge results.

Sentinel-1 data require corrections for systematic SAR processing effects and geophysical perturbations (atmosphere, solid Earth). To relieve users of these, ESA has commissioned an operational correction product for Sentinel-1 (Gisinger et al. 2019). The product will provide corrections for each Sentinel-1 SAR scene and can support applications like the proposed monitoring service.

Co-location with existing geodetic infrastructure through SAR reference markers like the ECRs of a Baltic network is also important for other SAR monitoring initiatives like the European Ground Motion Service (Solari et al. 2020).

The applied SAR methods and the Baltic ECR network allow usage of data other C-Band SAR sensors like the Radar Constellation Mission (Doyon et al. 2018). This could contribute to ESA cooperation initiatives with other SAR data providers. In the long-run, a multi-mission SAR data usage could also improve the tide gauge monitoring service and lead to the adoption of the techniques for other regions.

For international projects it is crucial to ensure the consistency of the tide gauge records (in terms of the common vertical datum and accounting for the vertical land motion, adopting common time epoch), such that they can be used for validation/verifications of new and emerging space technologies and data products. Complete metadata descriptions are required for tide gauge stations and data before they can be jointly analysed.

### 11.2.2 Recommendations for Future Studies and Applications

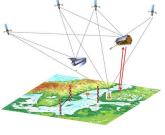
ECRs can give additional information for areas where no previous 3D position observations are available, but cannot replace current positioning techniques. In a wider perspective, the number of observations is very small compared to GNSS observations. Currently, together with hardware issues, it might not be reasonable to use geodetic SAR in geodetic applications as independent measurement technique, but it could be useful as a supporting technique collocated with GNSS stations.

Related to the main study goal, i.e. to link tide gauges to the global geometric network, the Baltic Sea project can be considered as a pilot study for the rest of the world. Assuming that operability requirements are met (see previous section), there is a great potential to use this observing system at remote locations, where it is hardly possible to install a permanent GNSS receiver. This opens the possibility to link many more tide gauge stations to the geometric network and to monitor the sea level also in an absolute sense and not only relative per tide gauge station as it is the case nowadays.

ECRs are not suitable to observe temporal 3D coordinate variations with shorter temporal resolution than a month as long as only radar images from the Sentinel-1A/B satellites are acquired (as a minimum about 10 images are needed to reach convergence for a robust positioning solution). But they can be used for observations of large movement (decimetre/month) in areas with critical slopes undergoing landslides, for volcanos and fast subsidence. ECRs might be a suitable tool for monitoring long term processes with larger signal amplitudes.

ECRs might be applicable for determining absolute reference coordinates to fix the orientation of SAR interferometry. Geodetic SAR positioning also is regarded as an interesting approach to support permanent GNSS networks. Several national agencies currently are installing passive corner reflectors at their national core stations. By installing also ECRs at these locations new possibilities for comparisons between active and passive reflectors in order to characterize the absolute and temporal behaviour become feasible.

Relative SAR positioning between two ECRs might become a more interesting technique capable to transfer ellipsoidal heights from a known position to an another place. If the system behaviour of ECRs is identical in terms of stability of calibration parameters and electronic delays, by the differential approach some of the major problems can be eliminated.

	<p style="text-align: center;"><b>BALTIC+ Theme 5</b></p> <p style="text-align: center;">Geodetic SAR for Baltic Height System Unification and Baltic Sea Level Research</p>	<p style="text-align: right;">Final Report</p> <p>Doc. Nr: SAR-HSU-SR-0022 Issue: 1.1 Date: 07.07.2021 Page: 169 of 170</p>
---	--	---

This could not be investigated in detail during the study, but some results indicate that height differences can be estimated with better accuracy than absolute heights.

In conclusion one can state, that for any future application, ECRs need to be fully characterized for systematic effects, which could otherwise result in absolute coordinate biases. Specifically, the long-term behaviour of such systematic effects need to be assessed and investigated. If this is under control and if the operability of the ECRs can be improved such that one can operate them without the need to visit the station frequently, ECRs can be used for many applications, where ellipsoidal coordinates are required over long observation periods. Specifically, coastal zones might be interesting as satellite radar altimetry in principle delivers equivalent information, but so far suffers from less good radar reflection and from less accurate geophysical corrections closer to the coast. Linking altimetric heights with geodetic SAR positions and also linking the satellite orbits of both might be an interesting approach from which both techniques might benefit. Generally, the integrated observation of the land/ocean transition zone is a key element to better understand the impact of climate change and geophysical phenomena on these highly populated areas. Therefore, implementing an observation system of this kind, which combines all satellite information of the Copernicus system in order to observe the geometry of the land/ocean transition zone is of great importance. The Baltic Sea with its excellent infrastructure could be a very good test case to develop such a system, which then should be transferrable to any other places in the world.